BIROn - Birkbeck Institutional Research Online

Enabling Open Access to Birkbeck's Research Degree output

Palaeolakes on Mars: geomorphology and hydrology at the planetary dichotomy

https://eprints.bbk.ac.uk/id/eprint/49832/

Version: Full Version

Citation: Dickeson, Zachary Ian (2022) Palaeolakes on Mars: geomorphology and hydrology at the planetary dichotomy. [Thesis] (Unpublished)

© 2020 The Author(s)

All material available through BIROn is protected by intellectual property law, including copyright law.
Any use made of the contents should comply with the relevant law.

Deposit Guide
Contact: email

Palaeolakes on Mars: Geomorphology and Hydrology at the Planetary Dichotomy

Zachary Ian Dickeson

Thesis submitted for the degree of Doctor of Philosophy

2021

Department of Earth and Planetary Science
Birkbeck College, University of London

Department of Earth Sciences
Natural History Museum

I, Zachary Ian Dickeson, confirm that the work presented in this thesis is my own. Where information has been derived from other sources, I confirm that this has been indicated.

Zachary Ian Dickeson

Abstract

Hundreds of palaeolakes have been identified on Mars; representing widespread ancient aqueous processes and potentially habitable conditions. Global catalogues serve to constrain past climatic conditions and regional controls on hydrology, while local studies are valuable in interpreting sequences of lacustrine processes over time. The goal of this thesis is to characterise the hydrological setting of the highland-lowland boundary during the Noachian and Hesperian, by linking high-resolution local studies into regional and global trends, and bridging the gap between disparate scales. The region of Arabia Terra is bounded to the north and east by the planetary dichotomy, and hosts few documented palaeolakes, presenting an opportunity to investigate the nature of a globally significant hydrological and morphological boundary through the observation of palaeolakes in an underrepresented area of the planet.

Geomorphological and topographic analyses in this thesis initially centre on two fluvio-lacustrine systems which terminate at the dichotomy: the first, represents a previously unknown chain of palaeolakes, showing evidence of prolonged and continuous drainage through the system; and the second, in the area of Oxia Planum, reveals an expansive lacustrine system draining into a possible palaeolake at the planned landing site of the ExoMars rover. Building on the results and methods of these detailed studies, a final analysis expands the scope of investigations to compile a comprehensive regional catalogue of fluvial and lacustrine features.

Analysis and correlation of multiple, temporally distinct palaeolake fill levels within individual palaeolake basins indicate a complex and prolonged history of aqueous processes in the region. While the discovery and cataloguing of hundreds of new palaeolakes allowed the delineation of drainage catchments representative of ancient Arabia Terra. Regional drainage patterns are shown to be strongly controlled by impact crater basins, and semi-arid climatic conditions, with limited highland areas acting as source regions for basins in the lowlands.

Contents

Abstract **5**

Contents **7**

List of Figures **11**

List of Tables **15**

Acknowledgements **17**

1 Introduction **21**
- 1.1 Mars 21
  - 1.1.1 Mars Observation and Exploration 24
  - 1.1.2 Climate and Hydrology 27
  - 1.1.3 The Planetary Dichotomy 29
  - 1.1.4 The Arabia Terra Region 30
- 1.2 Research Overview 33
  - 1.2.1 Aims and Objectives 33
  - 1.2.2 Methodology 34
- 1.3 Thesis Structure 35

2 Water Bodies on Earth and Mars **37**
- 2.1 Overview 37
- 2.2 Terrestrial Lakes and Palaeolakes 38
- 2.3 Palaeolakes on Mars 41
- 2.4 Ancient Oceans on Mars 43
  - 2.4.1 Global Palaeoshorelines 44
  - 2.4.2 Ocean Shoreline Evidence 47
- 2.5 Water Bodies and the Martian Climate 51

3 Data and Methods **55**
- 3.1 Overview 55
- 3.2 Orbital Instruments and Datasets 55
  - 3.2.1 Visual Image Data 60
  - 3.2.2 Topographic Data 61
- 3.3 Hydrological Analysis 63

3.3.1 Hydrology Coding Systems 63
3.3.2 Drainage Catchment Delineation 68
3.4 Research Applications 74

4 Palaeolake System at the Planetary Dichotomy 77
4.1 Introduction 78
4.1.1 Study Area in Western Arabia Terra 80
4.2 Data and Methods 81
4.2.1 Hydrological Analysis 82
4.3 Observations and Results 83
4.3.1 Fluvial Valleys 85
4.3.2 Sediment Fans and Basin Floor Deposits 86
4.3.3 Open Basin Palaeolakes 88
4.3.4 Highland Drainage Catchments and Lowland Sinks 91
4.3.5 Associated Morphological Features 92
4.3.6 Relative Age Relationships 95
4.4 Discussion 96
4.4.1 Analysis of Palaeolakes and Valleys 96
4.4.2 Nature of the Dichotomy Margin 100
4.4.3 Regional Hydrology and Martian Palaeolakes 102
4.4.4 Local Hydrological and Geological Evolution 104
4.5 Conclusions 106

5 Palaeolakes in the Region of Oxia Planum 109
5.1 Introduction 110
5.2 Data and Methods 113
5.2.1 Hydrological Analysis 114
5.3 Observations 115
5.3.1 Topographic Deformation 115
5.3.2 Fluvial Features 118
5.3.3 Sediment Fans 122
5.3.4 Open-Basin Palaeolakes 125
5.3.5 Closed-Basin Palaeolakes 127
5.4 Discussion 131
5.4.1 Palaeolake Confidence 131
5.4.2 Palaeolake Basin Deformation 133
5.4.3 Multi-Crater Palaeolake System 138
5.4.4 Lowland Basins and Water Bodies 140
5.4.5 Implications for Biosignatures and Sediment Transport 143
5.5 Conclusions 144

6 Catalogue of Palaeolakes and Drainage in Western Arabia Terra 147
6.1 Introduction 148
6.1.1 Dichotomy Scarp and Regional Scale Channels 151
6.2 Data and Methods 154
6.2.1 Hydrological Analysis 155
6.3 Observations 156
6.3.1 Dichotomy Drainage Catchments 157
6.3.2 Fluvial Features 159

6.3.3 Sediment Fans 166
6.3.4 Palaeolake Identification and Characterisation 167
6.4 Analysis and Discussion 175
6.4.1 Base-Level Correlation and Palaeolake Confidence 175
6.4.2 Fluvial and Lacustrine Distributions and Populations 178
6.4.3 Morphologically Derived Drainage Catchments 186
6.4.4 Constraining Drainage Sinks and Source Regions 189
6.4.5 Groundwater Influx and Surface Accumulation 194
6.5 Conclusions 196

7 Synthesis and Conclusions 199
7.1 Overview 199
7.2 Implications for Early Hydrology on Mars 199
7.2.1 Controls on Regional Drainage 199
7.2.2 Ground Water Influx and Surface Accumulation 201
7.2.3 Implications for Ancient Oceans on Mars 204
7.3 Palaeolake Environments on Mars 205
7.3.1 A Dynamic Landscape 205
7.3.2 Earth Analogues 206
7.3.3 Palaeolake Ecology and Astrobiology 208
7.4 Appraisal of Methods 209
7.4.1 Palaeolake Identification Criteria 209
7.4.2 Drainage Catchment Delineation 211
7.4.3 Data Resolution in Palaeolake Identification 211
7.5 Future Work 214
7.5.1 Palaeolake Datasets 214
7.5.2 Fluvial Datasets 220
7.5.3 Expanding Regional Palaeolake Catalogues 221
7.5.4 Proposed Landing Sites in Arabia Terra 223
7.6 Conclusions 226

References 229

Appendices 247
Appendix I – Photogrammetric Processing with SOCET SET 247
Appendix II – GIS Data Formats 248
Appendix III – Quantification of Morphology and Topography 250
Appendix IV – Catalogue of Palaeolakes in Arabia Terra 252

List of Figures

Figure 1.1 – Geological eons and periods for Earth and Mars. 22

Figure 1.2 – Map of Mars regions and major topographic features. 23

Figure 1.3 - Global map of past, present, and future surface missions to Mars. 26

Figure 1.4 – Regional map of Arabia Terra. 31

Figure 1.5 – Topographic profiles of Arabia Terra. 33

Figure 2.1 – Global distribution of rivers and lakes on Earth. 38

Figure 2.2 – Global distribution of valley networks and palaeolakes on Mars. 42

Figure 2.3 - Mapped ocean shorelines on Mars. 46

Figure 2.4 - Map of possible ocean evidence in Chryse Planitia and Arabia Terra. 48

Figure 2.5 - Examples of possible coastal morphologies on Mars. 50

Figure 2.6 - Schematic illustration of morphological evidence for water on Mars. 52

Figure 3.1 – Map of CTX and HiRISE image coverage. 60

Figure 3.2 – Map of topographic data coverage. 62

Figure 3.3 – Fluvial network ordering systems. 65

Figure 3.4 – Methods used to select relevant fluvial start and end points. 66

Figure 3.5 – Examples of rasters produced with the ArcMap 'Hydrology Toolbox'. 68

Figure 3.6 – Workflow diagram of the tools in the ArcMap 'Hydrology Toolbox'. 69

Figure 3.7 – Example drainage catchments filled to different depths. 72

Figure 4.1 – Study area context map, for dichotomy palaeolake system. 80

Figure 4.2 – Illustration of the method used to identify palaeolake basins. 83

Figure 4.3 – Detail images and longitudinal valley profiles. 84

Figure 4.4 – Preliminary mapping of basin floor and sediment fan deposits. 86

Figure 4.5 – Detailed views of basin floor and sediment fan deposits. 87

Figure 4.6 – Palaeolake extents and lake/valley system profiles. 89

Figure 4.7 – Highland drainage catchments for palaeolake systems. 92

Figure 4.8 – Morphological features associated with palaeolake basins. 93

Figure 4.9 – Scenarios accounting for the formation of negative slope outlet valleys. 99

Figure 4.10 – Chronology of fluvial and lacustrine processes in palaeolake systems. 105

Figure 5.1 – Context of Oxia Planum and Coogoon Valles in Arabia Terra. 111

Figure 5.2 – Examples of recent topographic features in Oxia Planum. 116

Figure 5.3 – Mapped morphological features around Oxia Planum. 120

Figure 5.4 – Detailed images of mapped fluvial valleys. 121

Figure 5.5 – Detailed images of the three large sediment fans. 122

Figure 5.6 – Detailed views of two possible sediment fans. 124

Figure 5.7 – Identified open-basin palaeolakes in the Coogoon Valles system. 126

Figure 5.8 – Possible ancient palaeolakes within the Oxia Planum basin. 129

Figure 5.9 – Example of possible palaeolake deposits. 132

Figure 5.10 – Detailed view of palaeolake L-CN1. 136

Figure 5.11 – Changing palaeolake levels within the multi-crater system. 138

Figure 5.12 – Detailed view of the outlet of palaeolake L-CC2. 141

Figure 6.1 – Context maps of the catalogue area. 149

Figure 6.2 – Drainage catchments produced on filled topographic data. 156

Figure 6.3 – Map of the major dichotomy drainage catchments. 157

Figure 6.4 – Map of catalogued fluvial features and sediment fans. 160

Figure 6.5 – Example of flow direction determination for fluvial features. 161

Figure 6.6 – Plots displaying the flow direction of fluvial features. 162

Figure 6.7 – Stream relationship classification. 164

Figure 6.8 – Examples of morphological classifications of fluvial features. 165

Figure 6.9 – All catalogued palaeolakes, with sizes and boundaries to scale. 168

Figure 6.10 – Open-basin palaeolakes identified in the area of Mawrth Vallis. 169

Figure 6.11 – Examples of closed-basin palaeolakes identified in the catalogue. 170

Figure 6.12 – Fluvial and open-basin palaeolake densities for the catalogue area. 176

Figure 6.13 – A comparison of open-basin and closed basin palaeolake populations. 179

Figure 6.14 – A comparison of open-basin palaeolake dimensions and properties. 182

Figure 6.15 – A comparison of closed-basin palaeolake dimensions and properties. 185

Figure 6.16 – Morphological drainage catchments. 187

Figure 6.17 – Morphological drainage catchments in the Becquerel system. 191

Figure 6.18 – Schematic model of surface runoff and groundwater processes. 197

Figure 7.1 – Trends in regional flow, relative to major regional depressions. 200

Figure 7.2 – Catalogued palaeolakes by elevation and distance from the dichotomy. 203

Figure 7.3 – Map of the Great Lakes region of East Africa. 207

Figure 7.4 – Palaeolake identification with topography data at different resolutions. 213

Figure 7.5 – Examples of possible palaeolake shorelines. 216

Figure 7.6 – Example of possible palaeolake deposits. 218

Figure 7.7 – Map of CRISM observations relative to mapped palaeolakes. 219

Figure 7.8 – Areas considered for future regional palaeolake catalogues. 222

Figure 7.9 – Landing site selection using ExoMars type mission criteria. 225

List of Tables

Table 3.1 – Selected orbital Mars instruments and technical specifications. 57

Table 4.1 - Palaeolake surface elevations and dimensions. 90

Table 5.1 – Elevations and dimensions of open-basin palaeolakes. 130

Table 6.1 – Characteristics and dimensions of the major dichotomy drainage catchments. 158

Table 6.2 – Volume to drainage catchment relationships. 195

Acknowledgements

To Peter Grindrod, who conceived this project, I am incredibly grateful for the freedom you gave me to follow my interests and intuitions, all whilst steering me away from dead-ends and towards interesting questions. I owe so much to the team of supervisors who have been ever enthusiastic in their support of my research, and generous with their time and advice. Thank you to Joel Davis, Ian Crawford, and Matt Balme, for the many hours of discussion, reading, editing and 'red-penning', that have made this work a cohesive and comprehensible whole.

However, to adapt a popular phrase; 'it takes a village', and beyond my 'official' supervisors I'm incredibly grateful to the academics who took an interest in my work and shared advice and ideas. Thank you to all the PhD students, studying everything from diatoms to dinosaurs, who I shared this experience with, and to the conference goers who lingered at my posters, asked questions about my research, or joined in a discussion of the work in progress. Doctoral study can be an isolating endeavor, but this community was my antidote.

To my family, thank you for getting me to the point where I could even consider this undertaking. Not least, thank you to my incredible wife, Katie, for weathering the moody ups and downs of my stress and self-doubt with bottomless kindness, understanding, and support. You've earned a secondhand PhD alongside me.

Finally, this thesis is for my father. He would have absolutely loved this stuff.

"Thought fights with thought;

out springs a spark of truth

from the collision of sword and shield."

- *W.S. Landor*

1

Introduction

1.1 Mars

Mars is the outermost of four terrestrial planets in the solar system, with a surface hosting features and landforms strikingly similar to the Earth (Herschel 1784, Masursky 1973, Kite 2019). The observation of analogous landforms on Mars has long fuelled speculation as to the environmental and climatic conditions on Mars, as well as the search for life beyond the Earth (Lowell 1908, Bowie 1971, Klein 1979, Vago, Westall et al. 2017).

The solid surface of Mars is understood to have formed contemporaneously with the Earth (~4.4 Ga)(Humayun, Nemchin et al. 2013), as both planets began to cool following accretion (**Figure 1.1**). Unlike the Earth, tectonic processes appear to have never initiated on Mars (Hauck and Phillips 2002, Carr and Head 2010), but the surface is still comprised of diverse terrains, divided into distinct geological regions (**Figure 1.2**), and dated within defined geological epochs as (**Figure 1.1**): Pre-Noachian ~4.6-4.1 Ga; Noachian ~4.1-3.7 Ga; Hesperian ~3.7-3.0 Ga; and Amazonia <3.0 Ga (Carr and Head 2010, Robbins, Hynek et al. 2013, Tanaka, Skinner et al. 2014). The action of major geological processes such as volcanism, tectonism, impact cratering, and aqueous erosion were largely limited to the early history of Mars, with most fluvial valley networks formed during the Noachian and tapering off towards the end of the Hesperian (Zuber 2001, Carr and Head 2010). Since then, relatively static conditions have persisted for billions of years through the Amazonian, permitting the widespread preservation of ancient landforms. Geological and geomorphological evidence indicates a past climate in which liquid water

significantly shaped the surface, through a variety of aqueous processes, including: fluvial (Hynek, Beach et al. 2010, Davis, Gupta et al. 2019), lacustrine (Goudge, Head et al. 2012, Goudge, Aureli et al. 2015), groundwater (Andrews-Hanna, Zuber et al. 2010), and marine (Di Achille and Hynek 2010, Rodriguez, Fairen et al. 2016).

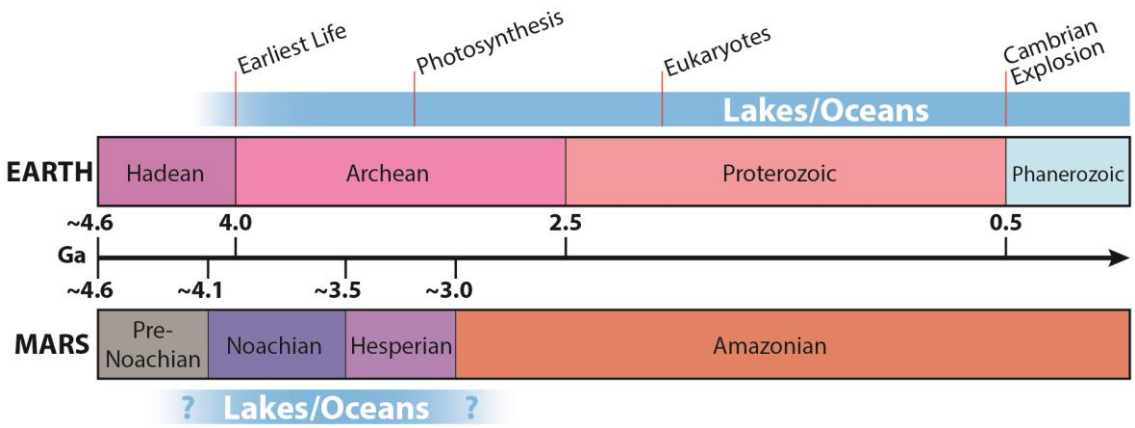

Figure 1.1 *– Geological eons and periods for Earth and Mars. Both planets formed at approximately the same time, and may have had lakes and oceans contemporaneously. Liquid water on Earth, in the form of oceans, lakes, and rivers, has remained a constant feature on the surface of the planet since the Hadean, part of a global hydrological system that has hosted major developments in the evolution of life. In contrast, liquid water on the surface of Mars is thought to have been largely restricted to the Noachian and Hesperian periods, and if life ever developed on Mars it may have been restricted to this relatively brief window.*

The present conditions on the surface of Mars are significantly different to those on ancient Mars, or on Earth. Temperatures range from +20 C° to –153 C°, but with a mean atmospheric pressure <1% that of the Earth, water is not stable as a liquid on the surface (Carr 2007). The thin atmosphere compounded with a weak magnetic field on Mars (Acuna, Connerney et al. 1998), results in high levels of ultraviolet and ionizing radiation at the surface (Hassler, Zeitlin et al. 2014). Despite these extremes, surface conditions on Mars are more similar to those on Earth than any other body in the solar system, and below the surface, vast reserves of water have been identified frozen in the polar caps and beneath the martian regolith (Carr and Head 2015). The availability, quantity, and chemistry of water are foremost amongst questions of habitability (Cockell, Bush et al. 2016), and although it is possible that habitable reservoirs of liquid water may exist at depth in the sub-surface or beneath the ice caps (Michalski, Cuadros et al. 2013, Orosei, Lauro et al. 2018), the present surface of Mars is likely inhospitable to life (Fairén,

Davila et al. 2010). As such, much of the astrobiological study of Mars is focused on habitable environments in the ancient past.

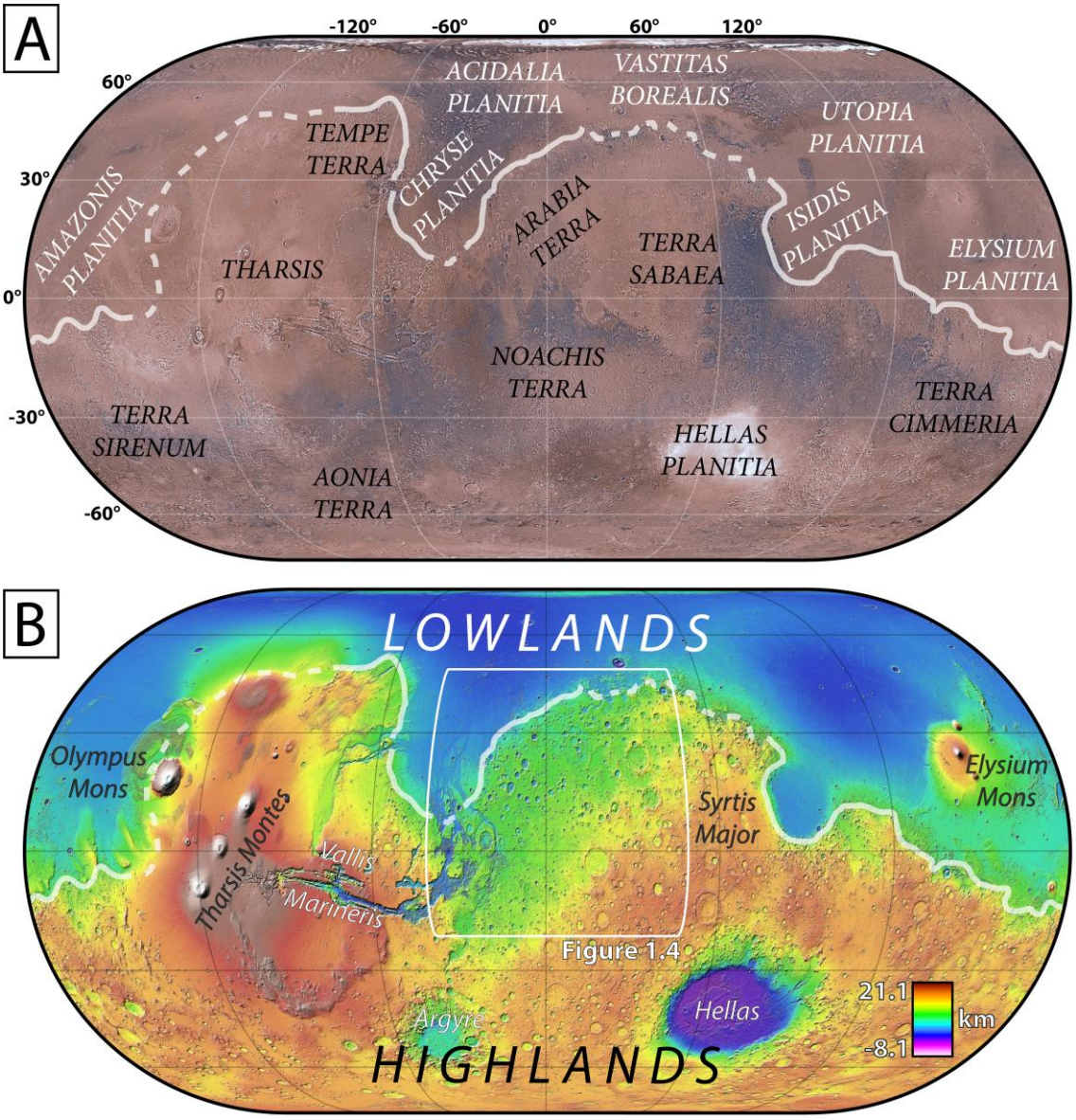

Figure 1.2 *– Map of Mars regions and major topographic features. (A) Global image mosaic of Mars surface with highland (black text) and lowland (white text) regions, and the position of the planetary dichotomy (white line; reproduced from (Zuber, Solomon et al. 2000, Zuber 2001)). (B) Global topography map indicating the distinct contrast between highlands and lowlands in relation to the planetary dichotomy, also showing major topographic features, including: volcanic edifices (black text); ancient impact basins; and Valles Marineris. (Viking imagery MDIM2.1 NASA-USGS, and MOLA topography NASA-JPL)*

That another planet should display evidence of processes so similar to those observed on Earth is significant beyond the search for extra-terrestrial life. The decline of aqueous processes early in the geological history of Mars, and the preservation of ancient geological and geomorphological evidence from this period, provide an opportunity to

better understand the evolution of the terrestrial planets in general, and the apparent exceptionalism of the Earth. Evidence of the early hydrology of the Earth has largely been destroyed by subsequent geological activity, and the divergent path followed by Mars allows for an analysis of the contrasting evolutions of different worlds, and the planetary surface processes in the early solar system.

1.1.1 MARS OBSERVATION AND EXPLORATION

Further from the Sun, and beyond the orbit of the Earth, the wider orbital path of Mars takes the planet on a longer and slower journey around the Sun. As a result, ground based observations and mission launches to Mars are only feasible every ~2.2 Earth years, during a window of a few weeks when the planets are in opposition (Pearce 1924), and Mars makes the nearest approach to Earth of any planet but Venus. However, unlike cloud shrouded Venus (Fegley Jr 2003), the surface of Mars is visible from Earth and from Mars orbit. This visibility and accessibility has allowed for a long history of observation and research (Herschel 1784, Lowell 1895), with Mars becoming the most imaged and studied planetary surface beyond the Earth and the Moon.

The position and motion of Mars across the sky have been observed and recorded for millennia, but the invention of the telescope enabled the first observations of features on the surface. Early astronomers observed and interpreted global scale albedo features as: landmasses (pale); oceans, seas and channels (dark); and polar ice caps (white) (Herschel 1784, Schiaparelli 1882, Lowell 1895). Whilst Earth based observations of the martian surface and atmosphere in the early twentieth century put constraints on climatic conditions, particularly the improbability of liquid water existing on the surface (Wright 1925, Menzel 1926, Hess 1950). However, the limitations of ground based observation meant that conclusive descriptions of the martian surface could not be further tested until the dawn of the space age (Lederberg and Sagan 1962).

The modern era of Mars exploration began in 1964 with the fly-by of Mariner-4, and acquisition of the first ever close-up images of the planet (Douglas 1964). At the mission outset there was not a consensus on martian surface conditions, but geologically

recent hydrological processes and even extant vegetation were considered possible (Barabashov 1963). The images however, revealed a heavily cratered ancient surface that was cold, arid, and with an atmosphere too thin to support liquid water (Leighton, Murray et al. 1965). Given these constraints, the search for habitable environments began to shift from the present to past conditions on Mars, through investigation of ancient landforms. In the 1970s the Mariner-9 and Viking orbiters imaged extensive areas of the surface at up to ~300 m/pixel (Masursky 1973). Coverage of wide areas of the surface allowed the geomorphology and geology of Mars to be studied on a regional scale, revealing ubiquitous landforms across the planet indicating the widespread presence and action of liquid water on the ancient surface of Mars (Pieri 1980).

A proliferation of orbital missions and instruments in the twenty-first century have revolutionised Mars research, with extensive coverage of the surface at a range of scales and with diverse observation methods, including: near global imagery coverage at ~6 m/pixel by the Context Camera (CTX) (Malin, Bell et al. 2007); a maximum image resolution of ~0.25 m/pixel with the High Resolution Imaging Science Experiment (HiRISE) (McEwen, Eliason et al. 2007); and orbital spectroscopy instruments such as 'Observatoire pour la Mineralogie, 'Eau, le Glaces et l'Activite' (OMEGA) (Bibring, Soufflot et al. 2004), on the Mars Express orbiter, and the Compact Reconnaissance Imaging Spectrometer for Mars (CRISM) (Murchie, Arvidson et al. 2007), on the Mars Reconnaissance Orbiter (MRO), allowing for the investigation of mineralogical and chemical composition form orbit.

In-situ observations from the surface of Mars were first returned by the Viking landers in 1975 (Chamberlain, Cole et al. 1976, Jones, Arvidson et al. 1979), and although landing on Mars is notoriously difficult (Braun and Manning 2006), a total of 12 robotic landers and rovers have since visited Mars, traversing a combined distance of more than ~70 km across the surface (**Figure 1.3**). The most recent landings are the CNSA Tianwen-1 'Zhurong' rover in May 2021, which was preceded just three months earlier by the NASA Mars2020 'Perseverance' rover and attached helicopter 'Ingenuity'. These new missions join the NASA Mars Science Laboratory (MSL) 'Curiosity' rover, active since

2012, and the stationary 'InSight' lander, active since 2018. The concurrence of four missions on the surface of Mars is unprecedented, and heralds a new era of Mars exploration, affording greater opportunities to compare and contrast observations at different points on the surface.

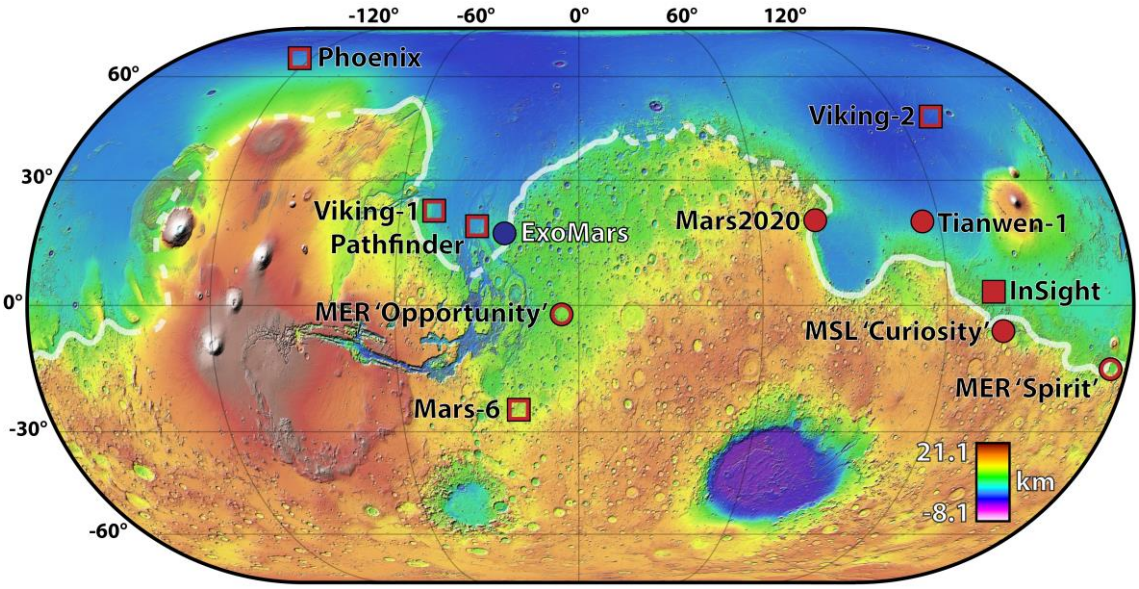

Figure 1.3 *- Global map of past, present, and future surface missions to Mars in relation to planetary dichotomy (white line), showing: active (red squares) and inactive (open red squares) stationary landers, active (red circles) and inactive (open red circles) rovers, and planned rover landing sites (blue circles). (MOLA topography and hill-shade)*

The landing sites for the 'Curiosity' and 'Perseverance' rovers were chosen as locations to study past aqueous processes (Milliken, Grotzinger et al. 2010, Goudge, Mustard et al. 2015), and both display evidence of probable palaeolakes in Gale crater and Jezero crater respectively, situated adjacent to the planetary dichotomy (see Section 1.1.3). The next planned landing is the ESA and Roscosmos ExoMars 'Rosalind Franklin' rover, which is due to land in Oxia Planum, within ancient aged terrains on the lowland side of the planetary dichotomy near a large sedimentary fan at the end of the Coogoon Valles valley network (Quantin, Carter et al. 2016). The primary mission objective is to drill into ancient phyllosilicate rocks formed in an aqueous environment, and examine the samples for the presence of biosignatures (Vago, Westall et al. 2017).

The focus and scope of Mars research has necessarily evolved along with observation and exploration of the planet. Early investigations were limited to the large

scale regional and global features resolvable with low-resolution imagery, but the current availability of high-resolution and dense data coverage from a range of observation methods now allows detailed studies on a local scale. The planned concurrence of three rover missions investigating hydrological processes at the planetary dichotomy presents an opportunity to contrast local investigations. With observations providing the basis to better understand hydrology at the dichotomy, the ancient climate, and by extension, possible habitable environments. More generally, integrating local scale studies into broader regional and global theories and models has the potential to once again revolutionise the understanding of Mars' past.

1.1.2 CLIMATE AND HYDROLOGY

Studies of geomorphology and mineralogy are in a broad consensus that Mars once experienced warmer and wetter climatic periods (Kite 2019), however, there is still much uncertainty as to: (1) how long conditions persisted, (2) the global or regional constraints on climatic and atmospheric conditions, and (3) what drove hydrological cycles at regional and global scales. The end members characterising ancient climate and hydrology on Mars are generally considered as either 'cold and dry' or 'warm and wet'.

In a cold and dry interpretation of ancient Mars, the climate is considered to have remained relatively consistent throughout the history of the planet, broadly reflecting the current surface conditions. In this scenario, landforms apparently formed by the action or presence of liquid water are often interpreted as being constrained to either limited time periods, or localised environments and processes. Geologically brief periods of warming and hydrological activity, on either global or regional scales, could have resulted from large bolide impacts (Wordsworth 2016), volcanic activity (Halevy and Head III 2014), or transient greenhouse warming (Wordsworth, Kalugina et al. 2017), and warmer conditions supporting liquid water could have persisted due to geothermal heating within isolated crater palaeolakes (Abramov and Kring 2005, Osinski, Tornabene et al. 2013). Alternatively, putative aqueous features may be accounted for by non-aqueous processes, such as: valleys carved by flowing lava (Leverington 2004), or ice (Ramsdale 2017), rather

than fluvial networks or outflow channels; aqueous mineralogy formed by sub-surface alteration processes (Carter, Poulet et al. 2010), rather than surface alteration, erosion, and deposition; or fluvial and lacustrine systems formed under extensive ice sheets spanning the highlands (Baker, Strom et al. 1991, Palumbo, Head et al. 2018).

A warm and wet interpretation of ancient Mars may be better classified as semi-arid, as the availability of water was likely limited even in the warmest models of the ancient climate (Wordsworth 2016). In this scenario, the ancient climate of Mars may have been similar to that of Earth, with a global hydrological cycle driven by evaporation and precipitation under an atmosphere thick enough to support liquid water on the surface (Luo, Cang et al. 2017, Barker and Bhattacharya 2018). For as long as these conditions persisted (Carr 2000, Abe, Numaguti et al. 2005, Wordsworth 2016), a wide range of aqueous landforms were formed by fluvial, lacustrine, and even possible marine processes. However, warm conditions eventually gave way to the present climatic conditions on Mars, with climate change thought to have been driven by atmospheric loss, including much of the planets water. A major constraint on warm and wet models is the mechanism and pace of that change, with many climate models unable to account for the loss of a relatively thick atmosphere and water budget (Erkaev, Lammer et al. 2014, Jakosky, Slipski et al. 2017).

The true nature of the ancient martian climate likely lies somewhere between these extremes (Fairen 2010, Wilson, Howard et al. 2016). Considerable evidence does indicate localised controls on hydrological and aqueous processes, but the ubiquitous observation of fluvial features across the planet strongly suggests a past epoch with a global hydrological system and a warmer climate. Each collected observation and description of hydrological processes at regional and local scales adds to the understanding of the ancient global climate, and when considered across the planet tend to suggest at least some prolonged climatic periods characterised by warmer temperatures than the present, yet semi-arid rather than wet.

1.1.3 THE PLANETARY DICHOTOMY

When the Mariner and Viking Orbiters imaged the entire surface of Mars through the 1960s and 1970s, one of the most prominent features was the planetary dichotomy; a steep scarp encircling the planet (**Figure 1.2**), separating the rugged southern highlands from the smooth, flat northern lowlands (Watters, McGovern et al. 2007). The contrasting appearance of terrains on either side of the dichotomy is striking, and crater counting indicates vastly different ages for the surfaces. The southern highlands represent a rugged and uneven terrain that is heavily cratered and generally aged as Noachian to early Hesperian (Robbins, Hynek et al. 2013), and host the majority of features indicating the past presence of flowing water (Hynek, Beach et al. 2010). At the dichotomy, the majority of valley networks and outflow channels terminate, and to the north the smooth flat lowland plains cover a third of the planet (Smith, Zuber et al. 1999). The crust of the northern lowlands is thinner than in the highlands (Zuber 2001), and terrains beneath the current lowland plains are thought to represent a surface as ancient as the highlands, which were then resurfaced (Frey, Roark et al. 2002). Evidence suggests multiple phases of resurfacing from the Hesperian through the Amazonian, although the possible processes responsible for resurfacing vary widely, including : volcanic flows, or air-fall deposits; mud or other fluid flows flooding from outflow channels; or marine deposits on the floor of an ocean (Tanaka, Skinner et al. 2003).

The origins of the dichotomy itself are not certain, but possible formation mechanisms include an early massive impact event, or early crustal or mantle processes (Lenardic, Nimmo et al. 2004, Andrews-Hanna, Zuber et al. 2008, Marinova, Aharonson et al. 2008), and an early interpretation of the dichotomy was that it represented the margin of an ancient ocean occupying the northern lowlands (Carr, Baum et al. 1972, Parker, Schneeberger et al. 1986).

Exposure and preservation of the dichotomy varies greatly with location, with wide stretches presumed to be covered by volcanic deposits associated with the Tharsis volcanic province, and in Syrtis Major (Zuber, Solomon et al. 2000). Along the southern

and eastern margins of Chryse Planitia the dichotomy is breached in numerous locations by massive outflow channels (Ivanov and Head 2001), and in the north of Arabia Terra and Terra Sabaea, highland areas along the dichotomy are dissected by chaos terrains, and periglacial or glacial landforms (Head, Nahm et al. 2006). This leaves Terra Sirenum, Terra Cimmeria, and western Arabia Terra as the best regions to observe well preserved long stretches of the planetary dichotomy.

1.1.4 THE ARABIA TERRA REGION

Evidence of past aqueous processes has been observed in nearly every region of Mars, however, to build a comprehensive picture of past climate and hydrology requires evidence of interactions between hydrological processes. The region of Arabia Terra is uniquely situated for these types of observations, with evidence for diverse and numerous hydrological processes closely associated within localised areas. Furthermore, the boundaries of Arabia Terra are approximately defined by distinct changes in geology and the expression of hydrological features, thus allowing a consistent research area to be defined within clear boundaries (**Figure 1.4**).

The southwest extent of Arabia Terra is truncated by Ares Vallis, a large outflow channel which begins in the highlands and terminates in the lowland basin of Chryse Planitia (**Figure 1.4**). The channel is thought to have formed in the late Hesperian, incising through older Noachian highland terrains and dissecting the dichotomy (Pacifici, Komatsu et al. 2009). The regional boundary to the east and southeast is delineated by a break in slope which rises into the higher terrains of Terra Sabaea and Noachis Terra. The majority of valley networks in Terra Sabaea and Noachis Terra terminate at or near this break in slope at the edge of Arabia Terra. One theory posits that this represents the palaeoshoreline of a northern ocean (Edgett and Parker 1997, Clifford and Parker 2001, Fairen, Dohm et al. 2003, Ormo, Dohm et al. 2004). However, a more parsimonious explanation may be that this boundary represents a transition in preservation style from erosional to depositional features, as water flowing down steep slopes spread out entering the flatter plains of Arabia Terra (**Figure 1.5**). Supporting this interpretation is the

correlation of valley network terminations, with the onset of sinuous ridges and raised layered basin fill, interpreted as representing depositional fluvial and lacustrine features (Davis, Gupta et al. 2019).

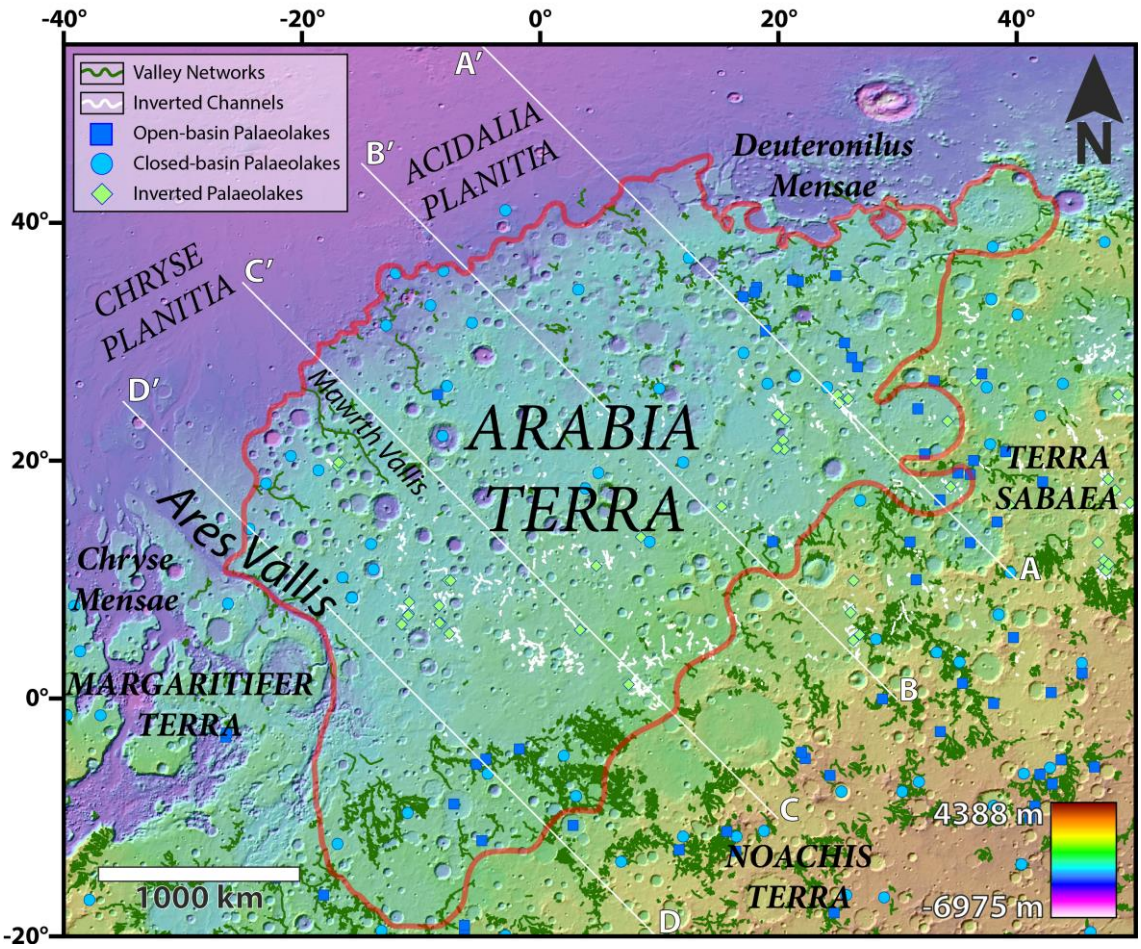

Figure 1.4 – Detailed map of Arabia Terra, showing the approximate boundaries of the region (red outline), and major terrains and features, including: valley networks (green lines)(Hynek, Beach et al. 2010), inverted channel networks (white lines)(Davis, Gupta et al. 2019), open-basin palaeolakes (dark-blue squares)(Goudge, Head et al. 2012), closed-basin palaeolakes (light-blue circles)(Goudge, Fassett et al. 2016), inverted palaeolake deposits (green diamonds)(Davis, Gupta et al. 2019). Location of topographic profile lines for (
Figure 1.5*) are indicated as A-A' – D-D'. (MOLA topography and hill-shade)*

Finally, the region is bounded to the north and west by the planetary dichotomy (**Figure 1.4**). The topographic expression of the dichotomy in Arabia Terra is ramped, presenting as a high, steep scarp in the north, with prominence decreasing southward to become a low, shallow slope at Ares Vallis (**Figure 1.5**). Incised valley networks, which are otherwise sparse throughout Arabia Terra are widespread nearer to the dichotomy, and nearly all terminate at the edge of the lowlands, some forming sedimentary fans (Di

Achille and Hynek 2010, Hynek, Beach et al. 2010). Much of the possible evidence for oceans in the northern lowlands has been identified near the dichotomy in Arabia Terra and Chryse Planitia (Carr and Head 2003, Rodriguez, Fairen et al. 2016, Ivanov, Erkeling et al. 2017), but the theory of an ocean remains difficult to reconcile with climate models and conflicting geological evidence (Wordsworth 2016). Towards the northern edge of Arabia Terra the dichotomy becomes less distinct in Deuteronilus Mensae, an area dissected by chaos terrain, chasms, mesas, and glacial valleys. The exact processes involved in these formations are not well understood, but appear to represent a later phase of modification that destroyed much of the dichotomy, including Protonilus Mensae and Nilosyrtis Mensae to the east.

Arabia Terra is also unusual in that it is situated within the Noachian aged southern highlands, but with a shallower slope and at an elevation significantly lower than most other highland terrains. This may account for the distinct expression of hydrological features in the region, and the apparent widespread occurrence of upwelling groundwater in western Arabia Terra (Andrews-Hanna, Zuber et al. 2010, Salese, Pondrelli et al. 2019). The region is sparsely represented in in global palaeolake catalogues (Goudge, Head et al. 2012, Goudge, Aureli et al. 2015), but high-resolution local scale studies near the dichotomy suggest complex hydrological systems and numerous palaeolakes (Wilson, Howard et al. 2016). Arabia Terra represents several distinct changes in hydrological features, transitioning with lowering elevation across the region, from: (1) a depositional setting characterised by inverted channels and palaeolake deposits; to (2) an area of ground water upwelling; and (3) an erosional setting characterised by palaeolake basins and valley networks; which (4) terminate at the planetary dichotomy, forming occasional sedimentary fans; and beyond (5) the flat, smooth lowland plains which exhibit few if any drainage features. The potential interplay of hydrological processes between all of these systems and localities has not been greatly studied, and a better understanding of this Arabia Terra could have important implications for the understanding of dichotomy settings elsewhere on Mars.

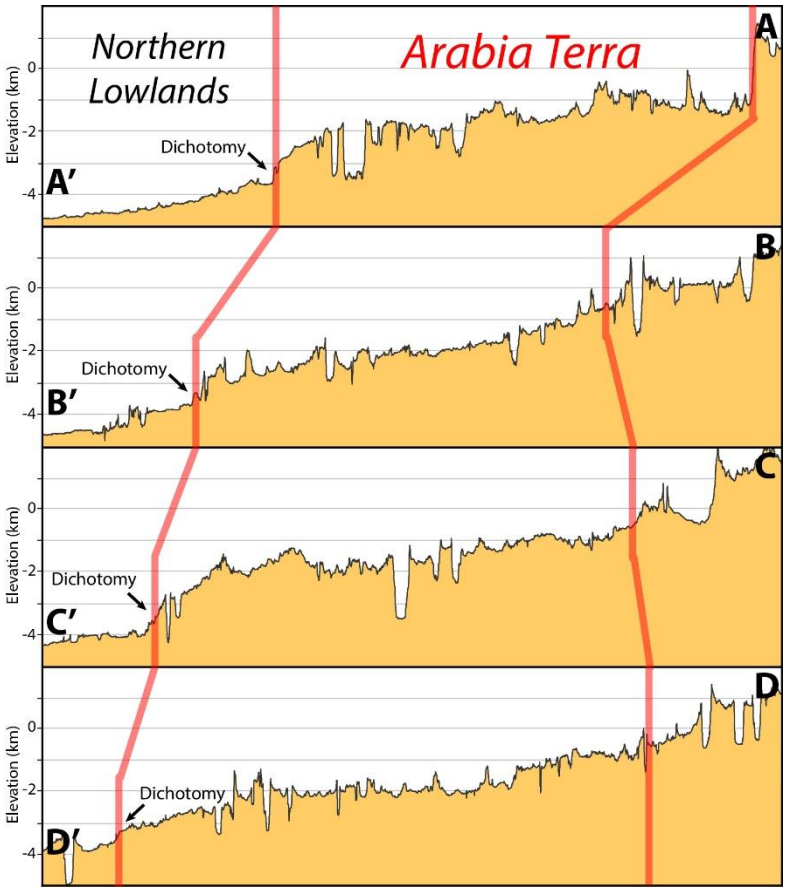

Figure 1.5 *– Topographic profiles of Arabia Terra (within red boundaries), arranged from north (A-A') to south (D-D'). The region is generally flat, and bounded by a break in slope to the eastward, and at the dichotomy to the west. However, the topographic prominence of the dichotomy is greater in the north, gradually reducing in prominence to the south. (MOLA topography data)*

1.2 RESEARCH OVERVIEW

1.2.1 AIMS AND OBJECTIVES

The broad goal of this thesis is to investigate the hydrological setting of the planetary dichotomy on Mars during the Noachian and Hesperian, and link high resolution local studies into regional and global trends in an effort to bridge the gaps between disparate scales. The specific aims of this research are twofold:

- To characterise the source to sink transport of water and sediment from fluvial and palaeolake systems in the highlands, to lowland basins and a possible ocean; and

- To integrate these findings into regional and global frameworks of hydrology and geology, and identify the implications for future exploration.

To achieve the aims of the thesis as stated above, the following objectives have been identified:

- To conduct a critical review of the evidence for palaeolakes and ancient oceans, identifying the most robust forms of morphological evidence and identification methods.

- To identify well preserved examples of highland drainage systems in Arabia Terra, which terminate at the planetary dichotomy, and produce high-resolution topographic data for these local areas.

- To produce detailed geomorphological studies of two dichotomy terminating drainage systems, using high-resolution topographic data, with a focus on defining sequences of palaeolake filling and drainage, and the veracity of palaeolake identification methods.

- To catalogue fluvial and lacustrine landforms across the wider region of western Arabia Terra indicated as a possible upland catchment for the northern lowlands basin, at the same level of resolution employed in the local studies.

- To characterise the dominant hydrological trends and reconstruct the ancient environment in Arabia Terra, and the planetary dichotomy in general, by producing drainage catchments supported by morphological observations.

1.2.2 METHODOLOGY

The objectives of this thesis were approached with remote sensing techniques applied to Mars orbital data, primarily by the observation and description of morphological forms on visual imagery and topography data. Geomorphology is the study of planetary surfaces, based primarily on interpretations of topography and form, to define the processes and conditions leading to the formation of a landform. This is

often achieved by comparing the morphology of a poorly understood landform to better understood analogues formed by known processes. However, a consideration of the limitations of these methods is important, and the particularities of Mars research present unique challenges.

Uniformitarianism is a fundamental principle of terrestrial geology and geomorphology which asserts that: processes which are currently observed to modify the surface of a planet are essentially the same as in previous geological eras. The implication is that unobservable past processes can be implied by the study of present day analogues. This principle is consistent with the majority of geological features on Earth, but some ancient landforms appear to be the result of processes with no modern analogue. The conditions and processes presently dominant on the surface of Mars are significantly different from those active in the distant past, and analogous examples may not exist in the history of the Earth. Therefore, care must be taken employing uniformitarianism even on the Earth, and on Mars, there are definite limitations to the use of terrestrial analogues.

A potential limitation of remote sensing in general is convergence of form, with features displaying similar morphological characteristics resulting from diverse processes. On Earth, findings of remote sensing are often tested and corroborated by in-situ observations, and in a similar way, data collected by landed Mars missions are invaluable to the understanding of Mars from orbit. However, the disconnected and narrow spatial coverage of data collected on the surface of Mars is selective, and the region of Arabia Terra has yet to be visited by surface missions. In the absence of in-situ observations, topographic and visual data are considered in conjunction wherever possible, and interpretations and findings are framed as to be tested by future landed missions, or improved observation techniques.

1.3 THESIS STRUCTURE

This thesis contains eight chapters: three chapters set up the motivation, background, and methods employed; three chapters comprise original research aimed at

discrete parts of a common objective; and a final chapter summarising the research results. Chapter 1 serves as a brief background and introduction to Mars research, sufficient to place the aims and objectives of this thesis into the context of Mars hydrology, the planetary dichotomy, and Arabia Terra. Chapter 2 presents a review of literature covering lakes, palaeolakes, and oceans on Earth and Mars, as well as the current paradigm on martian hydrology. Chapter 3 provides a summary of the spacecraft, instruments, and data utilised in this research, and a breakdown of the methods and analysis applied in this thesis. The next three chapters (4, 5 and 6) constitute the application, results, and interpretation of the original research conducted to meet the aims and objectives outlined above. Chapter 4 is a detailed study of a newly discovered system of palaeolakes terminating at the planetary dichotomy. Chapter 5 is a detailed study of palaeolakes in the drainage catchment of Oxia Planum, the landing site of the ExoMars rover. Chapter 6 presents a catalogue of palaeolakes and fluvial landforms covering a broader area of western Arabia Terra, including the planetary dichotomy and the areas discussed in Chapters 4 and 5. The catalogue applies the methods employed in Chapters 4 and 5, and provides a dataset and areal coverage large enough for the distribution and characterisation of lacustrine and fluvial features to be analysed in relation to global studies. Chapter 8 is a synthesis of results from the research chapters (4, 5 and 6), with a discussion of the methods employed, and how these findings concur and contrast with existing understandings of ancient martian hydrological systems. Final conclusions reached by this thesis are presented, and proposals for future studies and analysis to build on these findings, with a focus on current and future surface missions.

2

Water Bodies on Earth and Mars

2.1 Overview

Evidence for lakes and oceans is observed on a number of planetary bodies in the solar system, however, this broad statement is subject to significant caveats. Oceans of liquid water are thought to exist in the outer solar system, on Europa and Enceladus, moons of Jupiter and Saturn respectively. However, with no atmosphere, these oceans are trapped beneath kilometres of ice, only breaching the surface to ejecta vapour into space, and resurface parts of the moons' icy shells. Similarly, Titan, another moon of Saturn, has open lakes of liquid hydrocarbons, supported under a thick, but incredibly cold atmosphere. Given past and present solar radiation flux, evidence of uncovered, open bodies of liquid water are restricted to the inner solar system, within the ice-line. Venus and Mars, display evidence of large waterbodies in the ancient past, but only the Earth has oceans and lakes which have remained a constant feature to the present.

In this chapter, the nature of lakes on Earth is discussed in the context of distribution and landscape evolution, with a particular focus on evidence of terrestrial palaeolakes and observations made by remote sensing (**Section 2.2**). Evidence for palaeolakes on Mars and methods of palaeolake identification are considered, with a focus on the most robust forms of evidence (**Section 2.3**). Possible oceans on Mars, although contentious, are considered here as an extension of many of the same lines of evidence as palaeolakes, and are discussed in relation to the planetary dichotomy (**Section 2.4**).

Finally, palaeolakes and possible oceans are placed into the broader context of martian hydrology, including a summary of outstanding questions (**Section 2.5**).

2.2 TERRESTRIAL LAKES AND PALAEOLAKES

Present bodies of liquid water, open to the atmosphere, are a feature unique to the Earth within the solar system. The majority of surface waters on Earth are contained within the World Ocean, with a relatively small fraction held within lakes. However, lakes contain large volumes of the fresh water on Earth, and are important to interactions between the hydrosphere and lithosphere. The global distribution and characterisation of palaeolakes reveals broad trends in the hydrology of Earth, related to: topography, surface age, and precipitation (**Figure 2.1**).

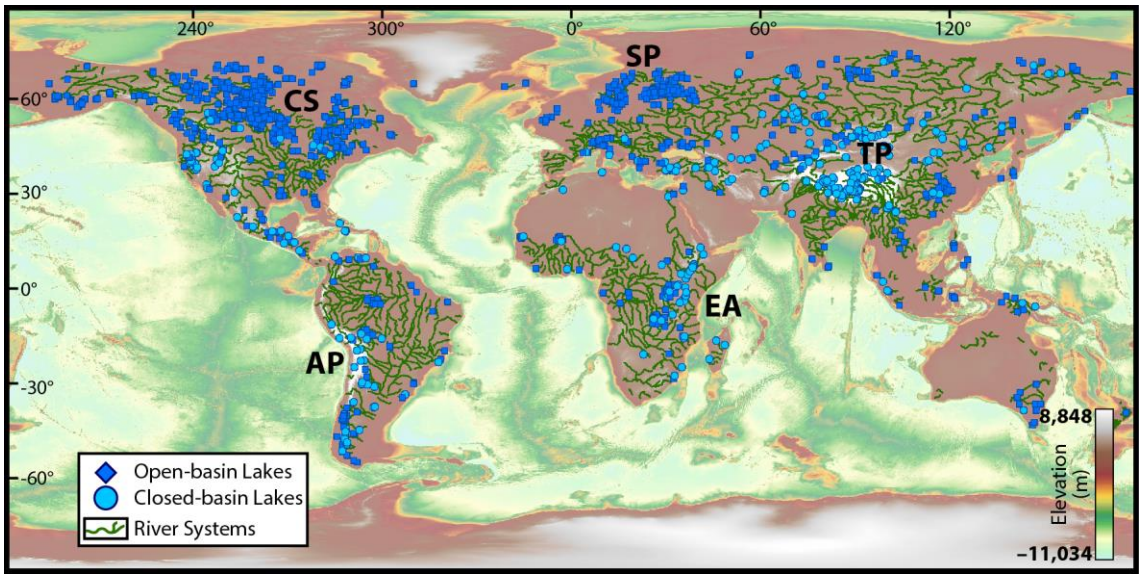

Figure 2.1 *– Map of the distribution of major river systems, open-basin, and closed-basin lakes on Earth, shown on a topography and bathymetry base-map. Regions are indicated which are characteristic of lake and river distributions, including: numerous open-basin lakes in the post-glacial landscapes of the Canadian Shield (CS) and Scandinavian Peninsula (SP); concentrations of closed-basin lakes in the upraised regions of the Andes Plateau (AP) and Tibetan Plateau (TP); as well as closed-basin lakes associated with the spreading region of the East African rift system (EA). River data obtained from Natural Earth (naturalearthdata.com), lake data obtained from Global Lakes and Wetlands Database (GLWD; https://www.worldwildlife.org/pages/global-lakes-and-wetlands-database)(Lehner and Döll 2004), with topography and bathymetry from ETOP1 1 Arc-Minute Global Relief Model (Amante and Eakins 2009).*

The broadest division within palaeolake populations is between open-basin and closed-basin types, with each group defined by a distinctive set of hydrological,

topographic, and ecological characteristics. Open-basin lakes are defined as being open basins, with an outlet which drains water from the lake, and are therefore typically fresh water. The distribution of open-basin palaeolakes is concentrated within impermeable bedrock terrains such as the Canadian Shield of northern North America or in on the Scandinavian Peninsula (**Figure 2.1**), where the geologically recent (~10 Ka) retreat of ice sheets has left an uneven surface with numerous local basins (Wolfe, Morse et al. 2017). Open-basin lakes constitute some of the largest lakes in the world, such the deep tectonic basin of Lake Baikal, and often forming cascading chains, such as the Great Lakes regions of North America or East Africa, where outlets and drainage from higher lakes goes on to become inlets feeding into lower lakes (Lehner and Döll 2004).

In contrast, closed-basin lakes are defined as endorheic basins with no surface outlets, and therefore these lakes become concentrated with dissolved minerals and salts, often forming hyper-saline environments far more saline than the World Ocean. Closed-basin lakes are common primarily in regions strongly controlled by tectonic processes, creating high drainage divides which isolate lake basins from integration with wider hydrological systems, such as the high plateaus of the Andes or Himalayas mountain ranges, or low rifting centres such as the Red Sea (**Figure 2.1**). Additionally, closed-basin lakes are found in arid regions where limited precipitation and accumulation of surface water are insufficient to fill a basin to the point of overspill, such as Lake Chad in central Africa.

Individual lakes on Earth represent relatively short-lived geological features, with lake basins eventually drained by progressive erosion of lake outlets, filled by sediment, or isolated by regional shifts in topography and tectonic processes. Therefore, for a lake to persist in a basin over geological time periods, generally requires a progressively deepening basin, such as the tectonically controlled basin of Lake Baikal (Brink and Taylor 2002), or closed-basin lakes within the East African Rift system (Cohen, Soreghan et al. 1993).

In addition to extant lakes, there are numerous examples of palaeolakes on Earth. In many instances, terrestrial palaeolakes are found within endorheic basins, with residual closed-basin lakes still extant at the deepest point. An example of this relationship in North America is the present closed-basin Great Salt Lake residing within the limits of Palaeolake Bonneville (Oviatt 1997, Lehner and Döll 2004). Evidence for palaeolakes on Earth is often found in the form of strandlines, wave-cut platforms, delta deposits, and evaporitic mineral deposits (White, McLaren et al. 2000, Drake and Bristow 2006).

In a similar vein, the ancient margins of oceans and seas on Earth are represented by palaeoshorelines. Unlike palaeolakes, which are situated on continental crust, the majority of the areas covered by oceans and seas are within the global oceanic basins over oceanic crust, and as Earth has retained its oceans since geological antiquity, oceans have always existed within these basins. There are therefore no true palaeo-oceans on Earth, but the past margins of Earth's extant oceans are located and preserved on some parts of the continental crust. Ocean palaeoshorelines, like the present ocean shorelines on Earth, are concentrated near continental margins. However, there are many examples of wide areas of continental crust on-lapped by past and present oceans, particularly at tectonic plate passive margins. Present examples include Hudson's Bay, the margin of the Arctic Ocean, the North American eastern seaboard, and the Australasian archipelago. A notable palaeoshoreline on continental crust is the Western Interior Seaway of North America which existed during the Cretaceous (~113-66 Ma), linking the Gulf of Mexico to the Arctic Ocean, with ocean floor deposits and palaeoshorelines observed across the present interior of the continent (Kauffman 1985, Chang and Liu 2021). Similarly, the Paratethys Sea in central Asia was isolated from the world ocean ~28 Ma, eventually shrinking to become the present Aral Sea and Caspian Sea (Rögl 1999, Popov, Shcherba et al. 2006).

Perhaps the nearest example to a palaeo-ocean in the history of the Earth existed briefly within the Mediterranean oceanic basin between 5.96 Ma and 5.33 Ma, a period known as the Messinian salinity crisis (Gautier, Clauzon et al. 1994, Krijgsman, Garcés et al. 1996). Isostatic sea-level fall resulted in isolation of the Mediterranean basin from the

wider global ocean, leading to a significant fall in base-level as runoff from local drainage basins was insufficient to offset evaporation. The gradual desiccation of this large saline water body resulted in the formation of extensive concentric evaporitic deposits, with distinct mineral assemblages marking progressively lower high-stands as the salinity of the residual water body increased. The eventual rise of global sea level caused a breach and rapid flooding of the basin, but the evaporitic deposits remain as a record the past lower levels.

2.3 PALAEOLAKES ON MARS

Hundreds of palaeolakes on Mars have been identified across a the southern highlands of Mars (**Figure 2.2**), and similar to palaeolake classifications on Earth, global catalogues of palaeolakes are considered separately as open-basin (Fassett and Head 2008, Goudge, Head et al. 2012), or closed-basin (Goudge, Aureli et al. 2015). The distribution of both palaeolakes and valley networks is almost entirely limited to highlands terrains, and even within the highlands there exist regional differences. At polar latitudes below 60°S, icy glacial and periglacial landscapes dominate the surface, obscuring any fluvial or lacustrine features which may have once existed there, and the Tharsis volcanic province similarly devoid of these features.

The identification of palaeolakes on Mars is primarily achieved by analysis of the relationships between valleys and topographic basins (Mangold and Ansan 2006, Fassett and Head 2008, Goudge and Fassett 2018), with open-basin palaeolakes identified where valleys are headed at the edges of basins, and closed-basin palaeolakes identified where valleys terminate within basins (Goudge, Aureli et al. 2015). In addition, the identification of deltas (Mangold and Howard 2013, Goudge, Mustard et al. 2015, Rivera-Hernández and Palucis 2019, Salese, Kleinhans et al. 2020), layered palaeolakes deposits (Goudge, Head et al. 2012), and possible shorelines (Di Achille, Hynek et al. 2009, Irwin and Zimbelman 2012), have all been considered in palaeolake identification.

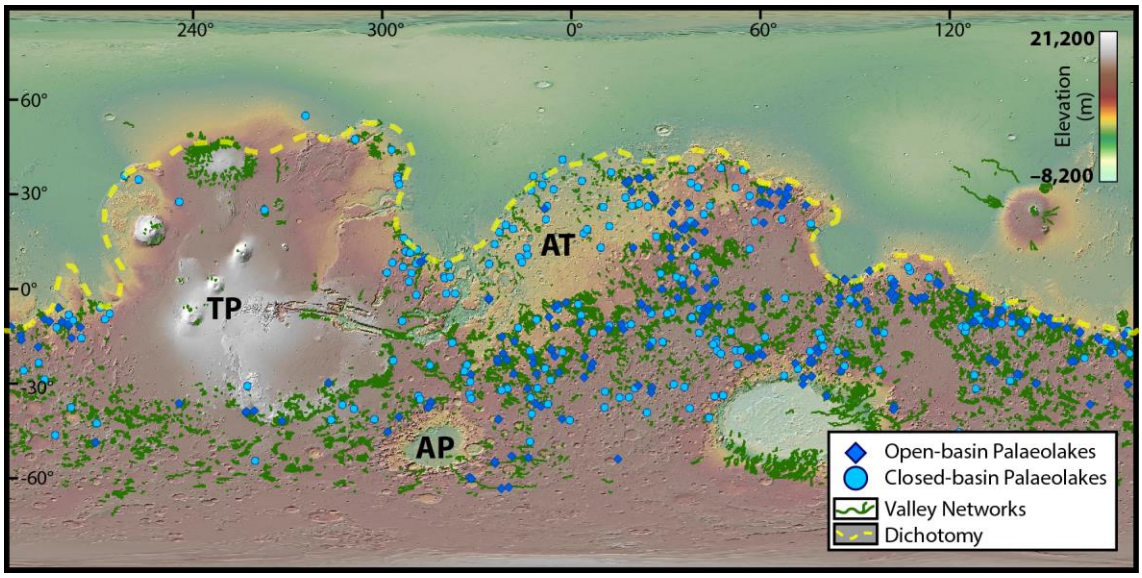

Figure 2.2 *– Map of the distribution of valley networks, open-basin and closed-basin palaeolakes on Mars. Regions of interest are indicated, including: Arabia Terra (AT) which hosts comparatively few open-basin palaeolakes, but numerous closed-basin palaeolakes; the Tharsis Volcanic province (TP) which accounts for a significant area of the highlands, but few fluvial or lacustrine features due to subsequent coverage by volcanic deposits; and Argyre Planitia (AP) which may represent the largest and deepest possible open-basin palaeolake on Mars.*

In addition to global catalogues, many regional studies have been undertaken, along with studies of individual palaeolakes and palaeolake systems. The outcomes of these detailed investigations often reveal far greater numbers of palaeolakes than global catalogues of the same areas (Wilson, Howard et al. 2016, Fawdon, Balme et al. 2021), but the particularities of local areas and differing methods of palaeolake identification often mean that results are difficult to compare between regions. Local investigations also present the opportunity to define detailed hydrological histories and lacustrine processes (Mangold and Ansan 2006, Goudge and Fassett 2018).

The most detailed investigations of palaeolakes on Mars are being undertaken by: the MSL 'Curiosity' rover in Gale Crater, identified as a closed-basin palaeolake; and the Mars2020 'Perseverance' rover in the Jezero Crater, identified as an open-basin palaeolake. The majority of data utilised for this work is from orbital observations, but the data and publications resulting from these missions offer in-situ observations of possible lacustrine and shoreline features, which are normally limited to investigation by remote sensing. The selection of Gale crater as a landing site was determined on the basis of aqueous mineralogy, apparently recording a transition from wet to arid conditions in

the region, and since landing, the mission has identified a detailed sequence of lacustrine processes as it climbs from the basin floor (Milliken, Grotzinger et al. 2010, Grotzinger, Gupta et al. 2015, Horvath and Andrews-Hanna 2017, Rapin, Chauviré et al. 2018). Jezero was identified as a palaeolake based on an outlet valley ultimately draining to the lowlands, and two inlet valleys beginning in the highlands, one of which terminates at a large sedimentary fan thought to be a delta (Goudge, Mustard et al. 2015, Kirk, Fergason et al. 2020, Salese, Kleinhans et al. 2020). Additionally, there is evidence the putative delta hosts aqueous minerals (Tarnas, Mustard et al. 2019). Landed investigations within the Jezero palaeolake are still within the first year, but one of the main goals of the mission will be to collect samples along this transect, and cache them for collection by a future sample return mission. Meaning that some of the first samples to be returned from Mars may represent palaeolake sedimentary deposits.

2.4 ANCIENT OCEANS ON MARS

Astronomers first suggested oceanic bodies of water on Mars over two centuries ago (Herschel 1784, Schiaparelli 1882, Lowell 1895), and although extant oceans on Mars were later proven to be an impossibility (Leighton, Murray et al. 1965), detailed imagery in the mid-twentieth century led to new hypothesis on the existence of oceans on Mars in the distant past. Most theories indicate a martian ocean during the Noachian or Hesperian, hosted within the wide basin of the northern lowlands, with a shoreline near the dichotomy, (Di Achille and Hynek 2010, Werner, Tanaka et al. 2011). However, within this general template exist a range of formation mechanisms, timings and ocean extents, with theories broadly divided into one of four scenarios: (1) a single ocean that gradually receded; (2) multiple, temporally separated oceans; (3) a frozen ocean; or (4) that Mars never had a northern ocean.

(1) The theory of a single basin filling event followed by a decline in water level and extent (Baker, Strom et al. 1991, Di Achille and Hynek 2010), commonly begins with an ocean forming shortly after a solid planetary crust (Clifford and Parker 2001), contemporary to ocean genesis on Earth at ~4.4 Ga (Wilde, Valley et al. 2001). Proposed ocean retreat rates are poorly

constrained and range from oceans vanishing by the early Noachian (Di Achille and Hynek 2010) to persisting into the Hesperian and Amazonian (Fairen, Dohm et al. 2003).

(2) Multiple, temporally separate basin filling events could explain the geographic and topographic variations recorded for proposed shorelines at different elevations (Head, Hiesinger et al. 1999). In this scenario the ocean may have been removed by desiccation or freezing between individual high stands, evoking a climate alternating between cold/dry and warm/wet extremes possibly driven by impact or volcanic events (Baker 1999, Fairen, Dohm et al. 2003). There is a spatial and age correlation between the older ocean boundaries and the Noachian-Hesperian transition peak in valley network activity (Di Achille and Hynek 2010, Hynek, Beach et al. 2010, Luo, Cang et al. 2017), and similarly between the younger ocean boundaries and the later Hesperian peak in outflow channel activity (Dohm, Ferris et al. 2001, Ivanov and Head 2001, Kreslavsky and Head 2002).

(3) An ocean with a partially, periodically or permanently frozen surface would fit many models of the ancient martian climate (Fairen 2010, Wordsworth 2016), and could explain the observed paucity of some landforms and mineral assemblages that would be suppressed in a frozen ocean (Clifford and Parker 2001, Fairen, Dohm et al. 2003, Ghatan and Zimbelman 2006, Fairen, Davila et al. 2011). Landforms indicative of a frozen ocean (Barnhart, Tulaczyk et al. 2005) or ice-bergs (Woodworth-Lynas and Guigné 2003, Fairén, Davila et al. 2010) have been identified on Mars but remain disputed. A frozen ocean could also have become buried and remain as an ice sheet under the current lowland surface (Janhunen 2002, Barker and Bhattacharya 2018)

(4) The final scenario is that the northern lowlands of Mars never contained an ocean. A dry northern lowlands basin is generally supported by models of the ancient martian climate and water budget (Von Paris, Petau et al. 2015, Wordsworth 2016). Additionally, many landforms along the dichotomy and in the northern lowlands could be explained by non-marine processes (Malin and Edgett 1999, Carr and Head 2003).

2.4.1 GLOBAL PALAEOSHORELINES

In the three billion years since the Noachian and Hesperian (~4.1 – 3.0 Ga), the northern lowlands has undergone widespread modification and resurfacing, including: volcanic deposits, the formation of a latitude-dependent mantling material between 30-60° north that supresses topographic features up to hundreds of metres depth (Kreslavsky and Head 2002), and glacial and periglacial deposits north of 60° (Kreslavsky, Head et al. 2008). The northern lowlands are also a basin for windblown sand and dust, which can

effectively block spectral observations of the surface with even thin coverings (10 μm; (Johnson, Christensen et al. 2002). Therefore, identifying direct evidence of an ocean within the northern lowlands is difficult, and many investigations instead focus on landforms along the planetary dichotomy, the putative ocean margin.

Collections of disparate landforms near the dichotomy are often grouped into contiguous regional or global lineations known as palaeoshorelines. Mapped palaeoshorelines are concentrated along three major trends, from widest areal extent and highest elevation to smallest and lowest they are known as the: (1) "Meridiani" (Edgett and Parker 1997, Clifford and Parker 2001, Fairen, Dohm et al. 2003, Ormo, Dohm et al. 2004, Ruiz, Tejero et al. 2006); (2) "Arabia" (Parker, Saunders et al. 1989, Clifford and Parker 2001); and (3) "Deuteronilus" (Parker, Saunders et al. 1989, Parker, Gorsline et al. 1993, Clifford and Parker 2001). Martian palaeoshorelines are generally interpreted as representing distinct ocean high-stands, and therefore expected to conform to an equipotential surface. However, plotting longitudinal shoreline elevations reveals that although the "Deuteronilus" shorelines are a reasonable fit to equipotential surfaces in some areas, the "Meridiani" and "Arabia" shorelines display large deviations in elevation at local and global scales (Head, Kreslavsky et al. 1998, Head, Hiesinger et al. 1999, Hiesinger, Head III et al. 2000, Carr and Head 2003). The fit to an equipotential surface is improved for some palaeoshorelines if subdivided into shorter regional sections (Carr and Head 2003, Ivanov, Erkeling et al. 2017), with each segment reinterpreted as representing an individual high stand (Webb 2004, Ivanov, Erkeling et al. 2017), and local scale deviations may be the result of multiple minor factors, including: imprecise placement of palaeoshorelines on low resolution images; and topographic changes due to volcanism, aeolian erosion, mass wasting, and impact cratering.

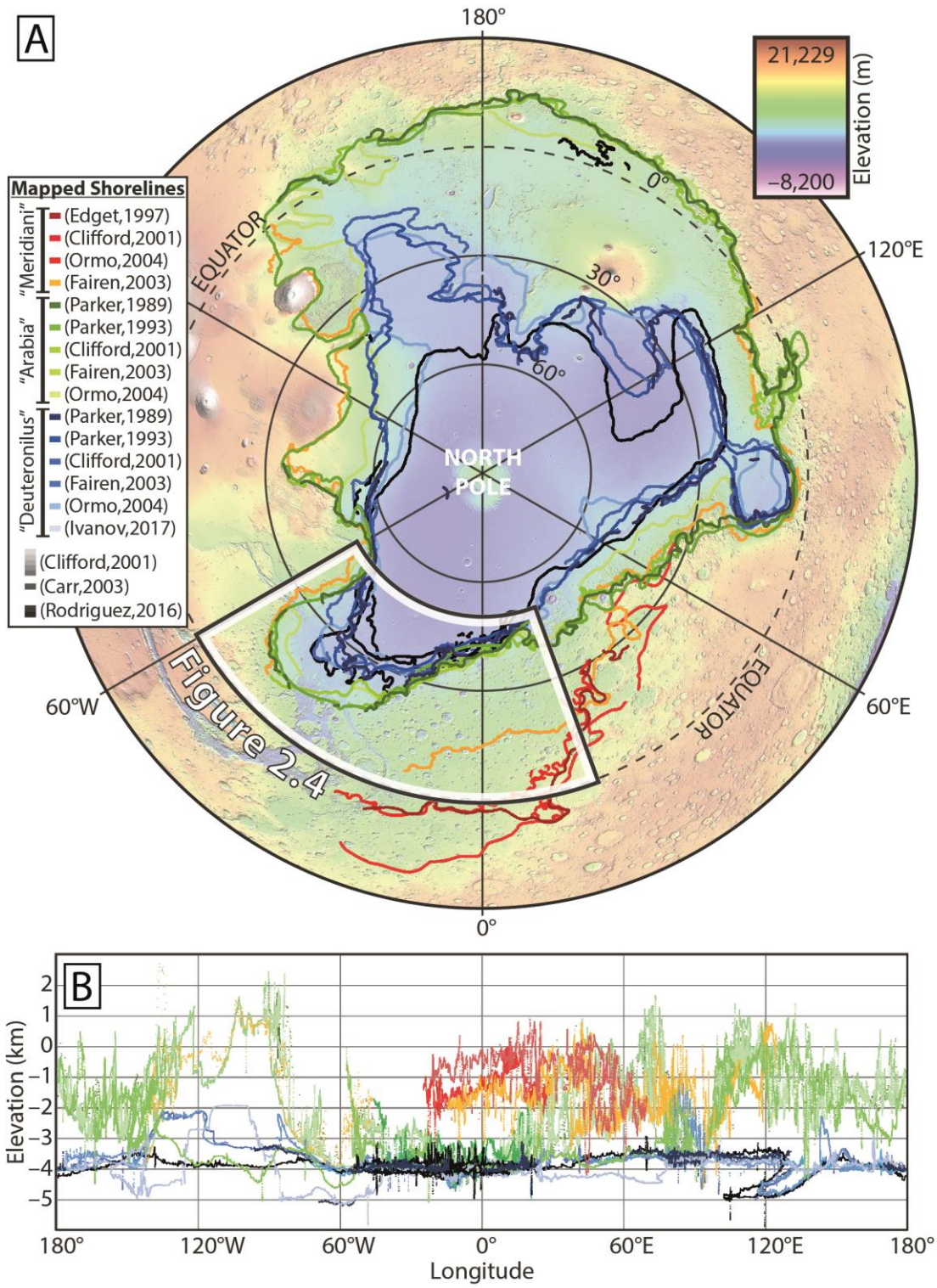

Figure 2.3 *- (a) Possible shorelines mapped from 1989 to 2017 compiled on polar centred MOLA topography (Azimuthal equidistant projection). Coloured lines indicate published shoreline names from highest and widest extent to smallest and lowest as the "Meridiani" (reds), "Meridiani/Arabia" (orange), "Arabia" (greens), "Deuteronilus" (blues), and other unnamed shorelines (grey-scale). The shorelines of isolated islands, seas and lakes have been omitted for clarity. (b) Plot of shoreline elevation against longitude illustrating the decent fit of long sections of "Deuteronilus" shorelines to a flat equipotential surface, and the significant local and regional deviations of the "Arabia" and "Meridiani" shorelines.*

Global scale deviations defy a simple explanation, but could be the result of topographic changes on a global scale, caused by: (1) isostasy following the emplacement of large volcanic provinces such as Tharsis and Elysium (Dohm, Ferris et al. 2001, Bouley, Baratoux et al. 2016, Citron, Manga et al. 2018), or the unloading of ice or liquid oceans (Hiesinger, Head III et al. 2000, Parker, Clifford et al. 2000, Webb 2004); or (2) warping of the martian geoid by true polar wander (TPW), as the rotational axis of Mars shifted to align the mass of Tharsis at the equator (Perron, Mitrovica et al. 2007, Bouley, Baratoux et al. 2016).

The poor fit of mapped palaeoshorelines to current equipotential surfaces raises doubts regarding the validity of these features when considered globally, and the numerous theories for topographic change tend to pose further questions. It has also been shown that the process of mapping and remapping of palaeoshorelines has resulted in significant variation in the positions of features that are ostensibly the same (Sholes, Dickeson et al. 2021). Interpreting the global boundaries of an ancient northern ocean are therefore problematic, and instead, mapped palaeoshorelines may be better considered as a general morphological trend, with the veracity of individual shoreline evidence investigated at local and regional scales.

2.4.2 OCEAN SHORELINE EVIDENCE

Parallel lineations and topographic steps are commonly observed features near the dichotomy and are sometimes interpreted as wave-cut platforms, benches or terraces (Parker, Saunders et al. 1989, Parker, Gorsline et al. 1993, Parker 1998, Webb 2004, Erkeling, Reiss et al. 2012, Świąder 2014, Sholes, Catling et al. 2017). Coastal process may explain the origin of these features in some localities where morphological observations best match terrestrial wave-cut platforms (Parker, Gorsline et al. 1993, Irwin and Zimbelman 2012), or where platforms are narrowly constrained by elevation over long distances (Webb 2004), however, the majority of these features are best described by other processes such as: debris aprons (Carr and Head 2003), or lithological layering exposed by differential erosion (Malin and Edgett 1999, Carr and Head 2003).

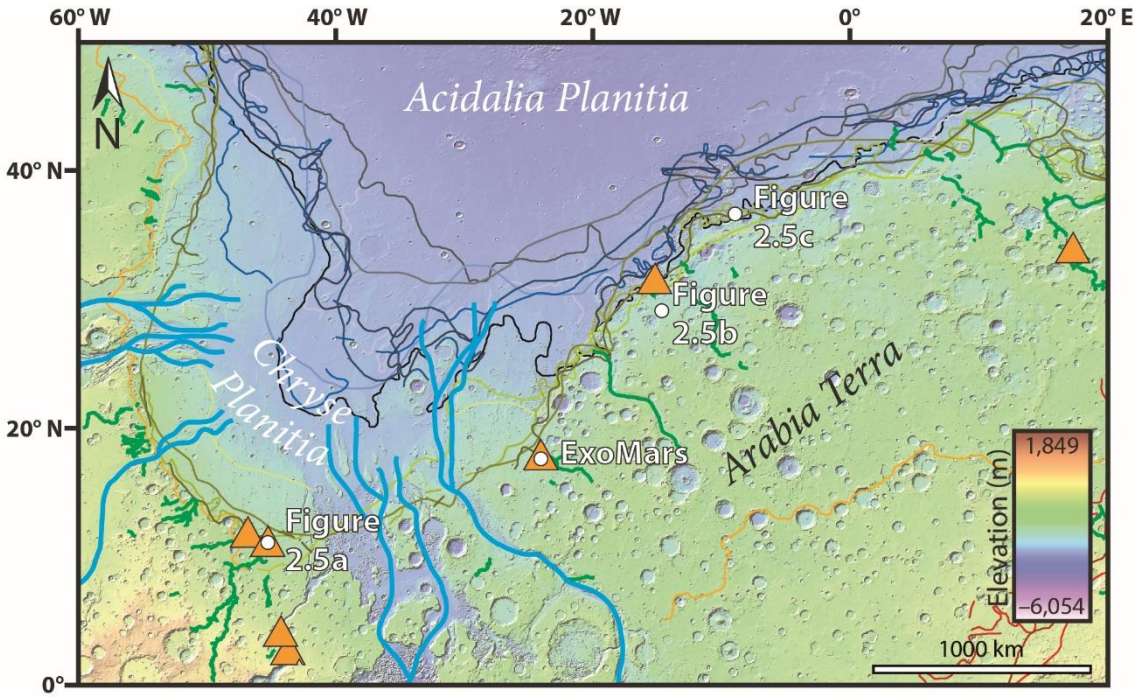

Figure 2.4 - Regional map displaying the flat, sparsely cratered lowlands of Chryse Planitia and Acidalia Planitia to the north and the rugged highlands of Arabia Terra to the south, with the scarp of the planetary dichotomy dividing the two where topographic colours transition from green to blue (MOLA topography). Terminations of valley networks (Carr 2000) and hydrologically open deltas (Di Achille and Hynek 2010, Quantin, Carter et al. 2016, Dickeson, Grindrod et al. 2018) are concentrated along "Arabia" shorelines, and the terminations of outflow channel terminations (blue lines) are closely associated with "Deuteronilus" shorelines. Marked sites of interest include the ExoMars rover landing site at Oxia Planum, and the locations of representative morphologies including: deltas (Fig.4a), platforms (Fig.4b), tsunami deposits (Fig.4c), polygonal terrain (Fig.5a), and 'ghost' craters (Fig.5b).

Just as terrestrial rivers terminate at sea level, the distribution of martian valley network terminations has been interpreted as recording the margins of an ancient sea level. Few valley networks are observed within the northern lowlands, and valley terminations are concentrated along the dichotomy at a narrow range of elevations near the "Arabia" shoreline (Di Achille and Hynek 2010, Hynek, Beach et al. 2010). In addition to valley terminations, many sediment fans at the dichotomy exhibit morphological and internal sediment structures consistent with deltas formed within standing bodies of water (Pondrelli, Rossi et al. 2008, DiBiase, Limaye et al. 2013). One example is the ~140 km long Hypanis delta, situated on the margins of Chryse Planitia at the terminus of a 10^5 km^2 catchment area, roughly equivalent to the Colorado River, which exhibits prograding channel and lobe structures which may record the retreat of a large body of water (Fawdon, Gupta et al. 2018). The Hypanis delta, and other deltas along the dichotomy,

are concentrated close to elevations of the "Arabia" shorelines (Di Achille and Hynek 2010), suggesting formation at an equipotential surface along the margins of a single water body. However, investigated regionally, deltas may be more consistent with a series of large lakes or small seas, rather than a hemisphere-spanning ocean, as has been suggested for deltas along the dichotomy in the area of Gale crater (Rivera-Hernández and Palucis 2019).

Outflow channels also appear to have formed by flowing water on Mars, but with widths up to hundreds of kilometres, they are an order of magnitude greater than the widest martian valley networks or terrestrial fluvial systems. Outflow channels typically begin in areas of collapsed or chaos terrain rather than being fed by branching tributaries and wide drainage catchments, and are thought to have formed by catastrophic floods that peaked in activity during the middle-Hesperian and early-Amazonian. A fitting terrestrial analogue may be the Missoula floods in North America occurring between 12,000-15,000 years ago, which resulted from the breach of an ice dam (Baker and Milton 1974). Outflow channels were the first features identified as potential sources feeding an ancient northern ocean (Parker, Schneeberger et al. 1986, Head, Hiesinger et al. 1999, Carr and Head 2003, Ivanov, Hiesinger et al. 2014), and the distribution of outflow channel terminations and landforms correlates with "Deuteronilus" shorelines (Mouginot, Pommerol et al. 2012, Duran, Coulthard et al. 2019). However, flooding through outflow channels was likely sporadic or episodic (Fairen, Dohm et al. 2003), and coincides with a probable martian climate and atmosphere that were too cold and thin to sustain liquid water for prolonged periods (Kreslavsky and Head 2002), and therefore outflow channels may be poor candidates as sources of a sustained and stable liquid ocean, but may have instead formed: an ice sheet (Ivanov, Erkeling et al. 2017), sublimation residue (Kreslavsky and Head 2002), layers of water-ice rich sediments (Carr and Head 2003), or muds (Parker, Schneeberger et al. 1986).

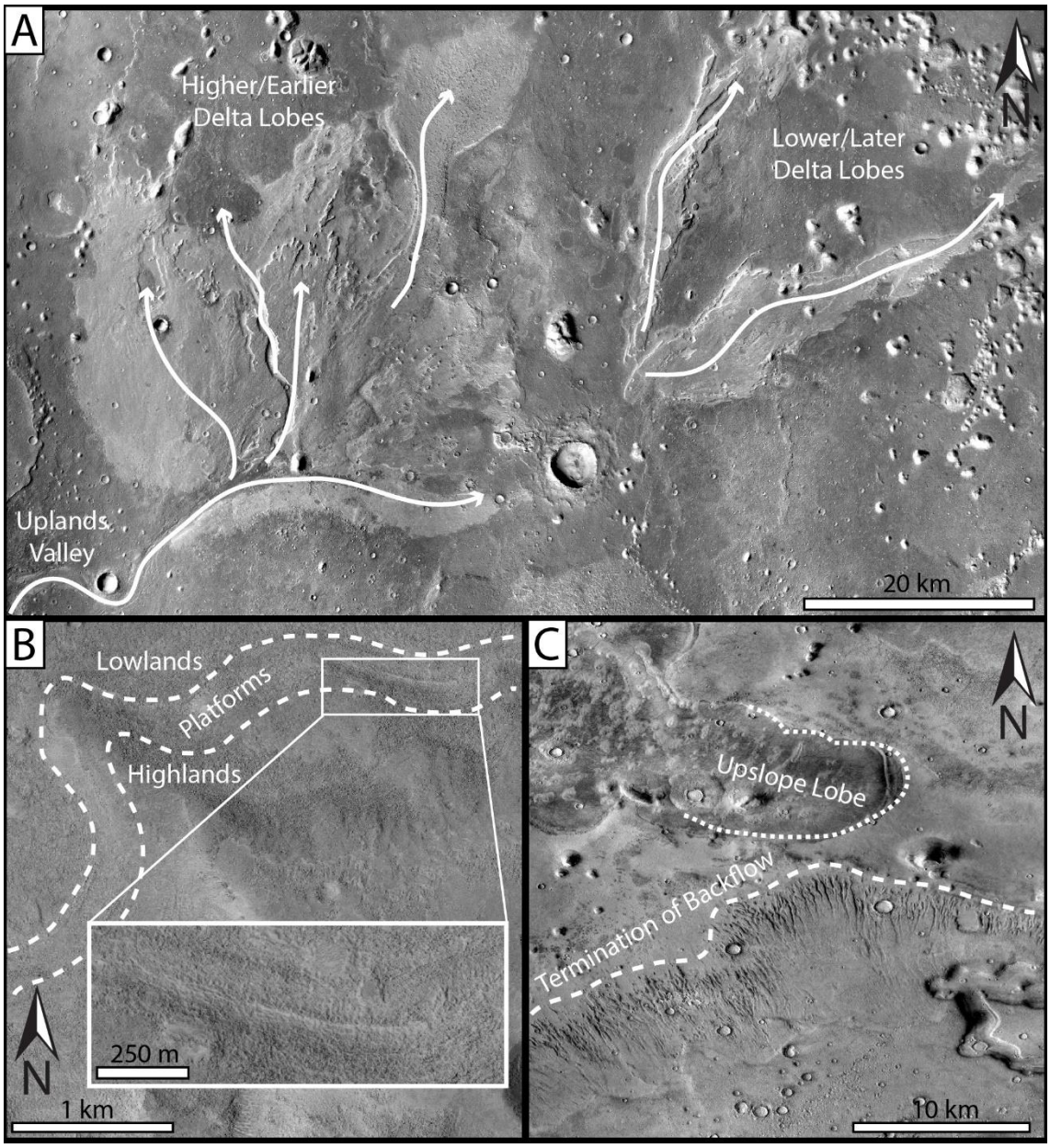

Figure 2.5 - Examples of possible coastal morphologies on Mars: **(a)** light toned deposits of the Hypanis delta at the end of an extensive valley network, with arrows indicating numerous branching lobes (CTX mosaic), **(b)** possible wave-cut platforms indicated between dashed lines on a scarp between the highlands and lowlands in western Arabia Terra, with detail inset (HiRISE), and **(c)** possible tsunami deposits in Deuteronilus Mensae including backflow channels ending at a common elevation (dashed line) and an upslope lobe of course material (dotted line) (CTX mosaic).

Possible palaeo-tsunami sequences have been identified in Chryse Planitia near the "Deuteronilus" shorelines (Rodriguez, Fairen et al. 2016), and are interpreted as resulting from two separate impact induced tsunamis occurring during the late Hesperian (3.61-3.37 Ga), with backflow channels of the higher tsunami deposits exploited by the lower and younger event, recording a ~200 m drop in sea level between events. The

"Arabia" and "Meridiani" shorelines would form the widest oceans, and the hypothesised timing of these oceans in the Noachian to early-Hesperian coincides with the high impact frequency of the late heavy bombardment (Frey 2008). Modelling of tsunami propagation based on the distribution of possible ocean impact craters (Matsui, Takamiya et al. 2001, Iijima, Goto et al. 2014, Costard, Sejourne et al. 2017) suggests that tsunami energy would be particularly focused on the "Arabia" shoreline and the planetary dichotomy (Mahaney, Dohm et al. 2010). The effect of impact tsunamis on shorelines could have been significant, and it is possible that the paucity of other martian shoreline landforms was the result of frequent tsunamis destroying coastal features such as terraces and deltas.

Evidence for a northern ocean on Mars has always relied on comparisons to terrestrial analogues, but with a different climate, gravity and system of moons, what is true of marine processes on Earth may not have been true for Mars. The current understanding of morphological and mineralogical evidence indicates waters of a different chemical composition to Earth, forming oceans unstable over geological time that may have experienced frequent impact induced mega-tsunamis; leading to the conclusion that if Mars once had a body of water in its northern hemisphere it was unlike any ocean on Earth.

2.5 WATER BODIES AND THE MARTIAN CLIMATE

The past climate of Mars was markedly different than at the present, but the precise nature of the ancient climate is not yet known. The timing and pace of climate change from a planet with large bodies of water to the present cold, hyper-arid climate also has important implications for the loss of water to space or the lithosphere (Lammer, Lichtenegger et al. 2003), (Clifford and Parker 2001, Carr and Head 2015). Overall, morphological evidence indicates extensive ancient fluvial and lacustrine processes across the highlands, draining into the hemisphere-spanning basin of the lowlands (**Figure 2.6**), which contained either palaeolakes or an ocean. Geomorphological evidence provides the means to place constraints on the past climate (Goudge, Fassett et al. 2016, Horvath and Andrews-Hanna 2017, Kite 2019), but a combination of work modelling the martian

climate, paired with constraints implied by geology and morphology will be necessary to answer these outstanding issues in the coming years (Kite 2019). The focus of this thesis is on evidence for palaeolakes in the martian rock record, but two principal climatic factors critical in supporting widespread palaeolakes or an ocean require consideration: (1) climatic and atmosphere constraints on the stability of liquid water; and (2) the ancient water budget and availability of near surface water. These concepts are addressed more extensively elsewhere (Wordsworth 2016), but area addressed here to highlight their importance to interpretations made in this thesis.

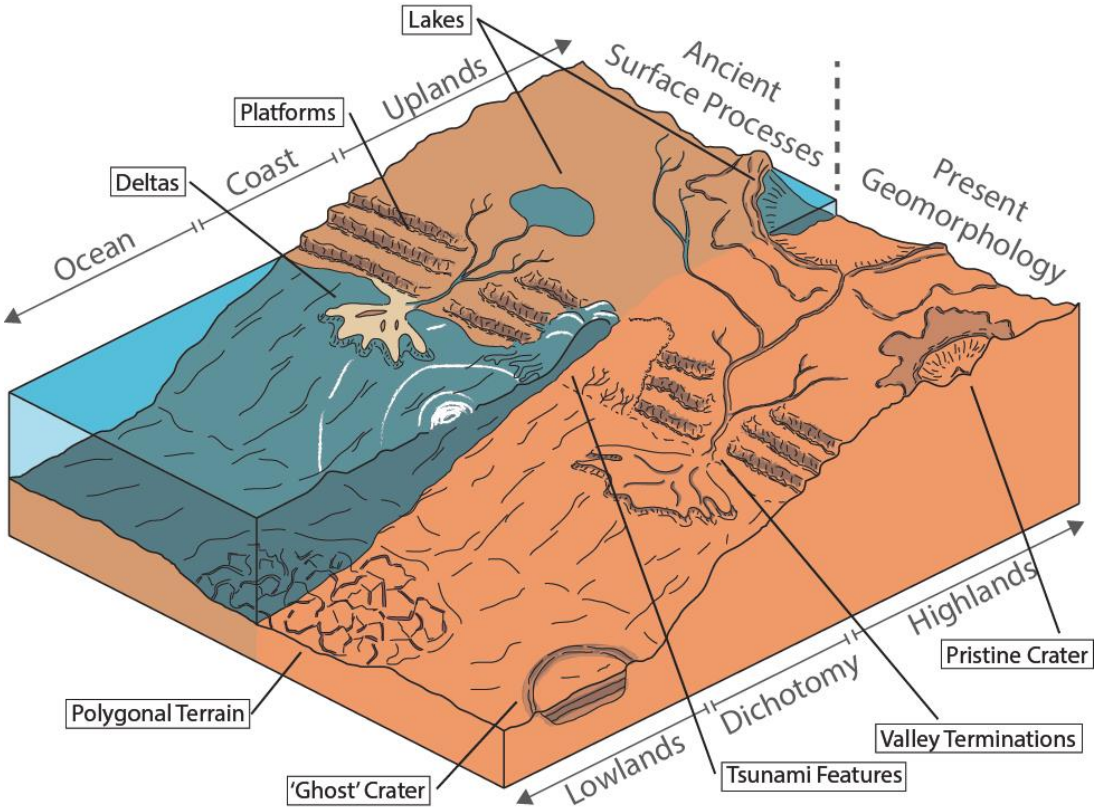

Figure 2.6 *- Schematic illustration showing the relative distribution of morphological evidence for oceans on the present surface of Mars (bottom right), and the possible ocean processes and environments existing on the surface during the Noachian (top left). Evidence can be followed from highland fluvial and lacustrine features indicating an active hydrological cycle, down to possible erosional platforms and deltas formed at the edge of a northern ocean, and still lower to filled craters and polygonal terrains occupying the deepest ocean floor settings.*

Models of the early martian climate generally assume a thick CO_2 atmosphere, producing a greenhouse effect (Pollack 1991), in association with other gases such as CH_4, SO_4 and H_2 (Wordsworth, Kalugina et al. 2017, Ramirez and Craddock 2018). Whilst an ancient, multi-bar CO_2 atmosphere is consistent with present atmospheric measurements

(Jakosky, Slipski et al. 2017), climate models produce conflicting results regarding the stability of liquid water for sustained periods (Ramirez and Craddock 2018), or limited to transient melting events (Forget, Wordsworth et al. 2013, Wordsworth, Forget et al. 2013, Halevy and Head III 2014, Wordsworth, Kalugina et al. 2017). High salinities could also allow for an active hydrological cycle with oceans or lakes at temperatures of at least ~245 K (Fairen 2010), but this is still warmer than many models predict.

The near-surface water inventory of Mars is often expressed as a global equivalent layer (GEL) spread across the entire planet. Values remain poorly constrained (~24 – 525 m GEL), and with major differences stemming from the method of calculation, including: water volumes required to carve valley networks (Rosenberg and Head III 2015, Luo, Cang et al. 2017), and outflow channels (Kereszturi 2012), water loss recorded by deuterium-to-hydrogen (D/H) ratio (137 m GEL; (Villanueva, Mumma et al. 2015), water ice in the northern lowlands (Oberbeck 2009), and the summation of water from near surface sources and sinks (~24 m GEL; (Carr and Head 2015). An ocean fitting the palaeoshorelines near the dichotomy would require volumes of water (130 – 599 m GEL; (Carr and Head 2003) far greater than is estimated to currently exist as ice on Mars (21 – 34 m GEL; (Carr and Head 2003, Villanueva, Mumma et al. 2015) and greater than many water inventories described above. In contrast, extensive coverage of the ancient surface of Mars by palaeolakes requires a far lower water inventory than filling the northern lowlands. Present catalogues of open-basin and closed-basin palaeolakes on Mars represent coverage of ~1% (1,570,003 km^2) of the surface by palaeolakes (Fassett and Head 2008, Goudge, Aureli et al. 2015), with a total volume of 593,771 km^3. This represents a GEL of ~4 m, and although present catalogues at a global scale are not comprehensive, the volume of water required to fill a great number of palaeolakes on Mars simultaneously is within even the lowest limitations imposed by water-inventory models.

The northern lowlands was undoubtedly a hydrological basin, into which ancient rivers and outflow channels converged, and the global distribution of deltas and valley network terminations at an equipotential along the dichotomy is consistent with a former

water level. Yet, analysis of high resolution images and topographic datasets reveal a more nuanced picture. At the margins of Chryse Planitia, the morphology of the Hypanis delta records a receding water level into a topographically open basin, whereas in the Gale crater region, numerous deltas form into a number of sub-basins along the dichotomy, which are closed to the northern lowlands.

Martian valley networks record water-driven erosion and the flow paths of ancient rivers (Carr 1995, Hoke, Hynek et al. 2011). These systems have large catchment areas and branching tributary networks feeding into larger valleys, many of which converge on the planetary dichotomy. The peak period of valley network activity corresponds to the Noachian age of the "Arabia" and "Meridiani" shorelines (Hynek, Beach et al. 2010), and open-basin palaeolakes on Mars are commonly fed by extensive valley networks of the same age (Fassett and Head 2008, Goudge, Fassett et al. 2016). These correlations suggest that standing bodies of water on Mars are closely tied to fluvial processes. However, the immature nature of many networks compared to terrestrial analogues suggests that they were only active for 10^4-10^7 years (Hoke, Hynek et al. 2011), and therefore the window when all these hydrological features existed on Mars may have been very brief.

3

Data and Methods

3.1 Overview

Research for this thesis was conducted with orbital datasets, using established remote sensing methods of observation and interpretation. Landforms indicating past aqueous processes were analysed and interpreted largely with visual imagery, but to understand the wider hydrological setting and how water may have flowed across the surface required the use of topographic data. Topographic data is also central to confirming the veracity of morphological features identified on imagery, and allowed for quantitative assessments of features such as volumes, slopes, and comparative elevations.

In this section, the principal datasets used in this thesis are identified and compared (**Section 3.2**), with a general appraisal of imagery (**Section 3.2.1**) and topography (**Section 3.2.2**) data available within the study area, and an overview of the method used to produce high-resolution digital elevation models from stereo image data (**Section 3.2.2.1**). Also included are summaries of existing methods for coding and grading fluvial systems (**Section 3.3.1**), and methods of drainage catchment delineation on Earth and Mars (**Section 3.3.2**), both considered in the context of Mars research.

3.2 Orbital Instruments and Datasets

As of 2021, there are eight active spacecraft in Mars orbit, while numerous other orbiters, landers and rovers have visited the planet over the past fifty years. Each mission carries an array of scientific instruments and experiments, contributing to an ever

growing body of observations and data. The majority of Mars missions are run by the National Aeronautics and Space Agency (NASA), and the European Space Agency (ESA), but collaboration with smaller national space agencies and private industry is common, with many instruments on NASA and ESA spacecraft designed, built and run by partner organisations. The use of Mars data in academic research requires full attribution of the mission and instrument, and where applicable, citation of published results and technical specifications, and/or data processed by a third party.

New orbital data and imagery is acquired and released regularly, and typically made available for immediate public use, although some data is subject to a proprietary period before wider release. Datasets can be browsed, searched, and downloaded from a range of sources. In the first instance, data from the majority of NASA and ESA missions can be accessed via either: NASA's Mars Orbital Data Explorer (Mars ODE; https://ode.rsl.wustl.edu/mars/), hosted by the Planetary Data Service (PDS; https://pds-geosciences.wustl.edu/); or through ESA's Planetary Science Archive (PSA; https://archives.esac.esa.int/psa/). Alternatively, some instruments host data on bespoke browser services, such as: the High Resolution Imaging Science Experiment (HiRISE; https://www.uahirise.org/); the Compact Reconnaissance Imaging Spectrometer for Mars (CRISM; http://crism-map.jhuapl.edu/); or digital elevation models (DEMs) from the High Resolution Stereo Camera (HRSC; https://maps.planet.fu-berlin.de). Lastly, a variety of derived data products, interpreted maps, and mosaics can be accessed from third party sources, such as: the extensive collection hosted by the Astrogeology Science Center of the United States Geological Survey (USGS; https://www.usgs.gov/centers/astrogeology-science-center/data-tools); or the global imagery mosaics produced by Murray Labs at the California Institute of Technology (http://murray-lab.caltech.edu/CTX/). In addition to existing datasets, systems are in place for researchers to request the acquisition of new imagery and data on Mars. Notably, the High Resolution Imaging Experiment (HiRISE) has a system allowing members of the public to request new image acquisitions (HiWish; https://www.uahirise.org/hiwish/).

Searching and downloading data from the above sources, for a given area, is often a multistep process, involving: (1) downloading data footprints (eg. https://ode.rsl.wustl.edu/mars/coverage/ODE_Mars_shapefile.html), (2) browsing footprints on a GIS base-map, and (3) downloading the required data. This process is streamlined where online data browsers and interactive maps are available, and the search results of many sources can be narrowed with criteria such as location, acquisition date, and other data attributes. Global Mars data and image footprints can also be browsed with a number of third party software options, such as the desktop version of Google Earth Pro (https://www.google.com/earth/download/gep/agree.html?hl=en-GB).

Table 3.1 *– Selected orbital Mars instruments and technical specifications, representing the data most used in this thesis. Also included are the spacecraft on which these instruments are mounted. '*' Denotes end date of prime observations with CRISM, although reduced quality observations are still made to the present.*

Instrument	Spacecraft	Operational Life	Imagery/ Data Type	Spectral Range (nm)	Max. Footprint (km)	Max. Image Resolution (m/pixel)	Max. DEM Resolution (m/pixel)
CTX	MRO	2006 – Present	Visual (Greyscale)	500 – 800	30 x 300	6	~20
HiRISE	MRO	2006 – Present	Visual (Greyscale/ Colour)	400 – 1000	6 x 60	0.25	~1
CaSSIS	TGO	2018 – Present	Visual (Colour)	500 – 950	9.5 x 45	5	~20
THEMIS	ODY	2002 – Present	Visual (Greyscale)	425 – 860	18.4 x 52	18	-
			Thermal	6780 – 14880	32 x 52	100	
HRSC	MEX	2004 – Present	Visual (Colour)	360 – 1050	62 x 206	2.5-25	150-200
MOLA	MGS	1997 – 2001	Laser Altimeter	-	0.168 x 0.168	-	463
CRISM	MRO	2006 – 2009*	Hyperspectral	362 – 3920	8 x 10	18	-

Orbital image and data resolution are typically communicated as the spatial dimension of individual pixels on the surface, given as metres per pixel (m/pixel), which is a function of: (1) the instrument specific image size in pixels; and (2) the spatial area coverage on the planet surface. The image footprint and therefore, image resolution, are dependent on the altitude of the orbiting spacecraft, and although the majority of Mars spacecraft are in approximately circular orbits, even slightly elliptical orbits result in

variations in image resolution for a single instrument. Typically, objects and features which are at least four times the image resolution can be effectively resolved; for example, 0.25 m/pixel imagery allows resolution of surface features >1 m in width or diameter.

The combined data from various instruments covers a wide range of the electromagnetic spectrum, from visible light to hyperspectral, at resolutions of up to ~0.25 m/pixel, and with nearly the entire surface of Mars represented at ~6 m/pixel. In addition, a single laser altimeter instrument has produced a detailed topographic map of the surface. The full breadth of available data is rarely required in a single project, and the following is a brief summary of the orbital instruments and datasets most relevant to this work (**Table 3.1**):

(1) **Context Camera (CTX)** (Malin, Bell et al. 2007) – The CTX instrument is a greyscale, medium/high-resolution camera on the NASA Mars Reconnaissance Orbiter (MRO), capturing surface imagery at a resolution of ~6 m/pixel in swaths ~30 km wide and up to ~300 km long. The primary function of CTX is to collect data simultaneously with high-resolution and spectroscopic instruments in order to characterise the wider context, and is an invaluable resource for Mars research due to its spatial, temporal, and stereo coverage of the surface. Since 2006, CTX has covered ~95% of the planet's surface, with many repeat images suitable for the production of DEMs. Additionally, tiled mosaics of CTX imagery are available for the entire martian surface (Dickson, Kerber et al. 2018).

(2) **High Resolution Imaging Science Experiment (HiRISE)** (McEwen, Eliason et al. 2007) – The HiRISE instrument is a greyscale/colour, high-resolution camera also on board MRO, capturing surface imagery at a maximum resolution of ~0.25 m/pixel in swaths ~6 km wide and up to ~60 km long, with acquisition of colour images limited to a ~1km wide central strip. Since 2006, HiRISE has covered ~3% of the planet's surface, but with a resolution an order of magnitude greater than the next best imager it is invaluable for examining fine detail on the martian surface. Despite the limited spatial coverage there are a large number of stereo observations suitable for the production of DEMs.

(3) **Colour and Stereo Surface Imaging System (CaSSIS)** (Thomas, Cremonese et al. 2017) – The CaSSIS instrument is a colour, medium/high resolution camera on the ESA ExoMars Trace Gas Orbiter (TGO), capturing imagery at a resolution of ~5 m/pixel in swaths ~9.5 km wide and up to ~45 km long. However, resolution and image width are

somewhat variable due to a more elliptical orbit than most other orbiters. CaSSIS images are all captured in colour, and are suitable for hyperspectral analysis, and interpretations of surface composition and mineralogy. CaSSIS also has the capability to acquire stereo imagery in a single orbital pass by pivoting its camera 180°.

(4) **Thermal Emission Imaging System (THEMIS)** (Christensen, Jakosky et al. 2004)– The THEMIS instrument is a visual and infrared imager on the NASA Mars Odyssey (ODY) orbiter. Visual greyscale images are captured at ~18 m/pixel, and infrared imagery is captured at ~100 m/pixel. Infrared imagery is typically captured for the same locations during day and night conditions, and by subtraction of these two datasets thermal inertia data can be produced to give an indication of surface composition and density.

(5) **High Resolution Stereo Camera (HRSC)** (Neukum and Jaumann 2004) – The HRSC instrument is a colour, medium/high-resolution camera on the ESA Mars Express (MEX) orbiter, capturing images at up to ~2.5 m/pixel, however, resolutions of ~12.5-25 m/pixel are more common. HRSC has the capability to acquire stereo imagery in a single orbital pass, and DEM coverage at a resolution of ~150-200 m/pixel is available for much of the martian surface (Jaumann, Neukum et al. 2007).

(6) **Mars Orbiter Laser Altimeter (MOLA)** (Smith, Zuber et al. 2001) – The MOLA instrument was a laser altimeter on the NASA Mars Global Surveyor (MGS), which made elevation measurements of the martian surface between 1997 and 2001. Data was collected as long tracks of individual ~120 m diameter shot points, with ~30 cm vertical resolution, and spaced at ~300 m from shot centre to centre. These shot points allowed for the production of global topographic maps with a spatial resolution of ~463 m/pixel, and remain the only absolute measurements of elevation to which all other DEMs are tied.

(7) **Compact Reconnaissance Imaging Spectrometer for Mars (CRISM)** (Murchie, Arvidson et al. 2007) – The CRISM instrument is a spectrometer on the NASA Mars Reconnaissance Orbiter (MRO) spacecraft, acquiring images in the range of 362 – 3920 nm, with a spatial resolution of ~18 m/pixel in swaths ~10 km wide and long. Good quality data CRISM data acquired between 2006 and 2009 still offers the most reliable orbital spectroscopy of the surface, but observations made after this time are of limited use as coolant for the instrument was exhausted, resulting in significant noise in many wavelengths.

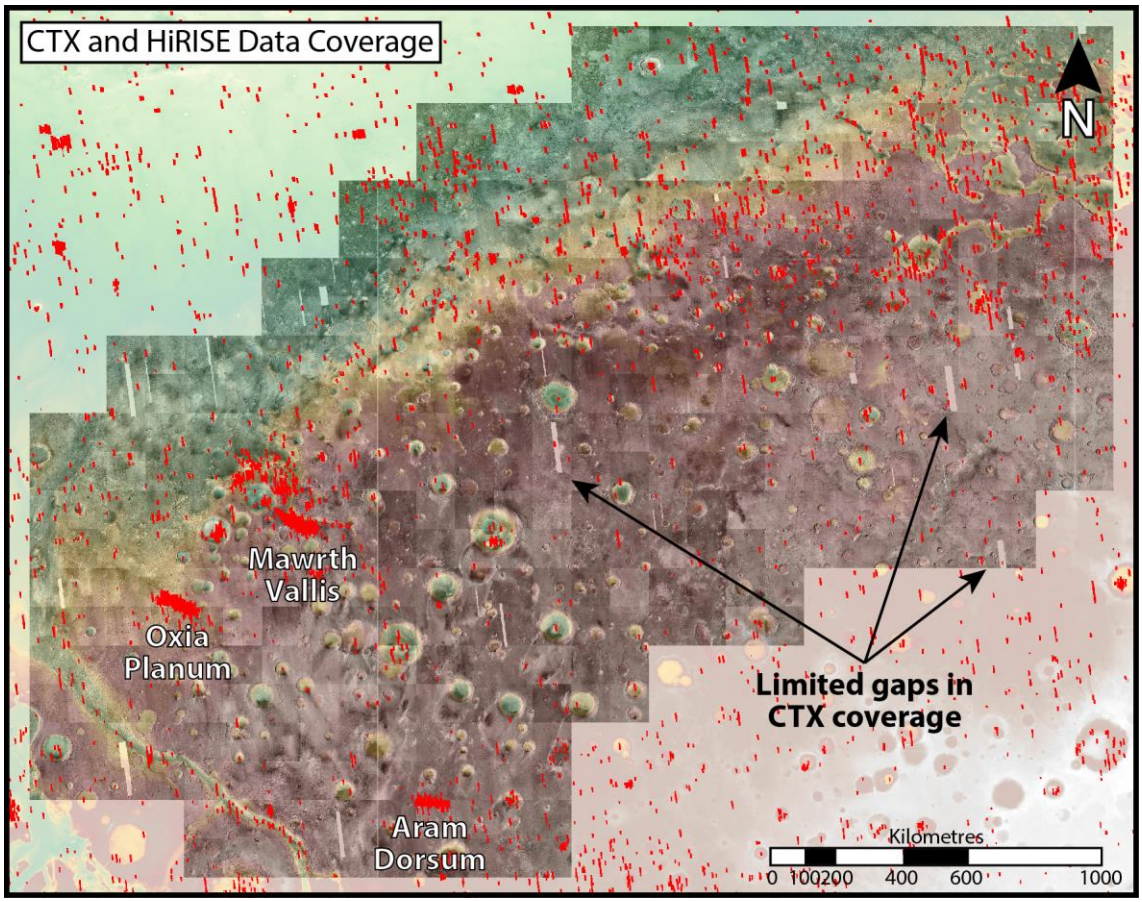

Figure 3.1 – Map of CTX and HiRISE image coverage for the area of western Arabia Terra investigated in this thesis. Coverage of CTX data represented by selected tiles of the global CTX image mosaic (Dickson, Kerber et al. 2018), indicating examples of limited gaps in image coverage. Coverage of HiRISE data footprints (red areas), indicating uneven distribution of coverage, with greater coverage: along the dichotomy; Ares Valles; and three candidate ExoMars rover landing sites at Mawrth Vallis, Aram Dorsum, and Oxia Planum. (overlaid with MOLA topography)

3.2.1 VISUAL IMAGE DATA

Visual and near infrared, greyscale imagery was used for the majority of observations and mapping applications in this thesis, primarily in the form of ~6 m/pixel CTX image data, and 0.25 m/pixel HiRISE image data. The coverage of CTX and HiRISE datasets are extensive for Arabia Terra, with near complete coverage of CTX imagery, and ~5% coverage by HiRISE, represented by 1,544 individual image observations (**Figure 3.1**). Evaluation of CTX images was generally carried out on third-party image mosaics (Dickson, Kerber et al. 2018), with the use of individual CTX and HiRISE images limited to focused study areas. Interpretation of greyscale image data was divided into two approaches: (1) morphological observations, interpreting three-dimensional forms from image data; and (2) albedo observations, concerning variations in tone as a result of

surface reflectance. Typical morphological observations include scarps, pits, valleys, craters, and any other features with prominences sufficient to cast shadows. Aiding morphological observations is the helio-syncronous orbit of the MRO spacecraft, hosting CTX and HiRISE, ensuring a constant angle of illumination for all observations. Albedo observations typically included qualitative descriptions of surface composition and texture, allowing identification of features with no apparent topographic profile.

Additional observations were made with colour imagery, although restricted by observation coverage, primarily in the form of ~5 m/pixel CaSSIS image data, and 0.25 m/pixel HiRISE image data. The nature of colour observations were generally qualitative, with colour data revealing clearer distinctions between mapped units, and useful in defining and describing layering within sedimentary deposits.

3.2.2 TOPOGRAPHIC DATA

Topographic data on Mars makes use of a datum defined by the average elevation of the surface as defined by MOLA observations (Smith, Zuber et al. 2001), or previously by the mean atmospheric surface pressure (Carr 2007). Values range from -8,143 m at the lowest point with Argyre Planitia to 21,241 m at the summit of Olympus Mons. The only global topographic dataset for Mars is the MOLA DEM which has a resolution of ~463 m/pixel (Smith, Zuber et al. 2001), and is the standard topographic dataset used in martian geomorphological research. In addition to the DEM products, original MOLA shot-points are also a useful resource for observing local profiles, or for detailed study of individual landforms. Topographic data from HRSC with a resolution of 150-200 m/pixel is available for many areas, and coverage along the dichotomy is particularly extensive (Neukum and Jaumann 2004, Jaumann, Neukum et al. 2007). However, only a few regional DEMs covering large quadrants of Mars have been produced, and there remain significant gaps in HRSC coverage. Lower resolution global and regional topography datasets are useful for investigating broad areas, and identifying major features. However, for this thesis, high-resolution topographic data was essential for the identification of subtle basins and fluvial feature attributes. Therefore HiRISE and CTX DEMs, with

respective resolutions of 1 m/pixel and 20 m/pixel were produced with orbital stereo imagery, for use in the detailed study areas of Chapters 4 and 5.

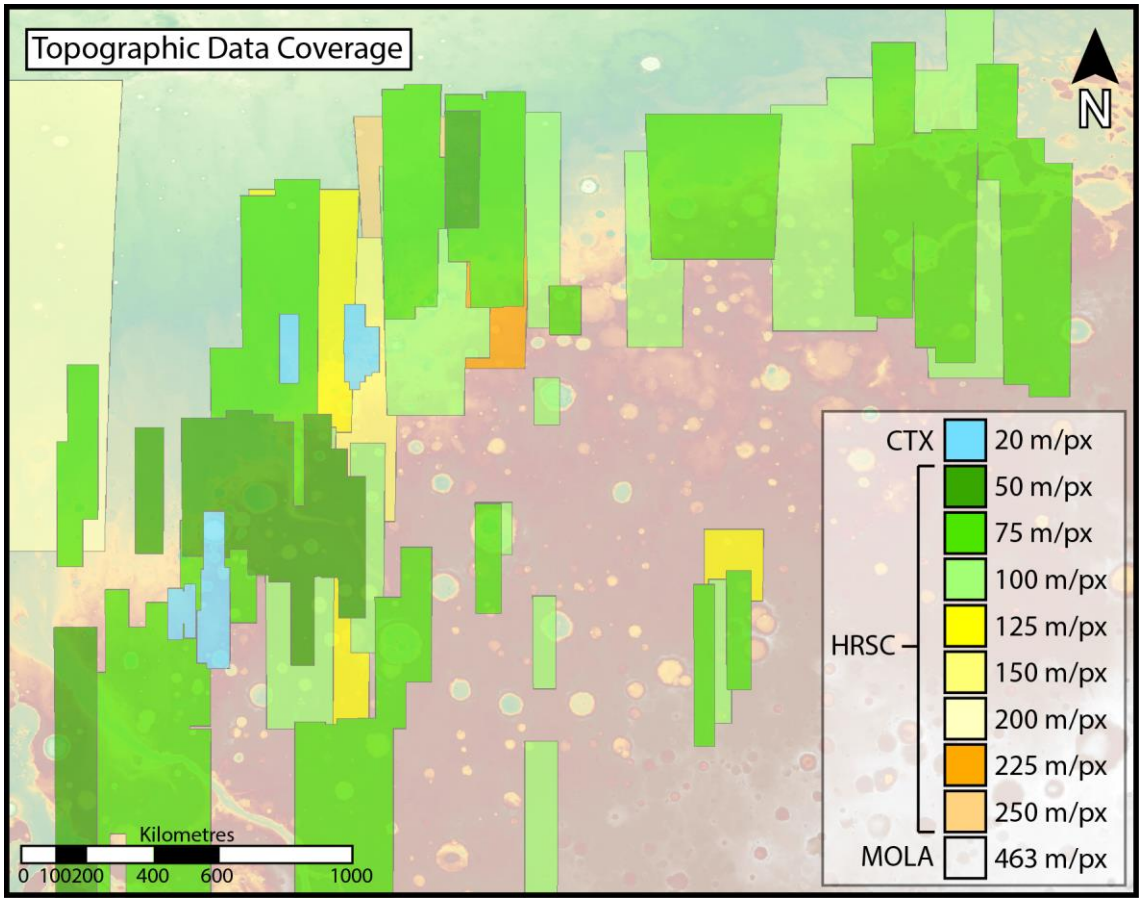

Figure 3.2 *– Map of topographic data coverage for the area of western Arabia Terra investigated in this thesis. The global MOLA DEM (~463 m/pixel) provides consistent and uninterrupted coverage of the region, while the dichotomy is well represented by 50-100 m/pixel HRSC DEMs, and the production of high resolution CTX DEMs was only deemed necessary for the detailed local studies presented in Chapters 4 and 5.*

3.2.2.1 DIGITAL ELEVATION MODEL PRODUCTION

Digital elevation models (DEMs) are produced based on the principal of stereo acuity. Where an area of a planetary surface is imaged multiple times from different angles, a three-dimensional model of the terrain can be calculated and then pegged to known elevation points on the surface. The production of DEMs for this work was carried out using ISIS and SOCET SET software and the 'USGS Tools' extension and associated workflow (Kirk, Howington-Kraus et al. 2008). Stereo imagery took the form of CTX and HiRISE data, with MOLA shot points providing absolute values to the terrain models, producing DEMs with an effective spatial resolution approximately factor of four less

than the original image. The process is memory and processer intensive and was therefore run on a set of dedicated machines. The total time of direct user input being roughly 45-60 minutes, with the processing time of one DEM taking roughly three hours for CTX or five hours for HiRISE. The workflow used in this work to create DEMs from both HiRISE and CTX stereo imagery is detailed in a document created by the United States Geological Society (USGS) entitled 'HiRISE Photogrammetric Processing using SOCET SET, with a brief summary of major steps in the process available in **Appendix I**.

3.3 HYDROLOGICAL ANALYSIS

The research of this thesis relies on topographic data in the identification and interpretation of geomorphological features, and in reconstructing past hydrological systems. In this section, methods applied to hydrological research on Earth and Mars, such as fluvial and basin grading systems are outlined and appraised in the context of Arabia Terra (**Section 3.3.1**), including descriptions of modifications and variations applied in this thesis. Crucial to the research of this thesis is the delineation of drainage catchments, and therefore a detailed account is provided of the methods for drainage catchment delineation used in previous works on Earth and Mars, and method favoured in this thesis (**Section 3.3.2**). A fuller description of ArcMap and GIS data, toolsets, workflows, and the methods used in this thesis to extract quantitative data from topographic features is available in **Appendix II and Appendix III**.

3.3.1 HYDROLOGY CODING SYSTEMS

Stream ordering systems provide a systematic means to divide fluvial networks into linear segments, and assign values based on tributary relationships. Values infer the relative importance and placement of fluvial segments within a wider network, differentiated segments fed by a greater number of tributaries for segments fed by fewer tributaries. Various stream ordering systems approach tributary relationships differently, and three major stream ordering systems considered here: (1) Strahler (Strahler 1957, Strahler 1964); (2) Shreve (Shreve 1966), and (3) Classic (Horton 1945). In addition to

fluvial coding systems handling linear features, systems such as the Pfafstetter coding system handle sub-basin areas within drainage catchments and fluvial systems (Verdin and Verdin 1999). A system of sub-basin delineation is considered for the unique setting of Mars and Arabia Terra in Chapter 6, but due to difficulties presented by the topography of Mars, existing terrestrial coding systems were generally not considered to be applicable.

In the Strahler and Shreve systems, branching networks are divided into segments beginning and ending at every intersection point, and therefore produce the same number of segments for a given system. In both Strahler and Shreve, the most peripheral segments of a system, those not fed by any other segments, are assigned a value of 1. Values in Strahler only increase where two tributaries of the same value meet to feed a segment, such that: a segment fed by segments with values of 1 is assigned a value of 2; a segment fed by segments with values of 2 is assigned a value of 3; but a segment fed by segments of differing value, for example values of 1 and 2, will only have a value of 2. Alternatively, Shreve stream order increases based on the sum of tributary values, such that: a segment fed by segments with values of 1 will have a value of 2; a segment fed by segments with values of 2 will have a value of 4; and a segment fed by segments with values of 1 and 2 will have a value of 3. Shreve stream ordering therefore produces a greater range of values or levels than Strahler stream ordering for a given system.

Classic stream ordering employs a different approach to dividing system segments. Instead of dividing systems at every intersection, a continuous segment is defined from the river terminus to the head of a distant tributary, and assigned a value of 1. Tributaries intersecting the segment with a value of 1 are assigned a value of 2, and form continuous segments from the intersection with segment 1 to the head of a distant tributary. Subsequent segments are similarly numbered so that all tributaries to a segment with a value of 2 are assigned a value of 3, and so on so that every segment has an open head. The Classic stream order therefore produces a lower number of segments, and the fewer levels for a given system. However, there is some subjectivity in which branches of a network are chosen to form each segment, although producing the longest possible segments is typically preferred, and because segments are not divided at every

intersection, values in this method do not convey the same information regarding relative order or importance of drainage input as the Strahler and Shreve methods.

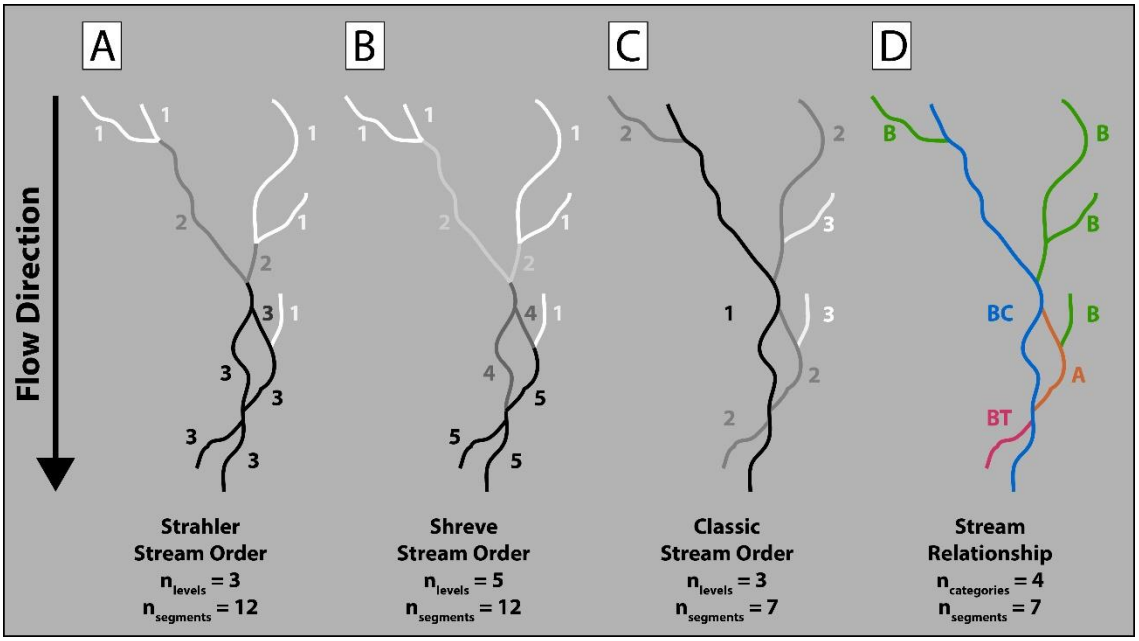

Figure 3.3 *– Demonstration of a fluvial network divided into segments and assigned values using existing stream ordering systems, as well as the stream relationship method employed in this thesis. The Strahler (A) and Shreve (B) methods divide networks into segments beginning and ending at every intersection, and thus both generate the same number of segments, with values assigned in such a way as to highlight the differences between upstream and downstream segments. Alternately, the classic stream ordering (C) method divides networks into segments which begin at open heads, and thus generates a lower number of segments and levels than Strahler or Shreve, while preserving information on the longest possible segments within a network. A stream relationship (D) method was employed in this thesis, as being an efficient means of representing only the information pertinent to this research, using the classic stream ordering method of dividing systems, while assigning categories based on segment relationships rather than values. The stream relationship categories are defined as: branching centre (BC; blue), the longest segment within a branching network, from head to terminus; branches (B; green), tributary segments with an unconnected start point; branching terminations (BT; pink), segments which start as a branch and terminate at an unconnected end point; and anabranching (A; orange), segments connected at start and end points to other fluvial segments.*

Mars presents difficulties in the use of existing stream ordering systems, not least because many valley systems mapped on Mars do not represent continuous branching systems, and instead, single valleys and networks with only a few levels of tributaries are common (Hynek, Beach et al. 2010, Alemanno, Orofino et al. 2018). Given the ancient age of fluvial processes on Mars (~3-4 Ga), limits on branching fluvial networks are likely to be at least partially the result of subsequent destruction and obscuration of fluvial landforms, and therefore, stream ordering values are of limited usefulness in regions such

as Arabia Terra where few extensive valley networks are observed. Additionally, hydrological processes on Mars may have been significantly influenced by upwelling groundwater or catastrophic flooding events (Andrews-Hanna, Zuber et al. 2010, Salese, Pondrelli et al. 2019, Goudge, Morgan et al. 2021), and therefore, terrestrial stream ordering systems intended to represent surficial drainage patterns driven by precipitation, may be of limited use. Still, some segmentation and organisation of drainage networks were deemed useful in this thesis, and existing stream ordering systems were adapted to this purpose.

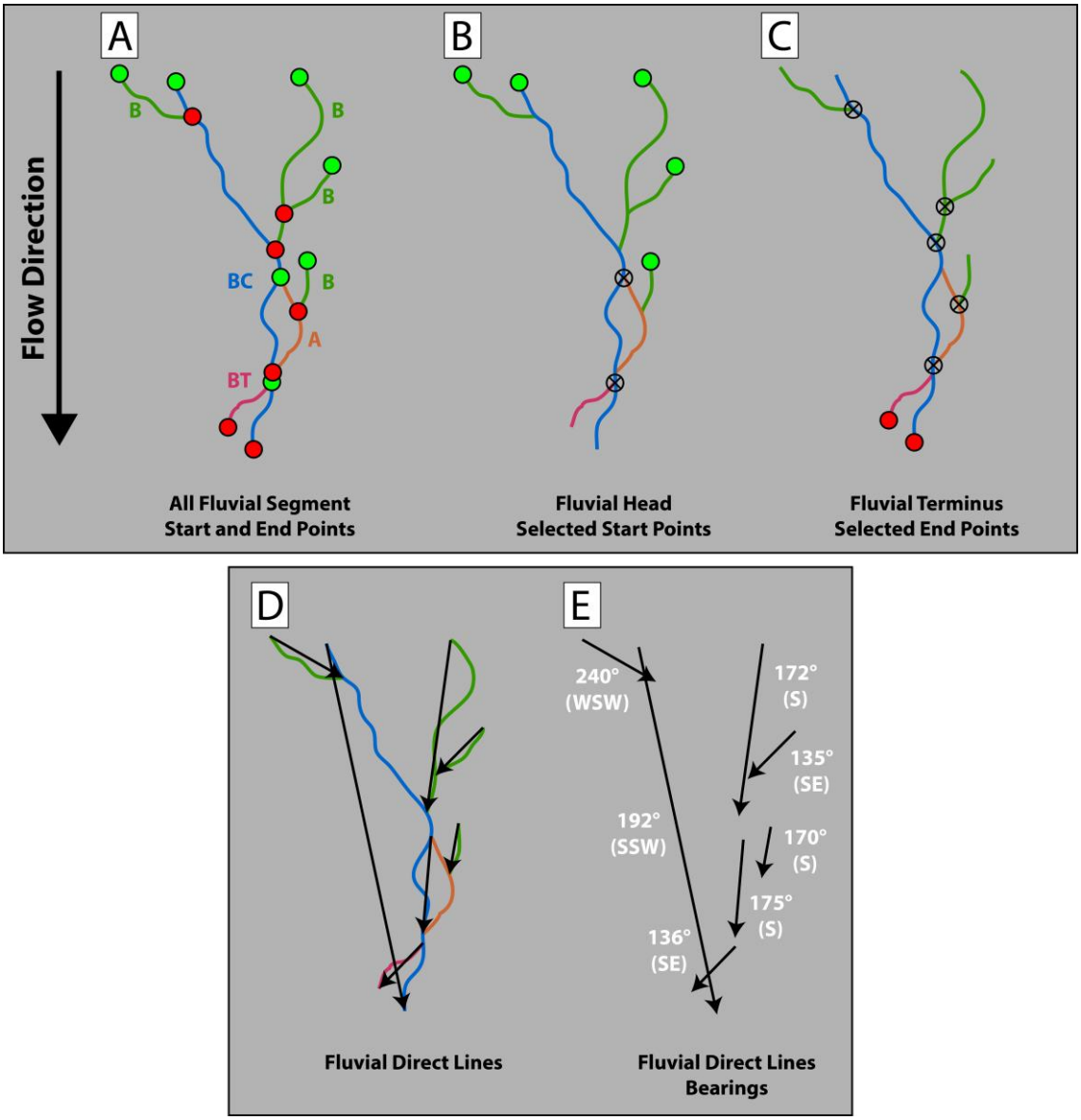

Figure 3.4 – Demonstrations of the methods used to select relevant fluvial start and end points, and generalised fluvial directions. (A) Start points (green dots) and end points (red dots) exist for each fluvial segment, with categories assigned as: branching centre (BC; blue); branching (B; green); branching termination (BT: pink); and anabranching (A; orange). Only some points

represent true fluvial heads and termini which are of interest to the identification of palaeolakes, with many additional points existing at intersections within the fluvial network, and not of diagnostic use. (B) Valley heads were defined as only the start points of BC and B segments, and (C) valley termini were defined as only the end points of BC and BT segments. To ascertain the overall direction of fluvial segments, (D) direct lines were generated for the start and end points of every fluvial segment, and (E) bearings and directions then measured for these direct lines.

The attributes of fluvial features most pertinent to the research of this thesis are: (1) maximum length; (2) flow direction; and (3) the position and elevation of fluvial heads and termini. The identification of these attributes across the large set ($n=10^4$) of features presented in Chapter 6 required a systematic approach to assessing these attributes. Numerical stream ordering values were not considered relevant to this research, but branching fluvial networks were divided into segments in the same manner as the Classic stream ordering system, meeting the requirements to produce the lowest number of segments and preserve maximum length data. Instead of stream order values, segments were designated as: single (S), open at both ends with no connecting segments; branching centre (BC), the longest segment within a network; branches (B), including all tributaries to BC and B segments; branching terminations (BT), branching off a network to form a termination in addition to the BC segment; and anabranching (A), connected at beginning and end to other fluvial segments. Segmenting and characterising branching systems in this manner allowed for a selective comparison of fluvial attributes considered most relevant to this research, and most importantly allowed the designation of fluvial heads and termini.

The study of palaeolakes, oceans, and regional hydrology on Mars often includes analysis of fluvial heads and terminations (Fassett and Head 2008, Di Achille and Hynek 2010, Goudge, Aureli et al. 2015), but fluvial segments within branching systems include start and end points which are not true heads or terminations. Therefore, analysis of fluvial heads in this study only considers the following start points (**Figure 3.4b**): non-branching single segments (S), branching centre segments (BC), and branch segments (B). Analysis of fluvial termini only considers the end points of: non-branching single segments (S), branching centre segments (BC), and branching termination segments (BC). Similarly, maximum fluvial feature length only considers: non-branching single

segments (S), and branching centre segments (BC). The individual start and end points for each fluvial segment are used to produce direct lines, from which a bearing or direction of flow can be derived.

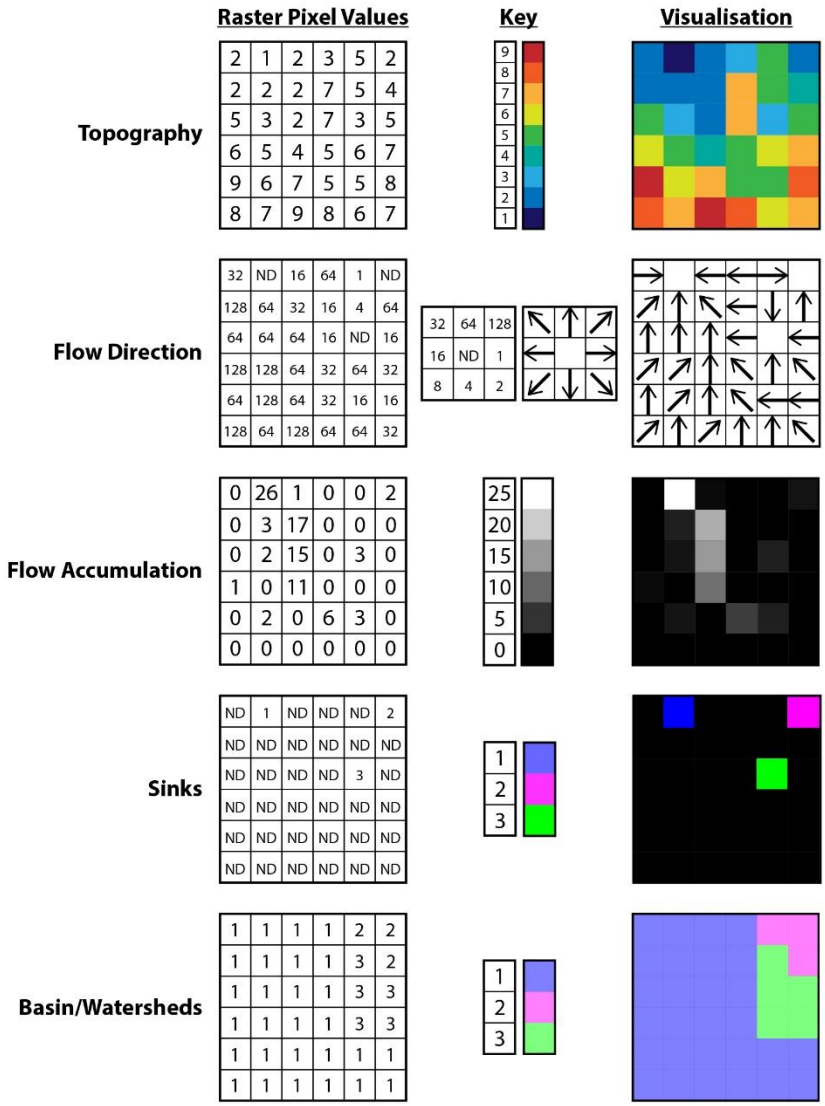

Figure 3.5 *– Simplified examples of the rasters produced as part of the ArcMap 'Hydrology Toolbox', and associated workflow, showing raster numerical pixel values (left), and a visual representation of those values (right): (1) Input topography data, showing high (red) and low (blue) areas; (2) Flow direction, defined as the direction to the lowest adjacent cell; (3) Flow accumulation, calculated as the sum of upland cell values, as defined by flow direction; (4) Sinks, defined as cells with no adjacent lower cell, and derived from flow direction; (5) Basins/Watersheds, defined by flow direction as the upland area draining to a set of points, in this case the previously defined sinks.*

3.3.2 DRAINAGE CATCHMENT DELINEATION

A drainage catchment is defined as the upland area which, given no infiltration or impediment, would contribute surface runoff and drain towards a given low area or pour-

point. Drainage catchments may be defined for individual tributaries, branches of a fluvial network, an entire lake or river, or as a continental watershed draining to an ocean. Drainage catchments can therefore define the limits of hydrological systems at a range of scales, and are important in characterising the interplay of hydrological processes, and the relationship between drainage catchment area and palaeolake dimensions has been highlighted as an important metric in characterising the balance of lake filling by surface accumulation or groundwater influx (Fassett and Head 2008, Stucky de Quay, Goudge et al. 2020).

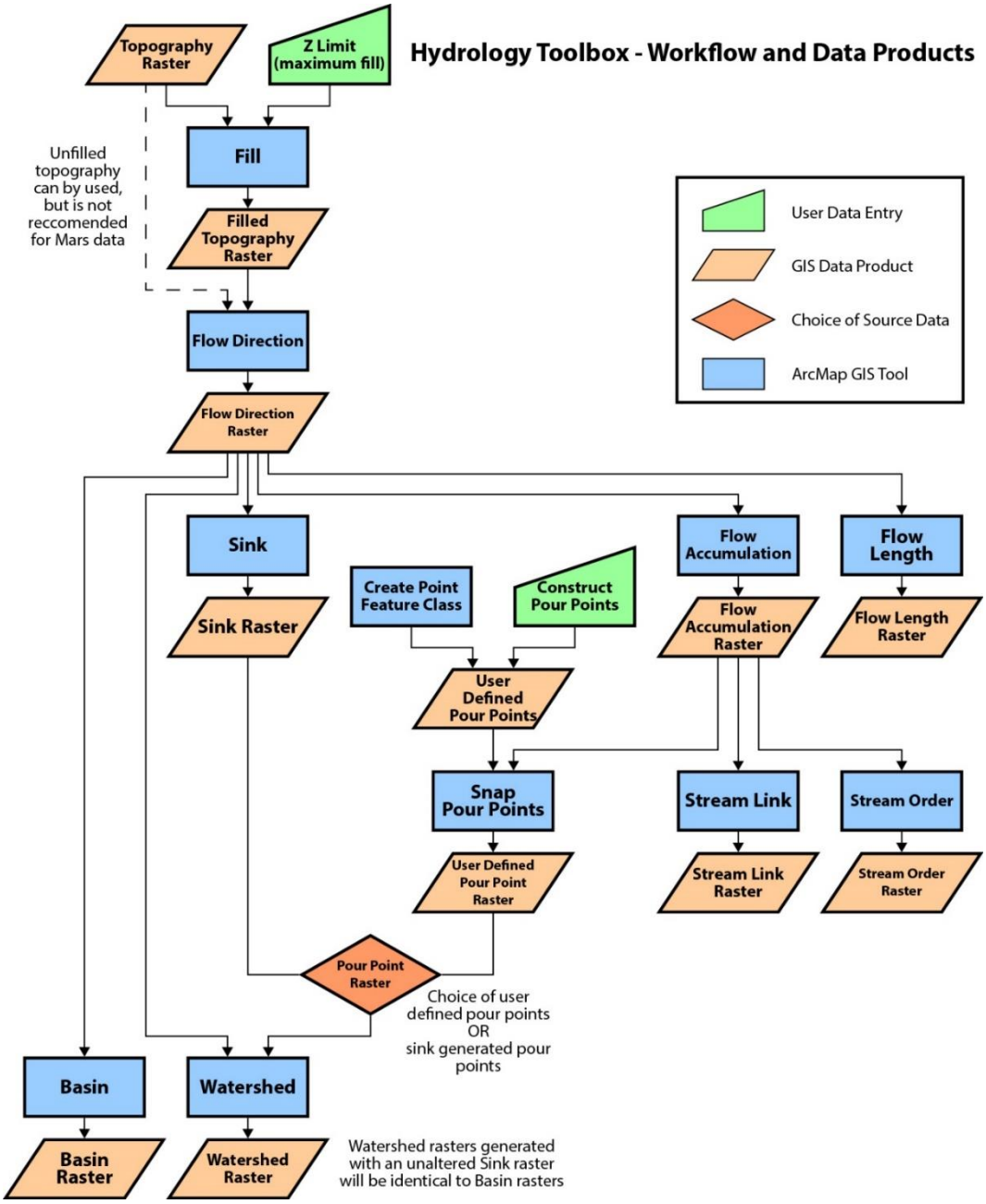

Figure 3.6 *– Workflow diagram of the tools in the ESRI ArcMap 'Hydrology Toolbox'.*

The 'Hydrology Toolbox' included in ESRI's ArcMap GIS software package includes tools and workflows for identifying and quantifying hydrological features from an input topographic surface, with the delineation of drainage catchments particularly pertinent to the research of this thesis. The workflow used to produce drainage catchments includes a number of intermediate steps, each producing a raster required as an input in subsequent stages of the process, starting with a topographic raster and ending with a raster identifying cells belonging to a drainage catchment (**Figure 3.5**). The flow accumulation raster can also be used to represent idealised drainage systems, and compared to morphological observations.

The process of drainage catchment delineation is outlined here in greater detail, as following the workflow and sequence of actions in the ArcMap 'Hydrology Toolbox' (**Figure 3.6**):

(1) The 'Fill' tool is applied to a topography raster, to remove isolated sinks and basins in the topography, with a user defined value describing the minimum sink depth to be filled, varying between: all sinks filled in a surface regardless of depth; or only sinks up to a minimum depth filled. The output is a filled topography raster.

(2) The 'Flow Direction' tool is applied to a filled topographic surface to generate a raster indicating relative relationship of flow between each individual cell of the raster. The output is a flow direction raster, returning an integer value for each cell indicating the direction of the lowest adjacent cell, and therefore the direction that liquid would flow from one cell to another. If a cell is itself lower than its eight adjacent cells then it is assigned a value calculated as the sum of all contributing cells, and designated as a sink.

(3) The 'Sink' tool can be applied to a flow direction raster, to generate a raster indicating all cells which are sinks, and therefore do not drain to any other cells. The output is a sink raster, with each sink, including those composed of multiple cells, defined by a unique value.

(4) The 'Flow Accumulation' tool can also be applied to a flow direction raster, to generate a raster indicating the cells and corridors with the highest accumulated contributing surface area. The output is a flow accumulation raster, returning an integer value for each cell which is the accumulated sum

of all the cells which drain into it based on the flow direction raster (**Figure 3.5**). This raster appears visually as a dendritic network which can be divided and quantified using the 'Stream Link' and 'Stream Order' tools, the results of which have been compared to mapped fluvial systems on Mars (Mest, Crown et al. 2010, Fawdon 2018).

(5) Drainage basins can be delineated with the 'Basin' or 'Watershed' tools. The 'Basin' tool is applied to a flow direction raster, to generate a raster with drainage catchments produced for every automatically identified sink. The 'Watershed' tool is applied to a flow direction raster, as well as a pour-point raster, to generate a raster with drainage catchments for every input pour-point. An input pour-point raster can either be: a sink raster, altered or unaltered to suit the specific research goals; or a pour-point raster produced by applying the 'Snap Pour Points' tool to manually placed point features and a flow accumulation raster. The 'Snap Pour Points' tool ensures that pour-points generate useful drainage catchments by shifting points to values of high flow accumulation. It should be noted that a basin raster will be identical to a watershed raster produced using an unaltered sink raster.

Filling sinks in topography data is an important preparatory step in advance of generating drainage networks and catchment areas (Tarboton, Bras et al. 1991). Sinks are cells or groups of cells on the topography data with no adjacent lower cells to which drainage flow, and represent the bottoms of closed basins in the topography. Which sinks are filled is determined by a user defined maximum fill depth, from sink bottom to overflow at the edge of the basin. For the ArcMap workflow, use of various fill depth values will have the following effects: (1) with no value entered, the default is to fill every sink in the topography to an unlimited depth (**Figure 3.7-Blue profile**); (2) a value of zero will result in no sinks being filled, producing an output topography identical to the input (**Figure 3.7b-Grey profile**); (3) values greater than zero will result in filling only sinks with a maximum depth less than the defined value (**Figure 3.7b-Red profile**). The relationship between fill depth and the number of drainage catchments produced is such that, for a given area: (1) a greater fill depth value will fill a greater number of local sinks, and produce a lower number of catchments; (2) drainage catchments produced with a greater fill depth will be sub-divisions of catchments produced with a lesser fill depth (**Figure**

3.7a). Therefore, smaller drainage catchments in a partially filled topography can be considered as constituent parts of a larger drainage catchment covering the same area.

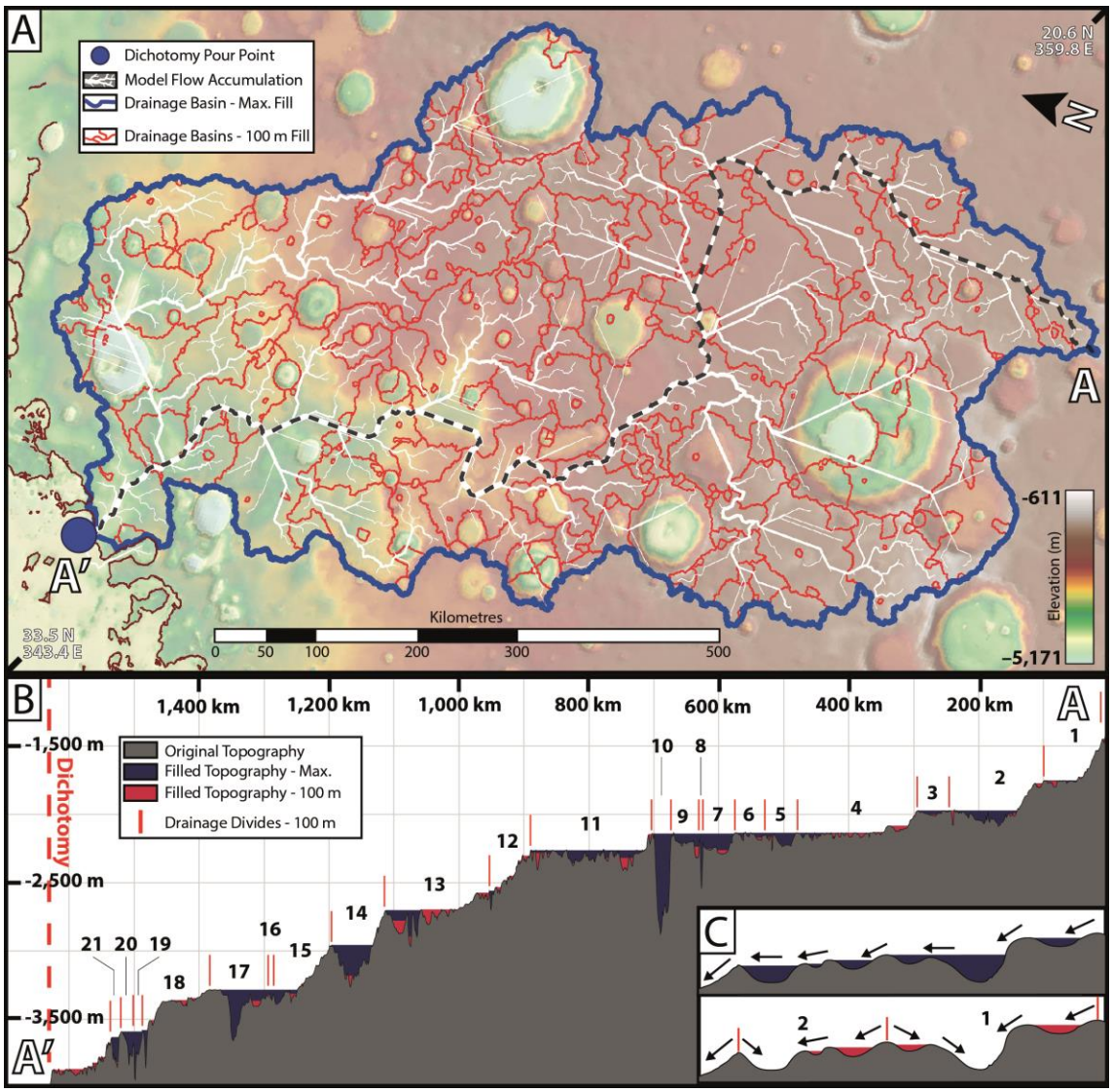

Figure 3.7 – Example of drainage catchments produced on topographic data filled to different depths, from a more detailed study in Chapter 6 of this thesis. (A) Map of an idealised drainage catchment (thick blue outline) and idealised drainage network (white lines), calculated on a topography with all sinks filled to an unlimited depth, for a pour point (blue circle) at the termination of a valley at the dichotomy. Also shown are a set of drainage catchments (thin red outlines) for the same area, but calculated on a topography with only sinks of a maximum depth <100 m filled. The profile traced from A-A' (dashed black line) is an example of the longest idealised flow accumulation stream (white lines) on the fully filled topography. (B) Profile of the longest idealised flow accumulation stream (A-A') within the idealised catchment, comparing the original topography (grey area), the topography with only sinks <100 m filled (additional red area), and the fully filled topography (additional blue area). The profile resulting from full filling represents one drainage catchment from highlands to lowlands. In contrast, the same profile on a partially filled topography transects 21 smaller sub-basins (numbered on profile) with drainage divides between them (vertical red lines). (C) A simplified schematic diagram of flow direction (arrows) on fully filled (blue infills) and partially filled (red infills) topographic profiles. The fully filled topography results

in a continuous flow from highlands to lowlands, and the partially filled topography results in multiple closed drainage catchments, each accumulating flow to an isolated sink. In this work we utilise fully filled topographic data as a broad, first order definition of possible drainage catchments, and partially filled (<100 m) topographic data to produce a granular breakdown of sub-basins. (MOLA topography data)

Terrains on Earth tend to display mature drainage networks, and any sinks in topography data which are greater than 10 m in diameter are typically considered to be erroneous (Mark 1988), unless the surface is dominated by karst or glacial features, or other known endorheic basins. On terrestrial topographies it is therefore advisable to fill all sinks to negate the effect of errors in the data which would otherwise result in erroneous sinks and discontinuous drainage networks. On Mars, evidence of hydrologically mature landscapes and drainage networks is rare (Stepinski and Stepinski 2005, Galofre, Bahia et al. 2020), and many local sinks, impact craters in particular, either postdate fluvial and lacustrine processes, or display no evidence of aqueous activity. Therefore, filling all sinks in a martian topography may produce unrealistic drainage catchments (Mest, Crown et al. 2010).

Despite the issues discussed above, filling all sinks in the topography is a method typically used to produce idealised drainage networks and catchments in Mars research (Goudge, Mustard et al. 2015, Fawdon 2018, Goudge and Fassett 2018). However, the use of full topographic filling may not be a validation of the usefulness of this method on Mars, and instead a pragmatic consequence of the additional complexity of partial filling of the topography. In this thesis, full topographic filling was considered useful for producing first order approximations of drainage catchments, representing a hypothetical scenario in which all local sinks were either filled with water to the point of overflow or did not exist at the time of fluvial and lacustrine processes (**Figure 3.7c**). Therefore, idealised drainage catchments may consolidate a number of minor endorheic basins into a broader catchment that is not consistent with the actual hydrological history of the area, and if groundwater rather than precipitation was the dominant source then drainage catchments delineated on surface topography would have little relevance. Additionally, changes in local topography postdating fluvial and lacustrine processes, such as raised impact crater rims and ejecta or wrinkle ridges (Fawdon 2018), may isolate

parts of an ancient catchment or create closed basins which would have originally been integrated with larger catchments.

Given that both fully filled and unfilled topographic data can produce unrealistic drainage catchments, some studies on Mars have made use of partially filled topographic data (Mest, Crown et al. 2010). Filling some small or erroneous sinks in the topography is still required to produce drainage catchments with a degree of connectivity which matches observed hydrological features, but determining the fill depth value to be used is potentially subjective, and will depend on the particular study area and research aims. For example, a study of drainage catchments in the Tyrrhena Terra region of Mars, determined that a fill depth of 575 m was most appropriate to the study, based on an iterative approach testing different fill depths (Mest, Crown et al. 2010). In Chapter 6, a fill depth of 100 m was considered appropriate to meet the particular research aims, however there is unlikely to be a universally applicable method, and studies in new regions with different aims will likely require further adjustments.

3.4 RESEARCH APPLICATIONS

Orbital investigations of the martian surface are served by a wealth of data, representing a wide range of observation styles. However, applying orbital data to research on Mars requires careful consideration of the limitations inherent in existing datasets and methods. The research questions of this thesis are primarily aimed at the identification and delineation of topographic basins which were once filled with water, and definition of the regional processes and controls which filled and sustained these water bodies.

As outlined in this chapter, the resolution and coverage of existing topographic datasets (eg. MOLA, HRSC) is sufficient to identify and characterise many aspects of lacustrine and fluvial morphology. However, to advance on previous studies, the work of this thesis also included production of high-resolution topographic data (eg. CTX and HiRISE DEMs) to aid in the identification of finer features. Additionally, geographically

constraining the study area to western Arabia Terra has allowed exploitation of the full detail of high-resolution CTX image data to identify and define morphological features.

Existing methods of palaeolake identification, fluvial coding, and drainage catchment delineation, are considered as useful starting points in this work, but care is taken to account for aspects of topography and geological history that are particular to Mars and the region of Arabia Terra. A major limitation to terrestrial methods applied to Mars is the ancient age of hydrological features, and the associated local and regional changes to topography which postdate fluvial and lacustrine processes. The identification of more subtle features with high-resolution topography data also has the potential to compound misidentification and misinterpretation. These issues are addressed throughout the research of this thesis, with careful attention paid to verifying results and interpretations derived from terrestrial methods, as well as established methods of Mars research applied at different scales and within different regions.

4

Palaeolake System at the Planetary Dichotomy

Hundreds of ancient palaeolakes have been identified and catalogued on Mars, indicating the distribution and availability of liquid water as well as sites of astrobiological potential. Palaeolakes are widely distributed across the Noachian aged terrains of the southern highlands, but Arabia Terra has comparatively few documented palaeolakes and even fewer examples of open-basin palaeolakes. This chapter presents a detailed topographic and geomorphological study of a previously unknown set of seven open-basin palaeolakes adjacent to the planetary dichotomy in western Arabia Terra. High resolution topographic data were used to aid identification and characterisation of palaeolakes within subtle and irregular basins, revealing two palaeolake systems terminating at the dichotomy, including a ~160 km chain of six palaeolakes connected by short valley segments. Analysis and correlation of multiple, temporally distinct palaeolake fill levels within each palaeolake basin indicates a complex and prolonged hydrological history, with drainage catchments and possible collapse features placing this system in the context of regional hydrology and the planetary dichotomy.

4.1 INTRODUCTION

The widespread occurrence of liquid water on ancient Mars is supported by evidence for hundreds of palaeolakes within the Noachian aged (>3.7 Ga) southern highlands (Fassett and Head 2008, Goudge, Head et al. 2012, Goudge, Aureli et al. 2015, Goudge, Fassett et al. 2016). The global characterisation and distribution of palaeolakes has helped to constrain past climatic and hydrological conditions on Mars (Milliken, Grotzinger et al. 2010, Wilson, Howard et al. 2016, Kite 2019), and to identify possible past habitable environments (Fairén, Davila et al. 2010). Studies of individual palaeolake systems have contributed to the understanding of regional hydrological histories, and although palaeolake ages generally coincide with the Noachian-Hesperian boundary peak in global fluvial activity, many examples indicate multiple episodes of locally or regionally controlled lacustrine activity rather than a global hydrological system stable over geological timescales (Mangold and Ansan 2006, Di Achille, Hynek et al. 2009, Salese, Di Achille et al. 2016, Wilson, Howard et al. 2016, Goudge and Fassett 2018). The continued incorporation of detailed palaeolake studies into regional and global contexts, including relationships to fluvial, groundwater and possible ocean systems, will provide a broader understanding of hydrology on Mars.

Martian palaeolakes are identified primarily based upon on morphological relationships between topographic basins and fluvial valley networks, and categorised as either open-basin or closed-basin. Open-basin palaeolakes are defined by outflow valleys, indicating a fill level sufficient to breach and overflow the basin (Fassett and Head 2008, Goudge, Head et al. 2012). Open-basin palaeolakes are therefore the strongest evidence for standing bodies of water and are commonly associated with regionally extensive drainage systems and branching valley networks (Goudge, Fassett et al. 2016). Conversely, closed-basin lakes exhibit only inlet valleys, and are typically fed by isolated, shallowly incised valleys (Goudge, Aureli et al. 2015, Goudge, Fassett et al. 2016). Open-basin palaeolakes therefore indicate a greater supply and duration of liquid water than a similarly sized closed-basin palaeolake which never filled to the point of overflow. Most palaeolakes currently described on Mars occur within conspicuous impact craters, while

a minority have been reported in tectonically controlled basins (Mangold and Ansan 2006), inter-crater basins bounded by the upraised rims and ejecta of multiple impact craters (Goudge and Fassett 2018), and other basins of undefined origin.

The distribution of catalogued martian palaeolakes (Fassett and Head 2008, Goudge, Fassett et al. 2016) approximately correlates to that of valley networks (Hynek, Beach et al. 2010, Alemanno, Orofino et al. 2018). Palaeolakes are thus almost entirely limited to the southern highlands, and many palaeolake and valley systems terminate at the boundary with the northern lowlands (**Figure 4.1a**). The processes leading to the formation and present morphology of the planetary dichotomy are not well understood (Watters, McGovern et al. 2007), but the dichotomy may represent the margins of an ancient hemisphere spanning ocean (Parker, Schneeberger et al. 1986, Clifford and Parker 2001, Di Achille and Hynek 2010, Duran, Coulthard et al. 2019). Regardless of the processes involved, the dichotomy appears to mark a distinct hydrological boundary, and analysis of the fluvial and lacustrine systems terminating here will be important to understanding the geological history of this planet encircling feature (Dickeson and Davis 2020).

This chapter presents a detailed investigation of a group of previously undocumented palaeolakes situated adjacent to the planetary dichotomy in Arabia Terra (**Figure 4.1**). Making use of high-resolution digital elevation models, topographic relationships are analysed between multiple equipotential palaeolake levels, sedimentary fans, longitudinal valley profiles, and associated geological features. The objective being to produce a detailed history of lacustrine and fluvial processes in the area, and place these processes within the context of regional hydrology models. The fluvial and lacustrine systems which intersect or terminate at the dichotomy in this area present an additional opportunity to investigate the origin and modification of the dichotomy scarp, as well as the existence of ancient lowland water bodies.

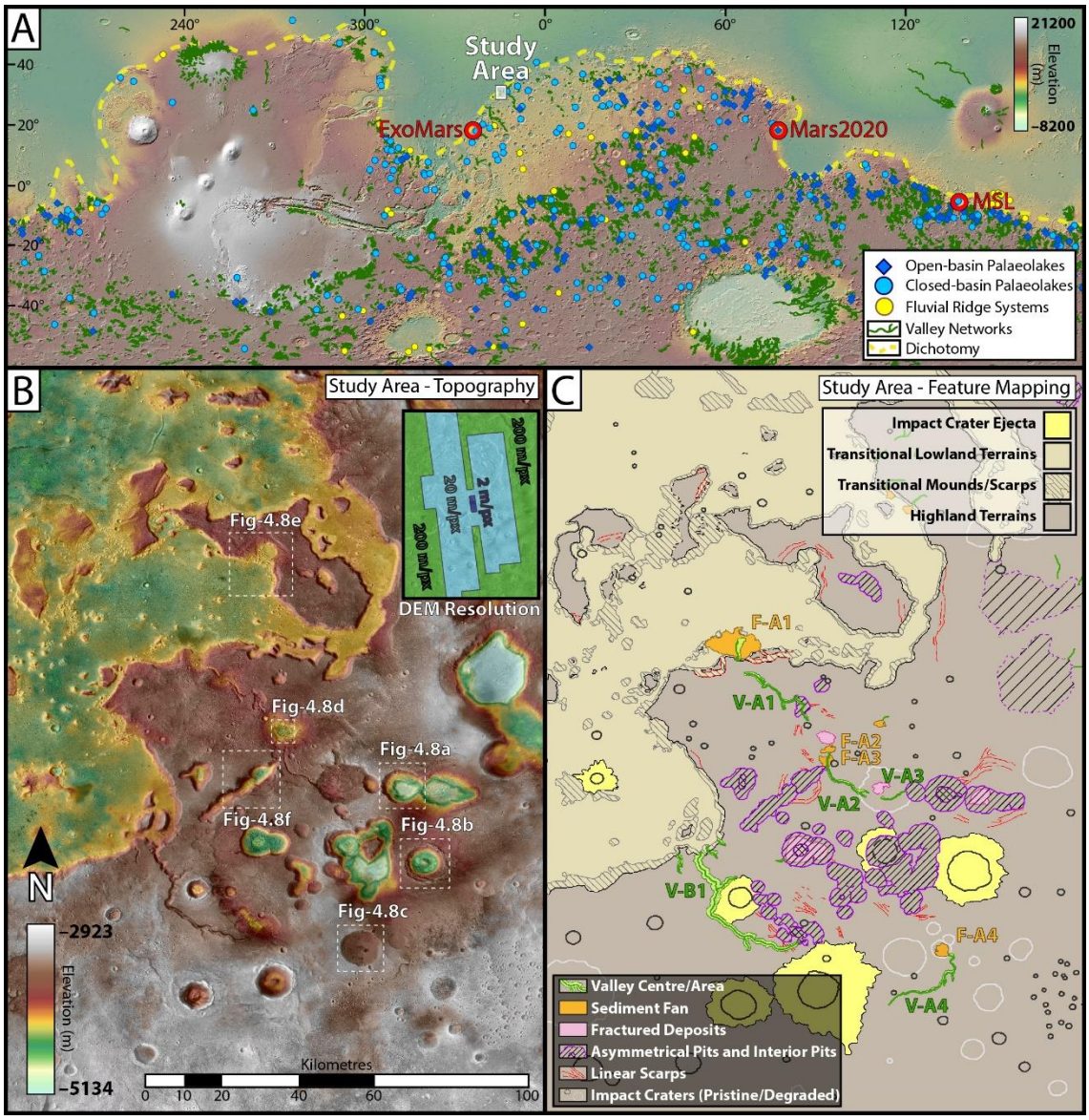

Figure 4.1 *– **(a)** Global topographic map (top) showing the study area in relation to globally catalogued open-basin (dark blue diamonds)(Goudge, Head et al. 2012) and closed-basin (light blue circles)(Goudge, Aureli et al. 2015) palaeolakes, valley networks (green lines)(Alemanno, Orofino et al. 2018), and fluvial ridge systems (yellow circles)(Dickson, Lamb et al. 2020) (MOLA shaded relief JPL), an approximation of the planetary dichotomy (yellow dashed line), and the planned (ExoMars) and presently active (MSL & Mars2020) rover landing sites. **(b)** Topographic and CTX mosaic map of the study area and DEM resolutions (inset). **(c)** Morphological features of interest on a high resolution remapping of highland (brown) and lowland (tan) terrains (mosaic including MOLA, HRSC and CTX).*

4.1.1 STUDY AREA IN WESTERN ARABIA TERRA

The Arabia Terra region of the southern highlands is predominantly Noachian in age and is bounded to the north and west by the planetary dichotomy, and sits at a markedly lower elevation than the majority of the southern highlands. The region exhibits a paucity of open-basin palaeolakes (Fassett and Head 2008, Goudge, Head et al. 2012)

and valley networks (Carr 1995, Hynek, Beach et al. 2010, Alemanno, Orofino et al. 2018), but an abundance of inverted channel systems indicative of a depositional fluvial setting (Davis, Balme et al. 2016, Williams, Moersch et al. 2018, Davis, Gupta et al. 2019, Dickson, Lamb et al. 2020). In addition, the lowest areas of western Arabia Terra, near the dichotomy, are suggested as sites of significant groundwater upwelling (Fassett and Head 2008, Andrews-Hanna, Zuber et al. 2010, Salese, Pondrelli et al. 2019), and numerous northern ocean palaeoshorelines have been mapped along this section of the dichotomy (Dickeson and Davis 2020).

This study focuses on an area of the dichotomy marking the topographic and geological boundary between the middle Noachian highland terrains (mNh), and the Noachian-Hesperian transitional lowland terrains (HNt) (Tanaka, Skinner et al. 2014). In this study, the geological units have been remapped at CTX resolution **Figure 4.1b**, with the contact tracing the steep scarp of the dichotomy and including large flat topped mesas to the east of the dichotomy as a part of the highland terrains (Tanaka, Skinner et al. 2003, Tanaka, Skinner et al. 2014).

4.2 DATA AND METHODS

Geomorphological feature mapping was carried out on imaging data from NASA's Context Camera (CTX; ~6 m/pixel) (Malin, Bell et al. 2007), with additional images from the High Resolution Imaging Science Experiment (HiRISE; 0.25–0.50 m/pixel) (McEwen, Eliason et al. 2007), and daytime infra-red images from the Thermal Emission Imaging System (THEMIS; 100 m/pixel; thermal) (Christensen, Jakosky et al. 2004).

High-resolution topographic data was used in the identification and characterisation of landforms, and to define the possible hydrological relationships between mapped landforms. Topographic data was created from mosaicked CTX (20 m/pixel) and HiRISE (2 m/pixel) digital elevation models (DEMs) with approximate vertical precisions of <8 m and <1 m respectively (Kirk, Howington-Kraus et al. 2008), and supplemented with High Resolution Stereo Camera (HRSC; 150–200

m/pixel)(Neukum and Jaumann 2004) DEMs and Mars Orbital Laser Altimeter (MOLA; 456 m/pixel) (Smith, Zuber et al. 2001) topography data. DEMs were produced from stereo CTX and HiRISE imagery and MOLA shot heights, using ISIS3 and SOCET SET software and the standard USGS workflow (Kirk, Howington-Kraus et al. 2008).

4.2.1 HYDROLOGICAL ANALYSIS

Mapping and analysis were carried out using ESRI ArcMap software, with 'Spatial Analyst' and 'Hydrology' toolboxes used to identify equipotential surfaces, basins, and drainage catchments. Palaeolake basins were defined by equipotential surfaces within closed topographic basins at the elevations of outlet valley heads. This was achieved by generating contours at 10 m vertical intervals, and selecting the highest closed contour at each outlet valley, thus defining an equipotential surface nearly overflowing the basin through the outlet valley, referred to here as the 'valley overflow' (VO) level. The valley overflow level is equivalent to the standard method of palaeolake identification used in previous palaeolake studies (Fassett and Head 2008, Goudge, Head et al. 2012), and here the concept was expanded upon to identify up to two additional palaeolake levels within each basin (**Figure 4.2**): (1) a higher equipotential surface identified as the highest contour with a single opening at the outlet valley, referred to as the 'basin overflow' (BO) level; and (2) a lower equipotential surface defined by the lowest closed contour at the outlet valley, referred to as the 'outlet extremity' (OE) level.

Drainage catchments were produced using the ArcMap 'Hydrology' toolbox on a mosaicked topography dataset of CTX and MOLA DEMs encompassing the wider highlands region. The 'Fill' tool was used to generate a topography with no local sinks. This preparatory step negates the influence of small sinks and noise in the topographic data to produce a maximum drainage catchment which is necessarily an approximation, as all sinks are filled regardless of depth, age, or origin.

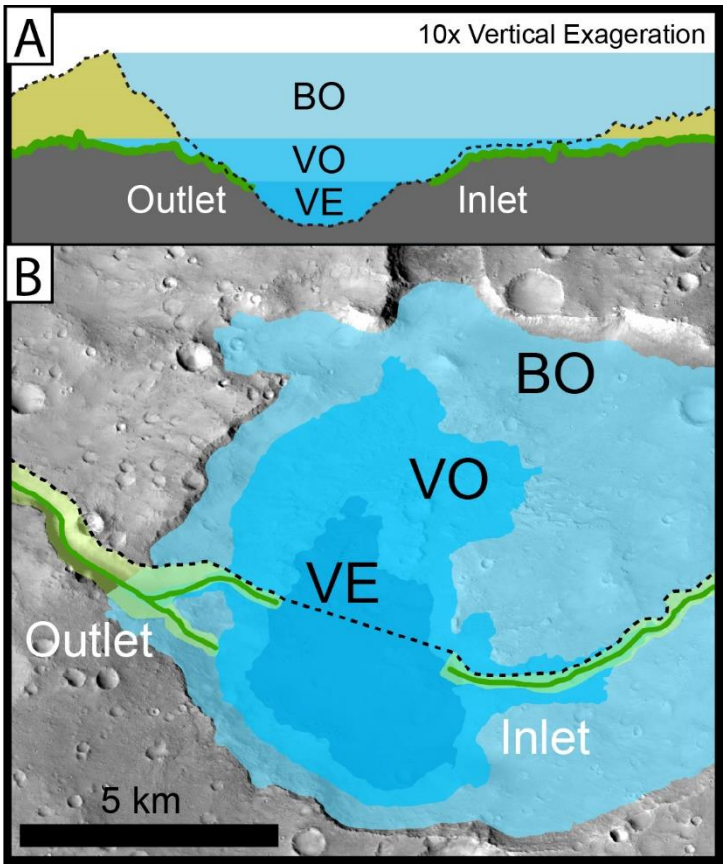

Figure 4.2 *– Illustration of the method used to identify palaeolake basins, and equipotential surfaces. (A) Cross-section of topographic basin exhibiting an inlet and outlet valley, with three palaeolake levels defined by elevations of the outlet valley: basin overflow (BO), defined as the highest elevation contour within the basin with a single opening at the outlet valley; valley overflow (VO), defined as the highest closed contour intersecting the outlet valley; and valley extremity (VE), defined as the lowest contour intersected by the outlet valley. (B) Map-view showing the three palaeolake extents (BO, light blue; VO, blue; VE; dark blue), describing equipotential surfaces defined by the elevations observed at the outlet valley.*

4.3 OBSERVATIONS AND RESULTS

The morphological features mapped for this study, were focused on the goal of identifying, and characterising palaeolakes. Valleys (**Section 4.3.1**) and sediment fans (**Section 4.3.2**) were mapped as the best evidence for liquid water in the study area, with valleys analysed in detail to identify and define palaeolake basins and levels (**Section 4.3.3**). Highland drainage catchments were mapped to define source areas, as were possible lowland sinks in the form of palaeolake basins (**Section 4.3.4**). Finally, additional morphological features were mapped which were observed closely associated with

palaeolakes (**Section 4.3.5**), along with an analysis of the relationships of these features to mapped valleys and palaeolakes (**Section 4.3.6**).

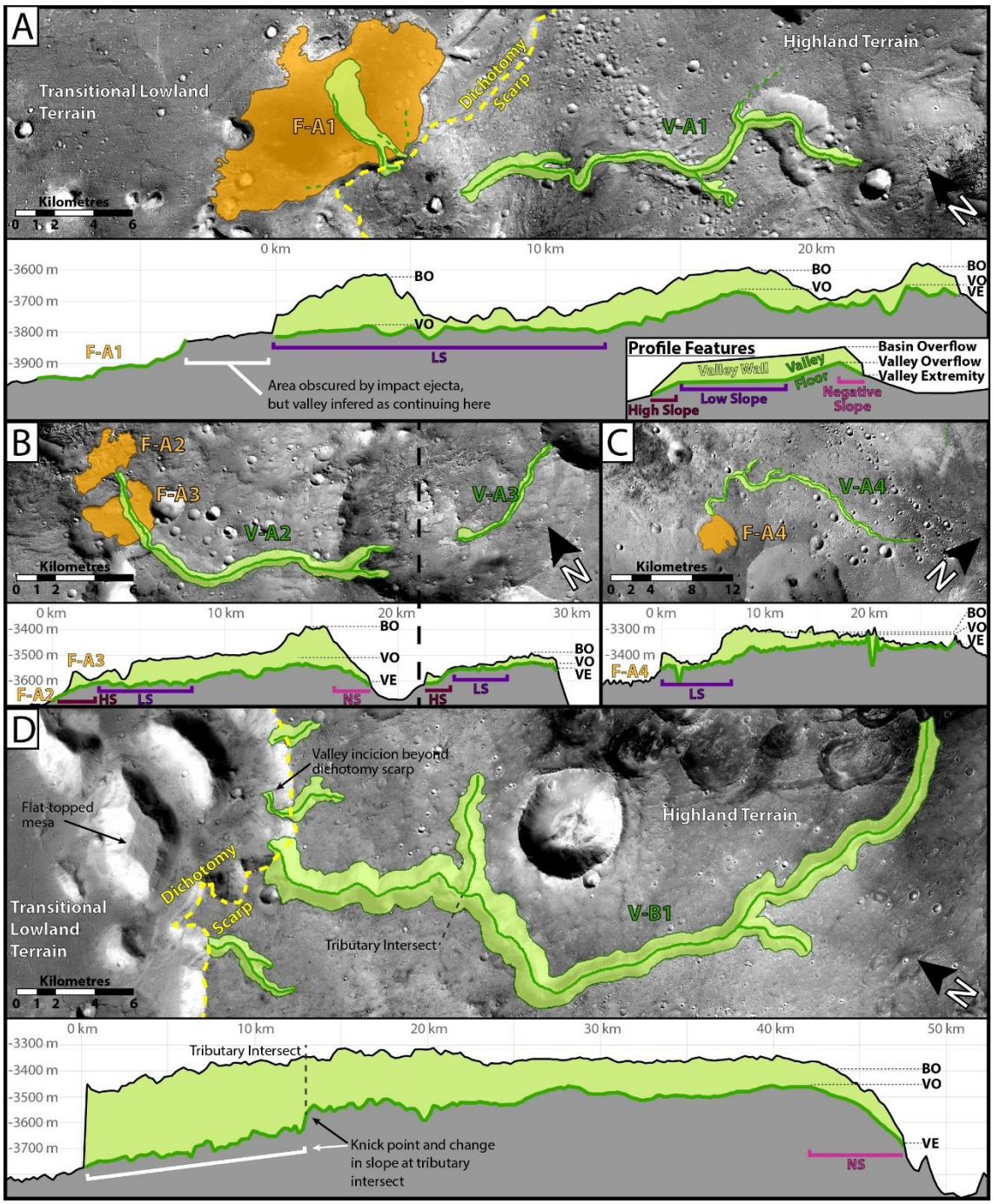

Figure 4.3 – Detail images and longitudinal valley profiles for the five major valleys (dark green valley centre and light green area between valley sides), with relationships to sedimentary fans (orange areas) and the dichotomy (yellow dashed line). Slope features indicated on valley profiles include: negative slope heads (NS, pink), low slope lower reaches (LS, purple), and high slope termini (HS, dark red), with three outlet valley elevations marked where valleys transect or begin within topographic basins at: headward valley extremity (VE), valley overflow at the maximum valley floor elevation (VO), and basin overflow at the maximum valley side elevation (BO). (CTX imagery)

4.3.1 FLUVIAL VALLEYS

Incised valleys were identified and mapped on CTX imagery, with valley centrelines following the lowest elevation along the valley floor, and valley sides mapped to ascertain width and incision depth. Analysis in this chapter focused on the five longest valleys, ranging from 7.5 km to 47 km in length, and numbered from the dichotomy in order of increasing elevation (**Figure 4.3**). A few short (<6.6 km) tributary valleys are also present, but do not represent significant branching networks. The valleys are typically 'V' shaped in profile, with narrow, flat floors dominated by aeolian bedforms and lacking interior channels. The heads of all major valleys begin within closed basins in the highland terrains. The two longest and deepest valleys (V-A1 and V-B1) terminate at the dichotomy, while the remainder (V-A2 to V-B4) terminate within highland closed basins.

Longitudinal profiles show a trend of increasing incision depth from valley head to terminus, and some common trends in slope along valley length (**Figure 4.3**). All valleys begin with a short section of negative slope in comparison to the overall trend of the valley, meaning the elevation of the valley head is 30–260 m lower than the maximum elevation of the valley floor. In addition, the lower reaches of all (V-A1 to V-A4) but one (V-B1) of the valleys are comparatively low slope compared to the upper reaches. Limited exceptions to this trend are short, high slope sections at the termini of valleys V-A2 and V-A3. Conversely, the lower reaches of V-B1 exhibit a higher slope than the upper reaches, with the transition between the two sections marked by a knickpoint coincident with the intersection of a tributary.

In close proximity to V-B1, are four short but deeply incised valleys. Three of these valleys terminate at the dichotomy, and unlike V-B1, appear incised into the dichotomy scarp (**Figure 4.3d**). The fourth valley nearby terminates within an asymmetrical pit in the Noachian highland terrains.

4.3.2 SEDIMENT FANS AND BASIN FLOOR DEPOSITS

Broad fan shaped features (F-A1 to F-A4) with areal extents of 5.1–69.7 km^2 are observed with apexes extending from the termini of three valleys (V-A1, V-A2, V-A4), with lobate, distal edges marked by steep scarps and a prominence of ~1–100 m above surrounding terrains. Fan surfaces are heavily degraded and cratered, but are flat overall with low and consistent slopes from apex to distal edge (**Figure 4.3**).

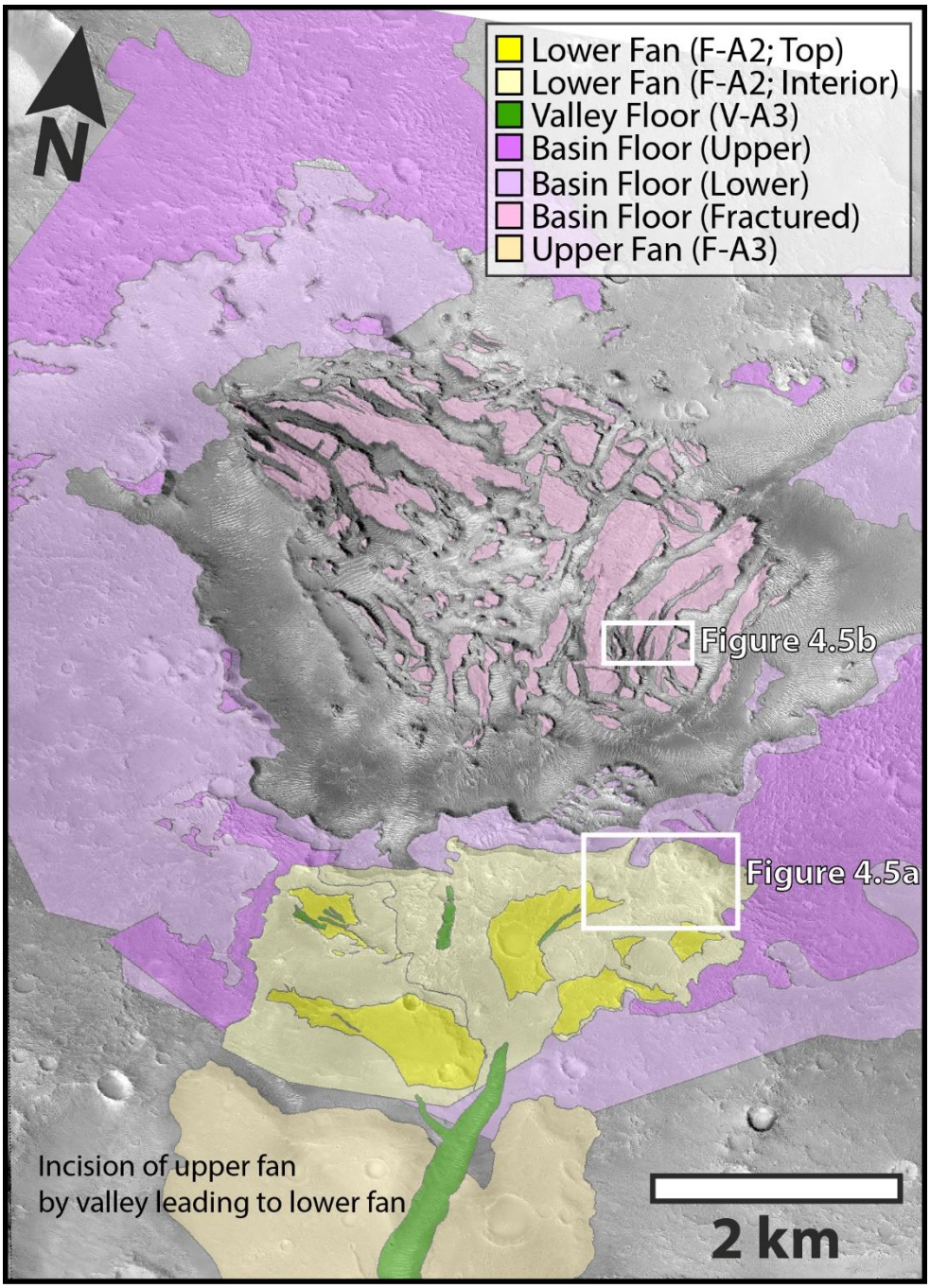

Figure 4.4 *– Preliminary mapping of basin floor and sediment fan deposits, in the basin between valley segments V-A2 and V-A3. Two fans are mapped at the south edge of the image, with the*

higher fan (F-A3) incised by the terminal end of valley V-A3, to form a lower fan (F-A2) which displays some areas of complex interior bedding structures. Marginal basin deposits appear to be layered (dark purple over light purple), and are thicker towards the centre of the basin, gradually thinning to an uncertain contact with the surround terrain. In the deepest parts of the basin, are heavily fractured deposits with a rippled surface texture.

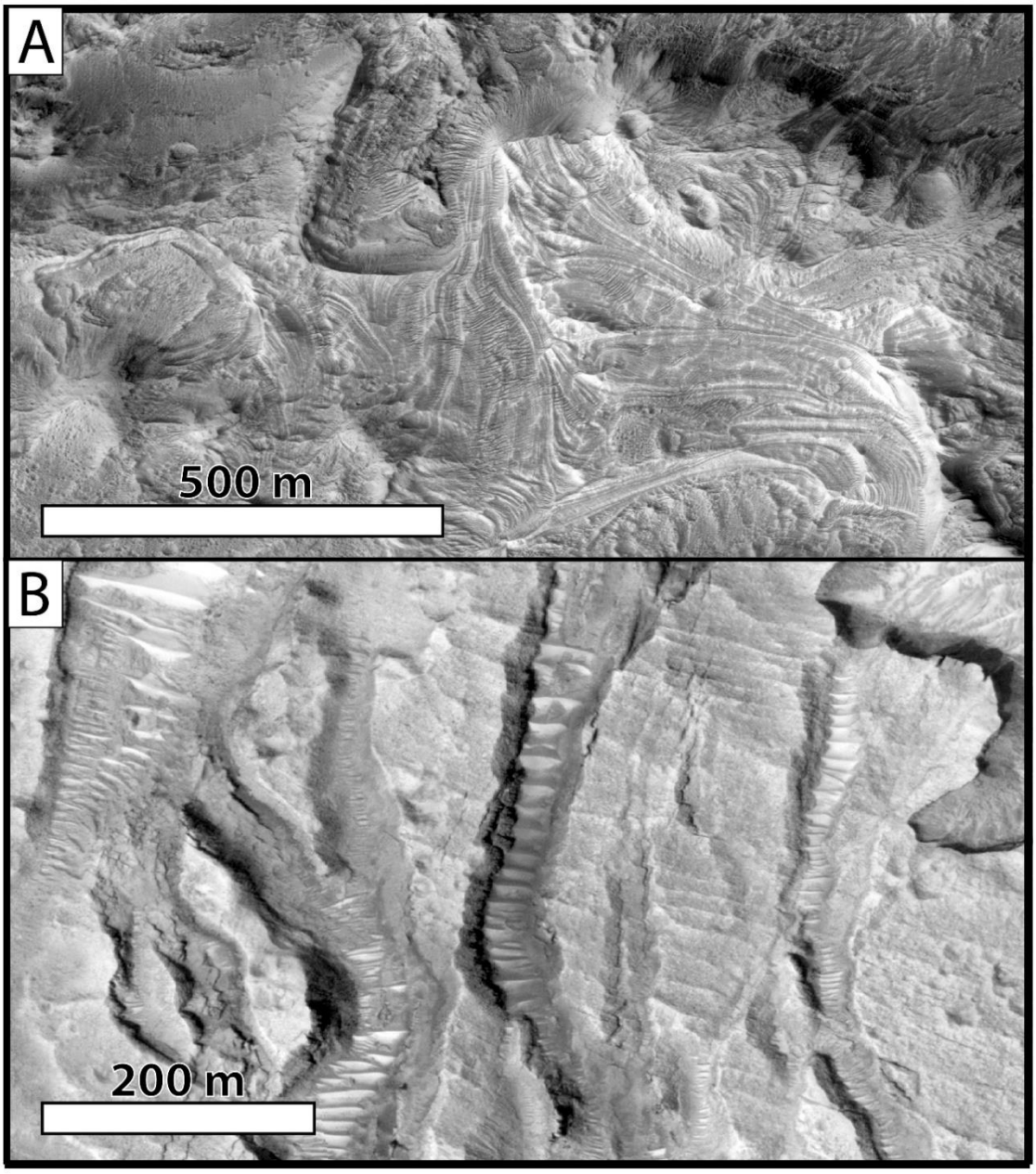

Figure 4.5 *– Detailed views of basin floor and sediment fan deposits, displaying: (A) Complex layering within sediment fan F-A2 at the termination of valley V-A2; and (B) fractured basin floor deposits within the deepest section of the same basin, characterised by angular fractures and a rippled surface appearance. (HiRISE ESP_032283_2115)*

Two fans at the terminus of valley V-A3 are situated at different elevations, with the upper fan (F-A3) incised by the valley which terminates at the lower fan (F-A2) (**Figure 4.4**). The upper fan (F-A3) has a sharply-defined lobate form with steep distal

edges, and sub-horizontal, parallel, ~1 m thick layering. The lower fan (F-A2) is heavily degraded, with poorly-defined edges, and an irregular surface topography. The internal structure of F-A2 appears to be complex (**Figure 4.5a**), with layering ~1–10 m thick, steeply dipping and possibly crosscutting with stacked lobes and channels also visible. Some areas are densely covered by aeolian bedforms suggesting a fine grained material comprises the fan. The fan (F-A4) at the terminus of valley V-A4 nearly covers the floor of an eroded impact crater. The fan surface is heavily cratered but overall sub-horizontal, with steep distal edges, a number of shallow channels, and ~1 m thick, sub-horizontal, parallel bedding exposed in the walls of impact craters.

Basin floor deposits with a fractured appearance are observed within deeper areas palaeolake basins L-A3, L-A4, L-A5 & L-B1 (**Figure 4.4**). These deposits are characterised by raised blocks separated by steep-sided, flat-floored fissures (**Figure 4.5a**). The sides of fractured blocks reveal fine (~1–10 m) layering, and the surfaces of some blocks display a corrugated appearance, with the orientation of minor fractures apparently influenced by the orientation of surface ripples.

The largest fan (F-A1) is situated at the dichotomy at the terminus of valley V-A1, although part of the valley is obscured by superposing impact craters. Distal lobes appear to deflect around raised mounds and mesas, and although the contact relationship is unclear the fan appears to lie above transitional lowland terrains (Tanaka, Skinner et al. 2014). The fan surface is marked by numerous channels and hosts a high concentration of aeolian bedforms compared to surrounding terrains, suggesting the fan comprising finer grained material. Exposed layering is ~1 m thick, sub-horizontal and parallel.

4.3.3 OPEN BASIN PALAEOLAKES

Seven possible palaeolake basins were identified where closed topographic basins are situated at the heads of valleys, or transected by valleys. These were numbered in order of increasing elevation from the dichotomy as follows; three (L-A1–L-A3) associated with valley V-A1, one (L-A4) with valley V-A2, one (L-A5) with valley V-A3, one (L-A6) with

valley V-A4, and one (L-B1) with valley V-B1 (**Figure 4.6**). Outlet valley elevations (**Figure 4.3**) for valley extremity (VE), valley overflow (VO), and basin overflow (BO) were recorded, with each level interpreted and mapped as representing a possible equipotential surface and palaeolake base level. Palaeolake volumes were calculated for each of the fill levels based on the current topography (**Table 4.1**).

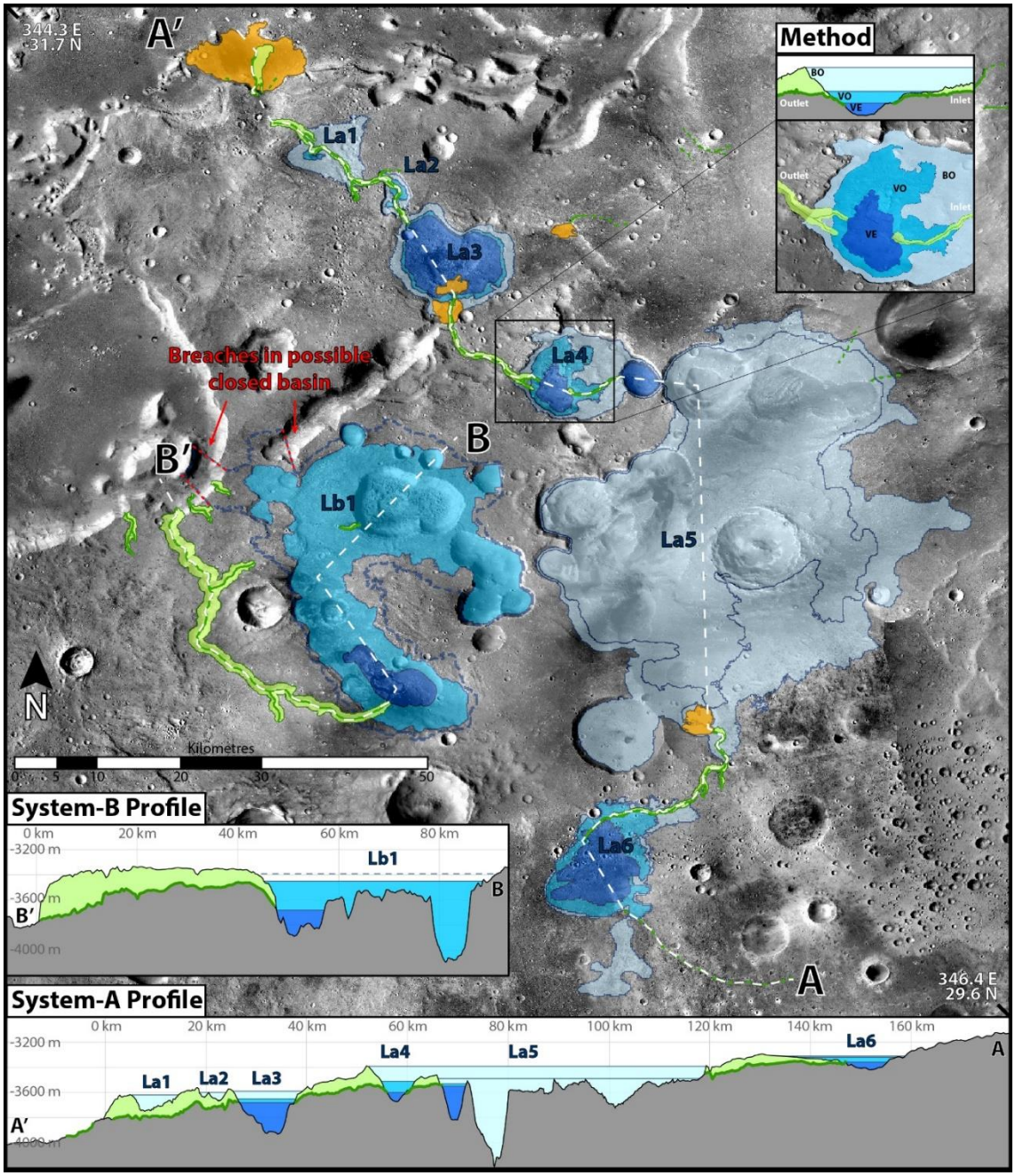

Figure 4.6 – Palaeolake extents and lake/valley system profiles based on outlet valley elevations: basin overflow (BO; light blue), valley overflow (VO; blue), valley extremity (VE; dark blue). System-A profile displays a close correlation of palaeolake surfaces with inlet valleys and sediment fans. System-B map and profile include an approximate basin overflow level (dashed blue line), defining

a nearly closed contour with the narrow areas open to the lowlands (red dashed lines). (both profiles displayed at the same scale and vertical exaggeration) (CTX imagery)

The basin overflow (BO) level represents the highest possible palaeolake level within each basin, based on a fill and spill model in which a basin filled with water and then overflowed on a topography existing before full incision of an outlet valley. The valley overflow (VO) level represents the lowest palaeolake level maintaining drainage through the outlet valley, based on overflow out of a water filled basin along the fully incised outflow valley floor. The valley extremity (VE) level, does not easily fit into a framework of basin overflow and outlet valley incision like the BO and VO levels, but has been recorded here as another possible indicator of palaeolake base level.

Table 4.1 *- Palaeolake surface elevations and dimensions for each of the three outlet defined fill levels (BO, VO, VE) within each of the seven palaeolake basins (L-A1-LA6, L-B1). Drainage catchment areas are shown for individual palaeolake basins and cumulatively for palaeolakes in the system-A chain*

			Correlated Base Level Elevations			Palaeolake Dimensions				Drainage Catchment	
Palaeolake	Fill Level	Surface Elevation (m)	Inlet Valley Term. (m)	Mean Sed. Fan (m)	Mean Low Slope Reach (m)	Area (km^2)	Volume (km^3)	Mean Depth (V/A) (m)	Max Depth (m)	Sub-basin (km^2)	Total Basin (km^2)
L-A1	BO	-3620	-	-	-	55	4.08	76	200	498	69,347
	VO	-3770	-	-	-	2.6	0.06	14	50	-	-
L-A2	BO	-3600	-	-	-	14	0.79	58	140	87	68,849
	VO	-3660	-	-	-	6.1	0.17	28	80	-	-
L-A3	BO	-3590	-	-3594	-3608	135	18.5	138	370	971	68,762
	VO	-3650	-	-	-	98	11.5	117	310	-	-
	VE	-3680	-3677	-3709	-	83	8.82	107	280	-	-
L-A4	BO	-3390	-	-	-3437	1,691	456	271	1,110	252	67,791
	VO	-3510	-	-	-3551	52	3.45	67	170	-	-
	VE	-3600	-3607	-	-	15	0.63	41	80	-	-
L-A5	BO	-3490	-3445	-3483	-	1,062	311	300	1,010	12,955	67,539
	VO	-3530	-	-	-	13	2.05	163	320	-	-
	VE	-3550	-	-	-	12	1.80	152	300	-	-
L-A6	BO	-3310	-	-	-	188	7.85	42	180	54,584	54,584
	VO	-3320	-	-	-	125	6.15	40	170	-	-
	VE	-3360	-	-	-	63	1.90	28	130	-	-
L-B1	BO	-3390	-	-	-	803	154	192	840	3,303	-
	VO	-3450	-	-	-	586	106	183	780	-	-
	VE	-3680	-	-	-	38	2.96	79	230	-	-

4.3.4 HIGHLAND DRAINAGE CATCHMENTS AND LOWLAND SINKS

Drainage catchments were calculated on a topography with all local sinks filled to determine the maximum extent of highland areas where accumulated surface water could drain into the northern lowlands (**Figure 4.7**). Two drainage end points were chosen where valleys V-A1 and V-B1 terminate at the dichotomy, describing two drainage basins, 'A' & 'B' respectively, separated by a drainage divide. Drainage catchment 'A' encompasses an area of 69,404 km^2 which extends south nearly to the edge of Mawrth Vallis. In contrast, the area of drainage catchment 'B' is an order of magnitude smaller at 3,393 km^2, and only extends a maximum of ~65 km from palaeolake L-B1. All the palaeolakes identified in this work fall within one of the two catchments, with the majority (L-A1 to L-A6) within catchment 'A' and only one (L-B1) within catchment 'B'. The drainage divide runs directly between the narrow (<2 km) distance between palaeolakes L-A5 and L-B1, the two largest in the study area, indicating no surface drainage connection between these two water bodies. Drainage sub-basins were calculated for each of the identified palaeolakes, and cumulative catchment areas calculated with higher sub-basins contributing to progressively lower sub-basins (**Table 4.1**).

Both drainage systems 'A' and 'B' terminate at the planetary dichotomy, at an elevation enclosing the entire northern lowlands. Locally however, the area surrounding the valley termini defines a nearly closed basin with only limited lower elevation gaps between flat topped mesas and mounds (**Figure 4.7**). The mean elevation of fan F-A1 is -3940 m, defining a possible basin with a total perimeter of ~408 km, which is closed along 99% of its length, with the maximum gap to lower elevation areas being 2.7 km. The maximum elevation of fan F-A1 is -3778 m, defining a wider possible basin with a perimeter of ~499 km, which is closed along 87% of its length, with the widest gap to lower elevation areas being 15 km.

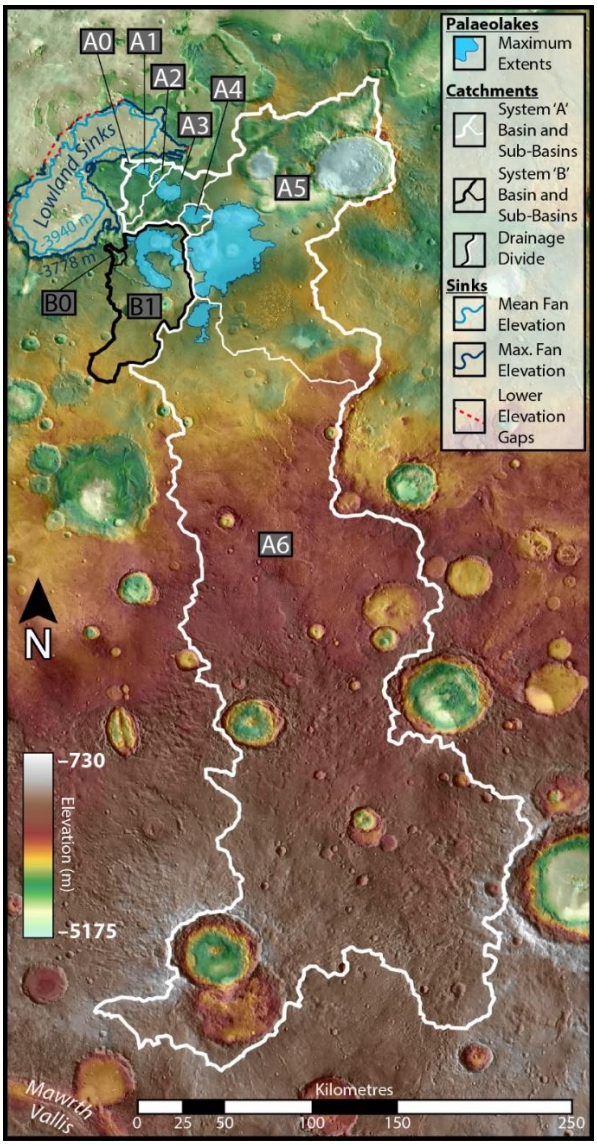

Figure 4.7 – Highland drainage catchments for palaeolake systems 'A' (white borders) and 'B' (black borders) terminating at the dichotomy, showing numbered sub-basins (thinner white and black borders respectively) for each individual palaeolake (light blue areas). Possible base levels within lowland sinks are shown for the mean (light blue dashed line) and maximum (dark blue dashed line) elevations of sediment fan F-A1, indicating basins open to the entire northern lowlands but only breached at narrow areas between flat topped mesas (red dashed lines). (THEMIS imagery, MOLA topography)

4.3.5 ASSOCIATED MORPHOLOGICAL FEATURES

4.3.5.1 BASIN MORPHOLOGY

Impact craters form ubiquitous topographic basins across the surface of Mars, and catalogued martian palaeolakes are often hosted within these conspicuous features (Cabrol and Grin 1999, Goudge, Aureli et al. 2015). The irregular palaeolake geometries exhibited in this study suggest a variety of basin origins, and described here are four basin

types defined by geometry, morphology and topographic profile as: (1) pristine impact craters, (2) filled/degraded impact craters, (3) asymmetrical pits, and (4) undefined basins. (**Figure 4.8**). These basins are then assessed in terms of relationship and influence on mapped palaeolake areas, depths and volumes.

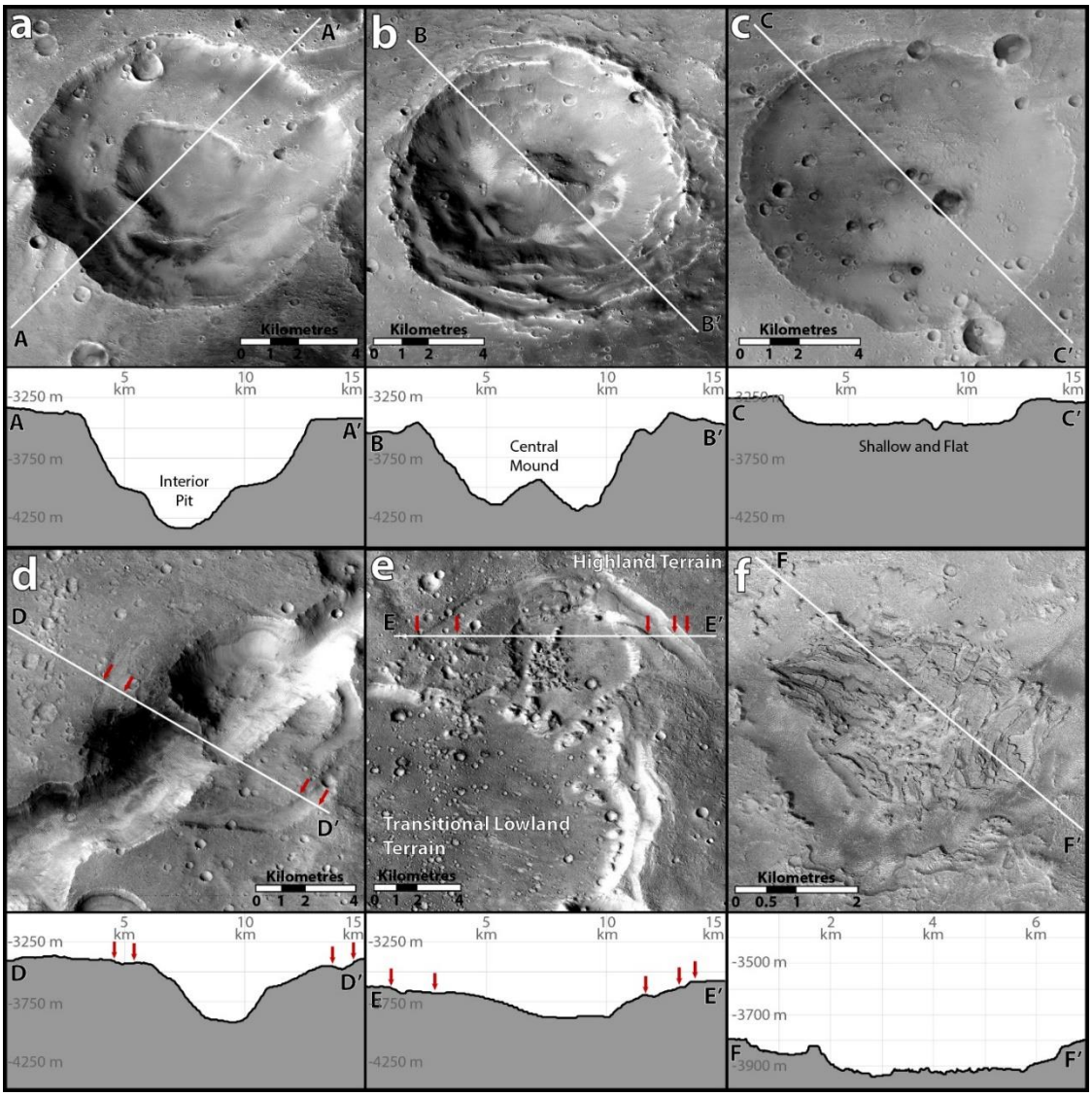

Figure 4.8 *– Morphological features associated with palaeolake basins, in plan-view and profile: (a) asymmetrical pit displaying no raised rim, steep sides, and a secondary interior pit, (b) pristine impact crater displaying raised rim, steep sides, and central mound, (c) degraded impact crater displaying slight raised rim and shallow flat floor, (d) an elongate asymmetrical pit apparently formed from coalesced circular and sub-circular pits, and surrounded by linear scarps (red arrows), (e) linear scarps (red arrows) arranged along the edge of a large flat-topped mesa, (f) fractured basin floor deposits. (North is up in all images. Profiles for a-e shown at the same vertical exaggeration) (CTX imagery)*

Pristine impact craters (**Figure 4.8b**) exhibit raised rims, steep interior sides, a uniform depth to diameter ratio, and often have raised central peaks and ejecta blankets.

These craters are thought to postdate the palaeolakes, but only the two largest palaeolakes (L-A5 and L-B1) overlap with large pristine impact craters or ejecta and do not appear significantly influence the palaeolake extents or dimensions. Filled, eroded, or otherwise degraded impact craters (**Figure 4.8c**) are typically shallow and flat floored in profile, with no uniform depth to diameter ratio. Palaeolake basin L-A4 is situated entirely within a degraded crater, and the southern edge of palaeolake basin L-A5 is partially defined by multiple craters.

Asymmetrical pits (**Figure 4.8a**) constitute a third distinct category of basins limited to the Noachian highland terrains and concentrated near the mapped palaeolakes. Small asymmetrical pits are bowl-shaped in profile and circular or semi-circular in plan-view. Larger examples appear to be composed of conjoined smaller pits, and are typically asymmetrical with cuspate or scalloped edges and narrow curvilinear interior ridges. Pit edges are sharply-defined, without raised rims, and have relatively consistent depths with no uniform depth to diameter ratio. Some asymmetrical pits also host secondary interior pits which are morphologically similar to the primary pits. Palaeolake L-A2 is situated completely within an asymmetrical pit, and although limited lengths of other palaeolake edges (L-A4, L-A5, L-B1) are defined by asymmetrical pits the majority are situated fully within palaeolake basins L-A5 and L-B1. Unlike pristine or degraded impact craters, asymmetrical pits appear to be the result of more complex formation processes. Asymmetrical pits appear to be one of the youngest features in the study area, forming abrupt, steep, sharp edges where they intersect degraded impact craters, valleys (V-A3), and the ejecta of pristine impact craters (**Figure 4.1c**). Given the significant depth of these features, the volumes in basins with asymmetrical pits (L-A4, L-A5, and L-B1) may be gross overestimates.

Besides the palaeolakes hosted within impact craters (L-A4) and asymmetrical pits (L-A2), and the limited sections of palaeolake extents partially defined by these features, the majority of palaeolakes (L-A1, L-A3, L-A5, L-A6 and L-B1) identified in this study are hosted within relatively shallow, irregular shaped basins without conspicuous edges or easily definable origins.

4.3.5.2 Dichotomy Scarp

The dichotomy scarp marks the sharp contrast between the highland and lowland terrains, and has a prominence of up to ~600 m in the study area, reducing to ~300 m and ~100 m at the terminus of valleys V-B1 and V-A1 respectively. In profile the dichotomy scarp is very steep, and in planform displays a cuspate geometry similar to the asymmetrical pits. These attributes are also shared by the scarps surrounding large flat-topped mesas, and may indicate a common formational origin for all three features.

The dichotomy scarp where intersected by valley V-A1 (-3900 m) is low and gently sloping, and sediment fan F-A1 appears to have formed over lowland deposits (**Figure 4.3a**). In contrast, valley V-B1 (-3800 m) terminates abruptly at the dichotomy with no sediment fan and without extending beyond the high steep scarp in this area (**Figure 4.3d**). These relationships suggest that in the area of valley V-A1 the dichotomy scarp predates fluvial activity, but that in the area of valley V-A1 alteration of the dichotomy scarp has occurred which postdates fluvial activity.

4.3.5.3 Linear Scarps and Troughs

Linear scarps with prominences of ~1–100 m are observed within the Noachian highland terrains, commonly as pairs and sets arranged in parallel, with depressed troughs between inward dropping scarps, or stepwise with scarps set progressively lower. In no cases do the low sides of parallel scarps face outwards to form a raised interior section. Linear scarps are concentrated near the margins of asymmetrical pits (**Figure 4.8d**), the dichotomy scarp and the edges of large flat-topped mesas (**Figure 4.8e**). They often mirror the geometry of these larger scarps, as inwardly depressed elliptical rings around asymmetrical pits, or parallel to the dichotomy and mesa edges, possibly indicating a linked origin or formation process.

4.3.6 Relative Age Relationships

Determination of absolute ages for martian valley networks is difficult due to the small and narrow areal extents available for crater counting. A method for buffered crater

counting has been successful in dating large valley networks (Fassett and Head III 2008), but the relatively short valleys (<47 km) in this study precluded this as an option and no valleys or palaeolakes coincide with impact ejecta blankets large enough for crater counting. As such, this work is limited to the apparent age relationships between features, and inferences based on the age of the terrains which host them.

All of the valleys within this study are incised into Noachian aged highland terrains, with some valleys (V-A2 to V-A4) and sediment fans (F-A4) clearly overlying degraded impact craters. Although valley V-B1 appears to be either incised through or partially covered by the ejecta of a ~5 km impact crater there are no unambiguous relationships between fluvial features and large pristine impact craters (**Figure 4.1c**). The approximate age of valleys, sediment fans and palaeolakes is therefore presumed as matching the Noachian and Hesperian peak in fluvial activity, postdating ancient degraded impact craters and predating pristine impact craters. However, a younger age cannot be excluded.

4.4 DISCUSSION

4.4.1 ANALYSIS OF PALAEOLAKES AND VALLEYS

4.4.1.1 PALAEOLAKE OVERFLOW AND VALLEY INCISION

Basin overflow (BO) and valley overflow (VO) levels are interpreted as marking temporally distinct base levels at the initiation and cessation of drainage out of each palaeolake basin, with an interceding period of falling palaeolake levels driven by outlet valley incision.

Basin overflow levels represent the base levels and extents of palaeolakes at the initiation of basin overflow and outlet valley incision, and have been similarly calculated in other palaeolake studies (Goudge and Fassett 2018, Salese, Kleinhans et al. 2020) (**Figure 4.6**). Basin overflow levels within catchment 'A' (L-A1 to L-A6) all define basins with the low edge coincident with an outflow valley, supporting a model of outlet valley

incision initiated as higher basins filled and spilled over to fill lower basins, in contrast to an alternate basin breaching model of sapping erosion and upstream propagation of valley heads from lower to higher basins.

In contrast, the basin overflow level in palaeolake basin L-B1 does not describe a closed basin, and the contour at this elevation (-3360 m) is open to the northern lowlands and inconsistent with a palaeolake on the current topography. As a maximum palaeolake level cannot be determined with certainty, the -3390 m contour was considered to be a useful approximation of palaeolake level prior to outlet valley incision, defining a nearly closed basin only broken at the dichotomy scarp and asymmetrical pits which appear to postdate palaeolakes and valleys. The outlet valley (V-B1) of basin L-B1 is also in close proximity to three large craters, and the valley sides may have been raised by ejecta postdating valley incision.

Incision of outlet valleys progressively lowered the elevation of valley heads, in turn lowering palaeolake base levels, reducing palaeolake extents and allowing inlet valleys to incise further and lower into palaeolake basins (**Figure 4.6**). Valley incision may have progressed gradually as a result of continuous drainage, or punctuated by multiple discrete overspill events. Valley incision and erosion rates have been calculated for other valley systems on Mars (Rosenberg and Head 2015), but are limited due to poorly constrained values defining lithology and rheology. Incision and flow rates were not quantified in this study, but palaeolake base level reductions resulting from outlet valley incision describe a trend from the top to bottom of system 'A', with a minimum change of 10 m in basin L-A6 to a maximum of 150 m in basin L-A1, indicating greater flow through and erosion for valleys towards the end of the system.

Outlet valley incision continued to reduce palaeolake extent until input to palaeolakes was no longer sufficient to overflow the basins, and the valley overflow (VO) levels represent the open-basin palaeolakes at the cessation of outlet valley incision.

4.4.1.2 CORRELATION OF PALAEOLAKE BASE LEVELS

Possible oceans in the northern lowlands and closed basin palaeolakes, which by definition lack outlet valleys, are often identified based on observations of valley terminations, channel topography, deltas, palaeoshorelines, and basin floor deposits (Di Achille and Hynek 2010, Goudge, Aureli et al. 2015, Goudge and Fassett 2018, Dickeson and Davis 2020). In isolation these diverse features may not conclusively indicate a standing body of water, but constitute supporting base level evidence where observed within outlet valley defined palaeolake basins and correlating with or situated below basin and valley overflow levels (**Figure 4.6**).

The observed location and elevation of valley terminations can result from cessation of incision at a standing body of water, or due to changes in lithology, slope, or subsequent destruction or burial of a valley. The three major valleys (V-A2 to V-A4) which terminate within palaeolake basins (L-A3 to L-A5) terminate on slopes which continue basinward and do not coincide with any obvious lithological changes. Two valley terminations (V-A2 & V-A3) correlate closely to valley extremity levels (L-A3, +3 m; L-A4, -7 m), and although valley V-A4 is poorly correlated to a basin overflow level (L-A5, +45 m) the elevation (-3445 m) falls between the basin overflow levels of L-A4 (-3390 m) and L-A5 (-3490 m).

Sediment fans are difficult to characterise as sub-areal alluvial fans or deltas, but the flat surfaces and steep distal edges of fans in this study support interpretation as possible deltas (Di Achille and Hynek 2010, Fawdon, Gupta et al. 2018). The mean elevation of two possible deltas (F-A2 & F-A4) correlate well to basin overflow levels (L-A3, -4 m; L-A5, -7 m), and that of fan F-A3 situated somewhat below the valley extremity level (L-A3, -29 m).

A stable base level at the terminus of an inlet valley can affect the valleys longitudinal profile, resulting in a low slope at the valleys lower reaches (Duran, Coulthard et al. 2019). The mean elevations of low-slope lower-reaches for palaeolake inlet valleys (L-A2 to L-A4) do not correlate well to basin overflow (L-A3, -18 m; L-A4, -

47 m) or valley overflow levels (L-A4; -41 m), but do fall below outlet defined palaeolake levels in each basin.

4.4.1.3 NEGATIVE SLOPE OUTLET VALLEYS

Unlike the basin overflow (BO) and valley overflow (VO) levels, the valley extremity (VE) levels do not easily fit into a framework of palaeolake overflow and drainage. In a draining palaeolake, the VE level would be expected to match the VO level, as the highest point of the outlet valley would be at the valley head. Instead, every valley extremity level observed in this chapter is lower than the corresponding valley overflow level. This is particularly evident within basins L-A4 (60 m) and L-B1 (260 m), and although basin L-A2 lacks a valley extremity level the valley floor within the basin is ~70 m lower than the valley overflow level (**Figure 4.3**). At the edges of these palaeolake basins the valley slope is negative relative to the overall trend of the valley, and considered here are three possible scenarios accounting for this observation.

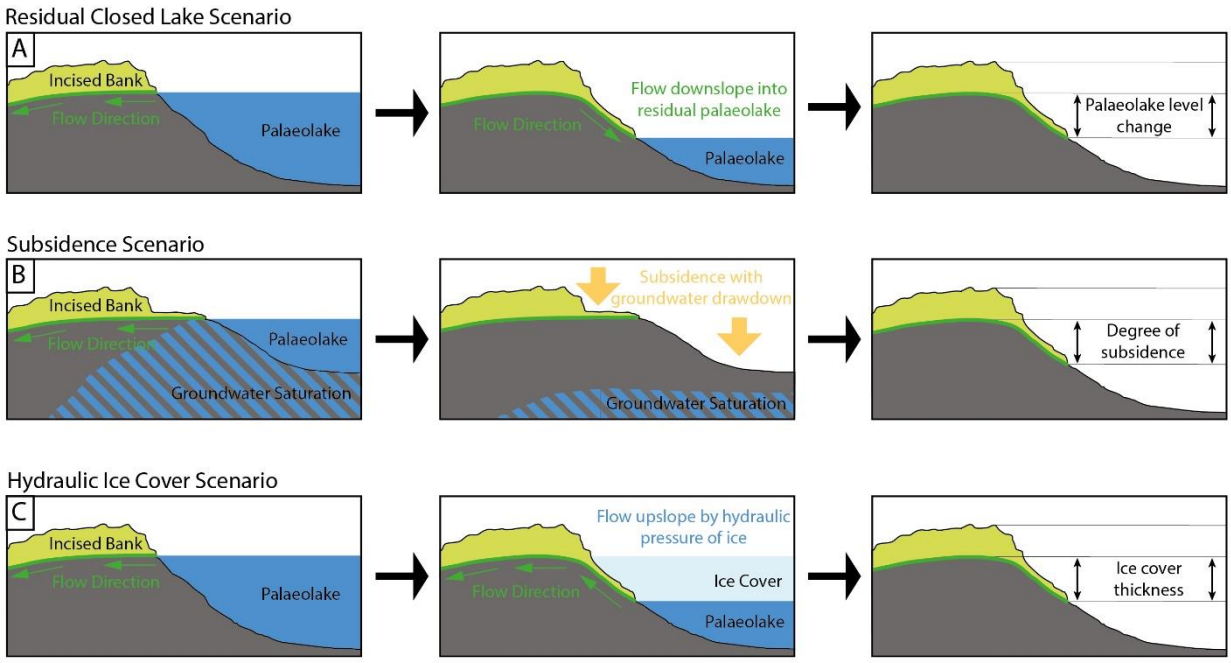

Figure 4.9 *– Scenarios accounting for the formation of observed negative slope outlet valleys.* ***(a)*** *Residual closed lake; in which a short and shallow section of valley is incised into the basin at a time after base level has fallen to form a closed basin palaeolake.* ***(b)*** *Subsidence; in which the outlet valley is formed by drainage out of the palaeolake followed by subsidence driven by groundwater drawdown within the basin.* ***(c)*** *Hydraulic ice cover; flow up and out of the basin is facilitated by significant pressure resulting from ice coverage.*

Valley extremity levels may represent the base levels of closed basin palaeolakes, with negative slope outlet valleys formed by a basinward flow of surfacing groundwater or minimal surface accumulation after cessation of palaeolake drainage through the system (**Figure 4.9a**). This scenario could also explain the similarly steep and shallowly incised inlet valley terminations which correlate to outlet valley extremity levels within basins L-A3 and L-A4.

Alternatively, subsidence in basins subject to significant desiccation or groundwater drawdown has been recorded in terrestrial basins on historical and geological time scales (Ireland, Poland et al. 1984). In this scenario, negative slope outlet valleys apparent on the current topography would have formed during palaeolake drainage, and later lowered by subsidence of the basin (**Figure 4.9b**).

A final consideration is that negative slope valleys formed by upward flow facilitated by the pressure of an overlying ice sheet, as observed in subglacial lakes on Earth (Cook and Swift 2012)(**Figure 4.9c**). Ice coverage would have profound implications on the interpretation of fluvial and lacustrine systems in this study and across the region, and other studies postulate periods of extensive ice coverage in the southern highlands (Baker, Strom et al. 1991, Head and Marchant 2014, Palumbo, Head et al. 2018). Glacial or sub-glacial landforms were not observed in this study, but this scenario should be revisited if further evidence of regional ice sheets comes to light.

4.4.2 NATURE OF THE DICHOTOMY MARGIN

Globally mapped shorelines of postulated lowland oceans are generally poorly constrained spatially or by elevation (Sholes, Dickeson et al. 2021). However, within Arabia Terra potential shorelines closely follow the dichotomy, accounting for a relatively narrow range of elevations within the study area; one transects palaeolake L-A1(−3770 m)(Parker, Saunders et al. 1989), three approximately follow the dichotomy near the termination of valley V-A1 (~−3900 - −3600 m)(Clifford and Parker 2001, Carr and Head 2003, Webb 2004), and a further three are traced through the lowlands ~60-70 km NNW of F-A1 (~−4000 m)(Parker, Saunders et al. 1989, Carr and Head 2003, Webb 2004).

Valley terminations and possible deltas have also been interpreted as representing the global margin and base level of a hemisphere spanning ocean on Mars (-2540 m)(Di Achille and Hynek 2010), and through detailed analysis of individual deltas (-2500 m)(Fawdon, Gupta et al. 2018). In contrast, topographic analysis of possible deltas in other regions indicate a number of lowland palaeolakes or small seas adjacent to the dichotomy rather than a hemisphere spanning ocean (Rivera-Hernández and Palucis 2019, García-Arnay and Gutiérrez 2020).

Situated at the dichotomy, sediment fan F-A1 (−3940 m), along with the termination (−3815 m) and low slope lower reaches (−3791 m) of valley V-A1 constitute possible base levels within the northern lowlands which correlate well to global shorelines mapped along the dichotomy, but are a poor match to delta defined ocean base levels. On the current topography the lowland base levels in this study would indicate a water body filling the entire northern lowlands, but on local topography altered by a few tens of metres would instead indicate a palaeolake limited to a local lowland basin as illustrated in **Figure 4.7**.

The morphological similarities between the dichotomy scarp, mesa scarps, and the sides of asymmetrical pits (**Figure 4.8**) suggest a possible common origin, consistent with collapse postdating fluvial and lacustrine activity. A similar origin has also been proposed for mesas in the Oxia Planum area to the southeast of this study (McNeil, Fawdon et al. 2021). Collapse along the edges of flat topped mesas would indicate a closed-basin palaeolake in the lowlands, and collapse along the dichotomy and within asymmetrical pits would explain the lack of a sediment fan or clear termination where valley V-B1 intersects the dichotomy and the open contour for palaeolake L-B1. Significant changes in the morphology and position of the dichotomy since the Noachian would have important global implications for the dichotomy and lowland ocean shorelines (Dickeson and Davis 2020).

Valley V-B1 also displays a pronounced knickpoint corresponding to the intersection of a tributary valley (**Figure 4.3**). This profile may indicate a significant

lowering of base level within the northern lowlands basin, and more recent drainage forming the knickpoint and tributary. Similar knickpoints elsewhere on Mars have been interpreted as representing multiple episodes of fluvial activity and changes in base level (Goudge and Fassett 2018, Duran, Coulthard et al. 2019).

4.4.3 REGIONAL HYDROLOGY AND MARTIAN PALAEOLAKES

Global palaeolake catalogues have so far identified only one open-basin palaeolake in western Arabia Terra (Fassett and Head 2008, Goudge, Head et al. 2012), but local studies to the north and south of the study have identified additional examples (Wilson, Howard et al. 2016, Fawdon 2018). The seven open-basin palaeolakes in this work therefore fill a gap in currently mapped palaeolakes and are significant in further characterising the style, distribution, and frequency of lacustrine processes in the region.

The palaeolakes and valleys discussed in this work are situated within Noachian highland terrains (Tanaka, Skinner et al. 2014), but this only affords an upper limit to their age. The peak in fluvial and lacustrine processes on Mars is generally agreed to have occurred during the late Noachian to early Hesperian (Fassett and Head 2008, Goudge, Head et al. 2012, Goudge, Fassett et al. 2016), although some studies suggest palaeolakes as late as the middle Amazonian (Wilson, Howard et al. 2016). One global study associates palaeolakes fed by extensive valley networks with an earlier period of formation prior to 3.7 Ga, and those fed by limited valleys with a later period of reduced hydrological activity (Goudge, Fassett et al. 2016). The palaeolakes in this study are difficult to categorise by these criteria, as they constitute a long chain of palaeolakes, only connected by short, non-branching valleys. However, the greater supply and duration of liquid water required to fill open-basin palaeolakes leads us to conclude that the palaeolake systems described in this work fit with the period of palaeolake activity prior to 3.7 Ga.

The palaeolakes in this study are slightly smaller and shallower than the mean of globally catalogued open-basin palaeolakes, but within the global range of dimensions (Fassett and Head 2008). A high ratio of palaeolake volume to catchment area has been highlighted as an indication of filling by groundwater rather than surface runoff, but only

for palaeolakes not fed by other palaeolakes as part of a chain (Fassett and Head 2008). Most palaeolakes identified in this chapter are fed by drainage from higher palaeolakes, and therefore a comparison is only useful for palaeolakes L-B1 and L-A6 which are not fed by higher palaeolakes, and L-A5 which is only fed by a much smaller palaeolake (L-A6). Of these three palaeolakes, only L-B1 displays a ratio indicative of groundwater as the dominant water source. Furthermore, palaeolakes L-B1 and L-A6 do not have inlet valleys, and although this is another possible indication of filling by groundwater, other studies have shown that significant accumulation and surface flow is possible with little to no channelization (Lamb, Dietrich et al. 2008).

Western Arabia Terra has been identified as a region of significant groundwater upwelling, particularly in areas adjacent to the dichotomy (Andrews-Hanna, Zuber et al. 2010), and groundwater was likely significant in filling palaeolakes across the region (Fassett and Head 2008). Although filling and overflow of the palaeolakes studied in this chapter appears to have been driven by drainage from higher palaeolakes, it is likely that upwelling groundwater played a role in the original filling of palaeolake basins, with early palaeolakes possibly existing as unconnected closed-basin palaeolakes before becoming sufficiently full to breach and drain. All the palaeolakes discussed in this chapter were identified in association with fluvial valleys, but if upwelling groundwater was the principal basin filling process then many other basins in the region could have hosted palaeolakes which never formed inlet or outlet valleys and thus remain unidentified.

The fractured basin floor deposits observed within some palaeolakes in this chapter are another feature common to many martian palaeolakes, with palaeolakes described to the north hosting a number of similarly fractured sedimentary deposits within the deepest modelled palaeolake basins (Wilson, Howard et al. 2016). Larger scale fractured floor deposits are found in association with numerous other palaeolakes on Mars (Goudge, Head et al. 2012), and in Xanthe Terra, to the south, these features are interpreted as forming by rapid discharge and eventual groundwater depletion within closed palaeolake basins (Sato, Kurita et al. 2010). Additionally, the rippled surfaces of some fractured floor deposits in this chapter appear analogous to the 'washboard' terrains

observed in Gale crater, where they are interpreted as aeolian dunes preserved beneath closed-basin palaeolake deposits (Milliken, Ewing et al. 2014). The Mars2020 mission is in the early phases of science operations in Jezero crater, but will hopefully soon provide examples of sedimentation within an open-basin palaeolake.

4.4.4 LOCAL HYDROLOGICAL AND GEOLOGICAL EVOLUTION

This section outlines the probable sequence of hydrological and geological processes leading to the palaeolake and valley landforms observed in this region of Arabia Terra. Palaeolake basin L-A6 is the only basin consistent with filling by surface accumulation, and is the highest basin in the area, and the strong correlation between inlet and outlet valleys indicates that all the other palaeolakes besides L-B1 were fed by inlet valleys ultimately draining from palaeolake L-A6.

In system 'A', a continuous chain of valleys and lakes drained water and sediment from the highlands to the lowlands, with palaeolakes cascading down through the system from basin L-A6 (BO), draining through valley V-A4 to form sediment fan F-A4 and fill basin L-A4 (BO), draining through valley V-A3 to form sediment fan F-A3 and fill basin L-A3 (BO), draining through valley V-A1 (**Figure 4.10e**). Valley V-A1 was originally three short isolated sections, with the first draining from L-A3 (BO) to fill basin L-A2 (BO), a second section draining L-A2 (BO) to fill basin L-A1 (BO), and a third section draining L-A1 (BO) and terminating at the dichotomy to form sediment fan F-A1.

In system 'B', the limited drainage catchment and lack of inlet valleys indicate that basin L-B1 (BO) was filled by groundwater, and then drained through valley V-B1 to debouch into the lowlands (**Figure 4.10b**). The close proximity and correlated elevations of basin overflow levels in L-A4 and L-B1 could also indicate groundwater communication between the two systems, with filling of L-B1 partially by groundwater from system 'A'.

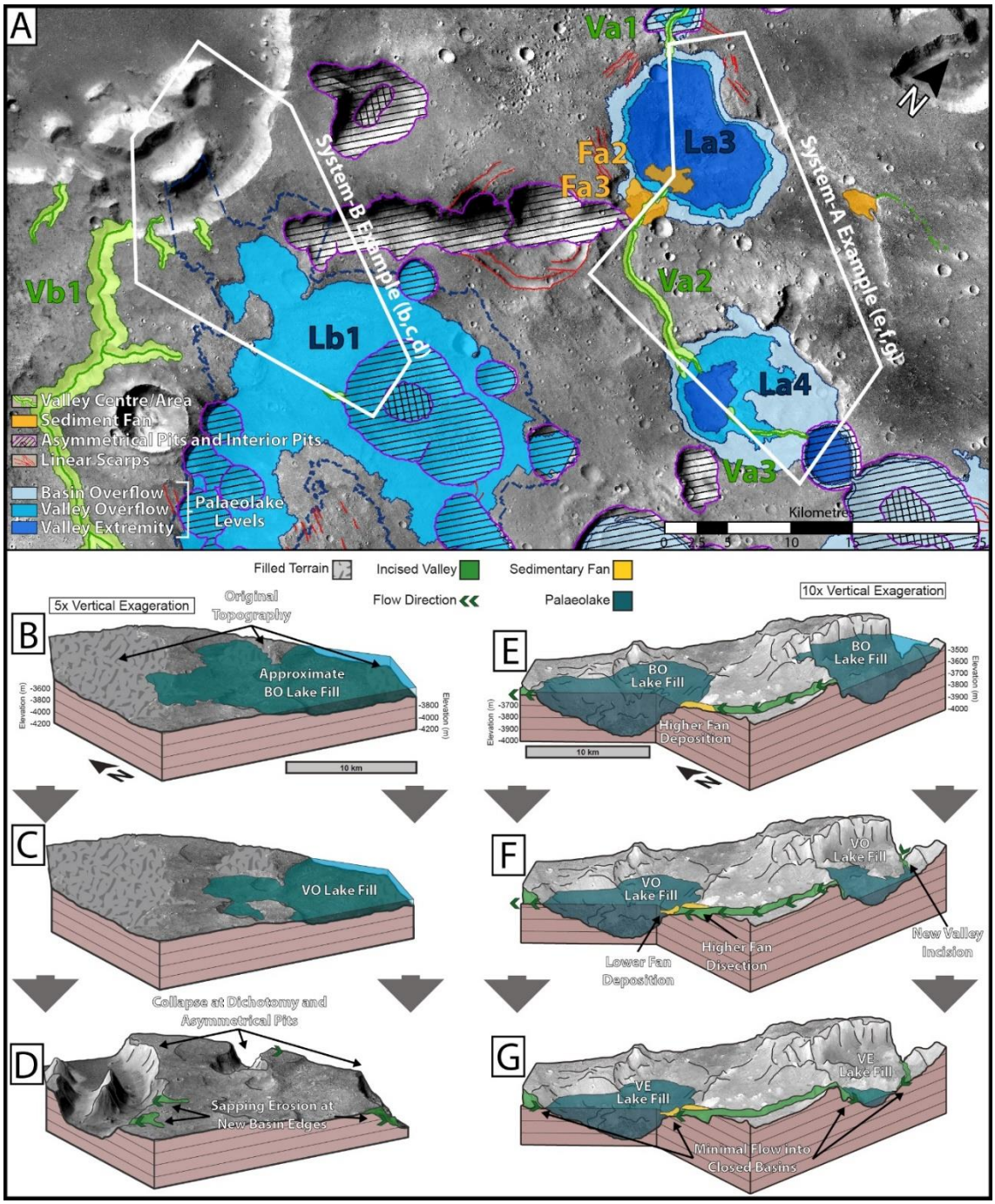

Figure 4.10 *– **(a)** Representative areas of system 'A' including palaeolake basins L-A3 and L-A4; and system 'B' including palaeolake basin L-B1 and the dichotomy scarp, and chronologies of fluvial and lacustrine processes in system 'A' **(e, f, g)** and system 'B' **(b, c, d)**. The top diagrams **(b & e)** show the highest palaeolake fill levels (BO) at the initiation of palaeolake drainage, **(e)** with the formation of fan F-A3 at the end of valley V-A2, **(b)** and an approximate topography with asymmetrical pits and the dichotomy scarp filled. The middle diagrams **(c & f)** show reduced palaeolake levels (VO) resulting from outlet valley incision while drainage out of the basins continued. **(f)** Fan F-A3 was incised through by valley V-A2 to form the new lower fan F-A2, and base level lowered within basin L-A4 so that valley V-A3 began to incise across the former lake floor. The bottom diagrams **(d & g)** show the lowest palaeolake levels (VE), likely fed by ground water or minimal surface accumulation, **(d)** and the current topography resulting from the formation of asymmetrical pits and the dichotomy scarp. (CTX imagery on CTX DEM topography)*

Continued drainage through both systems led to progressively lower palaeolake levels resulting from outlet valley incision (**Figure 4.10c, f**). Significant outlet valley incision resulted in complete drainage of the palaeolakes in basins L-A1 and L-A2, allowing inlet valleys to incise across the previously submerged lake floors to become one continuous valley (V-A1). Incision of valley V-A1 also caused base level to fall in basin L-A3 (VO), allowing inlet valley V-A2 to incise down and through sediment fan F-A3, with the apex of a new sediment fan (F-A2) forming further basinward at the new termination of valley V-A2. Incision of valley V-A2 caused a base level fall and significant reduction in extent within palaeolake L-A4 (VO), with the basin fed by a newly formed valley (V-A3) draining from palaeolake L-A5 (BO) and incising across the previously submerged palaeolake floor. The late exposure of V-A3 and sections of L-A1 in this area would also explain the relatively shallow incision depth of these valleys.

At the cessation of palaeolake overflow and drainage, palaeolakes were filled to the valley overflow level, and stable base levels of closed basin or ephemeral palaeolakes likely existed within some basins (L-A3–L-A6, L-A1) and evidenced by valley extremity levels (**Figure 4.10d,g**).

After drainage through the palaeolake systems had ceased, collapse within the highland terrains formed asymmetrical pits and modified the scarps at the dichotomy and the edges of flat topped mesas (**Figure 4.10d**). The result being a topography no longer commensurate with some calculated palaeolake volumes, or equipotential surfaces within basin L-B1 and a possible lowland basin.

4.5 CONCLUSIONS

High resolution CTX imagery and DEMs aided in the discovery and characterisation of this palaeolake system, and allowed for the precise calculation of palaeolake fill levels and drainage catchments. The inclusion of three temporally distinct palaeolake fill levels linked to different outlet valley elevations was key to understanding changes in palaeolake base level and valley incision over time, and allowed fully drained

palaeolake basins to be identified. Additional analysis of longitudinal valley profiles and possible deltas strengthened the evidence for these palaeolakes, and provided further insight into the hydrological evolution of the area.

That such a complex yet localised system has not been included in previous catalogues suggests that many more palaeolakes may exist on Mars than currently indicated, and will likely be revealed with the increased use of high resolution imagery and topography. Compared to crater hosted palaeolakes which are typically deep and exhibit clearly defined edges, palaeolakes of the type described here display more subtle topographic profiles and may be underrepresented in palaeolake catalogues. The conclusions regarding water sources, and regional hydrology from the features identified within this small study area warrant the undertaking of further detailed local and regional palaeolake investigations, and in depth analysis of palaeolakes that have so far only been catalogued and characterised generally. This study also shows the importance of small scale topographic features on local hydrology, and it is hoped that further investigations at this scale will be useful in defining regional hydrological trends and transitions from one region to another.

Continued discovery and classification of palaeolakes within the low-lying regions of Arabia Terra will increase the number of promising landing sites with prolonged histories of liquid water and astrobiological potential. The description of varied lacustrine and fluvial systems adjacent to the planetary dichotomy will also provide a broader understanding and context for the ExoMars and Mars2020 rover landing sites at Oxia Planum and Jezero Crater respectively.

5

Palaeolakes in the Region of Oxia Planum

The preceding chapter describes a previously undocumented system of palaeolakes, allowing a wide scope for novel observations and future work precisely due to the relative obscurity of the study area. In this chapter, the same methods of palaeolake identification and characterisation are brought to bear on Oxia Planum, the landing site of the upcoming ExoMars rover mission, and the high profile of the area presents advantages to the investigations in this chapter. Firstly, a wider range of orbital datasets and coverage, allows for more detailed observations and a broader comparison. Secondly, the research already undertaken and published in this area provides a detailed context in which to place findings, including: geological and hydrological histories; and tectonic deformation. Finally, the impending arrival of a rover to this area lends an increased immediacy and impact to any findings, and provides the rare opportunity for in-situ observation and verification of hypotheses made based on remote sensing. This chapter identifies and describes an extensive branching network of possible open-basin palaeolakes within the Coogoon Valles drainage catchment, which debouches at the planetary dichotomy within a possible closed-basin palaeolake in Oxia Planum. Palaeolakes in the area are also considered in relation to potential uncertainties in palaeolake identification due to subsequent topographic changes, addressed through the investigation of tectonic ridges and impact ejecta; and to identify probable eroded lake floor deposits which could have been transported to the landing site.

5.1 INTRODUCTION

Oxia Planum is a basin adjacent to the dichotomy in western Arabia Terra, which is set to become the landing site of the ESA-Roscosmos, ExoMars 'Rosalind Franklin' rover in 2023 (Quantin-Nataf, Carter et al. 2021). The site was selected to meet the primary mission aim to identify signs of past life, in an area with evidence of prolonged aqueous processes within Noachian aged terrains. The area primarily sits on the low side of the dichotomy, with the eastern end of the landing ellipse overlapping a possible delta at the terminus of Coogoon Valles, an extensive, branching valley network within the highlands (**Figure 5.1b**). This stretch of the dichotomy between Ares Vallis to the south and Mawrth Vallis to the north has also been interpreted as the palaeoshoreline of a northern hemisphere spanning ocean (**Figure 5.1a**) (Parker, Saunders et al. 1989, Parker, Gorsline et al. 1993, Clifford and Parker 2001, Ormo, Dohm et al. 2004), and although several palaeoshorelines are mapped through Oxia Planum, the veracity of these features is doubtful (Dickeson and Davis 2020, Sholes, Dickeson et al. 2021).

The ExoMars rover is equipped with a suite of instruments to detect chemical biosignatures, and will be the first mission with the capability to drill up to ~2 m under the martian surface to collect ancient samples shielded from the reducing conditions and harsh radiation on the surface of Mars (Vago, Westall et al. 2017). Orbital spectral observations indicate widespread phyllosilicate rich deposits within Oxia Planum, which will be the primary drilling targets thought to have the highest probability of hosting preserved biosignatures (Vago, Westall et al. 2017), and therefore, determining the origin of these deposits will be important in understanding the context of rover observations (Fawdon, Balme et al. 2021). Much work has focused on the geological and hydrological history of Oxia Planum (Hauber, Acktories et al. 2020, Ivanov, Slyuta et al. 2020, Quantin-Nataf, Carter et al. 2021), and possible upland source regions (Molina, Lopez et al. 2017, Fawdon 2018), yet the nature of phyllosilicate deposits in Oxia Planum is still debated, and may be either: authigenic, produced in-situ through diagenetic processes; or allochthonous, detrital material transported to the site and deposited. Possible depositional processes for the area are varied, and suggested origins include: volcanic air-

fall, or lava flows; aeolian sediments; and marine, or palaeolake deposits (Quantin-Nataf, Carter et al. 2021).

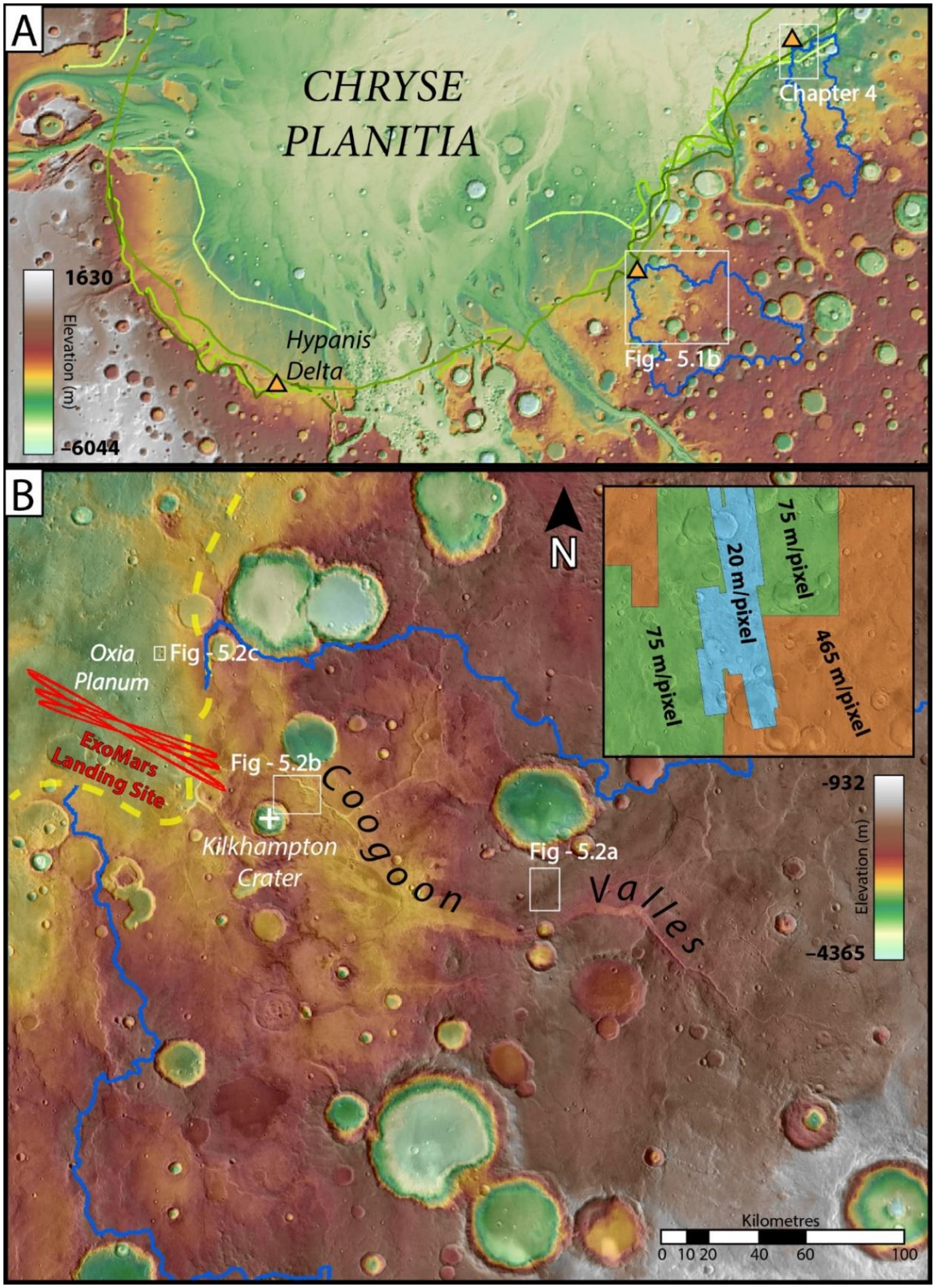

Figure 5.1 *– Context of Oxia Planum and Coogoon Valles in Arabia Terra and Chryse Planitia. (A) Idealised drainage catchments (blue outlines) defined by pour-points at sediment fans (orange triangles) at the dichotomy are shown for the Coogoon Valles drainage catchment (Fawdon 2018), and the palaeolakes studied in Chapter 4. Also shown are possible ocean shorelines as mapped in previous works (Parker, Saunders et al. 1989, Parker, Gorsline et al. 1993, Clifford and Parker 2001). (B) Study area of the present chapter, showing Oxia Planum and Coogoon Valles in relation to the*

landing ellipse of the ExoMars rover (red outlines), as well as the approximate position of the planetary dichotomy (yellow dashed line), and the idealised Coogoon drainage catchment (blue outline). Inset shows the resolution of available topography, including the 20 m/pixel CTX DEMs prepared in this thesis. (Top: MOLA DEM with hill-shade; Bottom: MOLA DEM with THEMIS daytime infrared)

Previous work on the source regions for Oxia Planum (Fawdon, Balme et al. 2021) have investigated the upland drainage catchments which could have contributed water and sediment to the Oxia Planum basin, and defined two drainage catchments based on the accumulation of drainage at different pour points. The principal drainage catchment (**Figure 5.1a**), with a pour point at the termination of Coogoon Valles, extends ~600 km to the east and covers an area of ~1.5×10^5 km^2; and the extended catchment, with a pour point at the low edge of the Oxia Planum basin, includes an additional area of ~0.6×10^5 km^2 to the south. The work includes a preliminary identification of possible crater-hosted palaeolakes within these catchments, based on a combination of topographic and morphological criteria given inundation of the landscape with a set depth of water, and characterised as: higher confidence large crater lakes (LCL), and lower confidence rimless crater lakes (RCL). Additionally, hundreds of irregular dark depressions (IDD) were identified within inter-crater basins and interpreted as possible remnant palaeolake deposits. The authors highlight palaeolakes as particularly relevant to possible biosignature detection in Oxia Planum, as ancient lacustrine environments in the drainage catchment could have hosted habitable conditions, and in turn contributed organic material and sediment to sinks at the landing site. However, fluvial processes within the drainage catchment are thought to postdate the formation of phyllosilicate deposits within the Oxia basin (Quantin-Nataf, Carter et al. 2021), thus complicating a direct comparison between source regions in the drainage catchment and the sediment sink at the landing site.

Palaeolakes on Mars are primarily identified based on morphological relationships between topographic basins and fluvial valley networks (Section **4.2.1**) (Fassett and Head 2008, Goudge, Head et al. 2012, Goudge, Aureli et al. 2015). However, the dependence of palaeolake identification on current surface topography introduces some uncertainty, given the ancient age of fluvial and lacustrine features on Mars, and the

major topographic changes known to have occurred as a result of: impact cratering (Quantin-Nataf, Carter et al. 2021); erosion (McNeil, Fawdon et al. 2021); tectonic deformation at regional (Woodley, Fawdon et al. 2021); and global scales (Perron, Mitrovica et al. 2007, Citron, Manga et al. 2018).

In this chapter, the Coogoon drainage catchment is investigated with a focus on possible open-basin palaeolakes. This expands on previous studies of crater-hosted palaeolakes in the area, to include the identification of palaeolakes within a diverse range of basins in the inter-crater plains, including an assessment of the possible topographic changes confounding palaeolake identification. Lowland basins at the termination of Coogoon Valles are also investigated in this work, to assess the possible existence of a northern hemisphere spanning ocean, or smaller closed-basin palaeolakes adjacent to the dichotomy within the local basin of Oxia Planum. These methods reveal a greater coverage of palaeolakes than previous studies, and a reconstruction source to sink palaeolake chains aids in the identification of palaeolakes partially or completely drained, allowing fluvial erosion and transport of lake bottom sediments into the Oxia Planum basin.

5.2 DATA AND METHODS

Context camera (CTX, 5 m/pixel) imagery provided the basis for feature mapping and geomorphological analysis, and was supplemented with HiRISE and THEMIS images. Topographic analysis at the scale of the entire catchment, such as for the production of system profiles and palaeolake extents, was carried out with MOLA DEMs due to the incomplete coverage of higher resolution topographic data over the entire study area (**Figure 5.1b**). High-resolution topographic data was utilised in the identification and characterisation of landforms at a local scale, and to define the possible hydrological relationships between mapped landforms. Topographic data was mosaicked from CTX (20 m/pixel) digital elevation models (DEMs) with approximate vertical precisions of <8 m (Kirk, Howington-Kraus et al. 2008), and supplemented with High Resolution Stereo Camera (HRSC; 150–200 m/pixel)(Neukum and Jaumann 2004) DEMs

and Mars Orbital Laser Altimeter (MOLA; 456 m/pixel) (Smith, Zuber et al. 2001) topography. DEMs were produced from stereo CTX and HiRISE imagery and MOLA shot heights, utilizing ISIS3 and SOCET SET software and the standard USGS workflow (Kirk, Howington-Kraus et al. 2008).

5.2.1 HYDROLOGICAL ANALYSIS

Drainage catchment areas as defined by Fawdon et al. (2018) were calculated on ~456 m/pixel MOLA DEM topography with all sinks in the topography artificially filled. As outlined in Chapter 3 (**Section 3.3.2**), drainage catchments produced on fully filled topography data are idealised approximations which may not be consistent with the palaeo-drainage catchment, and changes postdating fluvial and lacustrine processes, such as impact craters or wrinkle ridges, may result in closing off catchment areas which would have originally been connected.

As described in detail in Chapter 4 (**Section 4.2.1**), and in previous studies (Fassett and Head 2008, Goudge, Head et al. 2012), palaeolake basins were identified as equipotential surfaces within closed topographic basins at outlet valley elevations, on contours at 10 m vertical intervals. Three possible palaeolake levels were identified at: (1) the highest closed contour at the valley outlet, as the 'valley overflow' (VO) level; (2) the highest contour with a single opening at the outlet valley, as the 'basin overflow' (BO) level; and (3) the lowest closed contour at the outlet valley, as the 'valley extremity' (VE) level. Production of high-resolution topographic data not possible for the entire study area of the present chapter, due to incomplete stereo CTX coverage over this larger area, and therefore lower resolution MOLA DEMs were used to identify palaeolakes. The major consequence of this limitation was that the precise depths of all valleys could not be resolved on this lower resolution topography, and thus the elevation valley overflow levels in these cases may be closer to the actual basin overflow level.

5.3 OBSERVATIONS

Significant mapping and identification of features has been undertaken in previous studies of Coogoon Valles and Oxia Planum, and therefore, rather than a comprehensive remapping of the area, this study made use of past works to guide additional observations. In order to address uncertainty in the identification of palaeolakes due to topographic changes, features such as tectonic ridges and crater ejecta were mapped which superpose fluvial features and possible palaeolakes (**Section 5.3.1**). Finally, fluvial features (**Section 5.3.2**) and sediment fans (**Section 5.3.3**) were mapped, providing the preliminary evidence to identify open-basin (**Section 5.3.4**) and closed-basin palaeolakes (**Section 5.3.5**).

5.3.1 TOPOGRAPHIC DEFORMATION

A significant proportion (14%; n=30) of palaeolakes identified in global catalogues are relatively shallow (<25 m), with a mean depth of 112 m for the entire population (Fassett and Head 2008). Therefore, even relatively minor topographic changes occurring after palaeolake activity could affect the dimensions and detectability of palaeolake basins, or create basins which did not exist at the time of lacustrine activity. Basin morphology is described here to define the origin of identified palaeolake basins, and to assess the relative influence of processes known to have altered the topography of the local area, including regional compression, impact cratering, and erosion.

5.3.1.1 TECTONIC RIDGES

Major tectonic ridges, or 'wrinkle ridges', were mapped across the study area (**Figure 5.3**), as lineations with up-thrown and down-thrown sides indicated where apparent. Mapping and identification were guided by previous studies of wrinkle ridges identified in the study area (Molina, Lopez et al. 2017, Woodley, Fawdon et al. 2021), and typically presented as curvilinear, asymmetrical ridges, and occasionally arranged in staggered arrays. Past studies indicate a total relief of 80-250 m for wrinkle ridges in other Mars regions (Golombek, Anderson et al. 2001), and within the area of Oxia Planum these

features are confined to highland terrains and preferentially oriented north to south (Woodley, Fawdon et al. 2021). Wrinkle ridges are understood to form as a result of regional contraction, possibly as a result of crustal flexure following emplacement of the Tharsis volcanic province(Golombek, Anderson et al. 2001).

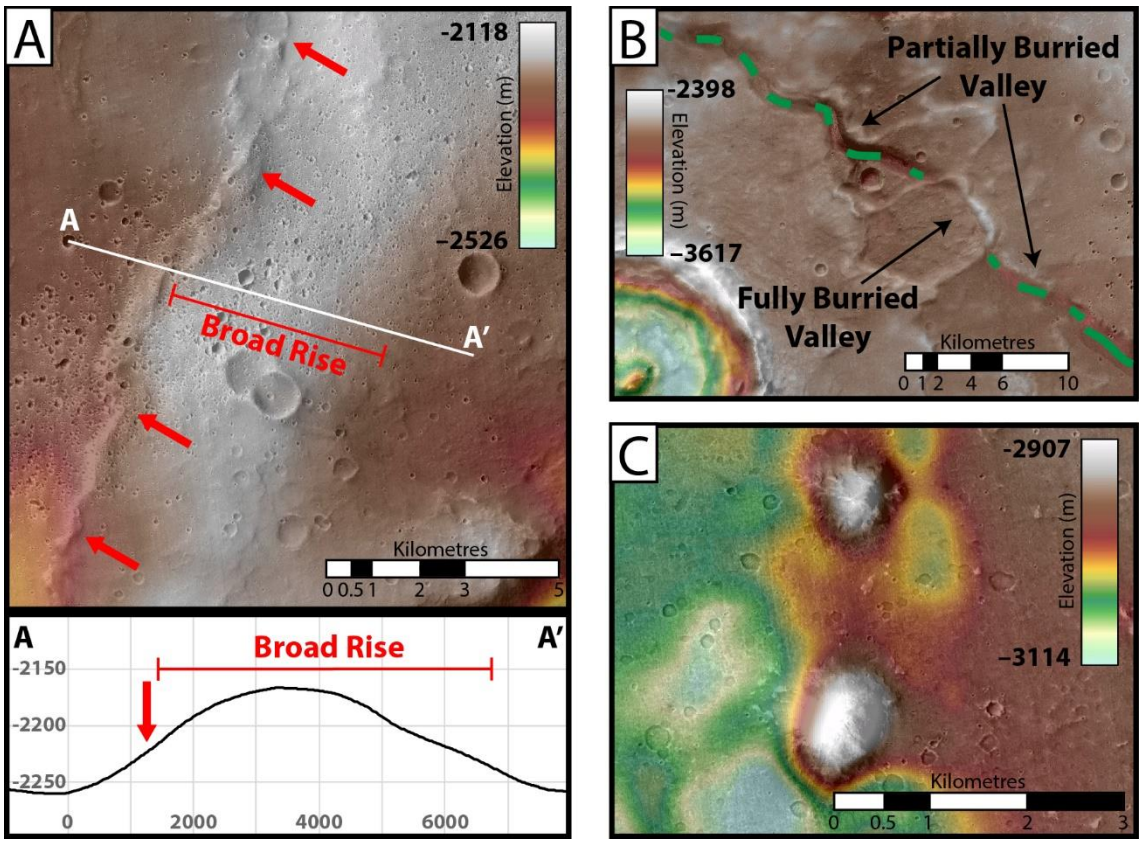

Figure 5.2 – Representative examples of recent topographic features in the study area which could influence the identification of palaeolakes, and basin dimensions. (A) Tectonic 'wrinkle ridge' running SSW-NNE, displaying a steep prominence at the ridge front (red arrows), with unaffected area to the west, and a broad rise extending to the east. (B) Impact ejecta of Kilkhampton crater overlying a section of Coogoon Valles (green lines), showing partial coverage in some areas, and complete coverage in others. (C) Mounds within the lowlands terrains, interpreted as remnants of a more extensive deposit which once covered Oxia Planum and the region. (HRSC DEM (75 m/pixel) over CTX image mosaic)

Ridges identified in this work typically display an asymmetrical profile, with a sharp ridge front rising steeply from lower terrain, and a broader topographic rise under the ridge extending to one side beyond the ridge front (**Figure 5.2a**). Where resolvable with MOLA topography (n=31), the maximum topographic prominence observed at ridge crests ranges from 30 m to 260 m, with a mean prominence of 89.5 m. The full width of the broader rise is more difficult to quantify given the gradual slope to the surrounding terrain, but was estimated where possible (n=11), and found to range from ~1.5 km to

~6.5 km. Although relatively insignificant on the scale of regional topography, these features are considered with regards to the potential influence they may have on the identification of local palaeolake basins.

5.3.1.2 IMPACT CRATERS

The majority of large impact craters in the area have a filled and heavily modified appearance, without raised rims or ejecta deposits, and were likely formed before fluvial activity in the area (Molina, Lopez et al. 2017, García-Arnay, Prieto-Ballesteros et al. 2019). However, two pristine craters are superimposed onto the channels of Coogoon Valles (**Figure 5.3**). The largest of these craters is the 16 km diameter Kilkhampton crater, which is situated just to the south east of the Coogoon terminus and delta, with an ejecta blanket partially obscuring ~50 km of the main valley channel (**Figure 5.2b**). The thickness of the ejecta blanket where it overlies the valley is ~60 m, with a range of thicknesses between different lobes and distance from the crater centre. A pair of smaller (~7 km and ~10 km) unnamed craters are situated directly in the centre of the main Coogoon channel approximately 150 km from the dichotomy. The prominence of the smallest crater where it intersects the valley is ~40 m at the edge of the ejecta blanket and ~200 m at the raised crater rim. As with tectonic ridges, the emplacement of recent impact craters onto an ancient fluvial valleys is considered here as potentially influencing the identification of palaeolakes in the area.

5.3.1.3 LOWLAND MOUNDS AND MESAS

Mounds and flat topped mesas are prominent features observed within the lowland terrains of Chryse Planitia, which are particularly concentrated near the dichotomy, and have been interpreted as remnants of widespread regional deposits formed in and then eroded during the Noachian (McNeil, Fawdon et al. 2021). A study including Oxia Planum by McNeil et al. (2021) records mounds and mesas in the region to have a mean height of 64.7 m and 167.9 m respectively (McNeil, Fawdon et al. 2021).

A full survey of mounds was not carried out in the present study, but 6 major mounds with a prominence of >25 m were identified in the lowlands, within and around Oxia Planum (**Figure 5.2c**). These mounds are concentrated along the dichotomy to the north of the Coogoon delta, and along the low edge of the Oxia Planum basin, where it opens to the lowlands (**Figure 5.3**). The highest mound sits along this basin edge, with a prominence of ~100 m, and a maximum elevation of -2990 m.

5.3.2 FLUVIAL FEATURES

Fluvial features were mapped across the study area including a range of morphological forms, including incised valleys and inverted channels. The majority of mapped fluvial features are incorporated into the Coogoon Valles valley network, which is composed of three main branches: central, north, and south (**Figure 5.3**). Incised valleys make up the vast majority of fluvial features in the area, presenting as up to ~50 m deep, with relatively constant widths of ~1 km, sharply defined banks and 'V' shaped in cross-section. Major exceptions to this generalised morphology are exhibited: along stretches of the central Coogoon branch, which exhibit wide (6 km) flat floored channels; and short, narrower channels observed within the inner walls of impact craters. A comprehensive range of distinct morphological valley types are described in detail in other works (Molina, Lopez et al. 2017, Fawdon 2018), but further classification of valleys was not considered necessary to meet the principal aims of this chapter to identify palaeolake basins.

The central branch of the Coogoon system covers a total distance of ~335 km from the most distant valley head in the highlands to a termination at the dichotomy on the edge of Oxia Planum (**Figure 5.3**), but does not represent a continuous unbroken valley of consistent morphology. The upper valley reaches exhibit the typical morphology described above, as a narrow, sharp sided channel for the first ~115 km, below which the valley morphology changes to a wide flat floored channel for a distance of ~100 km. The transition between these two morphologies, constitutes an overlap, with the narrow valley apparently incised into the wider channel floor for a distance of ~25 km. Another gradual

transition is observed towards the end of the flat floored channel, with a dark deposit along the floor of the wider channel extending out across a wide flat basin, referred to here as the central Coogoon basin (**Figure 5.3**). These dark deposits are analogous to the dark resistant unit mapped within the Oxia Planum basin (Quantin-Nataf, Carter et al. 2021), and are mapped in the central Coogoon basin as irregular dark depressions, interpreted as possible palaeolake deposits (Fawdon 2018).The continuation of Coogoon Valles from this point is uncertain, and the true termination of the flat floored channel may be obscured by Kilkhampton crater to the north-west (Molina, Lopez et al. 2017, García-Arnay, Prieto-Ballesteros et al. 2019). In the present study, the central branch of the Coogoon system is interpreted as continuing from the north edge of the central Coogoon basin, where a narrow, steep sided valley beginning at a short branching set of tributaries, and is incised the remaining ~90 km to the dichotomy. However, the majority of this final stretch is obscured by ejecta from Kilkhampton crater (**Figure 5.2b**).

The north branch of the Coogoon system joins the central branch ~75 km from the dichotomy, with a total continuous length of ~140 km (**Figure 5.3**). The morphology is generally consistent along the entire branch, exhibiting a steep sided channel, gradually increasing in width (~0.5-1 km) and depth (~10-40 m) along length, but with less sharply defined banks along a central stretch of ~40 km. This branch is also characterised by a number of branching and re-joining segments, some of which, identified in other works, have been interpreted as representing multiple phases of drainage (Fawdon 2018). Towards the intersection with the central branch of the Coogoon system, the valley exhibits two abrupt changes in direction: a set of two, near right-angle turns forming a short kink in the course of the valley (**Figure 5.4c**); and a near right-angle turn just before meeting the central branch, followed by a ~5 km stretch where the two branches run parallel before joining. An additional valley, in the northeast of the study area exhibits a similar right-angle turn, which coincides with a wrinkle ridge (**Figure 5.4c**).

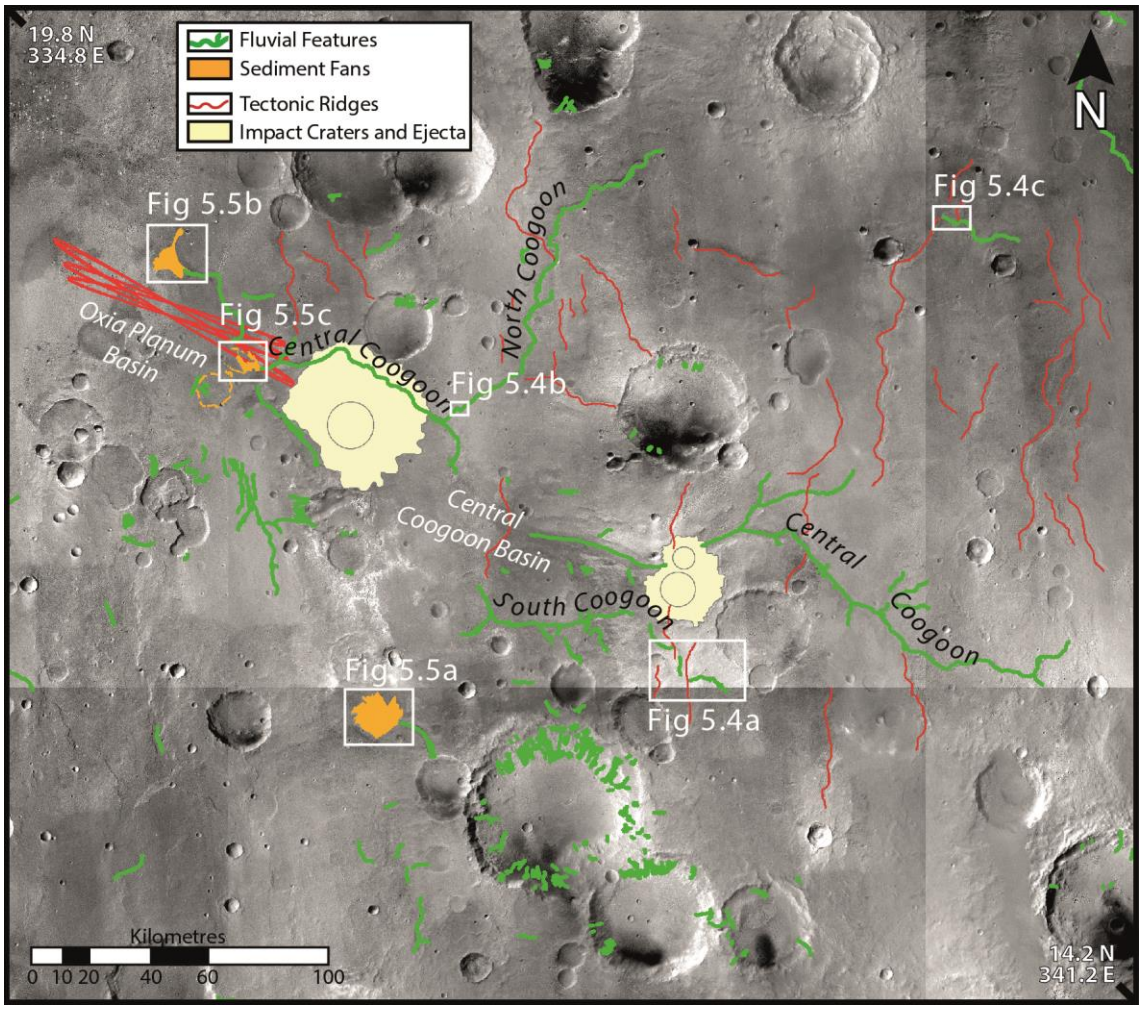

Figure 5.3 – Mapped morphological features within the area of the Coogoon Valles system, including: fluvial features (green lines), sediment fans (orange fill), tectonic ridges (red lines), and fresh impact ejecta (tan fill) overlying Coogoon Valles. Also indicated are the north, south, and central branches of the Coogoon system, as well as the Central Coogoon basin and the Oxia Planum basin with ExoMars landing ellipses (red outlines). (CTX image mosaic)

The south branch of the Coogoon system covers a total distance of ~100 km, and does not exhibit a clear join to the central branch valleys, and instead terminates at the edge of the central Coogoon basin (**Figure 5.3**). The valley has a similar morphology to the northern branch, and lower reaches of the central branch, with a width of ~0.6-0.8 km, but exhibits less sharply defined edges, and a shallower maximum depth of ~60 m. A ~35 km section of valley, beginning ~15 km from the valley head, is poorly defined, and difficult to identify in comparison to the valley sections above and below (**Figure 5.4a**).

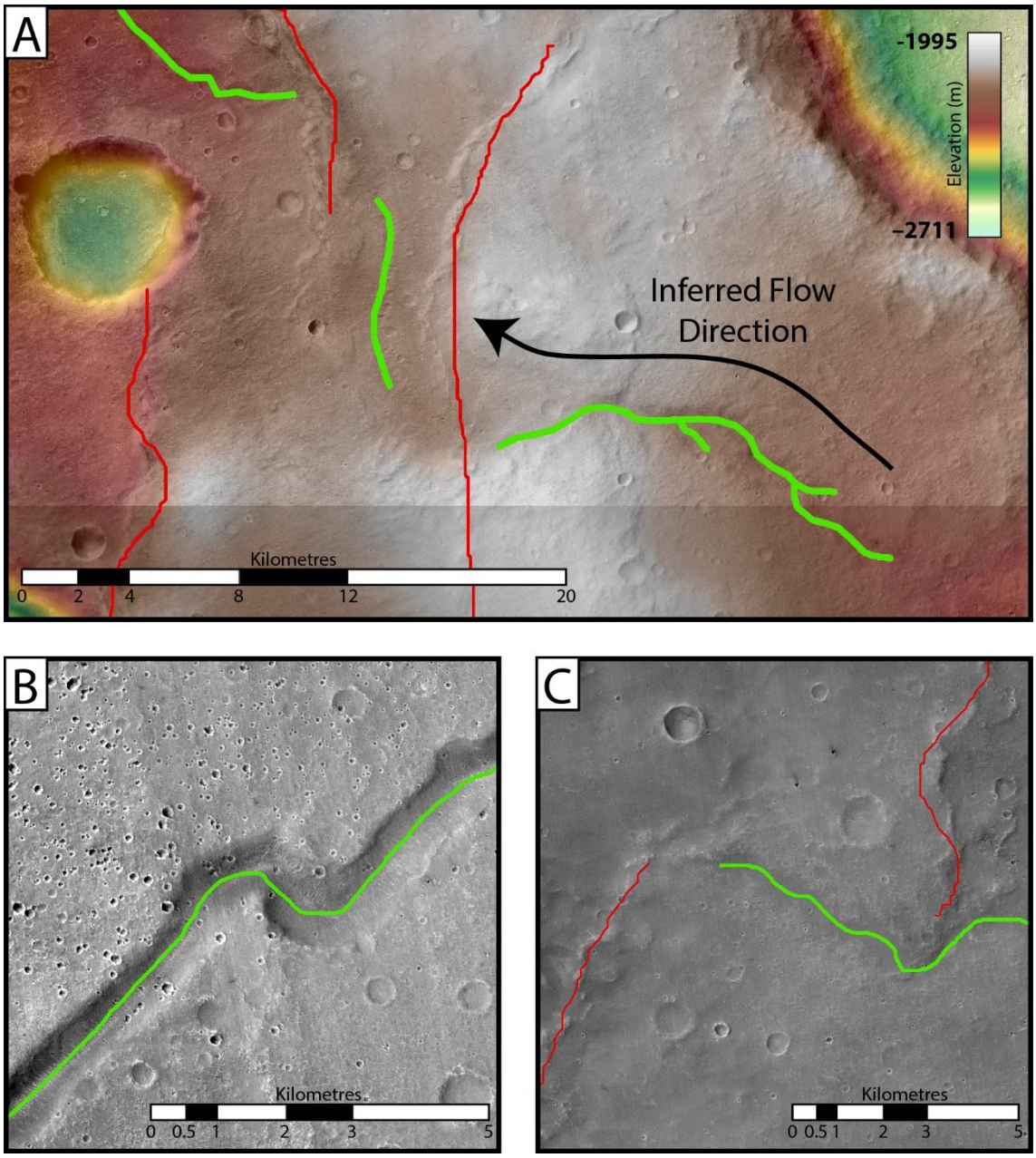

Figure 5.4 *– Detailed images of mapped fluvial valleys (green lines) apparently altered by subsequent tectonic processes represented by wrinkle ridges (red lines). (A) Valley section at the head of the south Coogoon branch which runs upwards out of a basin, apparently as a result of being uplifted, and broken by a series of wrinkle ridges. (B) Valley section on the north Coogoon branch, near the intersection with the central branch, displaying a distinct kink in the valley course, although without an apparent wrinkle ridge. (C) Valley section in the far northeast corner of the study area, displaying a lateral offset at the point of intersection with a wrinkle ridge. (HRSC DEM over CTX imagery)*

The flow direction of valleys was inferred by a combination of overall longitudinal valley profile, valley width along length, and the nature and angle of tributary intersects. Valley slope was generally consistent with inferred flow direction, with the exception of three limited valley sections exhibiting negative slope in relation to the overall flow

direction of the valley. The most pronounced example is situated on the Coogoon south branch, with a 14 km segment of valley rising ~170 m from the valley head (**Figure 5.4a**). The other two examples are situated on the Coogoon north branch, with a 5 km section rising ~60 m out of a deep basin along the valley, and a more gradual 15 km section rising 50 m from the valley head.

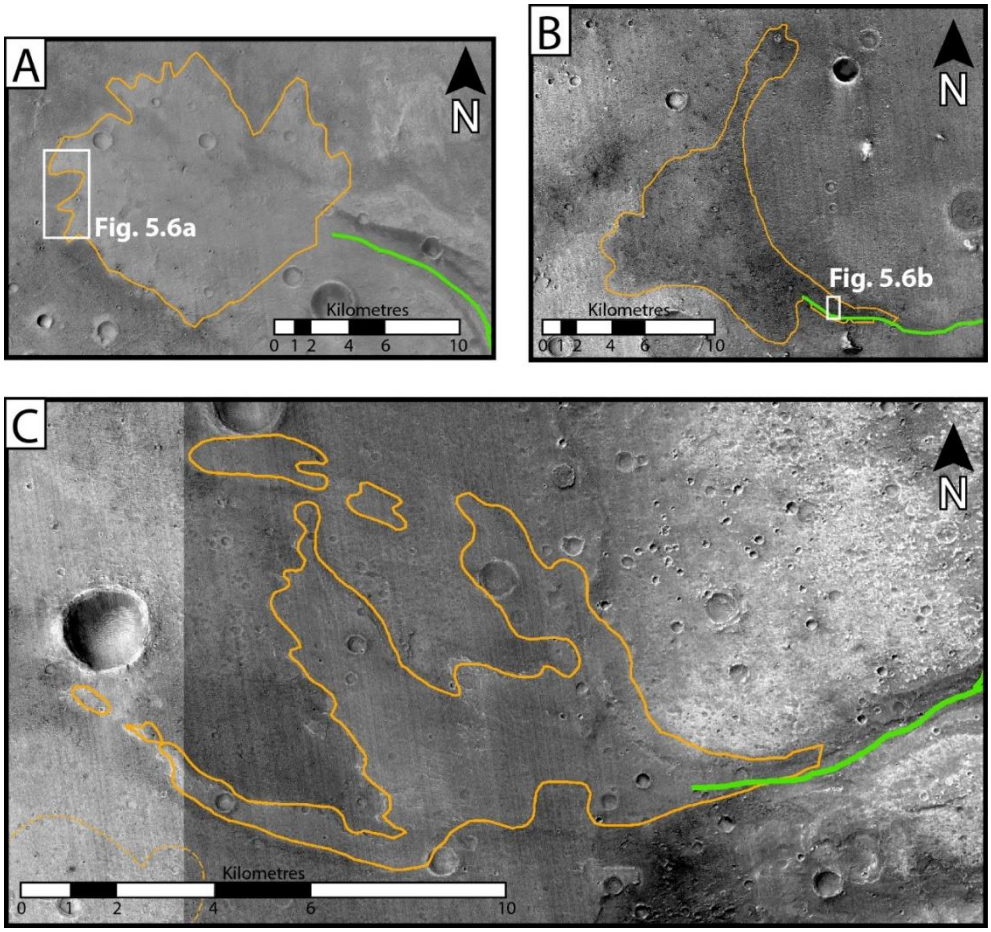

Figure 5.5 *– Detail images of the three large sediment fans discussed in this work. (A) Fan composed of light-toned material at the termination of a short valley, draining from a the multi-crater palaeolake in the highlands (Fawdon 2018). (B) Fan shaped deposits of raised, dark material within the lowest area of the Oxia Planum basin, at the termination of a valley exhibiting both raised and incised morphological profiles. (C) Putative delta at the termination of Coogoon Valles, well documented in previous studies (Quantin-Nataf, Carter et al. 2021), and a factor in the selection of Oxia Planum as the landing site for ExoMars. (CTX image mosaics)*

5.3.3 SEDIMENT FANS

The sediment fans described in this work, drew on a combination of previously identified features (Molina, Lopez et al. 2017, Fawdon 2018, García-Arnay, Prieto-Ballesteros et al. 2019, Quantin-Nataf, Carter et al. 2021), and the identification of

additional features based on established morphological criteria (Di Achille and Hynek 2010, Fawdon, Gupta et al. 2018). This section focuses on four large sediment fans within broad basins (**Figure 5.5**), although additional small sediment fans have been identified within deep impact craters in the highlands (Fawdon 2018).

The fan at the terminus of Coogoon Valles is a prominent feature in Oxia Planum (**Figure 5.5c**), and is widely interpreted as representing a delta formed at the edge of a standing body of water (Quantin-Nataf, Carter et al. 2021). The fan sits at an elevation of -2,996 m, and exhibits three major lobed deposits, with finely layered interior structure exposed at the margins. Situated directly SSE of the main Coogoon delta at an elevation of -2,953 m, a second set of similar deposits has also been interpreted as a second sediment fan (García-Arnay, Prieto-Ballesteros et al. 2019), although the upper part of this fan, and the fluvial feature that would have fed it appear to be obscured by overlying deposits, in particular, Kilkhampton crater.

Another set of fan shaped deposits located within the Oxia Planum basin sits at a mean elevation of -3,135 m, although characterisation as a sediment fan is made with a lower degree of confidence (**Figure 5.5c**). The long (~15 km), fan shaped deposit of raised, dark material is observed at the termination of a fluvial feature which begins at north edge of the main Coogoon delta (**Figure 5.3**). The fluvial feature leading to the possible fan displays a combination of incised, surficial and inverted channel morphological attributes, and towards the terminus appears to be composed of the same raised, dark material as the fan itself. Past mapping of Oxia Planum has identified these dark deposits as part of the 'dark resistant unit', which presents across the area as raised dark deposits with high crater-retention, and is interpreted as representing remnants of a volcanic unit (Quantin-Nataf, Carter et al. 2021). Therefore, the presently observed surface of this feature may not represent sediment deposits, but the fan shaped morphology and situation at the end of a fluvial feature may represent a sediment fan preserved under later deposits.

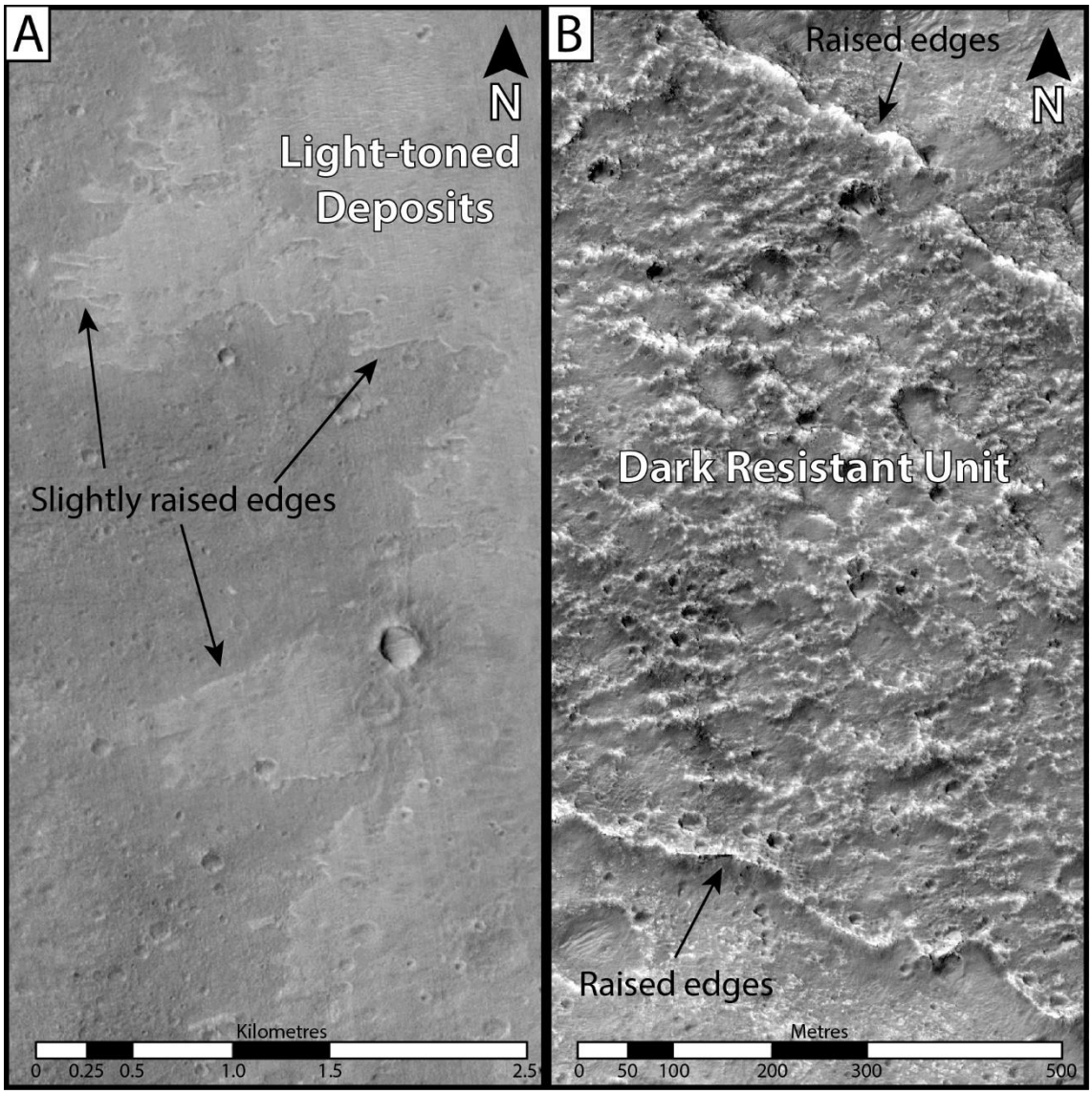

Figure 5.6 *– Detailed views of the two possible sediment fans identified in this work. (A) Sharply defined edge of the light-toned fan shaped deposits at the outlet of the multi-crater palaeolake, showing the clear contrast in albedo, and low relief over the surrounding terrain. (B) High, raised edges of dark deposits of the possible lower Oxia Planum sediment fan. Previous works have mapped this fan as part of a 'dark resistant unit' in Oxia Planum (Quantin-Nataf, Carter et al. 2021), and in this work it is interpreted as overlying a possible sediment fan deposits. The view here shows the narrow proximal end of the fan, apparently infilling the termination of the valley. (Left: CTX image mosaic; Right: HiRISE, ESP_044679_1985)*

A long (~26 km) possible sediment fan is also observed in the highlands at an elevation of -2,622 m (**Figure 5.5a**), with an apex at the terminus of a short, wide valley originating within a chain of coalesced craters identified as a palaeolake by Fawdon et al. (2018). The fan exhibits a number of curvilinear lobes along the margins, and is composed of smooth, light-toned material of a similar appearance to the Coogoon delta, and

although it displays no clear prominence on topographic data, the edges of these deposits appear to be slightly raised above the surrounding terrain observed on CTX imagery.

5.3.4 OPEN-BASIN PALAEOLAKES

A total of 17 possible open-basin palaeolakes were identified within the Coogoon Valles drainage system, where valleys originated within or transected through topographic basins, considering all valleys except for the wide flat floored sections of the central branch. These palaeolakes are all connected in branching chains, with a common terminus at the main delta at the edge of Oxia Planum. The 12 palaeolakes part of continuous chains on one of the main Coogoon branches are considered here in greater detail (**Figure 5.7**), including: five on the Coogoon central branch (L-CCn), five on the Coogoon north branch (L-CNn), and two on the Coogoon south branch (L-CSn). Palaeolakes were numbered with increasing distance from the dichotomy, along each of the main branches of Coogoon Valles, with the central and south branches meeting the at the boundary of palaeolake L-CC2 within the central Coogoon basin.

In all cases, the valley overflow level of palaeolakes defined closed basins on the present topography, and indicating palaeolake identification with a high degree of confidence. However, in three instances individual palaeolake levels were of lower confidence (**Figure 5.7**; dashed blue outlines), where topography was significantly influenced by crater ejecta (L-CC1) and wrinkle ridges (L-CS2) at the outlet valley, and where the equipotential surface did not define a closed basin (L-CN4 & L-CS2). The basin overflow level within palaeolake L-CN4, defines a basin almost completely closed (>98%) along the perimeter, with two narrow (~4 km) openings along the northern edge. In contrast, the basin overflow level within palaeolake L-CS2 defines a contour which is mostly closed on three sides, but with a large (~60 km) gap along the northern edge. The outlet defining palaeolake L-CS2 is also crossed by a series of wrinkle ridges (**Figure 5.4**a), further lowering the confidence in identification of a palaeolake within this basin. The valley overflow and basin overflow levels within palaeolake L-CC1 defined closed basins on the present topography, but because the outlet elevations were observed within the

area affected by the raised ejecta blanket of Kilkhampton crater (**Figure 5.2b**), identification of this palaeolake was also considered to be of lower confidence.

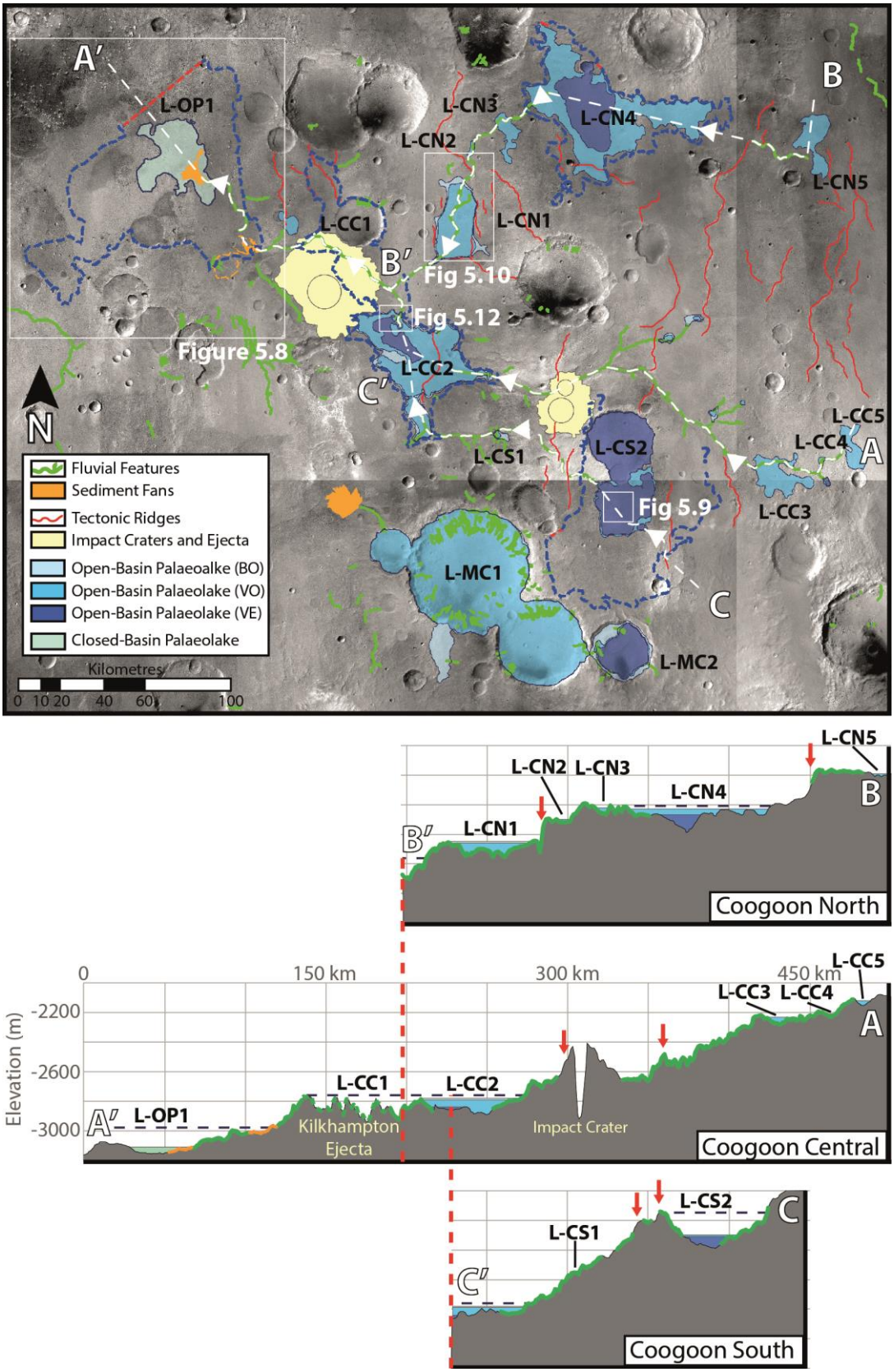

Figure 5.7 – Identified open-basin palaeolakes in the Coogoon Valles system and closed-basin palaeolakes in Oxia Planum, showing longitudinal profiles through the three main branches of

Coogoon Valles with sections of valley (green lines), and wrinkle ridges (red arrows). ***(A-A')*** *Shown on the Coogoon central branch, are open-basin palaeolake L-CC2 and the closed-basin palaeolake L-OP1 within Oxia Planum, also indicated are the influence of topographic features in the form of: two wrinkle ridges, although these are not associated with identified palaeolakes; and impact craters, in particular the irregular topography associated with Kilkhampton crater and the low confidence palaeolake L-CC1.* ***(B-B')*** *Shown on the Coogoon north branch are open-basin palaeolakes L-CN1 and L-CN4, the latter including the lower confidence basin overflow level defining a partially open-contour, also indicated are the positions of two wrinkle ridges associated with steep drops in the valley course.* ***(C-C')*** *Shown on the Coogoon south branch are open-basin palaeolakes L-CS2, and the relationship of this basin to two wrinkle ridges raising the outlet valley, and the edge of palaeolake L-CC2 where the south branch meets the central branch. (CTX image mosaics, and MOLA topography)*

An additional open-basin palaeolake meeting the same criteria as palaeolakes in the Coogoon system, and identified by Fawdon et. al. (2018) as the 'multi-crater palaeolake' is also considered in this study (**Figure 5.7**). The multi-crater palaeolake is not directly connected to the palaeolakes of the Coogoon system, and is hosted within a basin formed of four overlapping impact craters, actually composing two palaeolakes at different elevations: a higher palaeolake confined to the easternmost crater, with an outlet draining to the crater to the west; and a lower palaeolake composed of the other three craters, with an outlet breaching to crater wall and draining to the highlands.

All palaeolakes within the Coogoon system are hosted within relatively shallow basins in the highland inter-crater plains, although part of the boundary of palaeolake L-CS2 is defined by a filled and eroded impact crater, and the northern edges of palaeolake L-CN4 are partially defined by the raised ejecta of two large craters (**Figure 5.7**). The shallow and irregular nature of these basins make a definitive interpretation of basin formation and origin difficult, however a general interpretation of highland basins is that they represent heavily eroded and filled impact craters.

5.3.5 CLOSED-BASIN PALAEOLAKES

The identification of closed-basin palaeolakes was considered within a more limited range of topographic basins than open-basin palaeolakes, due to the greater uncertainty inherent in identifying closed-basin palaeolakes on Mars (Goudge, Aureli et al. 2015). Therefore, only two locations with the most robust evidence were considered in

the present study as the sites of possible closed-basin palaeolakes: (1) the basin of Oxia Planum, on the strength of exhibiting multiple possible deltas, and the terminus of the Coogoon Valles drainage system; and (2) within the multi-crater basin, at a lower level than the open-basin palaeolake in the same basin, on the strength of exhibiting >180 fluvial terminations concentrated at a narrow range of elevations.

The Oxia Planum basin is bounded to the south and east by the scarp of the planetary dichotomy, to the north and west, depending on the elevation traced on the present topography (**Figure 5.8a**), the basin is either: (1) broadly open to the northern lowlands (>-2,960 m); (2) narrowly open to the northern lowlands (-3,100 to -2,960 m); or (3) an entirely closed basin (<3,100 m). The maximum depth of the basin is ~70 m from the lowest point in the basin (-3,170 m) to the lowest point of the saddle opening to the northern lowlands (-3,100 m). The basin of Oxia Planum exhibits an irregular geometry, however, the raised edges to the east and north define a broad curve, and other studies have suggested formation as a substantially filled and modified impact crater (Quantin-Nataf, Carter et al. 2021).

Indicators of base level within Oxia Planum include: the main Coogoon delta (-2,996 m) and secondary delta (-2,953 m) at the dichotomy; a possible sediment fan deeper within the basin (-3,135 m); and the fluvial terminations of Coogoon Valles at the edge of the basin (-2,980 m), and the lower termination within the basin (-3,110 m). The Coogoon terminus and delta are at elevations commensurate with an equipotential surface open to the northern lowlands. A possible base level is defined at the level of the Coogoon terminus, defining a basin which is closed along the majority of its perimeter (90%; 422 km), with a 47 km wide opening to the lowlands along the northern edge (**Figure 5.8b**). The elevation of the lower sediment fan is situated at an elevation defining a closed basin, and the elevation of the fluvial termination leading to this fan is used define the extent of a possible close-basin palaeolake in Oxia Planum (**Figure 5.8b**).

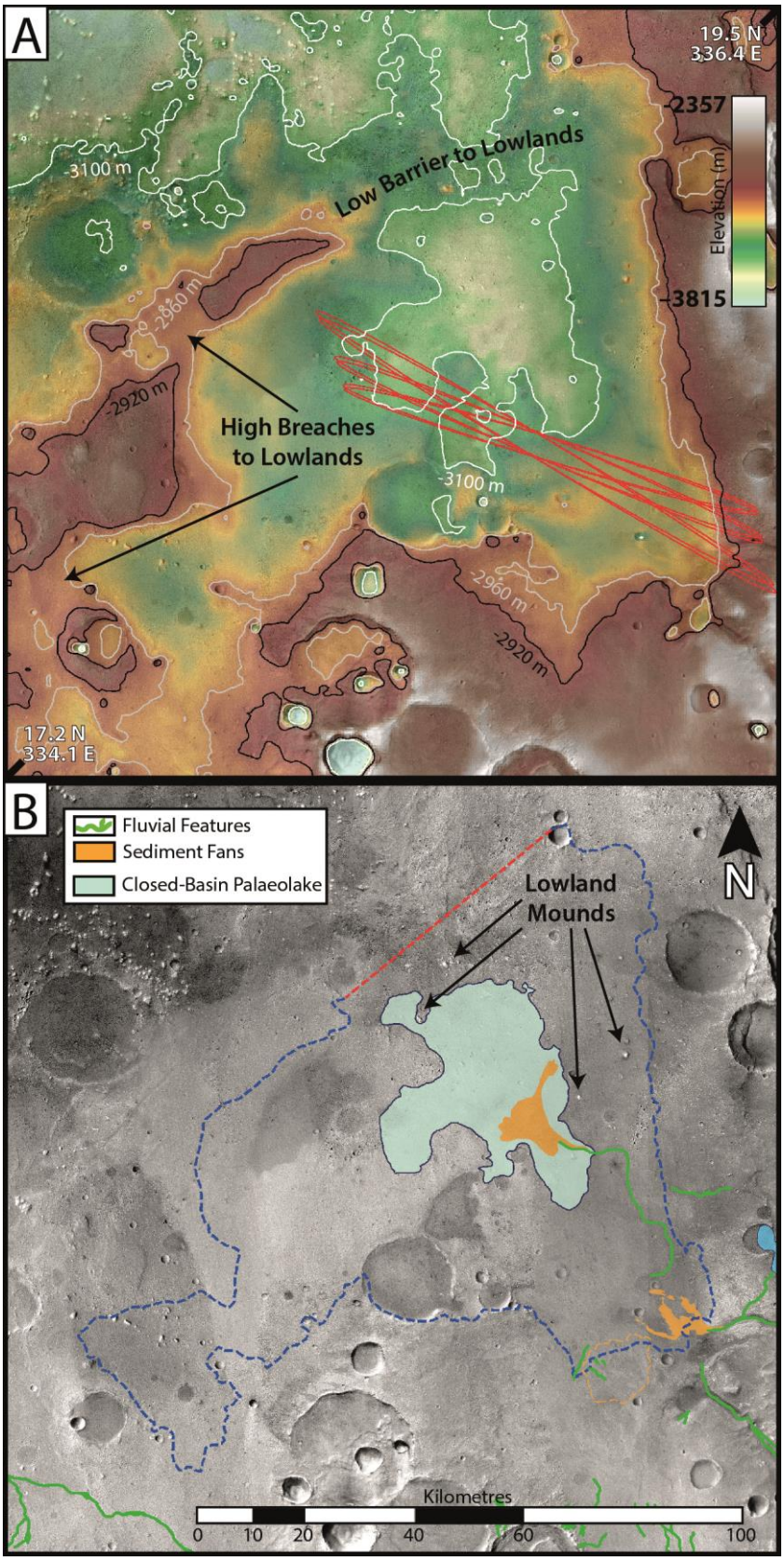

Figure 5.8 *– Illustration of the present topography, and possible ancient palaeolakes within the Oxia Planum basin.* ***(A)*** *The present topography of Oxia Planum indicates a basin fully closed to the northern lowlands at elevations below -3100 m (white contour), with elevations up to -2960 m (grey contour) breaching a low barrier only along the north edge of the basin, and the contour remains closed to the lowlands along all other sides. At elevations above -2960 m, with -2920 m (black contour) shown here as an example, the basin becomes widely open to the northern lowlands along*

the north, south, and west edges. ***(B)*** *Possible equipotential surfaces within Oxia Planum, defining: a closed-basin palaeolake (-3110 m) at a valley termination and possible sediment fan deep within the basin (light green area), and a possible base-level (-2980 m) defined by the Coogoon valley termination and delta (blue dashed line), which is open to the northern lowlands at the northern edge (red dashed line). Also shown are the locations of mounds within Oxia Planum and along the low barrier to the northern lowlands which may indicate the approximate level of the past topography. (MOLA DEM over CTX mosaic images)*

The two largest craters constituting the multi-crater basin, contain numerous (n=185) fluvial channels incised into the steep interior walls of the craters (**Figure 5.3**). Channels within each crater terminate within narrow elevation ranges, near the smooth, flat crater floors. Closed-basin palaeolakes are identified in this work at the 10 m contour where the greatest number of terminations are concentrated, defining possible palaeolakes with surfaces at -3400 m in the east crater, and -3600 m in the west crater.

Table 5.1 *– Elevations and dimensions of open-basin palaeolakes on the three main branches of the Coogoon Valles system (Central, L-CCn; North, L-CNn; South, L-CSn), as well as open-basin palaeolakes of the multi-crater system, and the closed-basin palaeolake within Oxia Planum (L-OP1). Only palaeolakes identified with a high degree of confidence are included here, notably excluding L-CC1, and the possible basin overflow levels of L-CN4 and L-CS2.*

Palaeolake	Fill Level	Surface Elevation (m)	Area (km^2)	Volume (km^3)	Mean Depth (V/A) (m)
L-CC2	BO	-2780	1570	68	44
	VO	-2790	1388	54	39
	VE	-2840	160	2.1	13
L-CC3	VO	-2230	308	5.8	19
L-CC4	VO	-2210	11	0.07	6
L-CC5	VO	-2120	143	2.4	17
L-CN1	BO	-2650	637	23	36
	VO	-2660	525	17	33
L-CN2	VO	-2500	15	0.13	9
L-CN3	VO	-2420	125	1.55	12
L-CN4	VO	-2430	2201	94	42
	VE	-2470	635	30	48
L-CN5	VO	-2190	259	2.9	11
L-CS1	BO	-2550	25	0.25	10
	VO	-2560	8	0.05	6
L-CS2	VO	-2300	1467	218	148
	VE	-2310	1212	203	168
L-MC1	BO	-2380	4546	3802	836
	VO	-2410	4267	3666	881
L-MC2	BO	-2310	596	201	337
	VO	-2490	441	109	260
	VE	-2560	394	79	202
L-OP1	-	-3110	802	18	23

5.4 DISCUSSION

The open-basin palaeolakes of the Coogoon system are assessed here in greater detail, to determine the veracity of identification by considering additional indications of base-level within the basins (5.4.1), and in relation to confounding topographic features which may have altered the detected basins (5.4.2). An assessment of the multi-crater palaeolake system, exhibiting evidence of open-basin and closed-basin palaeolakes highlights regional changes in palaeolake activity over time (5.4.3). Possible topographic changes and palaeolakes or oceans within the Oxia Planum basin are then discussed in relation to the ExoMars mission (5.4.4), with a final identification of probable source locations within the highlands (5.4.5).

5.4.1 PALAEOLAKE CONFIDENCE

The majority of open-basin palaeolakes identified in this study have continuous valleys running across the putative palaeolake floors, and there are therefore few examples of palaeolake inlets or deltas which might be compared to open-basin palaeolake extents as in Chapter 4. The limited examples within the present study area are (**Figure 5.7**): (1) valley terminations of the central and south branches of the Coogoon network, at elevations of -2867 m and -2820 m respectively, at the edge of palaeolake L-CC2 (-2780 m) within the central Coogoon basin; and (2) two shorter valleys, which are not part of the Coogoon system, terminating at elevations of -2761 m and -2818 m, at the edge of the lower confidence palaeolake L-CC1 (-2770 m). This may indicate a higher level of confidence for palaeolake L-CC2, but the additional topographic factors complicating identification of palaeolake L-CC1 are of greater importance in this instance.

Only one palaeolake extent out of the seven palaeolakes identified in the previous chapter did not define a closed basin, and this overall fit of outlet defined palaeolake levels to the present topography was considered as an indication that minimal topographic change had affected the area post-dating lacustrine activity. In the one case, a basin overflow level, which did not define a closed basin there appeared to be a clear evidence

of subsequent collapse near the dichotomy (**Sections 4.4.3 & 4.4.4**). In the present chapter, the possible basin overflow level measured at the outlet valley within palaeolake basins L-CN4 and L-CS2 did not define a closed basin on the present topography, and this is interpreted as a first indication of topographic change occurring subsequent to lacustrine activity. The nearly closed basin defined by the overflow level of L-CN4 is considered to be of greater confidence than the widely open basin of L-CS2 (**Figure 5.7**). However, the situation of palaeolake L-CN4 beyond the limits of the idealised Coogoon drainage catchment does indicate a topography no longer commensurate with the palaeo-drainage of Coogoon Valles (Fawdon 2018).

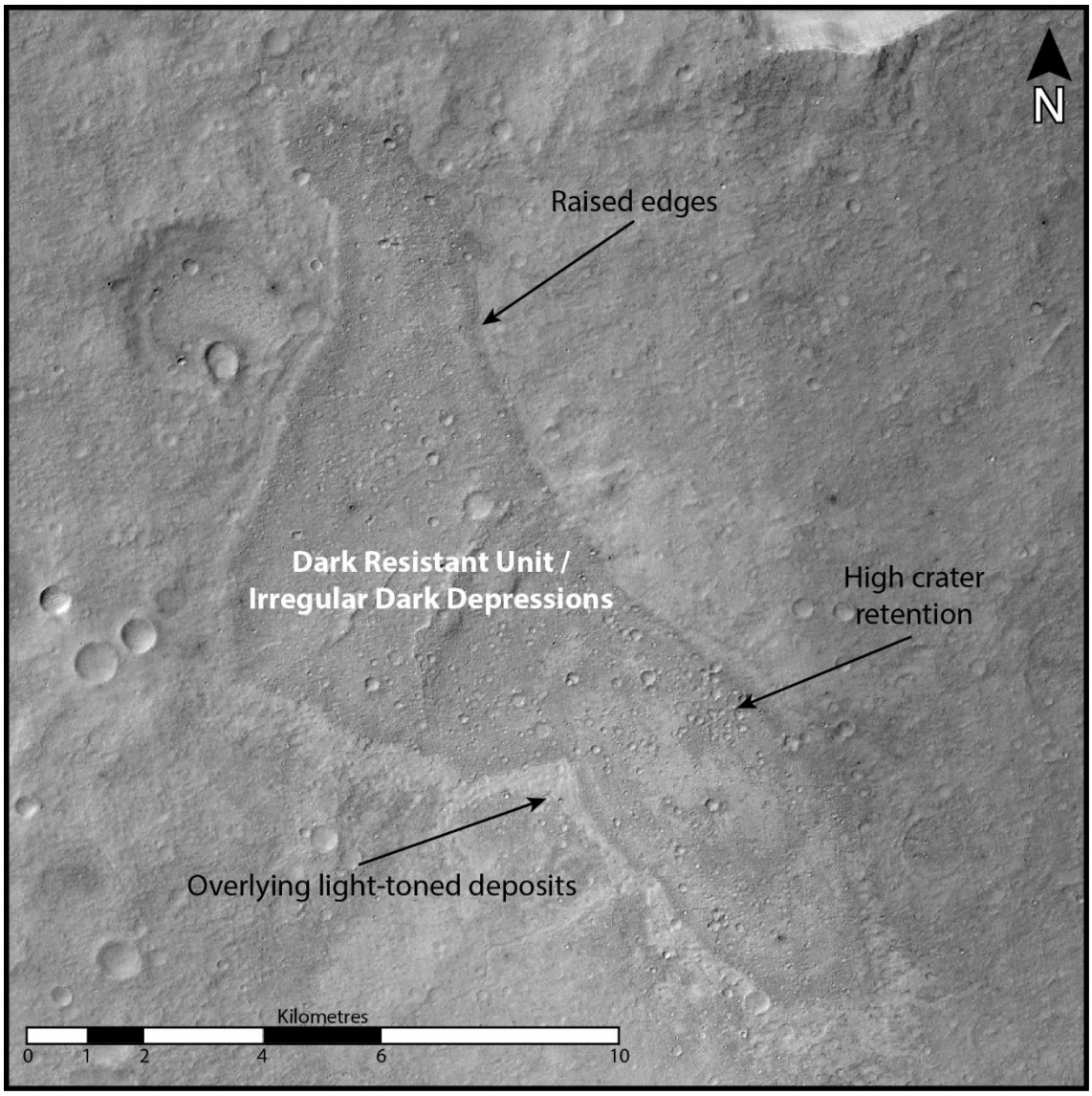

Figure 5.9 *– Example of possible palaeolake deposit, within the deepest area of palaeolake L-CS2. This unit was mapped as an 'irregular dark depression' in previous work, and may be analogous to the 'dark resistant unit' observed within the Oxia Planum basin. These resistant deposits are*

characterised by high-crater retentions, and raised edges, sometimes overlying light-toned deposits. (CTX image mosaic)

Possible palaeolake deposits, described as irregular dark depressions by Fawdon et. al. (2018), are observed within the boundaries of open-basin palaeolakes identified in the current work (L-CC2 & L-CS2) (**Figure 5.9**), and within the closed-basin palaeolake in Oxia Planum (L-OP1). These deposits are interpreted tentatively as possible palaeolake or playa deposits, and represent the only indication of palaeolakes within the inter-crater plains identified in previous studies (Fawdon 2018). The correlation of these features with open-basin palaeolakes identified using a different set of criteria in the present work, lends additional weight to interpretation of a lacustrine origin for these deposits.

5.4.2 PALAEOLAKE BASIN DEFORMATION

Methods of identifying and mapping palaeolakes based on outlet elevations are heavily reliant on topographic data, and on a presumption that the presently observed topography is a relatively true representation of past surfaces. Defining palaeolake extents of 10^4 km^2 based on the observation of elevation within a narrow 1 km width of outlet valley has the potential to compound small differences in elevation into interpretations indicating significant inundation of a surface. Therefore, in order to reduce the possibility of misidentification it is prudent to include a consideration of basin origin, and the relative timing of features defining palaeolake boundaries. Apart from the multi-crater palaeolake, all the other palaeolakes identified in this study are hosted within irregular shaped basins within the inter-crater plains. Compared to crater hosted palaeolakes, which are constrained to a relatively limited range of dimensions, basins in the inter-crater plains are more difficult to classify, with boundaries defined by a combination of features, often of unknown origin and age. The processes forming tectonic ridges and impact craters in the highlands, and mounds and mesas in the lowlands are believed to have occurred more recently than fluvial and lacustrine processes in the areas of Coogoon Valles and Oxia Planum (Quantin-Nataf, Carter et al. 2021), and the relative influence of these features on identified palaeolake basins is considered here to assess the veracity of palaeolake identification.

Where wrinkle ridges and recent impact craters define the upland side of a basin, away from the outlet valley, they may have an influence on the mapped palaeolake extent. However, the influence of these features is particularly pertinent where they define the lower edge of a basin near the outlet valley used in palaeolake identification, and in these instances, the presence of a wrinkle ridge or impact crater may be the control on whether or not a palaeolake is identified. In this study, there are three palaeolake basins which appear to be largely influenced by the upraised topography of relatively recent features: (1) palaeolakes L-CN1 and L-CS2 by wrinkle ridges; and (2) palaeolake L-CC1 by the Kilkhampton impact crater. The following sub-sections investigate these cases in detail, as well as indicating other minor instances of deformation which have a smaller effect on identified palaeolakes.

5.4.2.1 TECTONIC RIDGES

The basin of palaeolake L-CN1 is largely defined by wrinkle ridges along three edges (**Figure 5.10**), including: a ~10 km length along the south edge; a ~28 km length along the eastern edge; and ~10 km and ~5 km lengths along the western edge. The basin edges meet at near right angles, forming an approximately rectangular basin, with the outlet valley positioned at the southwest corner. This palaeolake falls within the area covered by high-resolution (20 m/pixel) CTX DEMs, allowing a detailed analysis of topography at the outlet valley, revealing that: (1) the palaeolake has a maximum depth of ~80 m at the basin overflow level; (2) the longitudinal valley profile diverts upwards by ~45 m at the edge of the basin, in a similar manner to the negative slope valley heads described in Chapter 4 (**Section 4.4.1.3**); and (3) although the prominence of the wrinkle ridges near the outlet valley are ~60 m, these features do not transect the outlet valley. This relationship suggests that although the wrinkle ridges have influenced the identified palaeolake boundary, the palaeolake basin would still be identified, although slightly smaller, on a topography unaffected by tectonic ridges.

Palaeolake L-CS2 affords the clearest evidence of an outlet valley and palaeolake extent affected by subsequent wrinkle ridges. The basin overflow level defines a widely

open contour that cannot represent an ancient palaeolake, and given the steep upward slope of the outlet valley where it has been uplifted by the wrinkle ridge (**Figure 5.4**), it is likely that the valley overflow and valley extremity extents have also been altered by this subsequent deformation. However, given the closed contours defined by the valley overflow and valley extremity levels identification of a palaeolake within this basin is still considered likely, although the exact dimensions and surface elevations are considered with lower confidence.

Wrinkle ridges in the present study appear to post-date fluvial and lacustrine processes, and therefore, palaeolake boundaries and dimensions calculated on the present topography are likely to be less accurate where influenced by subsequent tectonic deformation. However, detailed examination of the two examples above demonstrates that palaeolakes would still be identified within those basins, and thus palaeolake identification can still be made with relatively high confidence. Tectonically controlled lake basins, such as lake Baikal and the Red Sea, are common on the Earth, and although not represented in global palaeolake catalogues on Mars (Fassett and Head 2008), tectonically controlled palaeolake basins have been described in limited areas (Mangold and Ansan 2006). Additional examples of palaeolakes controlled by tectonic activity may be found by assessing the relative ages and relationships of tectonic features to new and existing catalogues of palaeolakes in the inter-crater plains.

In addition to the above examples linked to palaeolakes, two steep drops of ~75 m are observed to coincide with wrinkle ridges along the north Coogoon branch (**Figure 5.10**)(**Figure 5.7; north Coogoon profile**), with one also coinciding with a sharp turn in valley course (**Figure 5.4**), indicating a lateral as well as a vertical offset. Both ridges are situated near the boundary of the Coogoon drainage catchment, and previous studies have identified fluvial features crossing the drainage catchment boundary in this area (Fawdon 2018), which also includes palaeolake L-CN4. This further evidence of tectonic deformation in the study area highlights the need to consider recent topographic features in the calculation of drainage catchments in Oxia Planum or elsewhere on Mars (Goudge,

Mustard et al. 2015), and regional surveys of such features are likely to be important to future hydrological studies (Woodley, Fawdon et al. 2021).

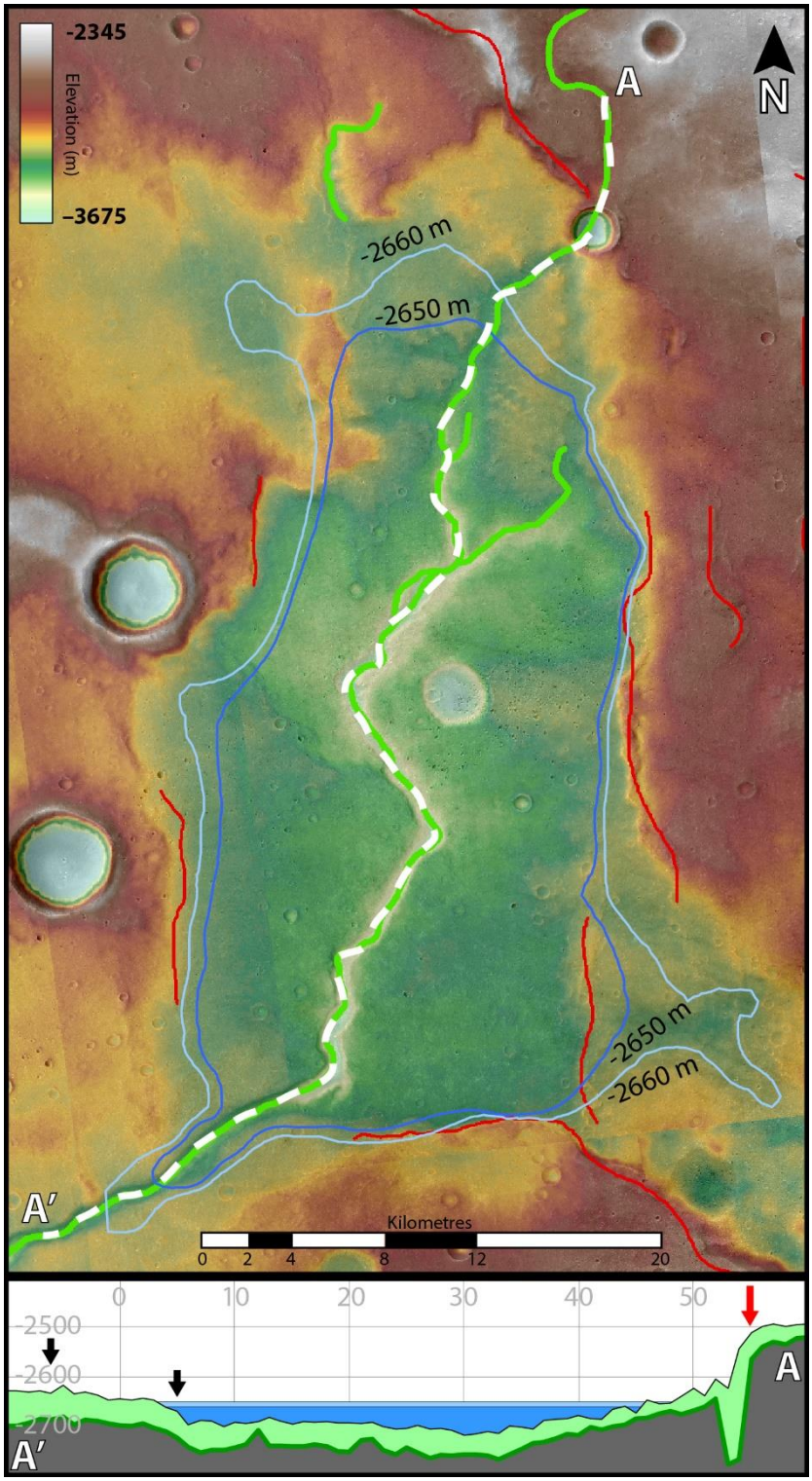

Figure 5.10 *– Detailed view of palaeolake L-CN1, with the benefit of high-resolution (20 m/pixel) CTX DEMs, showing the influence of tectonic processes on the basin geometry and longitudinal valley profile. Distinct wrinkle ridges (red lines) largely define the boundaries of basin overflow (light blue outline) and valley overflow (blue outline) palaeolake levels. The profile through the palaeolake shows the valley floor (dark green line) as well as the approximate elevation of the valley bank (light*

green area), measured as the average elevation at 1 km on either side of the valley centre-line. The profile shows a sharp drop in valley elevation correlated with a wrinkle ridge (red arrow) where the valley enters the basin, as well as a rise where the valley climbs out of the basin. The rise out of the basin is interpreted as an effect of the wrinkle ridges near the palaeolake outlet, and although there are two edges in the DEM mosaic in this area (black arrows), these artefacts do not appear to have a significant effect on the overall elevation trend.

5.4.2.2 IMPACT CRATERS

The topographic prominence of impact craters within this study is more readily recognisable than the sometimes subtle influence of tectonic ridges discussed above, with two pristine impact craters superposed onto the Coogoon valley network. The smaller crater is situated in the centre of the wide flat floored section of Coogoon Valles, with a prominence of >100 m forming a deep closed basin on the valley floor up-valley of the crater. However, due to the clear influence of the impact crater, mapping a palaeolake was not considered in this location. The effect of Kilkhampton crater on palaeolake identification is somewhat more complicated, due to the wide diameter (~45 m) covered by ejecta, and location of the crater near the end of Coogoon Valles. Although the ejecta of Kilkhampton crater only partially covers the presently observable termination of the valley network, it is thought that the crater itself is superposed directly onto a more ancient, wide and flat floor valley representing a palaeo-Coogoon system (Molina, Lopez et al. 2017, García-Arnay, Prieto-Ballesteros et al. 2019), and therefore there is greater uncertainty as to the topography existing prior to the crater.

The identification of palaeolake L-CC1 was made with a low degree of confidence due to the partial burial of the outlet valley under the ejecta blanket of Kilkhampton impact crater. To the north of Kilkhampton crater, beyond the ejecta blanket, the contour defined by the basin overflow level still defines a closed contour, and therefore it is possible that a palaeolake could have existed in this location, on a topography prior to the crate. However, in the absence of additional strong evidence supporting a palaeolake at this location, such as deltas at inlet valleys or mapped palaeolake deposits within the defined boundary, the identification of a palaeolake remains low confidence.

A small section (~23 km; 8%) of the perimeter of palaeolake L-CC2 is also defined by the raised edge of ejecta from Kilkhampton crater. However, only the basin overflow and valley overflow levels are affected by the topographic effect of the crater, with the valley extremity level sitting deeper within the central Coogoon basin. Additionally, the topographic effect of the crater is not observed at the outlet valley, where palaeolake level elevations were measured. Given these observations, the identification of a palaeolake in this instance is considered to be high, although the exact palaeolake extent may be slightly influenced by crater ejecta.

5.4.3 MULTI-CRATER PALAEOLAKE SYSTEM

The multi-crater palaeolake system, identified in the work by Fawdon et al. (2021), is a further example of a palaeolake basin with multiple fill levels, showing evidence of both open-basin and closed-basin palaeolakes within the same basin. The raised rims of the coalesced craters which compose the basin, act as a sharp drainage divide, severely limiting the upland area surrounding the craters which could have acted as a drainage catchment for surface accumulations, with only one shallowly incised valley breaching the crater rims to flow into the palaeolake, and therefore, palaeolake filling was likely driven by groundwater influx, as suggested by Fawdon et al (2021).

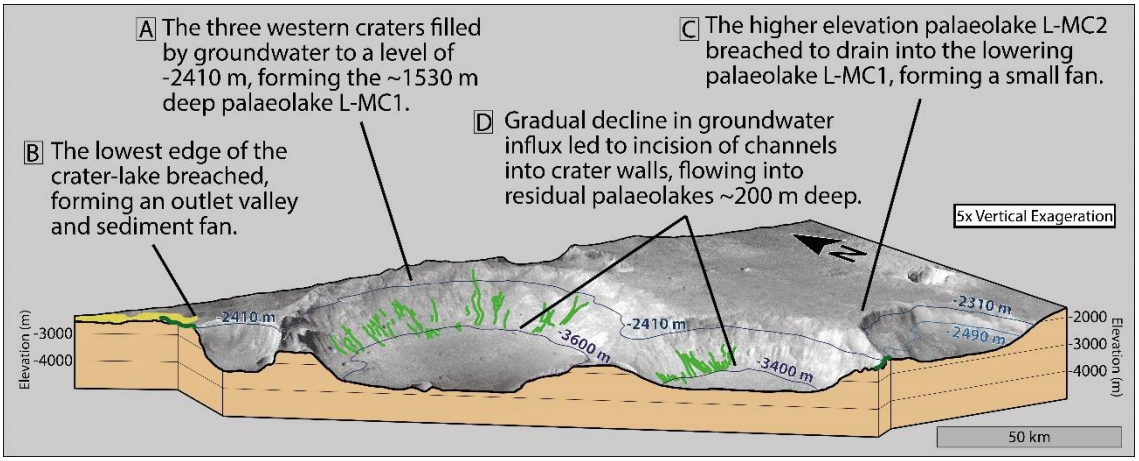

Figure 5.11 – Description of changing palaeolake levels, and transition from an open-basin to closed-basin palaeolake within the multi-crater system. (MOLA DEM topography with overlaid CTX images)

A probable sequence of events within these palaeolakes is (**Figure 5.11**): (1) filling of all four craters by groundwater influx, to an elevation near to that of the lower edge of the west crater; (2) breach of the west crater and rapid drainage of the palaeolake contained within the three western craters, with the flood forming a wide fan onto the surrounding terrain; (3) with water level lowered in the western craters as a result of the draining flood, the palaeolake in crater in the far east would be perched at a higher elevation; (4) breach of the crater wall of the far eastern crater, and drainage into the lower palaeolake to form a sediment fan; (5) gradual decline in groundwater influx, resulting in a lowering of palaeolake level, and the beginning of shallow incision of sapping valleys into the crater walls; and (6) further drop in the surrounding water table until only the deepest two crater, in the centre of the chain, had shallow ephemeral lakes.

The outlet of the multi-crater palaeolakes is short and terminates at the large sediment fan (**Figure 5.5**), with no clear continuation of incision or drainage beyond this point. On the present topography, any drainage from these palaeolakes would have flowed to the north into the central Coogoon basin containing palaeolake L-CC2, but the direction of the fan suggests flow towards the west. The short outlet, and lack of continued incision beyond the sediment fan suggests that drainage of the palaeolake was a single flooding event, and that little if any surface water or sediment reached the Oxia Planum basin.

The lack of fluvial features extending beyond the sediment fan, complicates efforts to link the multi-crater palaeolakes with palaeolakes in the Coogoon Valles system. However, evidence of groundwater influx and gradual desiccation as significant processes in the area, have implications for the overall hydrological and geological history of the landing site. If palaeolake L-CC2 was dominantly filled by groundwater influx, then it is probable that other palaeolakes identified within this chapter were also filled, at least partially, by the same process. This interpretation is in keeping with the lack of significant inlet valleys observed in palaeolakes at the origins of the three main branches of Coogoon Valles. As well as fitting into broader regional interpretations of groundwater upwelling in Arabia Terra (Andrews-Hanna, Zuber et al. 2010, Salese, Pondrelli et al. 2019), and

putting constraints on the potential importance of precipitation and surface accumulation. Overall drying throughout the study area, with later periods of limited aqueous processes also fits with the evidence for phased aqueous processes observed within the area of the landing site (Quantin-Nataf, Carter et al. 2021).

5.4.4 LOWLAND BASINS AND WATER BODIES

The present topography of Oxia Planum is such that depending on the elevation of possible equipotential surfaces, the basin could represent the edge of a water body spanning the entire northern lowlands or a small closed-basin palaeolake (**Figure 5.8**). The lower fan and valley termination within Oxia Planum at an elevation of -3110 m, indicate an equipotential surface defining a fully closed contour and a closed-basin palaeolake. While at an elevation of -2980 m, defined by the termination of Coogoon Valles, the basin is enclosed along the majority of its length (90%; 422 km), with a <47 km opening to the lowlands. The lowest point along the low barrier to the lowlands is -3100 m, giving a depth of ~120 m under the possible equipotential surface described above (**Figure 5.8a**). Therefore, even a minor change in local topography postdating a possible palaeolake, could have a significant impact on the nature and connectivity of the basin at various elevations. Besides the nature of the higher base-level as open or closed to the northern lowlands, the identification of two base-levels indicates a distinct change in water volume and depth in the basin over time.

Three proposed shorelines of a possible northern hemisphere spanning ocean are mapped within ~100 km of the termination of Coogoon Valles, two of which pass directly through Oxia Planum (Parker, Saunders et al. 1989, Parker, Gorsline et al. 1993, Clifford and Parker 2001). The global scale at which these shorelines were mapped makes them ill-suited as exact representations of a possible ocean margin (Sholes, Dickeson et al. 2021), and they are better considered as an indication that a global ocean shoreline may have existed in the area (Dickeson and Davis 2020). The elevations of the Coogoon Valles termination (-2980 m) and delta (-2996 m) are near to the range of elevations associated with possible ocean shorelines in Arabia Terra (-3000 m to -4000 m) (Dickeson and Davis

2020), and to the elevation of the Hypanis delta (-2500 m to -3000 m) which is situated ~1,300 km away on the margin of Chryse Planitia and has also been suggested as representing a possible ocean shoreline (Fawdon, Gupta et al. 2018).

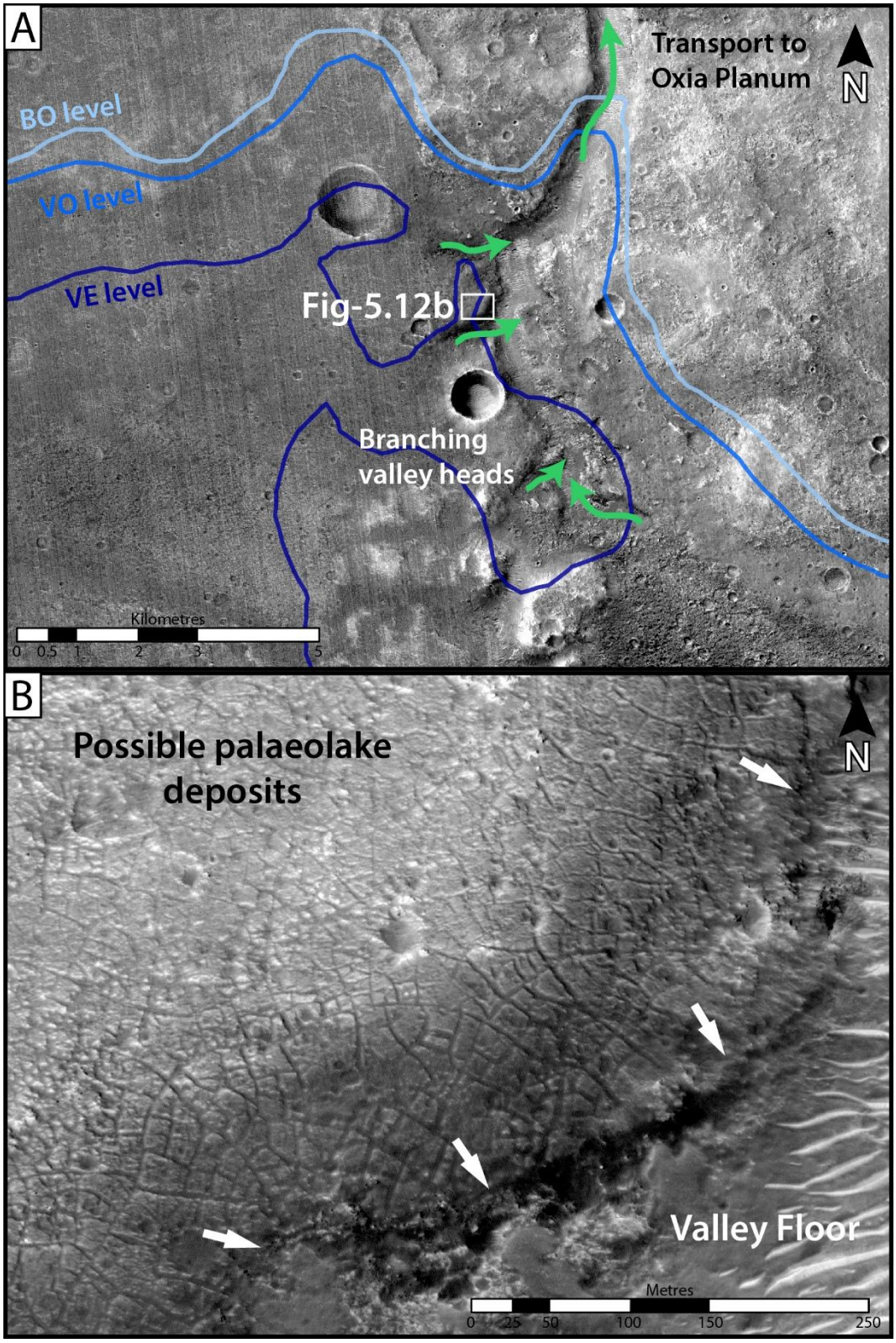

Figure 5.12 *– Detailed view of the outlet of palaeolake L-CC2, a probable site of palaeolake sediment deposition and subsequent erosion. (A) View of the outlet valley in relation to the mapped*

palaeolake levels, showing the incision of branching valley heads across the possible palaeolake floor. Also apparent is an albedo change along the north edge of the BO and VO levels, with darker deposits within the defined palaeolake. (B) Detailed image of the possible lake floor deposits, appearing as dark, and characterised by polygonal fracturing, and the sharply defined scrap (white arrows) where these deposits are interpreted as being incised by headward erosion of the outlet valley, as palaeolake level dropped. (Top: CTX image mosaic; Bottom: HiRISE image ESP_036714_1975)

It is known that substantial erosion has taken place in the region surrounding Oxia Planum (Quantin-Nataf, Carter et al. 2021), with mounds and mesas representing remnants of deposits covering the region (McNeil, Fawdon et al. 2021). A study of these features in the region by McNeil et al. (2021) reports the maximum height of mounds and mesas to be 453 m and 500 m respectively, with mean heights of 64.7 m and 168 m respectively. Although only a few mounds were identified in the present work, they are concentrated around the rim of the Oxia Planum basin. The tallest example has a prominence of ~100 m, with a maximum elevation of -2990 m, and is situated on the low rise which defines the opening of the Oxia Planum basin to the lowlands.

A testable hypothesis for the ExoMars rover will be to investigate the possible marine or lacustrine origin of sediments deposited at the landing site (Quantin-Nataf, Carter et al. 2021). A recent study by Quantin-Nataf et al. (2021) has indicated possible base-levels (-2960 m & -3120 m) within the Oxia Planum basin similar to those presented in this thesis, and concludes that these levels likely represent an ocean or sea if the current topography is representative of the past. However, based on stratigraphic relationships, mounds in the region are thought to be younger than the phyllosilicate-bearing unit that is the primary target of investigation by ExoMars (McNeil, Fawdon et al. 2021), as are base levels in Oxia Planum indicated by valleys and possible deltas within the basin (Quantin-Nataf, Carter et al. 2021). Therefore, if mounds observed in this study represent isolated remnants of a deposit covering the region, then the ancient topography of Oxia Planum would form a fully closed basin rather than an embayment on the edge of an ocean in the lowlands. Given the climatic and geological issues associated with supporting an ocean in the northern lowlands (Malin and Edgett 1999, Wordsworth, Forget et al. 2013, Wordsworth 2016, Sholes, Dickeson et al. 2021), the existence of a palaeolake within Oxia Planum is a more in keeping with the available evidence than an ocean. A series of

closed-basin palaeolakes in the lowlands, directly adjacent to the dichotomy, rather than a hemisphere spanning ocean, would also match observations made in other Mars regions (Rivera-Hernández and Palucis 2019).

5.4.5 Implications for Biosignatures and Sediment Transport

The palaeolakes previously identified within the drainage catchment of Oxia Planum indicate significant volumes and coverage of liquid water across the surface (Goudge, Aureli et al. 2015, Fawdon 2018), and therefore characterise a landscape representing a range of potentially habitable environments (Summons, Amend et al. 2011). However, the majority of previously identified palaeolakes represent endorheic basins, and cannot have contributed sediment to the basin in Oxia Planum, and the four open-basin palaeolakes that are identified are not clearly traced from source to sink. In contrast, the open-basin palaeolakes identified in this chapter are all integrated into the Coogoon Valles system, and represent sources of sediment and possible organic material that could have been transported to Oxia Planum.

Fluvial sediment delivered to Oxia Planum could have been eroded and transported from any of the geological materials which are incised by valleys in the Coogoon Valles system, representing a range of possible ages and origins (Tanaka, Skinner et al. 2014, Molina, Lopez et al. 2017). Palaeolake deposits on Earth often contain a high-proportion of organic material, with shallower palaeolakes associated with greater biological activity (Wetzel 2001), and shallow palaeolakes are considered as ideal settings to search for evidence of life on Mars (Fassett and Head 2008). Palaeolakes within basins in the inter-crater plains, like those identified in the present work, exhibit far shallower mean depths than crater-hosted palaeolakes, and may therefore represent areas of the greatest interest when considering sediment contribution to Oxia Planum.

The clearest example of incision, erosion, and transport from possible palaeolake deposits is observed at the outlet of palaeolake L-CC2 (**Figure 5.12**). The branching valley head incises into dark material, identified by Fawdon et al. (2018) as possible palaeolake deposits, within all three palaeolake levels defined. The interpreted sequence of events

within this palaeolake basin are as follows: (1) filling of the basin up to the basin overflow level; (2) breach of the basin to begin forming the outlet valley; (3) gradual erosion of the outlet valley, dropping the palaeolake surface to the valley outlet level, with parts of the former palaeolake floor beginning to be eroded; (4) continued erosion of the outlet valley, with the valley heads spreading further across the palaeolake floor, eroding more palaeolake deposits; and (5) palaeolake drainage finally ceasing with the residual palaeolake defined at the valley extremity level. The valley from this point continues ~95 km to the dichotomy, and Oxia Planum, without passing through further palaeolake basins which might act as sediment traps, and thus sediment eroded from palaeolake L-CC2 could have been transported the full distance downstream.

The sequence described above postdates the phyllosilicate deposits in Oxia Planum which are the main target of ExoMars, and therefore any sediment delivered would be found in other deposits. The outlet area of palaeolake L-CC2 has also been the subject of compositional analysis, comparing spectral observations made with CRISM at this possible source to locations within Oxia Planum (Turner, Fawdon et al. 2021). The preliminary results of that work indicate a strong association of light toned units at this location, with phylosilcate deposits at the landing site and across the region, but no analysis is included regarding the darker toned deposits. It is hoped that further analysis of CRISM data at this location will yield additional observations related to the possible palaeolake deposits identified in this chapter, allowing a comparison to future rover observations, similar to orbital and in-situ observations at Gale crater (Palucis, Dietrich et al. 2016).

5.5 CONCLUSIONS

This chapter expands on previous works defining the drainage catchment of Oxia Planum, by identifying open-basin palaeolakes constituting an extensive branching system, terminating at two possible closed-basin palaeolake levels within Oxia Planum. The open-basin palaeolakes represent a significantly greater coverage of water across the catchment area than previously identified, and present a wide range of possible habitable

environments which could have contributed sediment to the landing site. Contrary to previous investigations, this work suggests that water bodies existing within the basin of Oxia Planum were closed-basin palaeolakes, rather than the edge of a hemisphere-spanning ocean.

The identification of palaeolakes on Mars is heavily reliant on interpretations of the current surface topography, and the area of Oxia Planum presents a particular challenge to established methods of palaeolake identification due to a high prevalence of wrinkle ridges and impact craters. Examined in detail, the boundaries of some possible palaeolakes are defined by these more recent topographic features, and thus the palaeolake elevations, extents, and volumes are less accurate. However, examined in detail the total topographic prominence of wrinkle ridges and recent impacts is less significant than the basins defined by the underlying terrain, and therefore palaeolakes would still be identified within the same basins on a topography existing before tectonic or impact processes. This highlights the robustness of palaeolake identification by outlet elevation, but also suggests the application of caution in extracting values from identified palaeolakes such as palaeolake dimension and exact extent. Changes in topography also have the potential to exclude areas of the true palaeo-drainage catchment, as evinced by valleys and palaeolakes situated on the north Coogoon branch.

Specific examples of where lacustrine sediments, would have been deposited in the highlands, and then later eroded and transported, afford the opportunity to compare mineralogy between sources and sinks. Ultimately, these sediments, and any potentially organic material may be deposited and preserved within the Oxia Planum basin, and potential targets for ExoMars.

6

Catalogue of Palaeolakes and Drainage in Western Arabia Terra

The two preceding chapters describe individual palaeolake and valley systems with terminations at the planetary dichotomy, both representing highland drainage catchments which once contributed runoff and sediment to basins in the northern lowlands. The final aim of this thesis is to present a broader picture of drainage patterns across Arabia Terra, and to determine to what extent drainage from the highlands to the lowlands is representative of the region as a whole. To that end, the following chapter introduces a catalogue of possible fluvial landforms, palaeolakes, and drainage systems in western Arabia Terra. The methods and detailed observations of individual palaeolakes in preceding chapters provide the basis for a systematic survey of fluvial and lacustrine features, and a nuanced interpretation of palaeolake identification through topographic analysis. The regional scale of this catalogue fills a significant gap in the current hydrological understanding of Mars; systematically covering an area large enough to be compared to global palaeolake data, and undertaken at a high resolution matching that of detailed local studies. The results indicate a far greater number of palaeolakes in Arabia Terra than identified in previous global catalogues, and a high degree of connectivity between palaeolakes, forming long chains across the highlands. Linking palaeolakes and fluvial features into drainage systems demonstrates that the majority of open-basin palaeolake drainage constitute endorheic systems, terminating within deep sinks in the highlands, while few catchments terminate at the dichotomy, typically representing limited drainage catchments not extending great distances into the highlands.

6.1 INTRODUCTION

Studies of individual palaeolake systems have contributed greatly to the present understanding of regional hydrological histories on Mars, often indicating multiple episodes of locally or regionally controlled lacustrine activity rather than a global hydrological system stable over geological timescales (Mangold and Ansan 2006, Di Achille, Hynek et al. 2009, Salese, Di Achille et al. 2016, Wilson, Howard et al. 2016, Goudge and Fassett 2018). In particular, surface investigations by NASA's Curiosity and Perseverance rovers, within palaeolakes in Gale and Jezero craters respectively, have provide incredibly detailed outcrop-scale observations of lacustrine geology (Grotzinger, Gupta et al. 2015), and have prompted complementary research into the broader hydrological and climatic conditions which once existed in these regions (Milliken, Grotzinger et al. 2010, Horvath and Andrews-Hanna 2017, Rivera-Hernández and Palucis 2019). However, beyond these high-profile examples, research into regional palaeolake trends including relationships to fluvial, groundwater, and possible ocean systems is limited. The incorporation of local palaeolake studies into wider regional and global contexts is also hindered by a lack of intermediate, regional scale catalogues.

Global catalogues of Mars indicate up to 226 open-basin palaeolakes within a variety of morphological basins (Fassett and Head 2008, Goudge, Head et al. 2012), and up to 205 closed-basin palaeolakes within impact crater basins (Goudge, Aureli et al. 2015)(**Figure 6.1 a**). Western Arabia Terra includes a relatively high proportion of globally catalogued closed-basin palaeolakes (9%; n=18), but only one of the globally catalogued open-basin palaeolakes, with a few additional open-basin palaeolakes (n=6) tightly grouped near the Mamers Valles drainage system (**Figure 6.1 b**). These global catalogues were compiled primarily from observations of 232 m/pixel THEMIS IR daytime imagery, with ~463 m/pixel MOLA and 50 – 225 m/pixel HRSC topographic data, and palaeolakes were identified based on morphological relationships between topographic basins and fluvial valley networks. Open-basin palaeolake catalogues by Fasset et al. (2008) and Goudge et al. (2012) identified palaeolakes where outlets began within closed topographic basins, indicating a fill level sufficient to breach and overflow

the basin. The closed-basin palaeolake catalogue by Goudge et al. employed a more limited set of criteria, and only considered palaeolakes within impact craters, where an inlet was observed to breach the crater rim (Goudge, Aureli et al. 2015, Goudge, Fassett et al. 2016).

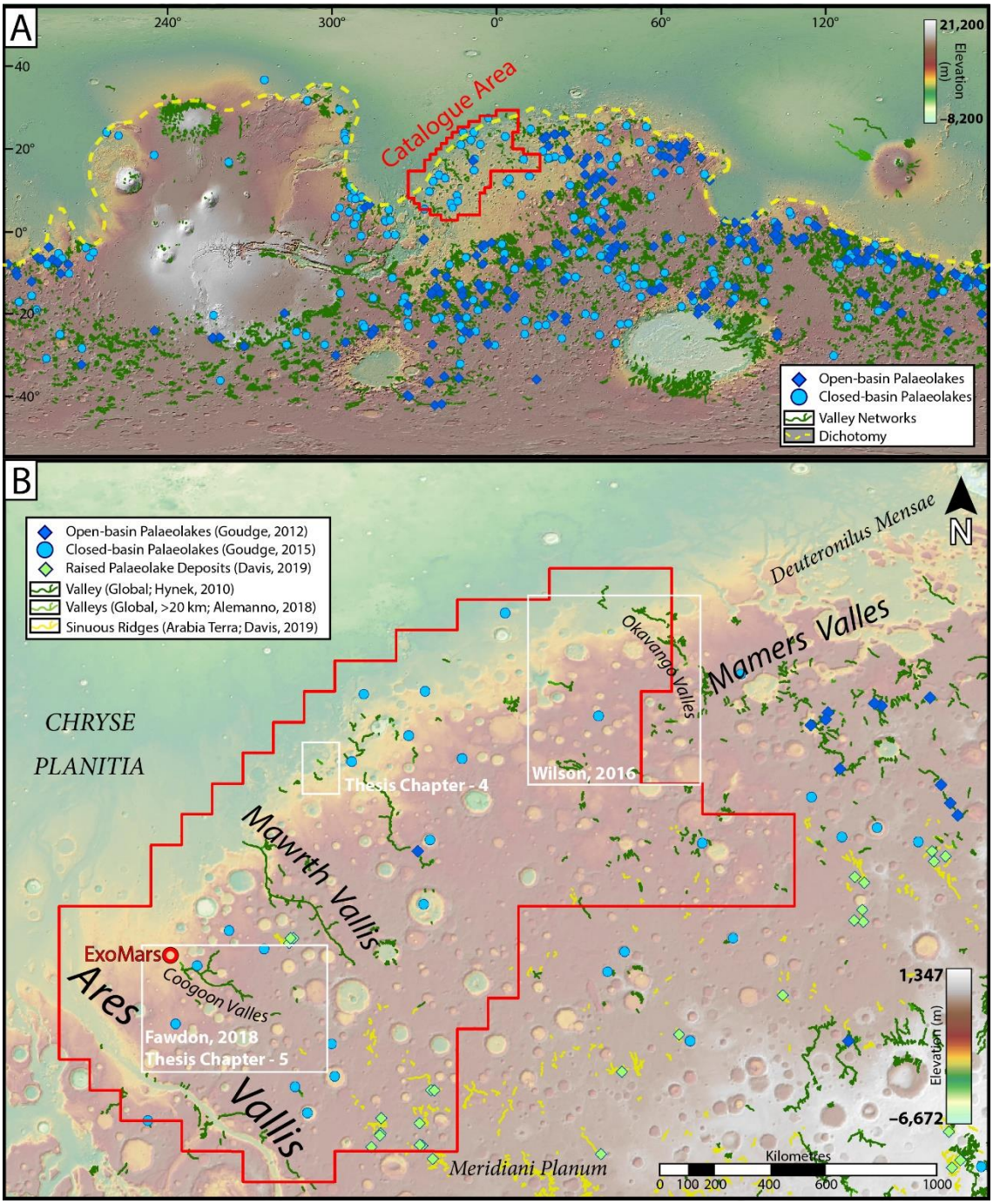

Figure 6.1 *– Global and regional maps showing the context of the study area, and the distribution of previously catalogued fluvial and lacustrine features. (A) Global context of the catalogue area straddling the dichotomy in Arabia Terra, showing the global distribution of: open-basin palaeolakes (dark blue diamonds; Goudge, 2012), closed-basin palaeolakes (light blue circles; Goudge, 2015), and valley networks (Hynek, Beach et al. 2010, Alemanno, Orofino et al. 2018). This global view highlights the low proportion of globally catalogued open-basin palaeolakes and valley*

networks within the low-lying region of Arabia Terra. (B) Regional map of western Arabia Terra, showing: named fluvial features and geographic features, the ExoMars landing site at Oxia Planum (red point), existing global catalogues of palaeolakes and valley networks, and a regional catalogue of depositional fluvial and lacustrine features (Davis, Gupta et al. 2019). Also shown are the extents of palaeolake and drainage studies within the catalogue area, as published by Wilson et al. (2016) and Fawdon et al. (2018), and the individual palaeolake system studies set out in chapters 4 and 5 of this thesis. (MOLA topography DEM with hill-shade)

The global distribution of catalogued martian palaeolakes (Fassett and Head 2008, Goudge, Fassett et al. 2016) approximately correlates to that of valley networks (Hynek, Beach et al. 2010, Alemanno, Orofino et al. 2018), and is therefore almost entirely limited to the southern highlands where most valley networks occur. Many palaeolake and valley systems terminate at the edge of the northern lowlands (Wilson, Howard et al. 2016, Goudge and Fassett 2018), and although the processes leading to the formation and present morphology of the planetary dichotomy are not well understood (Watters, McGovern et al. 2007), this planet-spanning feature may represent the margins of an ancient hemisphere-spanning ocean (Parker, Schneeberger et al. 1986, Clifford and Parker 2001, Di Achille and Hynek 2010, Fawdon, Gupta et al. 2018). The termination of fluvial systems at the dichotomy represents some of the most robust evidence for oceans in the northern lowlands (Di Achille and Hynek 2010), and therefore, constraining the upland extent of highland drainage catchments is important to understanding the hydrological input to possible oceans in the northern lowlands (Dickeson and Davis 2020).

Localised studies within Arabia Terra indicate additional palaeolakes in the area of Coogoon Valles (Fawdon 2018), and to the west of Okavango Vallis (Wilson, Howard et al. 2016)(**Figure 6.1 b**). These palaeolakes and palaeolake chains represent a mix of systems draining to the dichotomy, and endorheic systems ending at sinks within the highlands. However, the palaeolake identification criteria in these studies differ from those employed in global catalogues, and as a consequence, these palaeolakes are not readily comparable to the majority of other palaeolake studies on Mars.

Expanding on the palaeolake systems investigated in chapters 4 and 5 (**Figure 6.1 b**), this chapter compiles a regional catalogue of fluvial and lacustrine features in western

Arabia Terra, using high-resolution ~6 m/pixel Context Camera (CTX) mosaics. The catalogue covers an area of 3,541,649 km^2, equating to 2.5% of the martian surface or 3.5% of highland terrains. The southwest edge is defined by Ares Vallis and the Chryse Chaos terrains, and to the northeast by Dueteronilus Mensae and the drainage catchment of Okavango Valles, with terrain between these more recent catastrophic outflow and collapse features relatively undisturbed by younger features besides impact craters. To the north and northeast, the study area is approximately bounded by the planetary dichotomy, and coverage to the south and southeast was extended as far as to reach the limits of idealised drainage catchments (Fawdon 2018), a paucity of fluvial features (Hynek, Beach et al. 2010, Alemanno, Orofino et al. 2018), and a transition from erosional to depositional fluvial landforms (Davis, Gupta et al. 2019). The catalogue includes a comprehensive mapping and analysis of erosional and depositional fluvial landforms, sediment fans and deltas, and open-basin and closed-basin palaeolakes. Trends and distributions of hydrological features were analysed to identify the influence of regional topography, and the planetary dichotomy in particular, on local and regional hydrological processes. The principal aim being to identify drainage catchments and sinks based on linkages between catalogued palaeolakes and fluvial features, and thus to constrain the relative significance of highland areas contributing surface runoff to the lowlands or to endorheic highland basins.

6.1.1 DICHOTOMY SCARP AND REGIONAL SCALE CHANNELS

Throughout Arabia Terra, the planetary dichotomy is expressed as a scarp defining a boundary between ancient highland and younger lowland terrains. Previous global catalogues have identified very few fluvial features in the lowlands beyond the dichotomy (Hynek, Beach et al. 2010, Alemanno, Orofino et al. 2018), and this natural hydrological boundary marks the approximate north-western extent of the study area, although the catalogue of fluvial features extends ~100 km beyond the dichotomy to fully capture the transition from highlands to lowlands. The dichotomy, defined as the major scarp between highlands and lowlands, was mapped as a continuous line across the study area. The dichotomy scarp is less pronounced in the southwest of the study area near the

terminations of Ares and Coogoon Valles, where it displays a more gradual slope from highlands to lowlands, and a higher average elevation. The dichotomy is also less pronounced to the north-east where scarps associated with the Deuteronilus Mensae chaos formations complicate identification of the dichotomy. A longitudinal profile of the dichotomy shows large local variations in elevation, most likely a consequence of mismatch between the mapping of the dichotomy on high-resolution imagery, and production of the profile on lower resolution MOLA topographic DEM.

In addition to the fluvial features mapped in this catalogue, are three regional scale channels within the study area: Ares Vallis, Mawrth Vallis, and Mamers Valles. These features significantly influence the topography of the region, but are of an uncertain age in relation to the smaller scale fluvial features which are the focus of this work, and are therefore considered independently.

Ares Vallis defines the south-western limit of the catalogue area and is the largest outflow channel emptying into Chryse Planitia, with a width of ~100 km at the dichotomy terminus, and a length of ~1,700 km beginning at a nominal source region within Iani Chaos. However, the true length of the associated drainage system has been considered to include a chain of valleys and palaeolakes extending >3,000 km further south, and originating at the edge of Argyre Planitia (Parker, Clifford et al. 2000, Dohm, Ferris et al. 2011). As with the dichotomy scarp, the steep north bank of Ares Vallis was mapped to delineate the edge of the study area, and defines a ~1,500 m drop from highlands to channel floor. The formation of Ares Valles is thought to have occurred over an extend period of time, with the earliest flows during the late Noachian to early Hesperian, and the latest deeply eroding flows continuing into the late Hesperian and early Amazonian (Warner, Gupta et al. 2009). Timing the topographic influence of Ares Vallis on hydrology and drainage in the region is therefore uncertain. The global peak in fluvial and lacustrine activity is generally agreed to have occurred during the late Noachian to early Hesperian (Fassett and Head 2008, Goudge, Head et al. 2012, Goudge, Fassett et al. 2016), and as a result, some fluvial and palaeolake systems may have existed on a topography prior to full incision of Ares Vallis, and some may have drained into the incised channel.

Mawrth Vallis lies near the centre of this study area, and is on a similar scale to circum-Chryse outflow channels: with a width of ~60 km at the dichotomy terminus, a maximum depth of ~700 m, and extending for a length of ~750 km into the highlands. Although Mawrth Vallis displays a consistent width along length, it does not conform to many of the other morphological characteristics typical of outflow channels, and instead: does not originate in a region of chaos terrain; displays a heavily cratered and degraded appearance, with shallow sloping banks; and does not extend beyond the dichotomy. The age of this feature is not well constrained, but is likely to pre-date fluvial and lacustrine process within the study area (Poulet, Gross et al. 2020).

The Coogoon Valles system is also fully within the study area and displays some morphological characteristics indicative of a larger, regional scale landform. Although the majority of the channels in the system are typical of steep sided, branching, fluvial valley networks on Mars, some sections of the network display wide, flat floored channels similar in morphology to Mawrth Vallis. This has led to the interpretation that a palaeo-Coogoon Valles existed prior to the incision of smaller scale fluvial features (Molina, Lopez et al. 2017, Fawdon 2018).

Mamers Valles is ~1,000 km long from Cerulli crater to the channel head at the dichotomy within Deuteronilus Mensae, and outside the present study area. However, Cerulli crater appears to overprint the valley and it has been suggested that Naktong Vallis, Scamander Vallis, and an associated chain of palaeolakes would have originally fed into Mamers Valles (Fassett and Head 2008). The upper reaches of Mamers Vallis display morphological characteristics typical of fluvial valley network, and the channel is ~6 km wide and ~500 m deep where it enters the basin of Ismenius Cavus, but the lower reaches are far wider (~33 km) and deeper (>1,000 m) with flat floors dominated by ice and periglacial morphological forms. Although a number (n=9) of open-basin palaeolakes have been identified in previous global catalogues, the prevalence of icy features and uncertainty in the position of the dichotomy make the area surrounding Mamers Valles poorly suited for inclusion in the present study

6.2 DATA AND METHODS

Context camera (CTX, 5 m/pixel) imagery provided the basis for geomorphological mapping and analysis, and the CTX mosaics produced by Murray Labs were used to provide consistent coverage of the entire catalogue area (Dickson, Kerber et al. 2018). Additional CTX and THEMIS daytime infrared images supplemented the limited areas where CTX mosaics were of low or uncertain quality, or missing data.

Initial identification and mapping of features was carried out by systematically surveying CTX image mosaics. The Murray Labs CTX mosaics are downloadable as equidistant cylindrical projected 2° square tiles, with geodesic dimensions ranging from ~119 x ~118 km near the equator (4°N), to ~119 x ~85 km at the northernmost limits of the study area (44°N). Each tile was investigated by manual side to side scanning, beginning in an upper corner of the tile at a map scale of 1:30,000, affording view extents of ~5.5 x ~5.5 km in the south and ~5.5 x 4.0 km in the north of the study area. Features within the view extent were mapped as lines, and the view was then panned to the side to map features within the adjacent view extent. Upon completion of each row the view extent was shifted down with a ~20% overlap, then panned and mapped in the same manner back along the next row. This process was repeated to map features across the entire 2° tile. After completion of side to side scanning, map scale was reset at 1:150,000 to map any larger landforms within the tile which were not evident in narrower views, and then with the MOLA topography DEM overlaid to identify any additional channels not observed with visible imagery alone.

Following initial tile mapping across the entire study area, all fluvial features were reassessed in the context of surrounding geomorphology and topography at a range of scales, and with colourised MOLA and HRSC topography DEMs overlaid. In this phase of cataloguing attributes were added to every feature, ascribing: (1) a level of confidence in identification, (2) flow direction, (3) planform relationship to other fluvial features, (4) and dominant morphology.

Identification of putative palaeolakes was achieved by generating elevation contours at 10 m intervals, and examining the relationships of all high confidence valleys transecting, originating, or terminating within topographic basins. Contours were produced with ~456 m/pixel resolution MOLA data for the complete catalogue area.

6.2.1 HYDROLOGICAL ANALYSIS

Drainage catchment areas were calculated using the ESRI ArcMap 'Hydrology Toolbox' with ~456 m/pixel MOLA DEM topography (See, Data and Methods 3.3.3). Variations on the workflow were employed to produce two sets of hypothetical drainage catchments based on maximum or partial filling of the topography to represent drainage patterns within the catalogue area at two scales (**Figure 6.2**): (1) major drainage catchments were generated on a topography filled to remove all sinks, with pour points manually defined at the terminations of existing mapped valleys and outflow channels along the dichotomy; and (2) local drainage catchments were generated on a partially filled topography, only filling sinks with a maximum depth of 100 m, with pour points generated automatically for all remaining sinks.

In the present study, local drainage catchments produced on a partially filled topography are intended to meet the following objectives: (1) eliminate noise, and erroneous pixels in the data; (2) fill sinks of minor topographic significance on the scale of the study; (3) fill a majority of any open-basins palaeolakes which might exist on the topography; and (4) produce a manageable number of local drainage catchments, whilst providing a granular breakdown of sinks and drainage divides. A fill depth of 100 m was chosen to meet these requirements, representing local drainage on a topography with unknown continuity, connectivity and volume of ancient surface runoff. This depth also falls within the realistic range of palaeolake depth as identified in previous catalogues. The majority (>70%) of catalogued open-basin palaeolakes have a mean depth of less than 100 m (Fassett and Head 2008), and a fill depth of 100m produces a topography in which shallower (<100 m) palaeolake basins would be filled and integrated into a single drainage

catchment, and only deeper (>100 m) palaeolake basins would be superimposed across multiple drainage catchments.

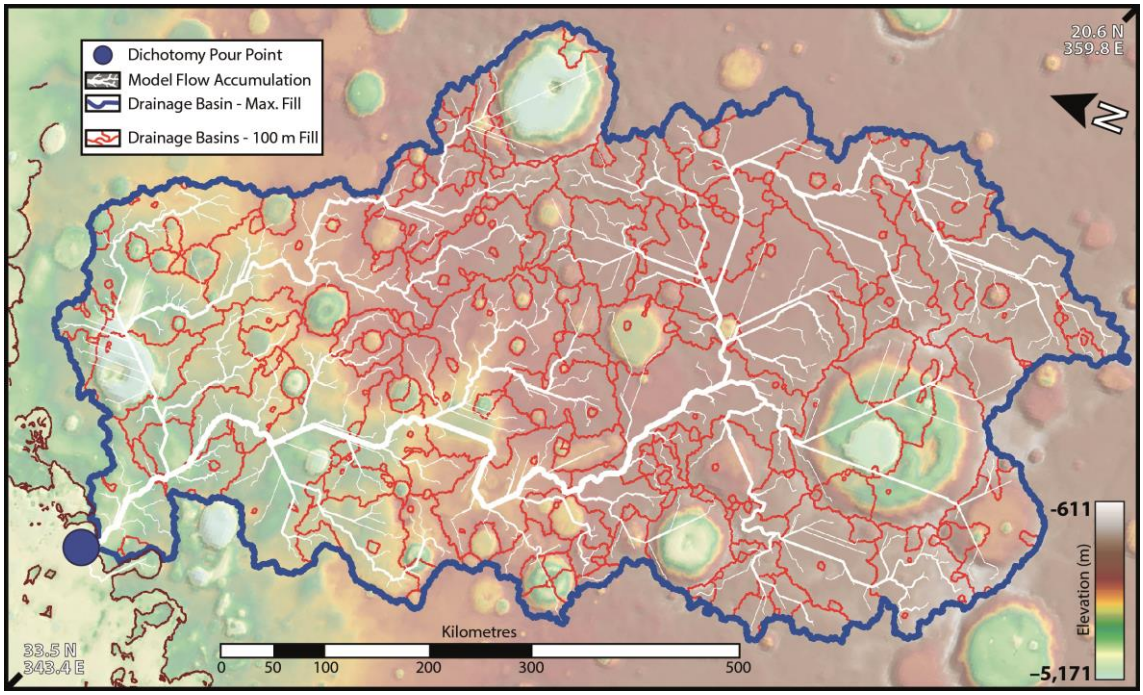

Figure 6.2 *–Example of a drainage catchment within the western Arabia Terra catalogue area, with basins produced on topographic data filled to different depths. An idealised drainage catchment (thick blue outline) and idealised drainage network (white lines), calculated on a topography with all sinks filled to an unlimited depth, for a pour point (blue circle) at the termination of a valley at the dichotomy. An additional set of local drainage catchments (thin red outlines) composing shallower sub-basins for the same area, were calculated on a topography only filling sinks with a maximum depth <100 m. The area mapped in this figure is shown in the context of wider region in Figure 6.3, and discussed in greater detail later in the chapter within section 6.6.4 and figure 6.16. (MOLA topography)*

6.3 OBSERVATIONS

In order to produce a catalogue of palaeolakes and drainage catchments in western Arabia Terra, morphological features were systematically surveyed and mapped, and then analysed in the context of regional and local topography. The scarp of the planetary dichotomy was mapped to delineate the limits of highland terrains, with major drainage catchments defined with pour-points at the dichotomy, in addition to local drainage catchments reflecting local scale drainage patterns and sub-basins (**Section 6.3.1**). Mapping and characterising fluvial features (**Section 6.3.2**) and sediment fans (**Section 6.3.3**) provided overall trends in fluvial activity, density, and flow direction, and most

importantly, the relationship between fluvial features and topographic basins allowed the identification and mapping of open-basin and closed-basin palaeolakes (**Section 6.3.4**).

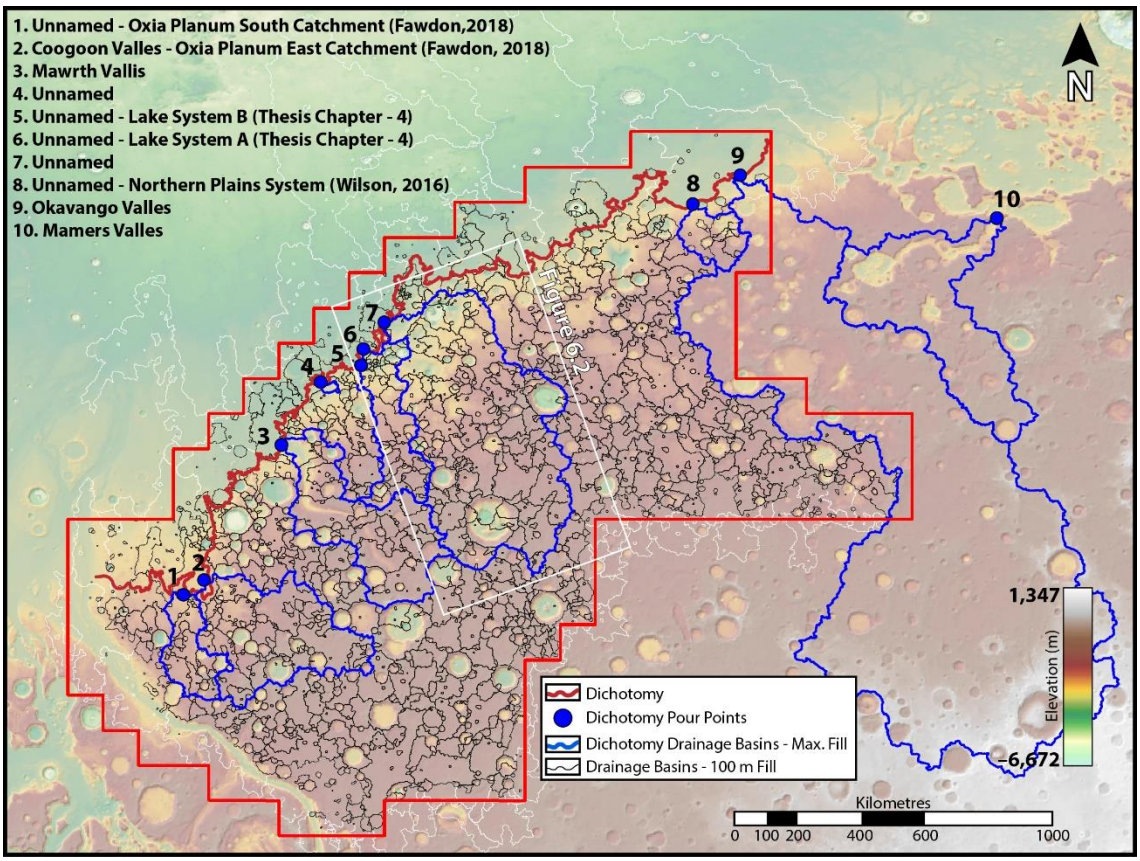

Figure 6.3 *– Map of the major dichotomy drainage catchments (blue outlines) as calculated on a fully filled topography, with pour points (blue circles) placed at existing mapped and published valley terminations at the dichotomy (purple line). Smaller drainage catchments, or sub-basins, calculated on a partially filled topography (<100 m), are shown by thin black lines where completely within the catalogue area, and by thin white lines where partially within the catalogue area. The 100 m sub-basins are shown in greater detail in* ***Figure 6.2****, and further details for all dichotomy drainage catchments are shown in* ***Table 6.1****. (MOLA topography and hill-shade)*

6.3.1 DICHOTOMY DRAINAGE CATCHMENTS

Idealised drainage catchments were calculated on a fully filled topography with pour-points positioned along the dichotomy at the terminations of valleys mapped in previous global catalogues (Hynek, Beach et al. 2010, Alemanno, Orofino et al. 2018), and regional studies within Arabia Terra (Wilson, Howard et al. 2016, Fawdon 2018)(**Figure 6.3**). A total of ten valley networks were identified (**Table 6.1**), including four named features: Coogoon Valles, Mawrth Vallis, Okavango Valles, and Mamers Valles; and six unnamed valleys, of which, four are the focus of published palaeolake studies (Wilson,

Howard et al. 2016, Fawdon 2018), and three are investigated in chapters 4 and 5 of this thesis. The Mamers and Okavango catchments fall outside the present study, with the catchment of the latter extending far to the south, and defining the eastern edge of the catalogue area (**Figure 6.3**). The calculated dichotomy catchments cover a large proportion of the catalogue area (24%; 833,961 km^2), although with two significant areas omitted: (1) a wide band between the Okavango catchment and unnamed catchment #7, here referred to as the 'Becquerel crater system', which contains no catchments due to a paucity of mapped valleys along this section of the dichotomy; and (2) an area in the southeast of the study, which mostly would drain towards Ares Vallis, but was not calculated as the channel marks the edge of the current study area and the full drainage catchment extends >3,000 km south to the Argyre basin.

Table 6.1 *– Characteristics and dimensions of the major dichotomy drainage catchments mapped in* ***Figure 6.3****, including: catchment area, elevation of pour point at the dichotomy, maximum elevation point within the catchment. Also included are previous detailed palaeolake studies where they exist for dichotomy drainage catchments, with valleys used in the placement of pour points sourced from previous catalogues and other published works (Hynek, Beach et al. 2010, Wilson, Howard et al. 2016, Alemanno, Orofino et al. 2018, Fawdon 2018).*

Dichotomy Catchment	Channel Name	Area (km^2)	Pour Point Elevation (m)	Maximum Catchment Elevation (m)	Palaeolake Study
1	-	46,087	-3041	-582	(Fawdon 2018)
2	Coogoon Valles	158,342	-3096	-578	(Fawdon 2018) & Chapter 5
3	Mawrth Vallis	147,990	-3852	-268	
4	-	1,632	-3756	-3069	
5	-	110	-3764	-3240	Chapter 4
6	-	72,745	-3977	-1149	Chapter 4
7	'Becquerel Crater System'	347,100	-3984	-526	
8	-	32,955	-3759	-1741	(Wilson, Howard et al. 2016)
9	Okavango Valles	1,218,219	-3720	1192	
10	Mamers Valles	215,678	-3342	-750	

Using a topography with only sinks deeper than 100 m filled, generated 2,276 drainage basins fully within the catalogue area, and 111 drainage basins only partially within the catalogue area (**Figure 6.3**). For the sake of consistency only the local drainage basins fully inside the catalogue area were considered for the bulk analysis. These drainage basins are also used to visualise the distribution and density of fluvial and lacustrine

features across the catalogue area, and to bin feature characteristics such as flow direction and fluvial feature type. Most importantly, these local drainage catchments are utilised in the latter part of the discussion to construct morphologically derived drainage catchments.

6.3.2 FLUVIAL FEATURES

A total of 33,441 linear features were initially mapped as possible fluvial features in the study area. A degree of confidence was then assigned to each linear feature to indicate the likelihood that it was the product of fluvial processes based on further observations of context, topography, and geomorphology. A large number of initially identified linear features were discarded (n=12,669) as likely being the result of non-fluvial processes, such as: radial furrows or concentric lobes associated with impact ejecta; fractures or chaos terrains; wrinkle ridges; or erosional scarps and steps.

The remaining 20,772 features, totalling 51,519 km in length were identified as being of fluvial origin (**Figure 6.4**), and subdivided as high (n=12,998) or low (n=7774) confidence. Features qualifying as high confidence typically displayed multiple characteristic fluvial morphologies such as branching, anabranching, or meandering, as well as traits indicating a good state of preservation such as clearly defined edges, and discernible extents. Topographic fit was also considered in the determination of confidence where features were sufficiently long or wide in relation to available topographic data. Uncertain features with longitudinal profiles incongruous with local and regional slopes, and those with no evident cross-sectional profile were often considered to be of lower confidence. More generally, low confidence features were those with only some characteristic fluvial morphologies, and in areas where observation was complicated by more recent destructive processes such as impact cratering and erosion.

All putative fluvial features, of high and low confidence, were attributed with additional observations characterising: (1) flow direction including start point, end point, and overall bearing; (2) planform relationship to other fluvial features, classifying the different parts of branching fluvial networks; (3) and broad morphological classification,

defined by cross-sectional profile. The following sub-sections describe these fluvial observations in greater detail, and present an initial analysis of fluvial trends in the catalogue area.

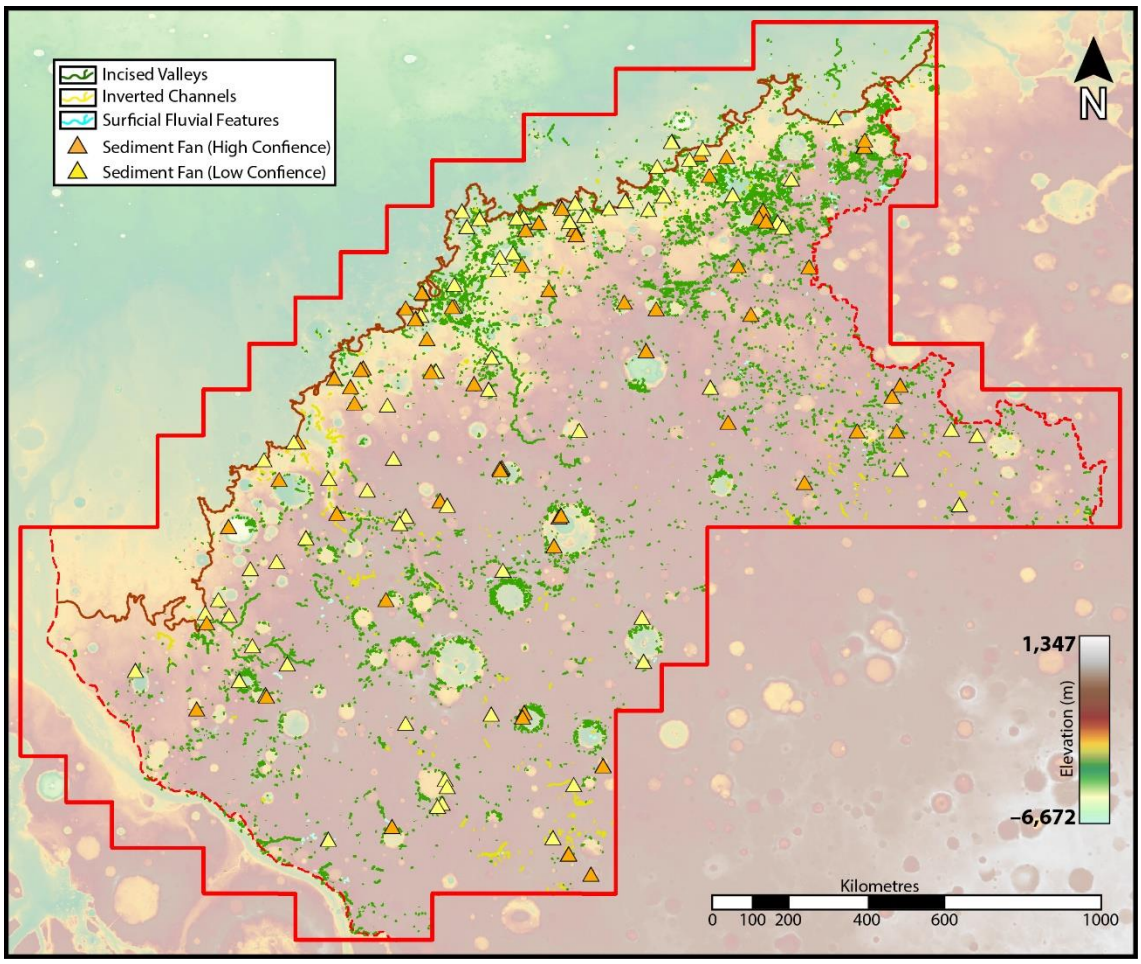

Figure 6.4 *– Map of catalogued fluvial features and sediment fans, and the planetary dichotomy. (A) Map of all catalogued fluvial features, with morphology denoted by colour: incised valleys (green), inverted channels (yellow), and surficial flow features (cyan). The locations of sediment fans identified with high (orange triangles) and low (yellow triangles) are also shown on the map. (MOLA topography)*

6.3.2.1 *FLOW DIRECTION*

Flow direction was inferred for each fluvial feature based on a combination of the overall longitudinal profile of valleys, valley width along length, and the nature and angle of valley intersections in branching networks (**Figure 6.5**). Flow direction allowed segment start and end points to be defined for each fluvial segment, and by creating a direct line between start and end points, each fluvial segment was attributed with an overall bearing.

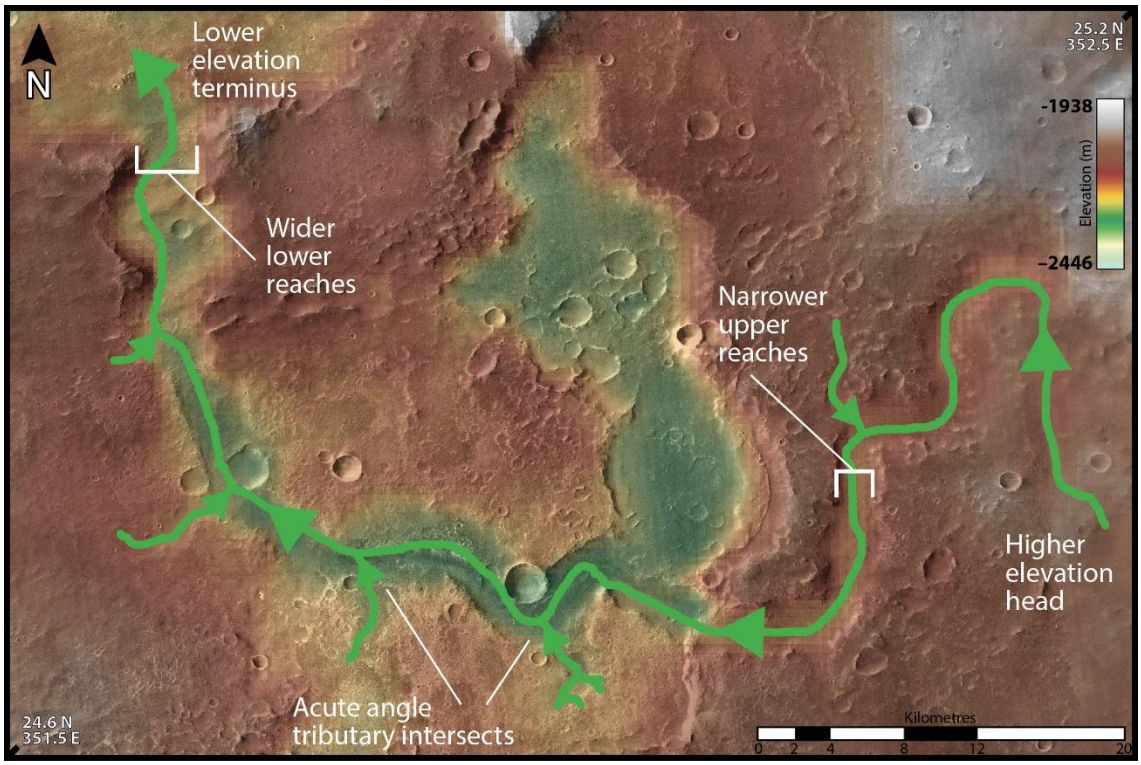

Figure 6.5 – Example of evidence used to infer flow direction of fluvial features, overall valley flow direction and tributaries shown with arrows based on a combination of: (1) overall valley slope and elevation from head to terminus; (2) widening of valley along length; (3) acute angle of intersecting tributaries. (MOLA topography on CTX mosaic)

The directional trend in the total population of fluvial features only shows a weak preference for northward flow when weighted equally (**Figure 6.6 a**), but the sum of fluvial feature length displays a stronger preference in westward and north-westward flow direction (**Figure 6.6 b**). A further breakdown of the relationship between individual fluvial segment length (l_F) and bearing indicates that the longest features (l_F >20 km; n=130) show a strong north-westerly trend (**Figure 6.6 c**), weakening with reducing length (l_F 5-20 km; n=2,096). The shortest features (l_F <1 km, n=7,508) display a northward preference, and the remaining segments (l_F =5-20 km), constituting the majority of features (n=11,026), do not show any directional trends.

A spatial breakdown reveals clear directional trends in relation to distance from the planetary dichotomy (d_D; **Figure 6.6 d**), with features terminating nearest the dichotomy (d_D <10 km; n=1,603) displaying a strong west to northeast trend towards the dichotomy, and weakening but still apparent at slightly greater distances (d_D =10-50 km; n=3,102). Features furthest (d_D >500 km; n=3,158) from the dichotomy show a strong

preference to be directed to the south, away from the dichotomy, with the majority of the study area between these extremes (d_D =50-500 km; n=11,759), displaying no evident trend in direction.

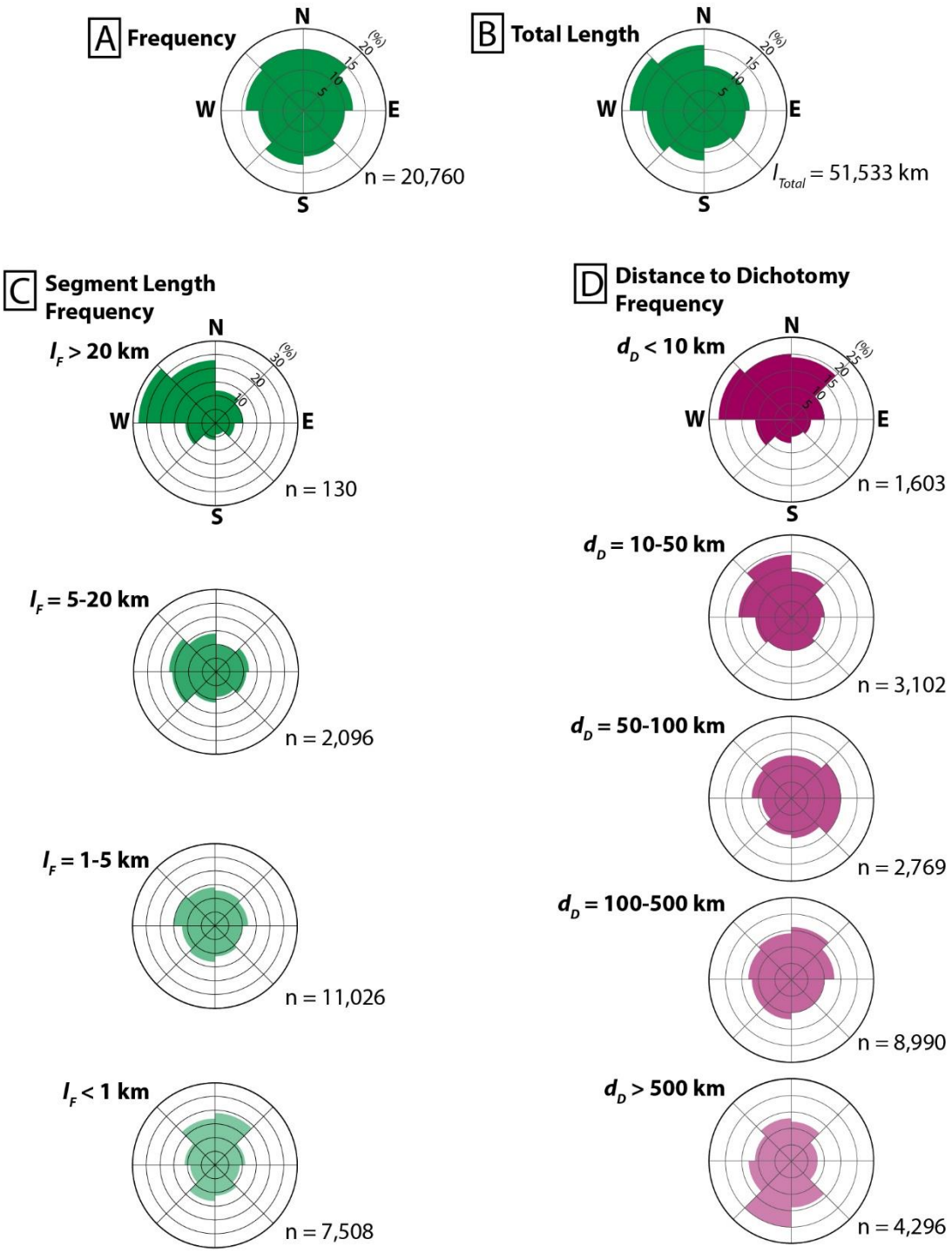

Figure 6.6 *– Plots displaying the flow direction of fluvial features as a percentage of the population. (A) The overall frequency of fluvial features does not exhibit a particular preference in flow direction, but (B) the total length of fluvial features is skewed towards westerly flow directions. (C) The directional frequency of fluvial features binned by length* (l_F)*, displays a clear north-westerly*

trend for the longest features (l_F >20 km), and a weak north and south dichotomy of direction for the shortest features (l_F <1 km). (D) The directional frequency of fluvial features binned by distance from the dichotomy (d_D), displays a similar clear west to north-easterly trend for features closest to the dichotomy (d_D <10 km), and a south-westerly trend for features furthest from the dichotomy (d_D >500 km).

6.3.2.2 PLANFORM RELATIONSHIPS

Fluvial features were segmented to preserve the longest lengths within branching networks, and categorised to describe the planform relationships between fluvial features (See, Data and Methods, 3.3.2). The five categories are based on how segments are connected to other fluvial features (**Figure 6.7 a**), including: (1) single segments, open at start and end, and unconnected to other fluvial features; (2) branching centre segments, open at start and end, with tributaries connected at intermediate points; (3) branching segments, with open start points and end points connected to other segments; (4) branching terminations, with start points connected to other segments and open end points; and (5) anabranching segments, connected at both start and end points to other fluvial features. This system allows a basic planform characterisation of fluvial features, but most importantly, allows for the true heads and termini within fluvial networks to be isolated from start and end points which are intersections within the network (**Figure 6.7a,c)**.

Single fluvial features, independent and unconnected to any other segments, make up 61% (n=12,638) of all fluvial features, and are relatively short on average (2.1 km) yet still constitute 53% (27,086 km) of the total length of fluvial features.

Branching and anabranching segments make up only 39% (n=8,117) of all fluvial features, but being longer on average (3.0 km) than single segments, constitute 47% (24,412 km) of the total length of fluvial features. Branching centre segments represent the longest segment within each branching or anabranching network, and constitute 12% (n=2,506) of all fluvial features, and are significantly longer on average (6.0 km), constituting 29% (14,907 km) of total fluvial length. The 8,117 branching and anabranching segments are grouped amongst 2,506 fluvial networks, with an average of ~3 segments per network, and a maximum of 31 segments. Anabranching segments are

the least numerous, comprising only 1% (493 km) of mapped fluvial features, and are most concentrated in the northeast extremity of the study area near the Okavango drainage catchment.

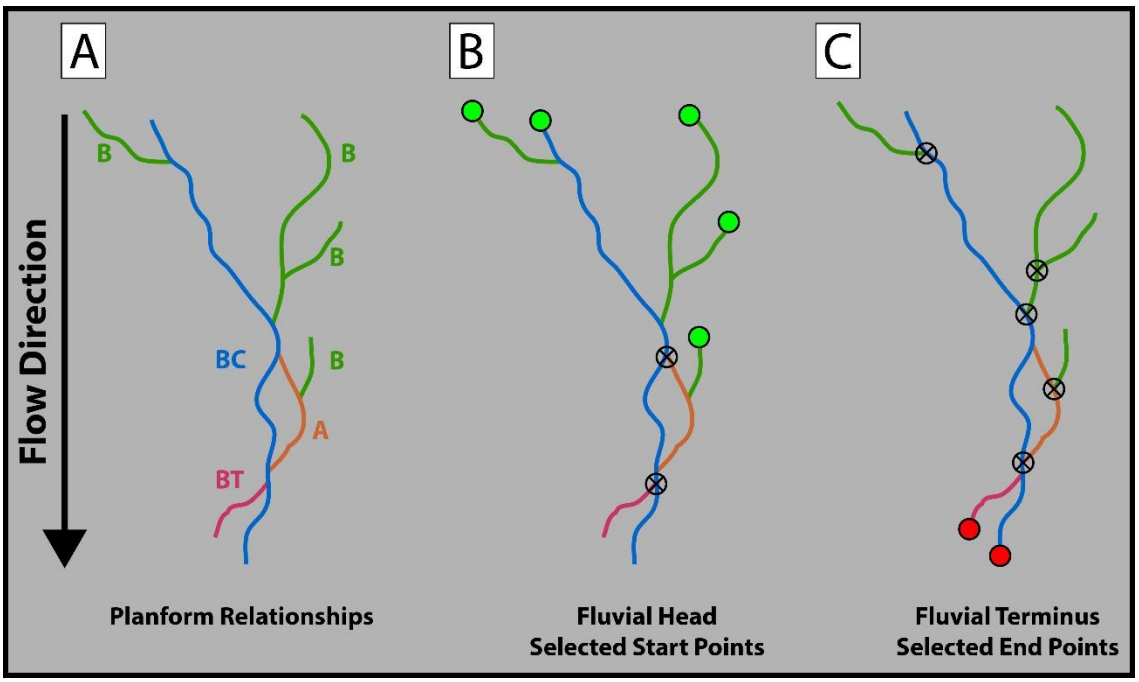

Figure 6.7 – (A) A stream relationship classification was employed with categories defined as: branching centre (BC; blue), the longest segment within a branching network, from head to terminus; branches (B; green), tributary segments with an unconnected start point; branching terminations (BT; pink), segments which start as a branch and terminate at an unconnected end point; and anabranching (A; orange), segments connected at start and end points to other fluvial segments. The classification of segments was used to sample for only true fluvial heads and fluvial terminations, to eliminate intersection points from analysis. (B) Fluvial heads were considered as only the start points of branching centre and branching segments (green points), and (C) fluvial terminations were considered as only the end points of branching centre and branching termination sections (red points), so that all other points were disregarded (crossed points).

6.3.2.3 *MORPHOLOGY*

Fluvial features were also categorised by morphology, with three broad categories defined principally by cross-sectional profile: (1) incised valleys, (2) inverted channels, and (3) surficial flow features (**Figure 6.8**). In cases where a fluvial feature exhibited some aspects of multiple morphologies (eg. an inverted channel on the floor of an incised valley), the dominant morphology contributing to the visibility of the feature was selected. However, where a fluvial feature changed morphology along length (eg. Transition from

an incised valley to an inverted channel), this was reflected in different morphological categorisation for each segment.

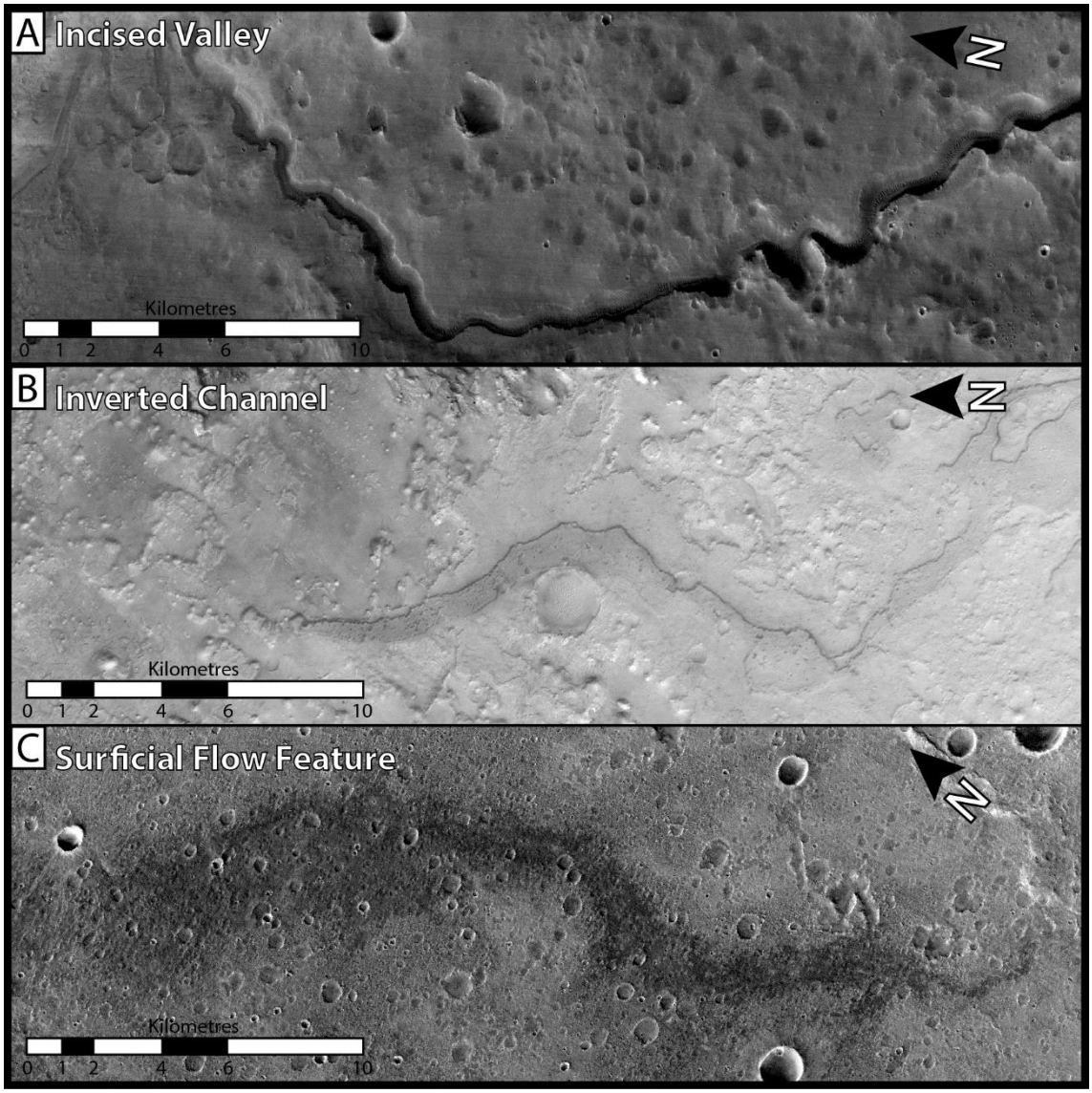

Figure 6.8 *– Representative examples of the three broad morphological classifications of fluvial features: (A) incised valleys, defined by a negative cross-sectional profile; (B) inverted channels, defined by a raised cross-sectional profiles; and (C) surficial flow features, with neither a clear positive of negative profile, but exhibiting other indications of fluvial flow. (CTX imagery – NASA)*

Valleys with negative cross-sections evident on the topography or an apparent negative expression viewed on imagery were classed as incised valleys (**Figure 6.8 a**). These features represent the most prevalent fluvial morphology on Mars (Hynek, Beach et al. 2010, Alemanno, Orofino et al. 2018), and in this work constitute the vast majority of fluvial features (92%; n=19,103), and the greatest total length (89%; 45,944 km). Catalogued valleys display a wide range of depths, with a maximum of >100 m, however,

the relatively low resolution of MOLA DEM (~463 m/pixel) data precluded observation of valley depth across the population.

Inverted channels were interpreted based on criteria established in previous global and regional catalogues (Davis, Balme et al. 2016, Dickson, Lamb et al. 2020), exhibiting quasi-sinuous planforms and positive cross-sectional topographic profiles (**Figure 6.8 b**). Overall, inverted channels account for 4% (n=905) of mapped fluvial features, and are the dominant fluvial morphology near the south west edge of the study area and in the vicinity of Mawrth Vallis. Although inverted channels constitute only 7% (3,733 km) of the total length of mapped fluvial features, anabranching features disproportionately display this morphological profile (32%; 74 km).

Surficial flow features were defined as features with a planform fluvial morphology, but with no apparent topographic profile in cross-section (**Figure 6.8 c**). The presumption is that these features represent very shallowly incised features, or very low profile depositional features. In either case, they appear to represent more limited fluvial activity than incised valleys and inverted channels, and may be analogous to the 'fresh shallow valleys' (FSV) described within the Wilson et al. palaeolake study in Arabia Terra, and interpreted as representing young Amazonian processes (Wilson, Howard et al. 2016). Surficial flow features account for 4% (n=761) of catalogued fluvial features and 4% (1,856 km) of total fluvial length. Surficial flow features do not constitute the dominant fluvial morphology in any particular area of the catalogue, but are more heavily concentrated in the area around and to the west of Okavango Valles which includes the Wilson et al. (2016) palaeolake study area.

6.3.3 SEDIMENT FANS

The locations of sediment fans were mapped at the same scale as fluvial features, and identified as fan shaped planforms, with positive relief, and displaying additional attributes common to sediment fans such as surface channelling or lobate edges. A total of 136 fans were identified, and further categorised as either high (48%; n=65) or low (52%; n=71) confidence (**Figure 6.4**).

Sediment fans were also broadly categorised by the type of basin in which they were observed. The majority (58%, n=79) are within impact craters in the highlands, 13% (n=18) are situated along the dichotomy, and the remaining 29% (n=39) are within undefined basins within the inter-crater highlands terrains.

6.3.4 PALAEOLAKE IDENTIFICATION AND CHARACTERISATION

Both open-basin and closed-basin palaeolakes were identified within the study area, using a variation on methods and criteria established in other palaeolake studies and catalogues on Mars (Fassett and Head 2008, Goudge, Aureli et al. 2015). Open-basin palaeolakes were identified where valleys begin within or transect through topographic basins, and closed-basin palaeolakes were identified where valleys terminate at the edges or within topographic basins. For the purpose of palaeolake identification, only high confidence fluvial features were considered.

6.3.4.1 *OPEN-BASIN PALAEOLAKES*

Three possible palaeolake levels were considered within each identified open-basin palaeolake basin, based upon three different elevations where fluvial features originated within topographic basins: (1) valley overflow, defined as the highest elevation closed contour within a basin; (2) basin overflow, defined as the highest elevation contour that is closed except at the outlet valley; and (3) valley extremity, defined as the lowest elevation closed contour which intersects the outlet valley (See, Data and Methods, and Chapter 4). A maximum distance of 5 km was allowed between outlet head and contour to allow for a small degree of uncertainty in the topography data, and for the simplification inherent in the use of 10 m contours. Valley overflow level is widely used as the criteria for open-basin palaeolake identification on Mars (Fassett and Head III 2008, Goudge, Head et al. 2012), and therefore palaeolakes identified by this established method are directly comparable to global catalogues. Accordingly, the principal analysis and interpretations within this work rely solely on palaeolakes defined by the valley overflow level, while basin overflow and valley extremity levels are discussed in a narrower context.

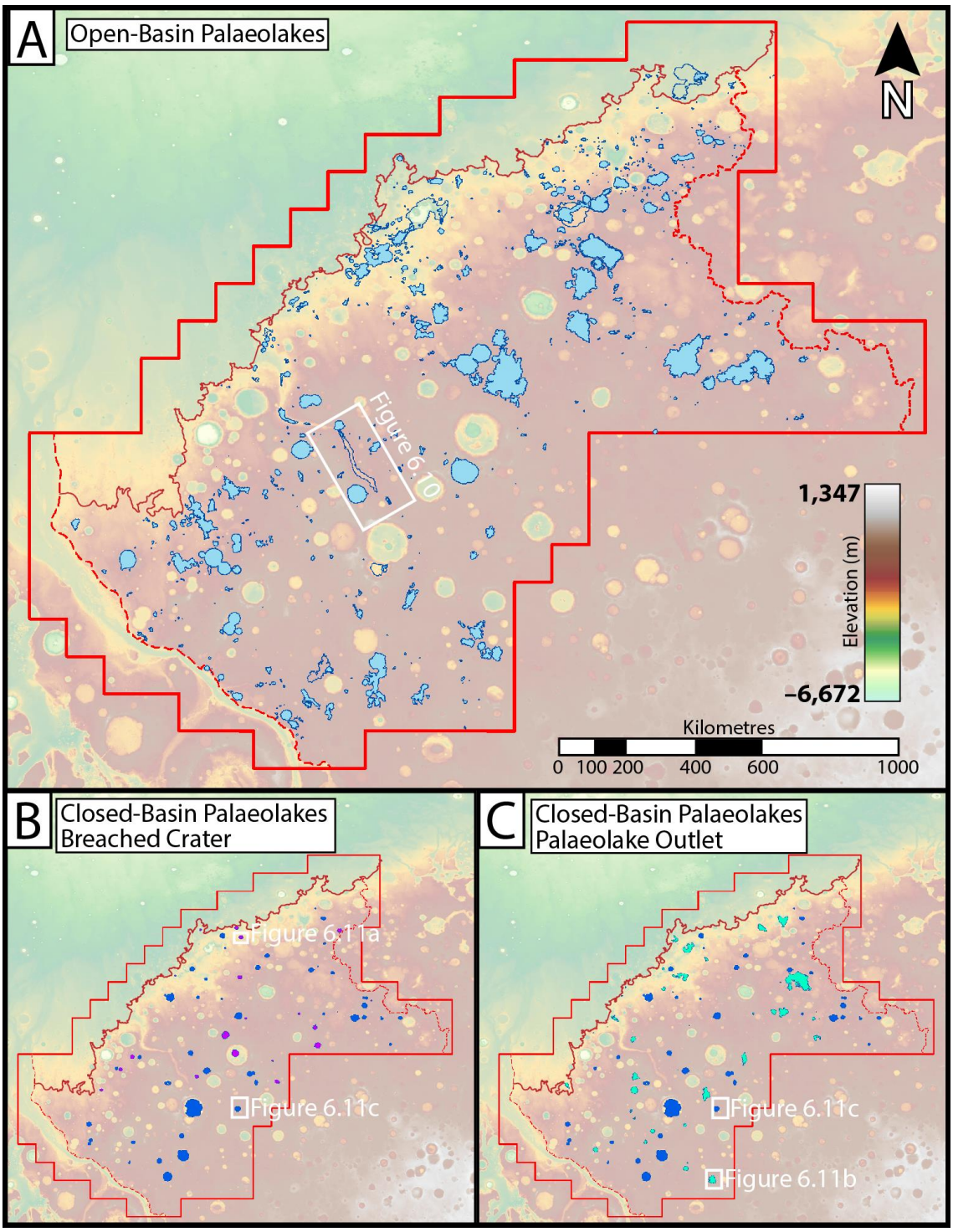

Figure 6.9 *– All catalogued palaeolakes, with sizes and boundaries to scale. (A) Open-basin palaeolakes based on the outlet overflow level (light blue fill), as well as wider palaeolake boundaries based on the basin overflow level (dark blue outlines). Notable examples where the basin overflow level describes a much larger boundary than the valley overflow level can be seen within Mawrth Vallis, and in the north east of the catalogue area near the dichotomy. (B) Closed-basin palaeolakes of the breached crater type (purple fill), defined as impact craters with inlets breaching the crater rim. (C) Closed-basin palaeolakes of the palaeolake outlet type (light green fill), defined as closed basins at the terminus of a fluvial feature headed at an open-basin palaeolake. The identification criteria for breached crater type and palaeolake outlet type are not mutually exclusive, and 29 closed-basin palaeolakes match both criteria (dark blue fill).*

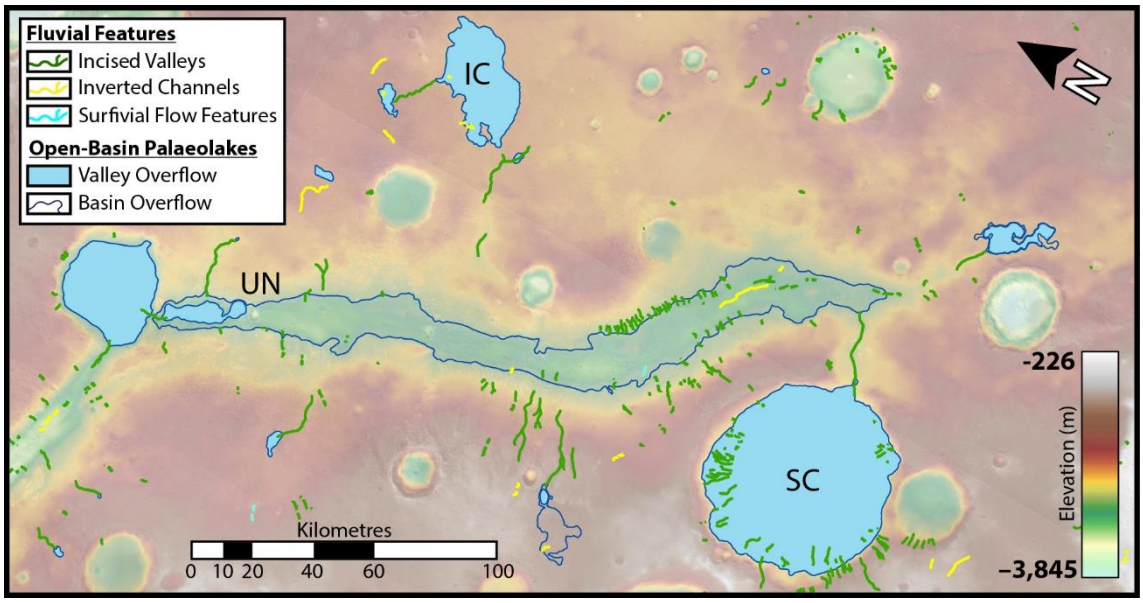

Figure 6.10 *– Examples of open-basin palaeolakes identified in the area of Mawrth Vallis. Open-basin palaeolakes identified based on the valley overflow level (blue fill) are the focus of this catalogue, and demonstrated here are the three main types of host basins: inter-crater plains (IC), single impact crater (IC), and unidentified (UN). Also displayed are palaeolake boundaries based on the basin overflow level (dark blue outline), which are only observed in some palaeolake basins. Basin overflow palaeolakes are usually only slightly different than valley overflow palaeolakes, but an example here is observed covering a far greater area along the floor of Mawrth Vallis, and in this case, the basin overflow level is a better match to valley terminations in the area. (CTX mosaics and MOLA topography)*

A total of 632 open-basin palaeolakes were identified based on the valley overflow level, ranging from <1 km^2 to >15,000 km^2 in area, with a mean size of 275 km^2 (**Figure 6.9 a**). Within 165 of the valley overflow palaeolakes, and using the same outlets, 101 palaeolake extents were identified based on basin overflow level, and 89 palaeolake extents based on valley extremity level. A breakdown of the number of palaeolake levels based on individual outlets is as follows: 465 palaeolakes with only a valley overflow level, 101 palaeolakes with only valley overflow and basin overflow levels, 87 palaeolakes with only valley overflow and valley extremity levels, and 23 palaeolakes with all three levels.

Basin morphology impacts the characteristics and dimensions of palaeolakes, and therefore palaeolakes were classified based on the dominant basin morphology defining the palaeolake boundary (**Figure 6.10**). The vast majority (72%; n=458) of palaeolakes are hosted within basins in the inter-crater plains, representing a range of possible origins, including: multiple upraised crater rims and ejecta, heavily eroded or infilled impact craters, regional deflation, tectonic deformation, erosion, or a combination of these

processes. A significant portion (17%; n=110) of palaeolakes are defined by impact craters, with 15% (n=96) within single craters and 2% (n=14) within multiple impact craters. The remaining 10% (n=64) of palaeolakes are within basins of an undefined or unknown origin, including those on the floor of Mawrth Vallis, and a number of irregular, steep sided basins near the dichotomy and Ares Vallis.

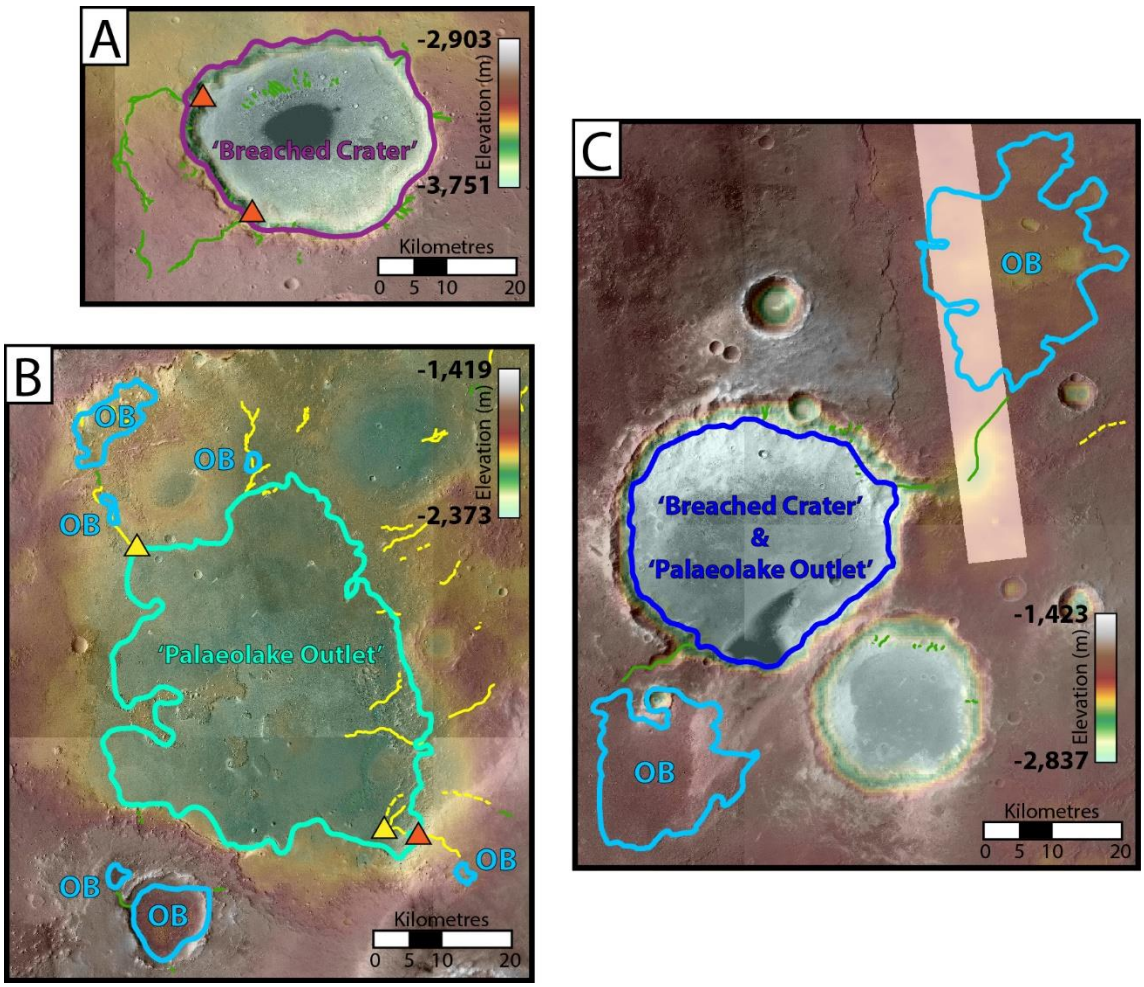

Figure 6.11 *– Examples of closed-basin palaeolakes identified in the catalogue, with other relevant features, including: incised valleys (green lines); inverted channels (yellow lines); sediment fans of high (orange triangles) and low (yellow triangles) confidence; and open-basin palaeolakes (OB; light blue outlines). (A) A total of 15 'breached crater' type palaeolakes were identified, where a fluvial inlet breached the crater rim, but was not sourced within an open-basin palaeolake. (B) A total of 37 'palaeolake outlet' type palaeolakes were identified, where a fluvial outlet from an open-basin palaeolake inlet terminated as an inlet within a closed topographic basin of any morphology. (C) A total of 29 identified closed-basin palaeolakes met the criteria of both 'breached crater' and 'palaeolake outlet' types, exhibiting inlets breaching a crater rim that originated within open-basin palaeolakes. (CTX mosaic images with MOLA DEM - North is up in all images)*

A sub-group of 16 open-basin palaeolakes was identified based on observation of a consistent set of morphological characteristics and topographic relationships, and are

here referred to as 'perched crater lakes'. All of the palaeolakes included in this classification met the following criteria: (1) hosted within impact craters with raised rims; (2) exhibiting fill levels higher than the surrounding terrain; (3) and draining by short, shallow outlets, which are not integrated with other fluvial networks. As a consequence of being hosted within craters with raised rims, none of these palaeolakes exhibit inlet valleys, and have virtually non-existent drainage catchments. In addition, exhibiting palaeolake levels which are above the surrounding terrain, distinguishes these examples from other open-basin palaeolakes, and suggests they may be illustrative of a particular basin filling process.

6.3.4.2 *CLOSED-BASIN PALAEOLAKES*

Fluvial outlets indicate, with a high degree of confidence, that a topographic basin was once filled with water, and thus the presence of an open-basin palaeolake. Conversely, closed-basin palaeolakes, which lack outlets by definition, are typically identified where fluvial features terminate within closed topographic basins (Goudge, Aureli et al. 2015). However, fluvial terminations do not always indicate a standing body of water, and are not conclusive evidence of a closed-basin palaeolake. The identification of closed-basin palaeolakes is therefore more complicated and subjective than open-basin palaeolakes, and additional criteria are desirable in order to achieve a higher degree of confidence in identification. One global catalogue of closed-basin palaeolakes addressed these difficulties by narrowing the criteria to only consider impact craters breached by an inlet (Goudge, Aureli et al. 2015). The rationale being that breaching a crater rim requires surface accumulation of water and subsequent incision into the crater. As a consequence, this method not only excludes possible palaeolakes in all other basin types, but also excludes possible crater palaeolakes filled by groundwater influx, both of which could be numerous, but very difficult to positively identify. For this catalogue, palaeolakes were identified based on consideration of two different, but non-exclusive criteria: (1) impact craters with fluvial inlets breaching the crater rim, as described by Goudge et al. (2015) (**Figure 6.11 a,c**); and (2) basins with a fluvial inlet which is also the outlet of an open-basin palaeolake (**Figure 6.11 b,c**). The inclusion of a criteria based on palaeolake outlet

terminations expands on the logic of sufficient surface accumulation as described by Goudge et al. (2015), and has the advantage of including a wider range of basin types, than only impact craters.

A total of 103 closed-basin palaeolakes were identified based on the above criteria, 62 of the 'breached crater' type (**Figure 6.9 b**), and 83 of the 'palaeolake outlet' type (**Figure 6.9 c**), with 42 meeting both criteria.

6.3.4.3 *MULTIPLE PALAEOLAKE FILL LEVELS*

As a result of the different criteria used to identify palaeolakes as described above, there are three circumstances in which multiple palaeolake levels are recorded within a single basin: (1) two valley overflow levels, defined by two outlets at different elevations; (2) a valley overflow level, and a basin overflow or valley extremity level, defined from the same outlet; or (3) an open-basin palaeolake level and a closed-basin palaeolake level, defined by outlets and inlets respectively. Palaeolake extents are defined by topographic contours, and therefore, multiple palaeolake boundaries are concentric and never intersect. The bulk of the analysis within this catalogue focuses on open-basin palaeolakes identified from a single valley overflow level, however, multiple palaeolake levels within a single basin can have implications for the interpretation of local and regional drainage, and in this section we outline some of the examples of multiple palaeolake fill levels.

Included in the total of 632 valley overflow open-basin palaeolakes are 29 palaeolakes situated within the boundaries and below the surface elevation of 17 other identified palaeolakes. These palaeolakes constitute two sub-groups, defined as 'below' and 'above', which could not have existed contemporaneously, and therefore only the 'above' group of larger palaeolakes is included in calculations of palaeolake areal coverage and volume for the entire population. Defining the relative ages of these palaeolake groups is difficult, but one of the two following scenarios is likely to apply: either that palaeolakes in the 'below' group could have formed first, with base level rising within the basin until a new outlet breached at the 'above' palaeolake level; or alternatively, the 'above' palaeolake was filled first, and base level then dropped forming residual

palaeolakes and valleys at the 'below' level on the former palaeolake floor. The second scenario, of higher fill levels before lower fill levels, may be more likely given the potential for evidence of palaeolakes in the 'below' group to be buried or destroyed by submersion under palaeolakes in the 'above' group. Some basins showing this relationship even indicate palaeolake chains completely under and within the boundary of a higher palaeolake.

In the 165 instances where multiple fill levels were indicated from the same outlet (ie. valley overflow, basin overflow, valley extremity), the average difference in elevation is relatively small, at 22 m higher for basin overflow levels and 54 m lower for valley extremity levels within a given basin. This translates to median differences in areal extents of 51% greater for basin overflow, and 59% for valley extremity in a given basin, with even greater differences expressed in relative volumes. However, some notable exceptions include a far greater palaeolake extent on the floor of Mawrth Vallis, and as part of the Becquerel crater drainage system. In these cases, the basin overflow level defines a boundary which is a better match for a larger number of valley terminations, and in particular terminations of valleys fed by other open basin palaeolakes.

There are 14 examples of open-basin palaeolakes and closed-basin palaeolakes within the same basin, in 13 of which the closed-basin level is below and within the open-basin level, and in one the closed-basin level is above. In terms of effect on interpreted drainage patterns in the catalogue area, only the closed-basin palaeolake which is above the level of the open-basin palaeolakes is relevant. This 'palaeolake outlet' type closed-basin palaeolake is above and encloses four open-basin palaeolakes within an irregular shaped, deep basin within the Becquerel crater drainage system. The relationship appears to indicate a higher palaeolake level within the basin, prior to the existence of the open-basin palaeolakes.

6.3.4.4 *PALAEOLAKE CHAINS*

It is common of open-basin palaeolakes on Earth and Mars to be arranged in cascading chains (Fassett and Head 2008), with the outlets of higher palaeolakes draining

into and filling lower palaeolakes. Palaeolake and fluvial chains indicate a degree of hydrological connectivity on the surface, and are important in modelling drainage catchments and patterns across the landscape. Identifying palaeolakes which are significantly sourced by other palaeolakes is also a necessary consideration in interpreting the relative importance of basin filling processes such as surface accumulation and groundwater. Only palaeolakes not significantly fed by other palaeolakes are good candidates for calculations of drainage catchments, which together with palaeolake volume and area are a proxy for interpretations of hydrological filling (Fassett and Head 2008).

The majority (65%; n=408) of open-basin palaeolakes identified in this catalogue are part of palaeolake chains; being either fed by, or draining into other open-basin palaeolakes. Inclusion as part of a chain was defined where the terminus of a fluvial outlet from one open-basin palaeolake was within or near the boundary of another open-basin palaeolake, with the position of each palaeolake relative to others in a chain indicated by an order number. An order value of '1' denotes palaeolakes draining into, but not fed by other palaeolakes, representing the majority of chained palaeolakes (40%, n=162). Order numbers >1 represent palaeolakes fed by at least one higher palaeolake, with the value indicating the total number of palaeolakes in a continuous chain. The highest order number in this catalogue is 12, representing the twelfth palaeolake in a continuous chain. However, chained palaeolakes were observed within a total of 104 networks, some with multiple head lakes (order values of '1'), with 23 palaeolakes in the Coogoon system being the highest number of palaeolakes within one network.

Overall lengths and bearings were calculated for palaeolake chains from the most distant palaeolake outlet head, to the terminus of the outlet from the final palaeolake in the chain, for all chains and branches with at least three palaeolakes.

6.4 ANALYSIS AND DISCUSSION

The fluvial and lacustrine features identified and described within this catalogue represent a significant new dataset for interpreting the hydrology of Arabia Terra, and global palaeolake trends on Mars. Presented in this section is a broad analysis of this new catalogue using similar approaches to previous regional and hydrological studies. The validity of catalogued palaeolakes are investigated (**Section 6.4.1**) to determine a degree of confidence in identification, and possible additional criteria for use in future palaeolake identification. Palaeolake and fluvial features are then analysed to identify trends in flow distribution, density, and elevation (**Section 6.4.2**), and compared to existing global catalogues. Next, the connectivity of palaeolake chains and valley networks are interpreted to produce morphologically derived palaeolake drainage catchments (**Section 6.4.3**), allowing an analysis of source to sink drainage and transport for the entire study area (**Section 6.4.4**). Finally, a preliminary assessment of palaeolake drainage catchments is presented to assess the relative influence of groundwater influx to surface accumulation in palaeolake filling (**Section 6.4.5**).

6.4.1 BASE-LEVEL CORRELATION AND PALAEOLAKE CONFIDENCE

Open-basin palaeolakes in this catalogue were identified exclusively based on evidence for fluvial outlets transecting through or originating at the edges of closed topographic basins. These criteria are common in martian palaeolake identification (Fassett and Head 2008, Goudge, Head et al. 2012), and unambiguous when palaeolakes are hosted in large, deep basins, and especially within impact craters. However, a result of the higher resolution imagery used to identify fluvial features and palaeolakes in this study, is that a large proportion of palaeolakes were identified within shallower, more subtle basins.

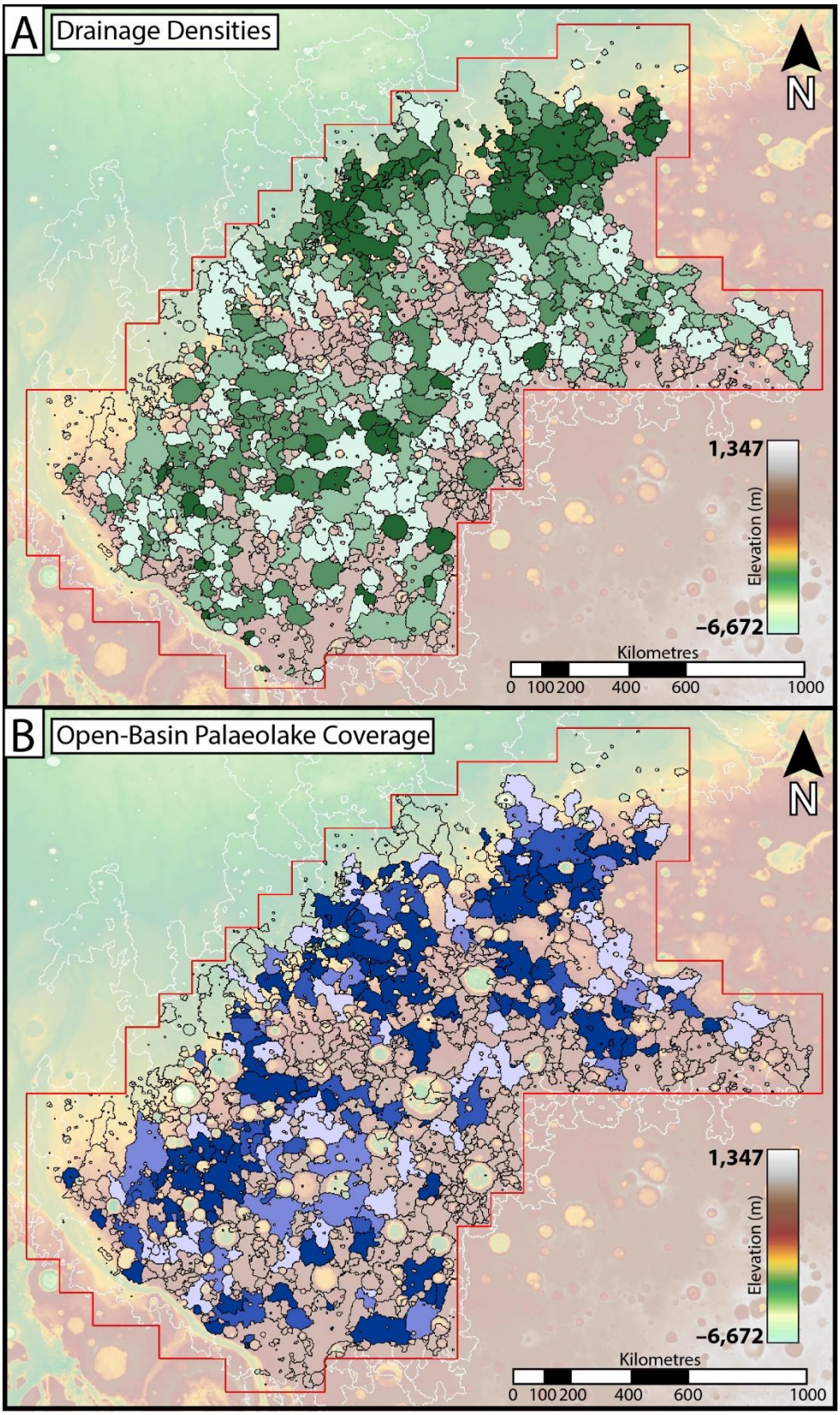

Figure 6.12 *– Fluvial and open-basin palaeolake densities for the catalogue area, spatially binned within local drainage catchments produced with sinks <100 m filled. (A) Drainage densities within local drainage catchments show the highest concentrations within two discrete areas along the dichotomy in the north of the catalogue area, and within isolated deep craters. (B) Open-basin palaeolake densities are most concentrated in higher elevation areas of the highlands, and within craters. Generally, higher densities are observed within the major drainage catchments of the area:*

Coogoon Valles, Mawrth Vallis, the Becquerel crater system, and the 'heart lake' area in the north-east. (MOLA topography)

In order to assess the veracity of palaeolakes identified within this catalogue, particularly those within subtle basins, additional indicators of base-level were considered. Concentrations of putative deltas and fluvial terminations at a common elevation are often considered in the identification of closed-basin palaeolakes and possible oceans on Mars (Di Achille, Hynek et al. 2009, Di Achille and Hynek 2010). As outlined previously (**Section 6.3.4.3**), this evidence is not conclusive of a stable base levels, but where observed in conjunction with stronger evidence, such as in close proximity to outlet defined open-basin palaeolakes, these features can be considered as supporting evidence. In this work the position and elevation of sediment fans and multiple fluvial terminations are considered where they correlate to mapped open-basin palaeolake boundaries and elevations.

A large proportion (40%; n=54) of mapped sediment fans occur in close proximity to the boundaries of open-basin (2%; n=15) and of closed-basin (29%; n=30) palaeolakes. A total of 18 fans, five high-confidence and 13 low-confidence, were observed correlated with the boundaries of 15 different open-basin palaeolakes, and a total of 38 fans, 20 high-confidence and 18 low confidence were correlated with the boundaries of 23 different closed-basin palaeolakes. A further breakdown of fans by type of closed-basin palaeolakes reveals a roughly even divide, with: 16 'breached crater' palaeolakes associated with 14 high-confidence and 6 low confidence sediment fans; and 17 'palaeolake outlet' palaeolakes associated with 10 high-confidence and 13 low-confidence sediment fans. Although closed-basin palaeolakes were correlated with a greater number of sediment fans, this is likely due in part to the natural association of sediment fans with inlets rather than outlets.

Many of the palaeolake boundaries identified for both open-basin and closed-basin groups appear to be well correlated with the terminations of multiple fluvial features, including outlets from other palaeolakes. In the case of closed-basin palaeolakes, this is partially a consequence of identification criteria based on inlets, however, for open-

basin-palaeolakes identified by outlet valleys, this correlation represents additional supporting evidence for a palaeolake. Although the observed elevation and location of fluvial terminations can be explained by a number of processes, it is often an indication of a standing body of water. Additionally, the confidence in identified palaeolakes was considered to be greater where more than one palaeolake criteria coincided. Firstly, in palaeolakes (n=42) identified as both 'breached crater' and 'palaeolake outlet' types (**Figure 6.11c**), and secondly, for closed-basin palaeolakes (n=23) in which where the terminations of multiple palaeolake outlets described the same level (**Figure 6.11 a,b,c**). An extension of this logic confers greater confidence to the many open-basin palaeolakes (36%; n=229) which are fed by higher palaeolakes, as part of a chain. This is quantified for all palaeolakes, open-basin and closed-basin, as the number of inlets from other palaeolakes.

6.4.2 FLUVIAL AND LACUSTRINE DISTRIBUTIONS AND POPULATIONS

The overall distributions of fluvial and lacustrine features are correlated within the catalogue area, as a result of the identification of palaeolakes being dependent on the observation of fluvial features. However, there are notable differences between the distributions of drainage densities and lacustrine coverage across the study area. Density maps were calculated within local drainage catchments, produced on a topography with sinks <100 m filled, and only considering sinks wholly within the catalogue area, and high confidence fluvial features and open-basin palaeolakes.

Drainage densities were calculated as total length of fluvial features within a local drainage catchment (A_C/L_F) (**Figure 6.12 a**). The greatest densities are in the north-east of the catalogue area near the dichotomy, near the terminus of the Becquerel crater system, and within isolated deep impact craters. All three of these areas are dominated by short and shallowly incised features. The areas around Coogoon Valles and Mawrth Vallis represent the next highest densities, but are relatively similar to the catalogue on average. Significant areas with no fluvial features exist between Mawrth Vallis and the Becquerel system, and to the east of the Becquerel crater system. Drainage density also becomes

sparse towards the south-east extent of the catalogue area, with coverage of incised features completely limited to within deep craters, and the only fluvial features within the inter-crater plains represented by inverted channels (Davis, Gupta et al. 2019).

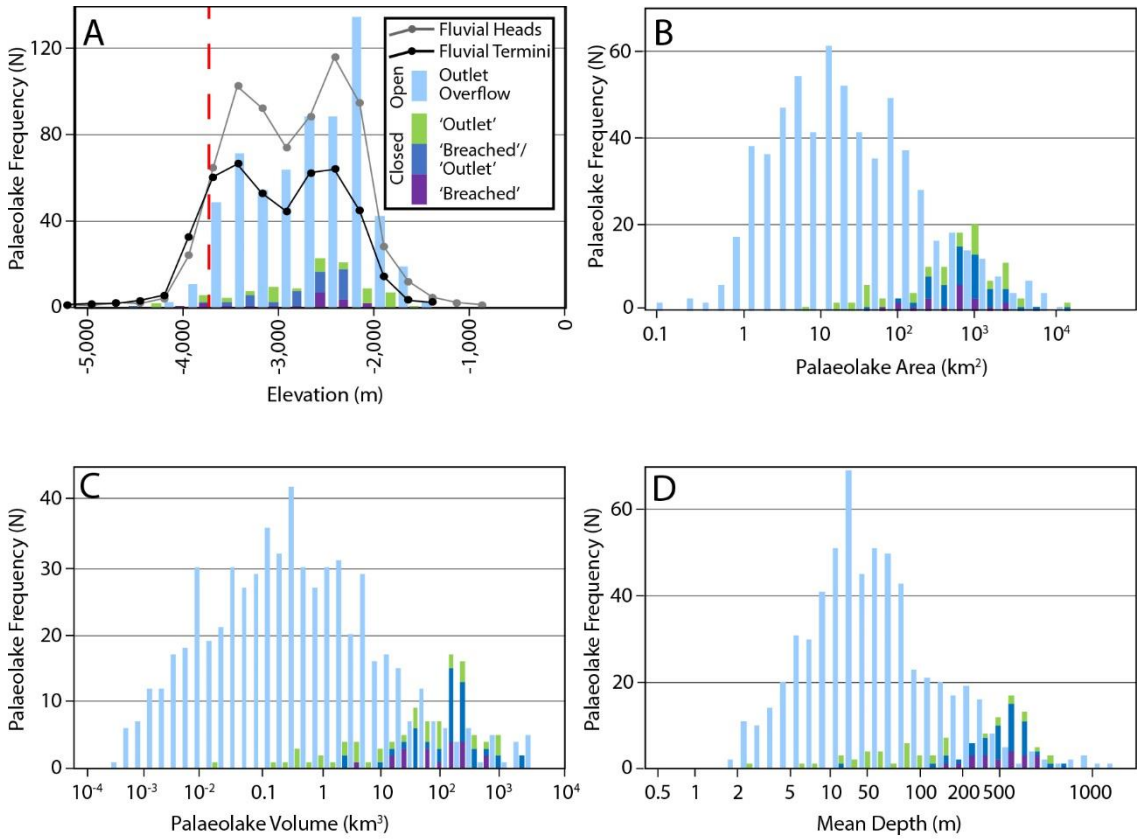

Figure 6.13 – A comparison of open-basin (n=632) and closed basin (n=103) palaeolake populations in this catalogue. (A) Plot of palaeolake elevations, inlet defined elevations for closed-basin and outlet defined elevations for open-basin palaeolakes, showing two peaks roughly corresponding to fluvial inlet and outlet elevations, and also the mean elevation of the dichotomy (dashed red line). Palaeolake dimensions as plotted by area (B), volume (C), and mean depth (D) indicate that closed-basin palaeolakes are larger and deeper, primarily as a consequence of mostly being hosted within deep impact craters.

Palaeolake density was calculated as coverage of open-basin palaeolake area over a local drainage catchment (A_C/A_L), with the greatest densities corresponding to areas in the highlands with the largest palaeolakes, rather than areas nearer to the dichotomy at lower elevations which host numerous smaller lakes (**Figure 6.12 b**). Higher palaeolake densities are concentrated within the major catchments of Coogoon Valles, Mawrth Vallis, the Becquerel crater system, and the area surrounding the 'heart lake' system identified by Wilson et al. (2016). Between these concentrations are areas with no palaeolake coverage, supporting an interpretation that major drainage divides exist

between these major catchments. The south-east edge of the catalogue area is almost devoid of palaeolakes, with the exception of, like drainage densities, palaeolakes defined by inverted channels. The imbalance of low palaeolake density in the highest areas of the catalogue and higher densities towards the dichotomy, suggests higher elevations as source regions.

Correlations were also considered between the populations of fluvial feature heads and termini, open-basin palaeolake elevations, and closed-basin palaeolake elevations (**Figure 6.13**). Two distinct peaks are observed in the populations of fluvial heads and termini, one near the elevation of the dichotomy and the other at approximately -2750 m elevation (**Figure 6.13 a**). The peak at the dichotomy represents the high concentration of fluvial features, although generally short, that are observed along the dichotomy, indicating intense but localised fluvial activity in this area. The higher peak is not clearly attributable to a regional trend or process, and the average elevation of the catalogue area is near an elevation of -2750 m, and thus the abundance of fluvial features at this elevation could be a consequence of the regional elevation. However, a horizon of aqueous processes within the highlands, such as would be expected by intersection with regional groundwater could also cause such a concentration within a narrow elevation range.

The peak in open-basin and closed-basin palaeolakes is also observed near an elevation of -2,000 m, with a secondary smaller peak in open-basin palaeolakes near the elevation of the dichotomy (**Figure 6.13**). As with the elevations of fluvial features, these horizons of palaeolake elevation indicate a strong regional topographic control on aqueous processes. It is also notable that the peak in fluvial termini is a very good match to the elevation closed-basin palaeolakes, while the peaks in open-basin palaeolake elevation are a better match to the higher elevation peaks in fluvial heads. Additional comparisons of palaeolake dimensions reveal closed-basin palaeolakes to be on average; larger, deeper, and containing a greater volume than open-basin palaeolakes (**Figure 6.13 b,c,d**). This relationship is overall a consequence of most identified closed-basin palaeolakes being hosted within steep-sided, deep craters, but also indicates the greater

volume of water that could be held in these basins which are typically fed by multiple open-basin palaeolakes. An exception in the population of closed-basin palaeolakes are those identified solely as 'lake outlet' type, and not hosted within impact craters (**Figure 6.13, green bars**). As a whole, the dimensions of 'lake outlet' palaeolakes are in line with the frequency displayed by open-basin palaeolakes.

Most palaeolakes currently described on Mars occur within conspicuous impact craters, while a minority have been reported in tectonically controlled basins (Mangold and Ansan 2006), inter-crater basins bounded by the upraised rims and ejecta of multiple impact craters (Goudge and Fassett 2018), and other basins of undefined origin (Wilson, Howard et al. 2016). Within this catalogue, the majority of open-basin palaeolakes area identified within irregular basins in the inter-crater plains, and the 'lake outlet' type closed-basin palaeolakes are likewise hosted within undefined basins. This places the palaeolakes within this catalogue as an important addition to the knowledge of palaeolakes on Mars, but in addition to the higher resolution used in this catalogue, complicates comparison to global catalogues.

6.4.2.1 *OPEN-BASIN PALAEOLAKES*

A direct comparison of palaeolake dimensions and elevations between the current Arabia Terra catalogue and existing global catalogues is presented here, revealing interesting commonalities and divergences, while addressing the differences in survey resolution, identification criteria, and the morphological and hydrological characteristics particular to the Arabia Terra region. The open-basin palaeolake catalogue by Fasset and Head (2008) primarily relied on 232 m/pixel THEMIS daytime infrared global image mosaics to survey the martian surface between 90° S and 60° N, identifying 210 open-basin palaeolakes, only 52 of which had been identified in previous studies. Their identification criteria required a closed basin with an observed outlet, and is thus a good match to the open-basin palaeolakes identified with the valley overflow level in the present study. Although subsequent studies have increased the global total of open-basin palaeolakes to 226 (Goudge, Head et al. 2012), the catalogue by Fasset et al. (2008) remains

the most comprehensive analysis of martian palaeolake populations, dimensions, and characteristics.

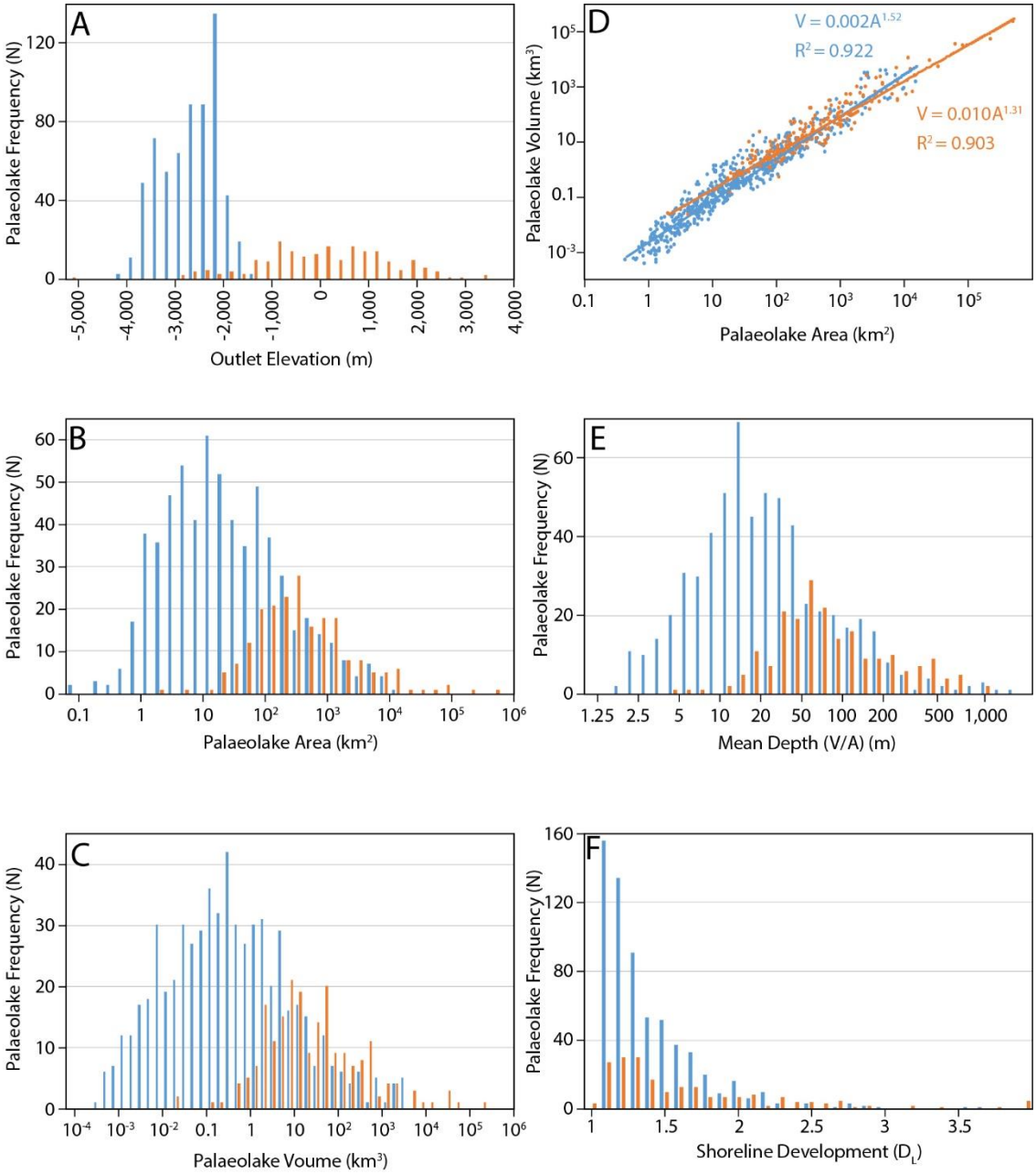

Figure 6.14 *– A comparison of open-basin palaeolake dimensions and properties between the present Arabia Terra catalogue (blue) and the global open-basin palaeolake catalogue (orange) by Fassett et al. (A) Outlet elevation demonstrates the most significant difference between the two catalogues, and is likely the result of the lower average elevation of Arabia Terra compared to the majority of highland terrains where palaeolakes are found. Palaeolake area (B), volume (C), and mean depth (volume/area) (E), indicate a greater number of small palaeolakes in the Arabia Terra catalogue, but importantly, still identify larger palaeolakes. The cut-off in palaeolake dimensions is also steeper for the global catalogue, which may indicate a limit of detectability in this study. (F) Shoreline development index quantifies palaeolake circularity, and is interpreted as an indication shoreline processes generating more complex palaeolake boundaries. However, the skew towards smaller palaeolakes within the Arabia study may limit the usefulness of this metric.*

The most striking difference between the global and Arabia datasets is palaeolake outlet elevation, analogous to the surface elevation or base-level of each palaeolake. Frequency distributions for global palaeolakes show a sharp drop in the number of outlet elevations below -1,250 m, with only 21 palaeolakes below this elevation, whereas outlet elevations in the present Arabia catalogue (n=632) are entirely confined to elevations below -1,250 m (**Figure 6.14 a**). This divergence is a consequence of the low elevation of Arabia Terra in comparison to the rest of the highlands, and therefore any catalogue limited to Arabia Terra will reflect lower elevations than the global data set.

The paucity of open-basin palaeolakes within Arabia Terra, as shown in previous catalogues, therefore appears to underrepresent low-elevation palaeolakes on Mars, which could influence interpretations of regional and global hydrology (Andrews-Hanna, Zuber et al. 2010, Salese, Pondrelli et al. 2019). Previous investigations have identified Arabia Terra as a region which experienced significant groundwater upwelling to the surface (Andrews-Hanna, Zuber et al. 2010), and palaeolakes identified as being fed by groundwater influx (Fassett and Head 2008), correlate well to the areas of greatest groundwater upwelling indicated by Andrews-Hanna et al (2010). Although the greater number of Arabia Terra palaeolakes identified in this catalogue is primarily a result of higher resolution imagery, if groundwater influx is a major process driving palaeolake formation in Arabia Terra, then the increased number of palaeolakes identified in this catalogue may be a function of hydrology in the region.

The frequency distributions of palaeolake dimensions, including area (**Figure 6.14 b**), volume (**Figure 6.14 c**), and mean depth (**Figure 6.14 e**), for both the global and Arabia Terra catalogues, reveal similar and relatively symmetrical distributions, but with the peak shifted towards smaller water bodies in the Arabia Terra data. The global palaeolake data shows a slightly steeper cut-off towards smaller and shallower palaeolakes, but it is unclear whether this is a true representation of palaeolakes, or a consequence of drop-off in detectability. The detection of a greater number of fluvial features and palaeolakes in the present catalogue is to be expected given the use of ~6 m/pixel CTX imagery compared to 232 m/pixel imagery used in the global catalogue.

However, it is significant that in addition to revealing a greater number of small palaeolakes, using higher resolution imagery also revealed larger palaeolakes nearly as numerous within Arabia Terra as in entire global catalogues (**Figure 6.14 b**). This suggests that the major factor impacting martian palaeolake detectability is not the dimension of a palaeolake basin as limited by the resolution of the topographic data, but the dimensions and expression of the outlet feature as limited by the resolution and quality of the imagery.

An additional metric examined in the global catalogue is the shoreline development index (**Figure 6.14 f**), a measure of irregularity in palaeolake shapes, with D_L=1 being a perfect circle, and greater values representing more irregular shapes. The formula, where L is the shoreline length, and A is the palaeolake area, being:

$$D_{\mathrm{L}} = \frac{L}{2\sqrt{\pi A}}$$

The shoreline development index is intended as a relative measure of shoreline processes acting on a lake shore, with higher values indicating a greater degree of alteration from a circular outline (Hutchinson 1957). Fassett and Head (2008) point to the relatively low values globally, as a consequence of the majority of palaeolakes in that study being hosted within impact craters. Whereas the palaeolakes with the largest values represent basins of varied morphological origin, and in particular larger, shallower basins formed by flooding wide areas of irregular, inter-crater terrain. The results in Arabia Terra show an even greater majority of low shoreline development values, suggesting very circular palaeolake basins. However, this may be misleading due to the smaller dimensions of palaeolakes identified in Arabia Terra, with 27% (n=171) of open-basin palaeolakes being <5 km^2, approaching the useful resolution of the topographic data (~436 m/pixel; MOLA) to define palaeolake outlines. At the limits of topographic resolution, the complex shapes of palaeolake outlines may be simplified, and as there is a strong correlation between the smaller palaeolakes and low shoreline development indices in this study, it is suggested that the high frequency of very low D_L is not reprehensive of the overall irregularity of palaeolake basins. Overall, the geometries of palaeolake boundaries in this catalogue

appear to be dominantly controlled by basin origin, and there are no clear examples of shoreline modification to refute this interpretation.

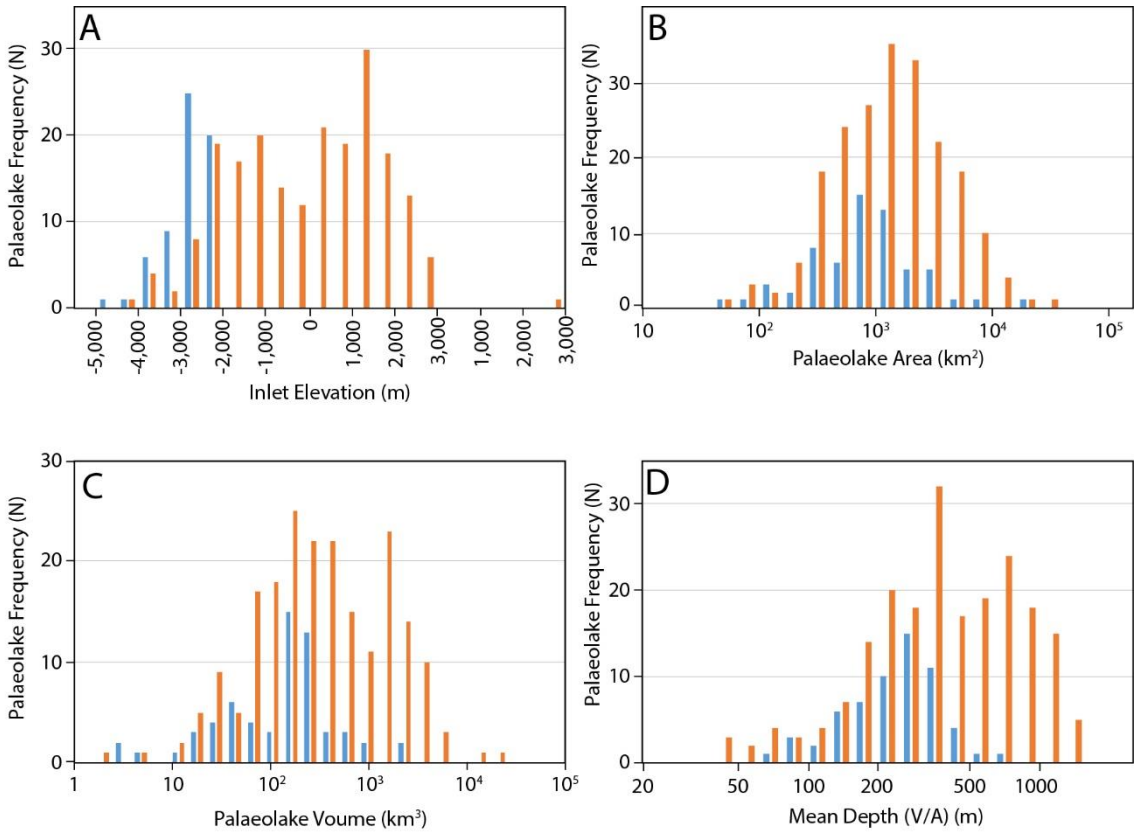

Figure 6.15 *– A comparison of closed-basin palaeolake dimensions and properties between 'breached crater' palaeolakes in the present Arabia Terra catalogue (blue; n=103), and the global closed-basin palaeolake catalogue (orange; n=205) by Goudge et al. (A) Inlet elevation, or maximum palaeolake level, demonstrates the most significant difference between the two catalogues, and is likely the result of the lower average elevation of Arabia Terra compared to the majority of highland terrains where palaeolakes are found. The frequency distribution of area (B), volume (C), and mean depth (volume/area) (E), indicate a slight preference towards small palaeolakes in the Arabia Terra catalogue, but are largely in-line with the global catalogue.*

6.4.2.2 *CLOSED-BASIN PALAEOLAKES*

Closed-basin palaeolakes in this catalogue were compared to a global catalogue compiled by Goudge et al. (Goudge, Aureli et al. 2015). The global catalogue (n=205) only considered palaeolakes within impact craters breached by an inlet, and therefore only closed-basin palaeolakes identified as 'breached crater' (n=62) were compared from the present Arabia Terra catalogue, including 'breached crater' types that were also observed to be 'lake outlet' types. A total of 18 palaeolakes from the global catalogue are situated within the Arabia Terra catalogue area, and of these, the current catalogue agreed with

identification in 14 of these cases, with four excluded based on uncertainty in the positive identification of the fluvial inlet.

As with the elevations of open-basin palaeolakes, the population of closed, basin palaeolakes within Arabia Terra is at the low end of the global dataset, and again this is likely due to the overall lower elevation of Arabia Terra compared to the rest of the highlands (**Figure 6.15 a**). However, in the case of closed-basin palaeolakes, the examples in Arabia Terra are still in line with global distributions, rather than at far lower elevations. This may be explained by a broad similarity in impact crater depth, and that Arabia Terra was indicated as particularly important in the global distribution of palaeolakes (Goudge, Head et al. 2012). The dimensions of closed-basin palaeolakes in Arabia Terra is generally consistent with global populations (**Figure 6.15 b,c,d**), and is likely a consequence of the narrow range of morphological variation observed in impact craters in general. However, populations of closed-basin palaeolakes within Arabia Terra are at the smaller and shallower end of global dimensions.

6.4.3 MORPHOLOGICALLY DERIVED DRAINAGE CATCHMENTS

Topographically derived drainage catchments produced with Mars topography data are idealised approximations, due in large part to the necessity of filling sinks in the topography (Tarboton, Bras et al. 1991, Mest, Crown et al. 2010). Filling sinks which exhibit no supporting morphological evidence of aqueous filling can produce exaggerated drainage catchments, incorporating additional areas which were not integrated with the ancient watershed. Conversely, changes to topography postdating fluvial and lacustrine processes, such those produced by tectonic deformation or impact cratering, can result in underestimated drainage catchments with areas of ancient watersheds isolated on the present topography. To what extent an idealised drainage catchment represents the true ancient catchment therefore depends on the particular area being investigated. Past work demonstrates the validity of idealised catchments in the area of Coogoon Valles (Fawdon 2018), but numerous closed-basin palaeolakes identified near the dichotomy in the north of the present catalogue area (Wilson, Howard et al. 2016), are at odds with a drainage

catchment produced on a fully filled topography. These difficulties can be mitigated in part by calculating drainage catchments on topographic data that has only been partially filled, rather than fully filled, with a final verification comparing calculated drainage catchments to observed geomorphology (Mest, Crown et al. 2010) (See, Data and Methods 3.3.3).

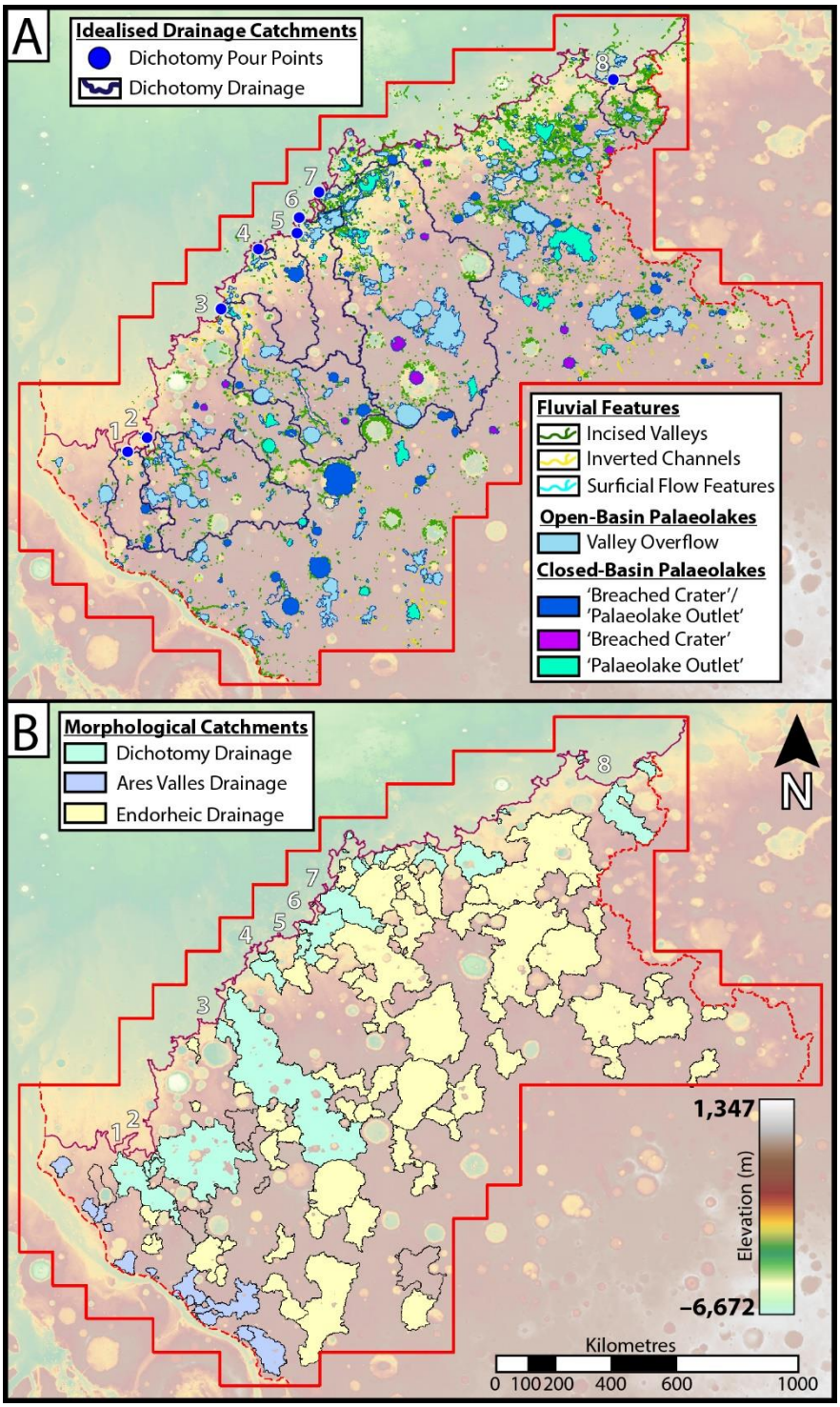

Figure 6.16 – Comparison of full catalogue of fluvial and lacustrine features, with topographically derived drainage catchments and morphologically derived drainage catchments. (A) Map of fluvial

and lacustrine features mapped in the catalogue, including all open-basin and closed-basin palaeolakes, with the coverage of major drainage catchments calculated on a fully filled topography (blue outlines), and the pour points used in the catchment calculations (blue dots). The overall distribution of features reveals that many fall outside the idealised drainage catchments, and large areas within the drainage catchments show no evidence of surface drainage or accumulation. (B) Map showing the extents and classifications of morphologically defined drainage basins based on three types of sink: dichotomy drainage (light green), Ares drainage (lilac), and endorheic drainage (yellow). (MOLA topography)

In this section, a new method for producing morphologically derived drainage catchments is employed, which has two main advantages in interpreting and characterising drainage. First, by only including basins with strong evidence of past fluvial and lacustrine processes, morphological drainage catchments are a more conservative approach to representing past hydrology. Second, and most important, by only partially filling the topography, the presence of closed sinks and endorheic basins can be accounted for and understood.

Producing morphologically derived drainage catchments was achieved by combining local drainage catchments as sub-basins of a larger drainage catchment. Local drainage basins were produced on a partially filled topography, using a fill depth of 100 m, so that only shallower sinks were filled, as described in section 6.2.1 (see also, Data and Methods 3.3.3). Neighbouring drainage catchments were combined where warranted by morphological evidence, using one of the following criteria: (1) where open-basin and/or closed-basin palaeolake extents overlap multiple local drainage catchments, indicating submersion under a palaeolake; (2) where fluvial features and palaeolake chains cross local drainage divides, indicating flow across the drainage divide; or (3) where a geologically recent feature, such as a pristine impact crater, is overprinted onto a fluvial or lacustrine feature and defines a drainage divide. To select for morphologically derived catchments with the strongest evidence of aqueous processes and surface accumulation, only catchments containing at least one open-basin palaeolake were considered.

To accurately include the relevant areas where drainage terminated at the planetary dichotomy or Ares Valles, an additional drainage catchment was produced on the 100 m filled topography, with a pour point placed at each fluvial termination. This

extra step was necessary as many of the local catchments straddling the dichotomy and Ares Valles, extended far below and beyond the actual fluvial terminations, and inclusion of the full catchment would therefore be a gross overestimate. Accordingly, no such additional calculations were required for endorheic drainage catchments.

Morphologically derived drainage catchments were classified based on three types of terminal sink: (1) dichotomy drainage catchments, with the final outlet valley terminus at the planetary dichotomy; (2) Ares drainage catchments, with the final outlet valley terminus at the bank of Ares Vallis; and (3) endorheic basins, with the final outlet valley terminus within a closed basin in the highlands. In a few examples, the terminus of a drainage system lacked a clearly definable sink within the highlands, and in these cases the drainage catchments were classified as uncertain.

A total of 111 morphologically defined drainage basins were mapped in the catalogue area (**Figure 6.16**), the combined area of which covers 30% (1,057,918 km^2) of the study area, similar to the 24% (833,961 km^2) covered by the topographically derived, dichotomy drainage basins discussed in section 6.3.1. However, the morphologically defined drainage basins indicate only a small portion of the catalogue area draining directly to the dichotomy (8%; 274,093 km^2), with an additional small area (1.5%; 51,511 km^2) draining to the lowlands indirectly through Ares Vallis. Endorheic basins account for the greatest coverage (21%; 732,314 km^2) of the catalogue area, and it is presumed that uncertain drainage catchments (2%; 54,132 km^2) were also likely to be endorheic, despite lacking clear sinks. Furthermore, without morphological evidence of fluvial or lacustrine features, it is presumed that the remaining majority of the catalogue area was either completely dry, or would have also drained into endorheic basins.

6.4.4 CONSTRAINING DRAINAGE SINKS AND SOURCE REGIONS

Major drainage catchments terminating at the dichotomy were produced on fully filled topographic data, and cover wide areas of the highlands extending hundreds of kilometres from the dichotomy, and indicating the highland areas which could have contributed surface runoff to the northern lowlands. Independent of any other

observations, these major catchments suggest that drainage in the catalogue area was dominated by surface accumulation and flow from sources in the highlands to sinks in the lowlands. However, these major catchments are only idealised representations of drainage, and therefore morphologically derived drainage catchments were produced to account for observed fluvial and lacustrine features, and endorheic basins.

Drainage catchments produced with both methods are broadly in agreement for Coogoon Vallis, Mawrth Vallis, and for some of the smaller idealised dichotomy catchments (**Figure 6.16**). Comparing the two sets of dichotomy catchments, the areas covered by the more conservative morphological drainage catchments are smaller, for the most part as a result of the exclusion of areas with no evidence of fluvial or lacustrine features. However, the catchments which are in agreement are not representative of the area as a whole, and formation of the regional depressions controlling drainage in Mawrth Vallis and Coogoon Valles likely predates the fluvial and lacustrine processes which are the focus of this catalogue. The overall trend in drainage catchments across western Arabia Terra is markedly different, with the majority of morphologically derived drainage catchments representing endorheic basins, which terminate within sinks in the highlands, and only limited areas contributing drainage to the lowlands.

The Becquerel drainage system represents the most significant mismatch between the two methods of drainage catchment production, and is examined here in greater detail (**Figure 6.17**). The Becquerel drainage catchment, calculated on a fully filled topography, is the largest of the major dichotomy catchments, indicating a significant portion of the catalogue area (11%; 347,100 km^2) as draining into the lowlands, and although the nine morphologically derived drainage catchments within the same boundary cover a significant area (8%; 214,456 km^2), they illustrate a far smaller highland area (<1%; 16,239 km^2) which actually drained to the lowlands. All but one of the drainage catchments (n=8) within the Becquerel system area are endorheic, terminating within sinks in the highlands, representing closed-basin palaeolakes in impact craters (n=4), and other deep basins (n=4). The areas within the Becquerel system which are excluded from the

morphologically derived catchments are almost completely without fluvial features of any kind, thus supporting this more conservative method of drainage modelling.

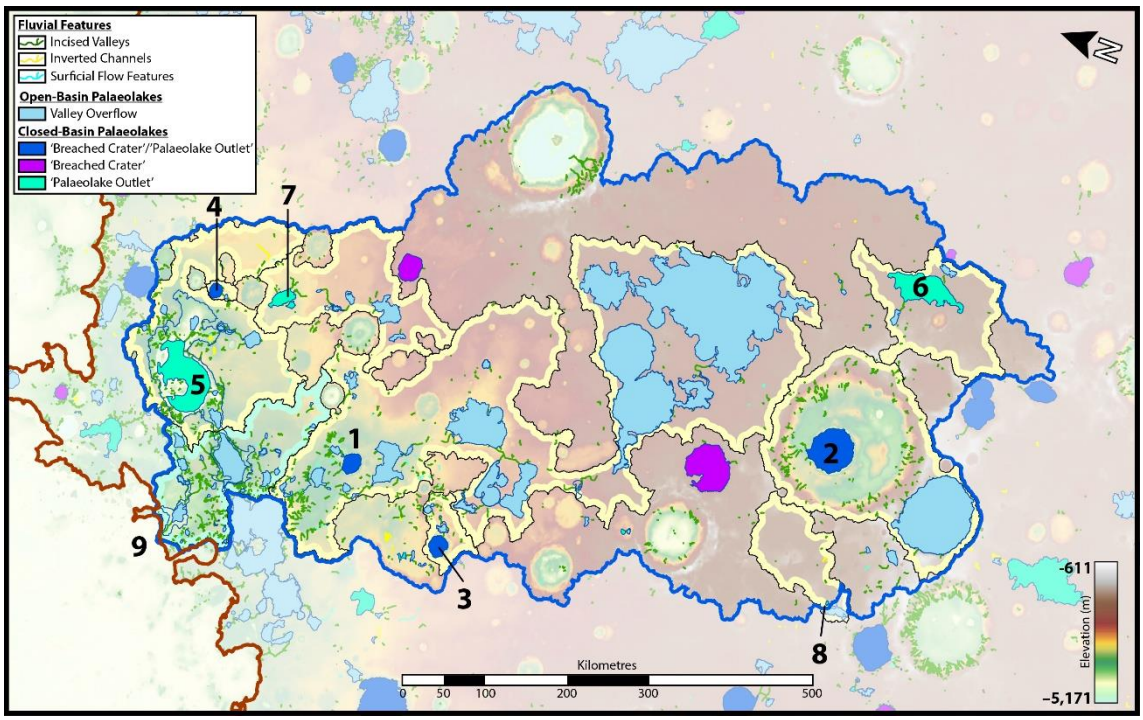

Figure 6.17 – Detailed map of morphologically derived drainage catchments within the broader dichotomy drainage catchment of the Becquerel system. The dichotomy drainage catchment of the Becquerel system (blue outline), was calculated based on a pour point (9) at the dichotomy (red line), and a topography with all sinks filled. The morphologically derived palaeolakes drainage catchments, produced by combining local drainage catchments with only <100 m sinks filled: indicate a dichotomy drainage system (light green outline) with the same pour point (9), but covering a far more limited area; and a number of endorheic drainage catchments with terminations (1-9) within closed-basin palaeolakes in the highlands. The endorheic catchment ending at sink #1 is the largest in the study area, and shows evidence of intense fluvio-lacustrine activity, despite not continuing to fill basins and drain down into the lowlands. (MOLA topography)

The largest drainage catchment within the Becquerel system also contains the largest palaeolake in the catalogue area, the longest chain of palaeolakes, and the longest fluvial feature. Yet even this significant drainage system is endorheic, and ultimately terminates within a very small closed-basin palaeolake (**Figure 6.17; sink 1**). The considerable volume of water contained and transported within this catchment over the duration of its activity, seems likely to have exceeded the volume of the sink into which it drained. It is therefore hypothesised that infiltration through the floor of this deep crater was a significant factor in the ultimate fate of water in this catchment, and possibly for the other endorheic drainage catchments across the catalogue.

6.4.4.1 *DICHOTOMY DRAINAGE*

Drainage catchments terminating at the dichotomy are in the minority, by area covered, and implied volume based on palaeolakes within those systems. Additionally, endorheic drainage catchments are situated within very short distances (>10 km) of the dichotomy, indicating flow away from the dichotomy and towards local sinks even very near to the dichotomy. The few drainage catchments which do terminate at the dichotomy cover a limited area (8%, 274,093 km^2), and besides Coogoon Valles and Mawrth Vallis, only extend ~200 km from the dichotomy. This raises an important question: how much of the highlands in Arabia Terra can be said to be a catchment for the lowlands? Given the limited extent of morphologically supported drainage catchments contributing to the lowlands, it appears that surface flow from the highlands to lowlands was limited in Arabia Terra.

One of the most robust lines of evidence for the existence of an ancient ocean in the northern lowlands are the globally consistent elevations of deltas and valley network terminations at the planetary dichotomy (Di Achille and Hynek 2010). The global study by Di Achille et al. identifies zero deltas and ~20 valley terminations within the area of the present catalogue in western Arabia Terra, and the results presented in this chapter increase this number to 14 possible deltas and hundreds of additional valley terminations, 26 of which drain open-basin palaeolakes at the dichotomy (**Figure 6.4**), with elevations a good match to those indicated globally, and the elevations of mapped northern ocean shorelines (Dickeson and Davis 2020, Sholes, Dickeson et al. 2021). This catalogue also reinforces the striking paucity of fluvial features beyond the dichotomy, within the lowlands, although a few fluvial features are situated below the dichotomy in this study, as well as one open-basin palaeolake. Detailed studies of dichotomy terminating drainage systems in other Mars regions, do indicate extensive catchment areas well supported by morphological evidence (Dohm, Ferris et al. 2001, Dohm, Ferris et al. 2011, Goudge, Mustard et al. 2015, Fawdon, Gupta et al. 2018, Goudge and Fassett 2018), and Arabia Terra may not be typical of drainage patterns across Mars. However, the contrast between idealised drainage catchments and morphologically supported catchments demonstrated

in this region, advocates for the application of caution in calculating water budget based on valley networks or palaeolakes as potential sources feeding an ocean.

6.4.4.2 *ENDORHEIC DRAINAGE*

That so few areas drained to the dichotomy indicates that the volume, and flow of water was not sufficient to fill all basins to the point of overflow, even for long palaeolake chains such as the Becquerel crater system, which extends ~500 km across the highlands towards the lowlands, but ultimately terminates within a deep sink less than 200 km from the dichotomy (**Figure 6.17**). If the volume of water and rate of flow had been greater, and sustained of longer periods, then it would be expected to have filled and overflowed all intervening basins until eventually debouching into the hemisphere spanning basin of the lowlands. The close proximity of endorheic catchments even directly adjacent to the dichotomy highlights the need to fully map fluvial and lacustrine features in an area, to be certain of the sink into which drainage would have occurred.

However, the prevalence of endorheic drainage basins may have more to do with the extreme depth of craters, than the overall supply of water. The sinks at the terminations of most (23%; n=25) endorheic catchments in this catalogue, are closed-basin palaeolakes hosted within deep craters. These basins are typically steep sided and deep, and in many cases the volume of closed-basin palaeolakes at the terminations of drainage catchments is far greater than the volume of the upstream palaeolakes which fed into them. Therefore, even a steady supply of water through open-basin palaeolake chains would require a relatively long time to fill the closed-basin palaeolakes acting as sinks. The relatively low slope of Arabia Terra could also have contributed to the prevalence of endorheic drainage systems, with relatively wide shallow basins to fill and overflow before flow could continue downslope towards the dichotomy. This would fit with an interpretation of Arabia Terra as dominated by depositional fluvial environments, as indicated by the prevalence of inverted channel systems beginning at the south-east edge of the present study area, and that by Davis et al. (2019).

6.4.4.3 *ARES VALLES DRAINAGE*

Drainage catchments terminating at the edge of Ares Valles only constitute a small proportion of the catalogue area (<1%, 51,511 km^2), and are difficult to fit into a broader understanding of the region. Although the palaeolake and fluvial systems defining these catchments terminate at Ares Valles, ultimately, flow could have continued downslope towards the dichotomy and into the lowlands. However, due to uncertainty in the age of Ares Valles in relation to the majority of fluvial and lacustrine feature in this catalogue, it is unclear whether systems drained into the present topography of the channel, or if systems were truncated by later incision of the channel.

Overall, the topographic influence of Ares Valles is limited to the immediate area adjacent to the channel, with Ares drainage catchments extending no more than ~250 km from the channel bank. Beyond these limited catchments, drainage in the south of the catalogue area is dominated by endorheic basins. Two palaeolakes adjacent to Ares Valles have inlets and outlets which appear to be integrated with the outflow channel, indicating that at least in these cases, the source of palaeolake filling was as a result of bank overspill during flooding of the outflow channel, and further supports an interpretation that the processes controlling hydrology near Ares Valles may not be relevant to Arabia Terra in general.

6.4.5 GROUNDWATER INFLUX AND SURFACE ACCUMULATION

In addition to the sinks and sources described above, another important aspect in characterising the hydrology of Arabia Terra is the relative influence of groundwater influx, or surface accumulation and precipitation in palaeolake filling. A method of approximating the balance between these processes was applied in the study by Fassett et al. (2008) for 34% (n=72) of the open-basin palaeolakes in that catalogue, and achieved comparing the catchment area (A_C) of individual palaeolakes to palaeolake volume (V_L) and area (A_L). Based on terrestrial studies, V_L values >15 m were taken to indicate groundwater influx as the dominant input, and V_L values <15 m to indicate surface accumulation as the dominant input (Fassett and Head 2008). However, the methods

used to derive catchment areas appears to have been largely subjective, and difficult to replicate, with the palaeolake inclusion criteria stated as: (1) palaeolake basin without volumetrically important basins as sources, such as palaeolakes fed as part of chains; and (2) palaeolakes not exhibiting evidence of major resurfacing within their watersheds, which might complicate watershed definition. Palaeolake drainage catchments were then estimated, and although there is no indication of the method used in estimation, it appears that watershed delineation was achieved by a subjective analysis of the landscape, topography, and fluvial features rather than calculated digitally. A study of the drainage catchment of the palaeolake within Jezero crater specifically addresses the significant disparity between the drainage catchment defined manually in previous studies (Fassett and Head III 2005, Fassett and Head 2008), and the idealised drainage catchment calculated topographically (Goudge, Mustard et al. 2015).

Table 6.2 *– Preliminary volume to drainage catchment relationships for large >2,000 km palaeolakes identified in this chapter, ordered by palaeolake area. Including morphological palaeolake basin types: inter-crater plains (IC); single impact craters (CS); multiple impact craters (CM); and unidentified (UM).*

Palaeolake	Basin Type	Area (A_L) (km^2)	Volume (V_L) (km^3)	Catchment Area (A_C) (km^2)	Volume/Catchment (V_L / A_C) (m)
32	IC	15,208	1,435	30,102	48
705	IC	9,701	863	22,367	39
680	IC	9,345	775	30,670	25
14	IC	6,053	351	36,324	10
298	CM	5,303	673	26,925	25
426	CS	5,172	3,498	7,873	444
314	IC	4,996	366	13,782	27
207	CM	4,267	3,665	7,609	482
21	CS	2,769	1,855	4,598	403
138	CM	2,665	2,865	3,647	786
377	CM	2,639	2,325	4,015	579
204	IC	2,470	150	13,437	11
483	CS	2,415	2,985	3,193	935
91	UN	2,191	193	5,621	34
142	CM	2,133	845	3,901	217

Despite the difficulties in calculating drainage catchments on Mars, the benefits of further characterising the hydrology of palaeolakes warrants a preliminary calculation of individual palaeolake drainage catchments, and the analysis presented here considers only the largest (n=23) palaeolakes identified in this chapter, with areas >2,000 km^2 and eliminating palaeolakes: (1) thought to be of lower confidence (n=2), based on the

detailed studies in Chapters 4 and 5; or (2) fed by higher palaeolakes of significant relative volume (n=6), defined here as >50% volume of the palaeolake being considered. Drainage catchment areas were defined for the remaining 15 large palaeolakes, using the morphologically derived catchment boundaries produced in section 6.4.4.

Two of the analysed palaeolakes display V_L/A_C values <15 m, indicating palaeolake filling driven by surface accumulation, with the remaining (n=13) palaeolakes indicating groundwater influx as the dominant process, including three palaeolakes displaying V_L/A_C values of <30 m. A stark contrast is observed based on the morphological type of basin hosting the palaeolake, with palaeolakes hosted within craters displaying much higher mean values of V_L/A_C (n=8; 484 m) than palaeolakes hosted within basins in the inter-crater plains and other undetermined basins (n=7; 28 m). This division may reflect the generally high volumes of impact crater palaeolakes relative to shallower inter-crater basins, or alternatively, that a greater number of impact crater palaeolakes intersect the water table at depth.

The analysis presented here only considered the largest palaeolakes by area, but the total volume of these 15 palaeolakes comprises ~64% (22,850 km^3) of all the open-basin palaeolakes, and therefore the filling mechanism indicated for these examples should be relatively representative of the entire population. However, it should be noted that given the uncertainties in calculating drainage catchments on Mars these values are approximations, and with an unknown margin of error, values of 15-30 m may also represent significant filling by surface accumulation. Although the method of drainage catchment delineation applied here was suitable at the scale of the entire catalogue area, a more detailed approach may be required at the scale of individual palaeolakes.

6.5 CONCLUSIONS

This catalogue presents a significant new body of data quantifying hydrological processes in western Arabia Terra, central to which are 632 open-basin palaeolakes and 103 closed-basin palaeolakes. The combined area of these palaeolakes cover ~7% of the

total catalogue area, representing substantial submersion of the region. This degree of coverage is on a par with some of the most densely lake covered regions on Earth, such as the Canadian Shield of northern North America at ~12%. Such extensive coverage by water across Arabia Terra has important implications for the past habitability of the region as well as the geological and chemical processes and deposits that would be expected to accompany such widespread inundation.

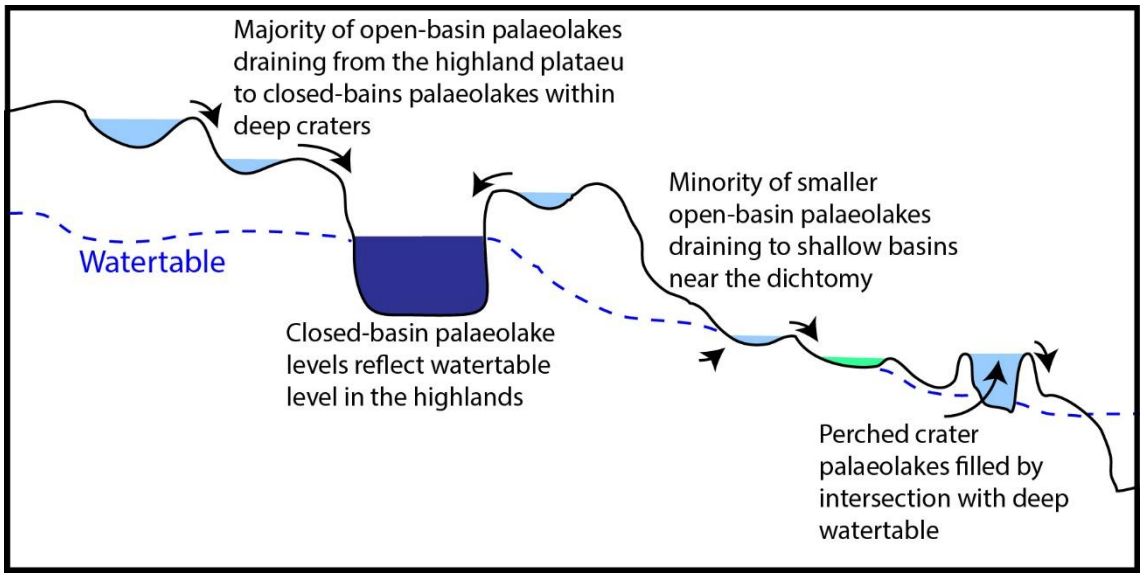

Figure 6.18 *– Schematic model of surface runoff and possible groundwater processes characterising the hydrology of Arabia Terra.*

Far from being isolated features, the vast majority of open-basin and closed-basin palaeolakes identified within this catalogue are connected into chains of palaeolakes and fluvial networks, indicating wide connected systems stretching across the highlands. Furthermore, analysis of individual palaeolakes and systems reveals complex histories of changing fill levels within palaeolake basins, driven in some cases by steady erosion of fluvial outlets and in others by reduction in drainage input. These changes resulted in a dynamic shifting of drainage patterns as palaeolake levels dropped to uncover previously submerged basins, with subsequent drainage catchments defined by the new palaeolake levels. From a global perspective, the existence of this apparently complex and widespread population of lakes necessitates a climate and atmosphere sufficient to allow stable liquid water on the surface.

A major finding of this work is the overall contribution of highland terrains as drainage catchments, ultimately facilitating surface accumulation of water, and the transfer of sediment to basins in the lowlands. The morphologically derived drainage catchments produced in this work provide a stark contrast to the idealised drainage catchments which are typical of hydrological research on Mars. Instead of wide areas of Arabia Terra draining to the lowlands, very little of the region can be considered as a catchment for the northern lowlands based on the present topography. The ancient terrains of Arabia Terra are likely a good representation of past topography, as the majority of large impact craters were already present at the time of the fluvial and lacustrine processes discussed here. The majority of morphologically derived drainage catchments end within endorheic basins in the highlands, producing a hydrological landscape similar to the closed basins of Central and East Africa, including closed-basin lakes such as Lake Chad or Lake Turkana. Very few drainage systems actually terminate at the planetary dichotomy, and those that do typically represent extremely localised catchments. This indicates that although Arabia Terra was once significantly covered by standing water bodies, basin filling was generally not sufficient to overflow the deepest basins, and this places significant limitations to the volume of water that could have reached the lowlands and a possible northern ocean on Mars.

7

Synthesis and Conclusions

7.1 Overview

This chapter brings together the major findings of the three research chapters of this thesis, and presents a discussion of results and methods as applicable to the region of Arabia Terra and Mars in general. The broader regional and global implications of this research are discussed with a focus on the major topographic controls and hydrological constraints on drainage (**Section 7.2**), allowing the identification of palaeolake settings and environments on Earth which represent the best analogues to the hydrology of ancient Mars and Arabia Terra (**Section 7.3**). The methods central to this thesis are then compared and contrasted between research chapters, and to previously published studies, with the aim of improving methods for future studies (**Section 7.4**), with a discussion of suggested areas of future work, building on the this thesis (**Section 7.5**). Finally, a brief conclusion sets the research of this thesis into the study of Mars and the search for life (**Section 7.6**).

7.2 Implications for Early Hydrology on Mars

7.2.1 Controls on Regional Drainage

Regional scale channels in Arabia Terra, such as Mawrth Vallis and palaeo-Coogoon Valles, drain north-westward towards the planetary dichotomy, a trend shared by major (>20 km) valleys described in Chapter 6 (**Section 6.3.2.1**) and previous studies (Hynek, Beach et al. 2010, Molina, Lopez et al. 2017, Alemanno, Orofino et al. 2018,

Fawdon 2018). The palaeolake systems investigated in Chapter 4 and 5 are additional examples of flow from the highlands to the lowlands, however, for the entire population of fluvial features in the region, flow direction is only controlled by the dichotomy locally. Further south-east, upslope into the highlands, flow is largely directed into regional sinks in the highlands rather than towards the lowlands, and longer fluvial features and palaeolake chains are the only exceptions.

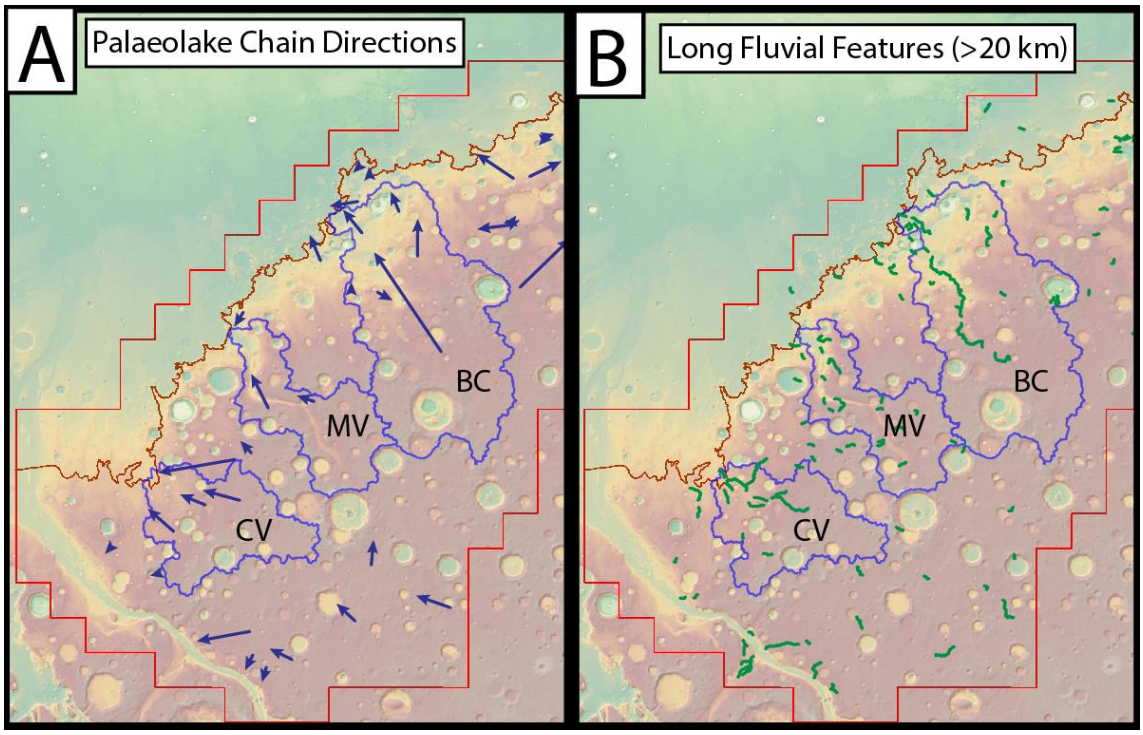

Figure 7.1 *– Trends in regional flow, relative to major regional depressions, illustrated with the idealised drainage catchments for Coogoon Valles (CV), Mawrth Vallis (MV), and the Becquerel crater system (BC). (A) Distribution of long palaeolake chains, with direction and length from start to end, including only chains of at least three open-basin palaeolakes. Demonstrates the preference of flow direction towards the dichotomy, particularly within the three idealised catchments. (B) Distribution of the longest fluvial features (>20 km), concentrated within the three idealised drainage catchments.*

The majority of long fluvial features and palaeolake chains are concentrated within three regional scale depressions which trend north-west: Coogoon Valles, Mawrth Vallis, and the Becquerel crater system described in Chapter 6 (**Figure 6.16**). The morphology and geology of both Coogoon Valles (Molina, Lopez et al. 2017), and Mawrth Vallis support origins as regional scale ancient fluvial systems, which have since been eroded and eventually overprinted by more recent valley networks. The Becquerel system defines the centre of a similar northwest oriented depression, influencing drainage

patterns and flow directions for great distances into the highlands (~1,000 km), and is characterised by a wide flat floored channel where it terminates at the dichotomy, much like Mawrth Vallis and palaeo-Coogoon Valles. Given these similarities, the Becquerel system may share a similar origin, and represent another ancient drainage system in Arabia Terra. These ancient drainage systems appear to display a greater degree of hydrological maturity than many younger valley networks on Mars, and probably indicate an early martian climate that was wet and warm enough for liquid water to flow on the surface for prolonged periods.

The majority of palaeolakes in this thesis are situated on ancient aged terrains (Tanaka, Skinner et al. 2014), and identified based on observations of typical martian valley networks, and are therefore interpreted as coinciding with the global peak in valley network activity in the Noachian and Hesperian (~3.7-4.0 Ga). The greatest influence on these fluvial and lacustrine systems is not the regional depressions described above, but deep local basins in the highlands. Nearly half of open-basin palaeolakes (48%; n=304), containing the majority of total volume (70%; 35,909 km^3) ultimately drain to closed-basin palaeolakes in the highlands, with the majority of terminal closed-basin palaeolakes hosted within deep impacts craters. That these craters remained as closed-basin palaeolakes, indicates a supply of water insufficient to fill to the point of breach and overflow. However, the volumes of terminal palaeolakes are often greater than the open-basin lakes draining into them (**6.4.2**), and the total capacity of these deep craters is greater still. The prevalence of deep craters in the landscape acted as essentially unfillable sinks, severely limiting the connectivity and continuity of drainage across Arabia Terra. The effect of deep craters is particularly acute given the semi-arid or arid conditions indicated by the work in this thesis as well as past studies (Ramirez and Craddock 2018), but even with a greater supply of water, the disruptive effect of impact craters on drainage continuity would likely have been significant.

7.2.2 GROUND WATER INFLUX AND SURFACE ACCUMULATION

The relationship between drainage catchment area and lake volume is an indication of the relative importance of groundwater influx and surface accumulation to filling of a palaeolake (Fassett and Head 2008). The drainage catchments of individual palaeolakes are difficult to calculate objectively and accurately on Mars, but the preliminary analysis of these relationships presented in Chapter 6 (**6.4.5**) suggests the filling of palaeolake basins was predominantly by the influx of groundwater. This would fit with the results of Fassett and Head (2008), highlighting the correlation between palaeolakes dominantly fed by groundwater influx and a global study indicating Arabia Terra as a region of significant groundwater upwelling (Andrews-Hanna, Zuber et al. 2010).

In addition to the relationship between drainage catchment and palaeolake dimensions described above, an analysis of palaeolake elevation and distance from the dichotomy shows a general trend following the rise in topography into the highlands, expressed differently for each type of palaeolake, with trends suggesting differences in the relative importance of palaeolake filling processes across the region.

Open-basin palaeolakes, and 'lake outlet' type closed-basin palaeolakes are situated at the highest elevations, and display the greatest range in elevation. Open-basin palaeolakes include the largest palaeolakes by area and volume, and although the largest examples are situated in the relatively flat plateau of the highlands, a greater number of smaller open-basin palaeolakes is concentrated along areas nearer to the dichotomy. These groups were found to not be generally connected at the surface, with most of the larger palaeolakes in the highlands draining into endorheic basins, and with little surrounding higher terrain, likely sourced by near-surface water.

In contrast, closed-basin palaeolakes within impact craters have a well-defined upper elevation limit of ~-2500 m, which may indicate a past water table level only intersected within deep craters in the region. Closed-basin palaeolakes within craters also define a lower elevation limit to palaeolakes in the region, at ~-3500 m in the plateau area, and steeply lowering towards the dichotomy. The mean elevation of the dichotomy in the

region is also ~-3500 m, and therefore a wider base-level within the lowlands may have influenced ground water up to ~600 km into the highlands.

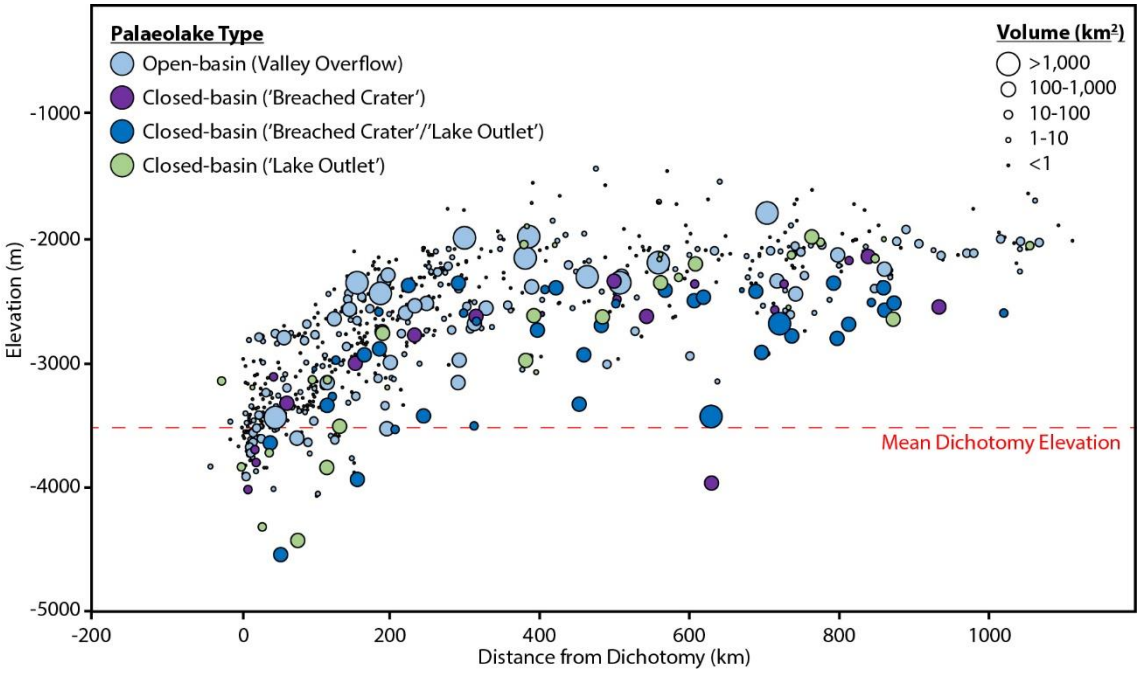

Figure 7.2 *– Complete population of catalogued palaeolakes (n=735) plotted by elevation and distance from the dichotomy, and weighted by volume. Overall palaeolake distribution shows the trend in topography from the steeper low-lying areas adjacent to the dichotomy, to the wider flat plateau of Arabia Terra, with a greater concentration in the number of palaeolakes lower and near the dichotomy, but with the largest palaeolakes higher and more distant. Open-basin palaeolakes (light blue) are the best fit to the overall topography, and show a wide spread of positions and elevations, and 'lake outlet' closed-basin palaeolakes (light green) match this general trend. Due to all being set within craters, 'breached crater' (purple) and 'breached crater' and 'lake outlet' type (dark blue) closed-basin palaeolakes are at a lower elevation, and regardless of distance from the dichotomy, are concentrated at elevations between -2500 and -3000 m.*

Perched crater lakes are a subset (2.5%; n=16) of open-basin palaeolakes, defined as being hosted within impact craters with raised rims and surrounded by terrain at an elevation lower than the palaeolake level. This topographic relationship implicates groundwater influx in the filling of these basins, as the catchment area available for surface accumulation is essentially non-existent. Beyond simply being fed by groundwater, the high elevation of the palaeolake surface, above the surrounding terrain, precludes the palaeolake level as representing the level of the water table. Instead, it appears that the crater must intersect the water-table at depth, and that there is sufficient hydraulic pressure released to fill the crater above the level of the surrounding terrain.

7.2.3 IMPLICATIONS FOR ANCIENT OCEANS ON MARS

Whist not the primary focus of this thesis, any investigation of the planetary dichotomy or palaeolakes on Mars will have implications on possible water bodies in the lowlands. The palaeolake systems investigated in Chapter 4 and 5 terminate at deltas at the dichotomy, but the ultimate fate of water into the lowlands, and the nature of possible waterbodies at these terminations is ambiguous. The extent of these possible water bodies indicate either closed-basin palaeolakes or a hemisphere spanning ocean depending on the exact elevation, and in both locations the basins are only narrowly open to the northern lowlands, and there is evidence of topographic change postdating fluvial and lacustrine processes (McNeil, Fawdon et al. 2021). The conclusion reached in this thesis is that these systems likely drained into closed-basin palaeolakes rather than an ocean, and topographic modifications to the dichotomy as observed in Arabia Terra should be considered in global ocean interpretations which are based on fluvial system terminations at the dichotomy (Di Achille and Hynek 2010, Rivera-Hernández and Palucis 2019). It is also significant that the vast majority of palaeolake drainage systems do not reach all the way to the dichotomy, so that only a small area of Arabia Terra acts as a catchment area for a possible ocean. Therefore, attempts to define the volume of water input from highland fluvial systems to support an ocean in the lowlands (Luo, Cang et al. 2017), may be significant overestimates. However, that the landscape was so densely covered by lakes also raises questions as to the source of such great volumes of water. Extensive lake covered regions on Earth are only possible due to a global hydrological cycle driven by evaporation from the World Ocean, and to sustain regional palaeolake activity on the scale shown in this thesis without such a water body may prove difficult. To prove or refute the existence of ancient oceans in the northern hemisphere of Mars is not likely to be possible with the presently available set of orbital data. The findings of this thesis serve to advance the incremental process of evaluating the evidence for an ocean and the constraints placed on such a water body, and leads to the overall impression of additional doubt in the theory of long prevailing oceans on Mars.

7.3 PALAEOLAKE ENVIRONMENTS ON MARS

7.3.1 A DYNAMIC LANDSCAPE

Evidence of multiple fill levels within individual palaeolake basins indicate a complex and changing fluvial and lacustrine landscape, particularly where open-basin palaeolakes drained completely, or open-basin palaeolakes transitioned to closed-basin palaeolakes. Dropping levels within open-basin palaeolakes reflect the erosion of outlet valleys, and indicates sustained drainage through the system and supporting climatic conditions. Sufficient water input and climatic conditions to fill and support fully connected palaeolakes chains eventually ceased before the landscape was fully integrated into drainage catchments, or closed-basin palaeolakes filled to overflow and become open-basin palaeolakes. However, the persistence of closed-basin palaeolakes within formerly open-basin palaeolakes suggests that these changes were not abrupt, and that groundwater supported residual palaeolakes for some time after surface drainage declined. In the most extreme cases, the reduction of base-level within a palaeolake midway along a chain, has changed the direction and fate of drainage for a wide area. It is also likely that impact events occurred which blocked the established course of palaeolake drainage, with a possible candidate observed near the dichotomy within the Becquerel crater system.

An observation made throughout this thesis was of negative slope outlet valleys, where fluvial features appear to climb upwards out of palaeolake basins along their upper reaches. The preferred interpretation of this observation is of residual flow back into a closed-basin, but some valleys clearly exhibit this morphology at both ends. Both ends of these arched valleys can equally be interpreted as inlet or outlets, and are here interpreted as representing a dynamic shift in flow direction to and from palaeolakes at either end. This shift could have been the result of unequal groundwater influx at one end of the system, raising one palaeolake level higher to reverse the flow, or as a longer term consequence of changing global topography tilting the entire terrain (Perron, Mitrovica et al. 2007, Citron, Manga et al. 2018).

7.3.2 EARTH ANALOGUES

The most densely lake covered terrains on Earth are found in the far north of North America and Eurasia (**Section 2.2**), representing a relatively hydrologically immature landscape, freshly uncovered from beneath by ice sheets (Wolfe, Morse et al. 2017). The density of palaeolake revealed in this thesis is similar to the Canadian Shield of North America, and the shallow nature of the numerous palaeolakes described here indicate a similar level of hydrological immaturity, with fluvial processes not continuing long enough for the majority of outlet valleys to incise and drain the palaeolakes.

An aspect lacking in the analogy of post-glacial landscapes is the presence of closed-basin palaeolakes, which this thesis shows to be an important part of the ancient drainage systems and hydrology of Arabia Terra. The largest closed-basin palaeolakes on Earth are generally found within the centres of continents, such as the Caspian Sea in Central Asian and Great Salt Lake in North America, with smaller examples often confined to deep tectonically controlled basins such as the Great Lakes of Africa or the Dead Sea within rift regions (Carroll and Bohacs 1999). The majority of closed-basin palaeolakes identified in this thesis are hosted within deep impact craters, and although crater hosted lakes are not significant on Earth, a fitting terrestrial analogue on may be steep sided rift basins, which act as persistent deep basins in a similar manor to palaeolakes on Mars.

Changes in flow direction, as described for 'arched valleys' in the previous section, are not unheard of on Earth, and the Tonlesap River in Southeast Asia reverses direction on a semi-annual basis as the balance of water input at either end changes through the year (Kummu, Tes et al. 2014). When input from the Mekong River, at the east end of the Tonlesap is greater, flow is directed westward to fill a large shallow palaeolake ~100 km to the west, and when level of the Mekong River drops, the lake begins to drain, and the Tonlesap flows to the east. However, in the case of the Tonlesap, this is only possible given the low topographic gradient between either end of the river, and a reversal of flow in martian 'arched valleys' a much greater gradient of water surface levels would be required from one end of the valley to the other.

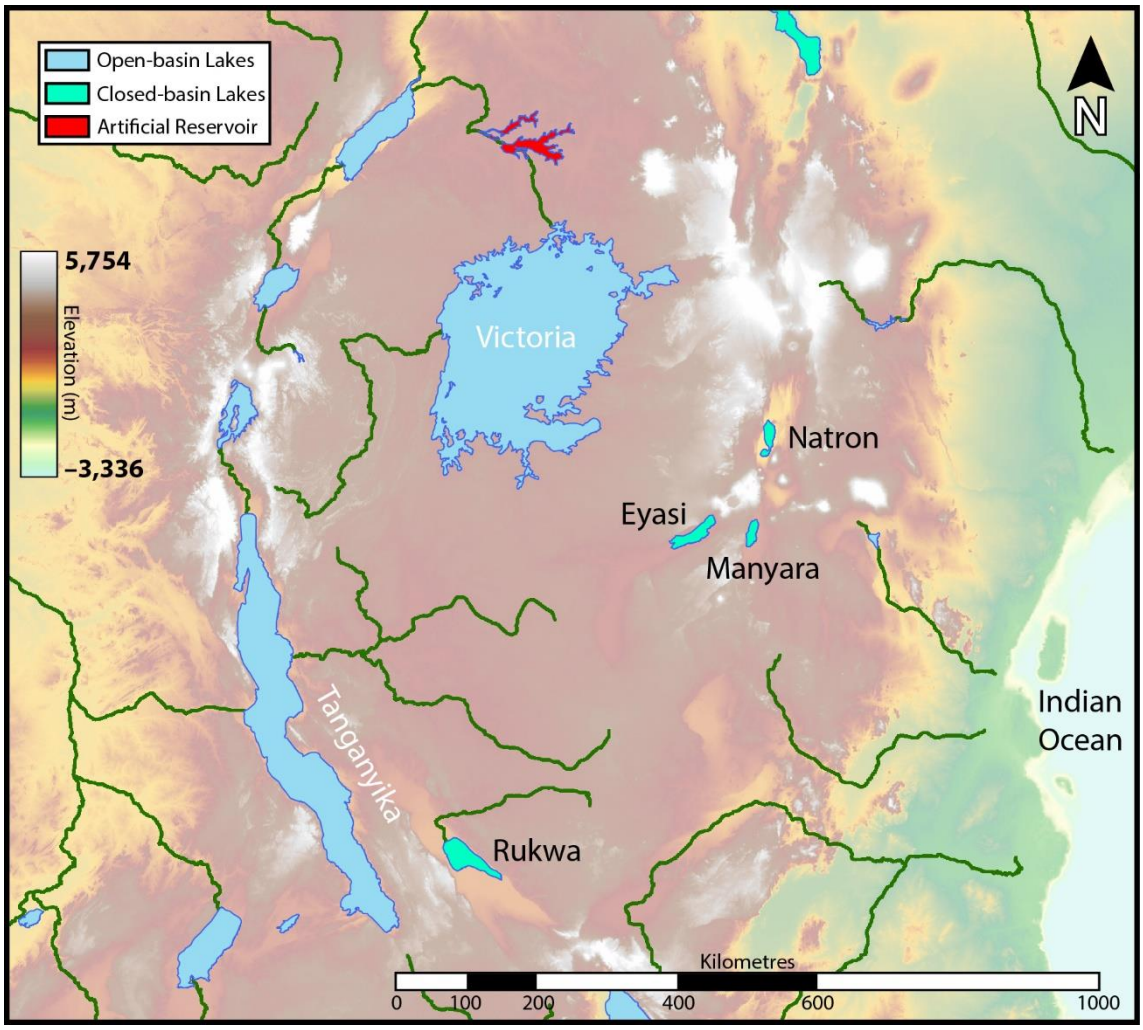

Figure 7.3 *– Map of the Great Lakes region of East Africa, as a possible analogue to the hydrological setting of Arabia Terra. Drainage patterns in the region are largely controlled by the upraised edges, and downthrown floors of continental rift valleys, considered here as a fitting analogue to the role of impact craters on Mars in controlling drainage. In this model, the wide and shallow basin of Lake Victoria is analogous to palaeolakes hosted in the inter-crater plains as identified in this thesis, with closed-basin palaeolakes hosted within the rift valleys, just as many closed-basin palaeolakes on Mars are hosted within craters. Further strengthening this analogy is the inlet valley of Lake Rukwa which appears to breach the upraised edge of the rift valley, in a similar manner to 'breached crater' type palaeolakes described within this work. A major difference noted between East Africa and Arabia Terra is the full filling and overflow of the deep rift basin which holds Lake Tanganyika, indicating a supply of water exceeding that existing on ancient Mars. River data obtained from Natural Earth (naturalearthdata.com), lake data obtained from Global Lakes and Wetlands Database (GLWD; https://www.worldwildlife.org/pages/global-lakes-and-wetlands-database) (Lehner and Döll 2004), with topography and bathymetry from ETOP1 1 Arc-Minute Global Relief Model (Amante and Eakins 2009).*

As for the closed-basin palaeolakes on Mars situated along the lowland side of the planetary dichotomy, a similar arrangement of fluvial terminations and small palaeolakes is observed along the steep margins of mountain ranges in some arid regions on Earth. The northern edge of the Iranian Plateau in central Asia exhibits this arrangement of

drainage and closed-basin palaeolakes, as do the edges of the basin and range province between the Rocky Mountains and the Coastal Mountains of North America.

Taking in all these considerations, a fitting terrestrial analogue to the hydrology of Arabia Terra as an entire region, may be the region in and around the East African rift system. The area exhibits a mix of open-basin and closed-basin lakes in close proximity, with some open-basin lakes in the plateaus between rifts draining into the continental fluvial system of the Nile River, and others breaching the edges of the rift valleys, to terminate in closed-basin lakes on the rift floors (Lehner and Döll 2004).

7.3.3 PALAEOLAKE ECOLOGY AND ASTROBIOLOGY

The exploration of Mars has traditionally followed the mantra of 'follow the water', with a central aim of searching for evidence of life on Mars (Fairén, Davila et al. 2010). Considering a wide range of criteria, standing bodies of water such as lakes and oceans represent a wide range of habitable environments on Earth, and given the lack of consensus on ancient martian oceans and significant resurfacing of lowland terrains (Tanaka, Skinner et al. 2003, Dickeson and Davis 2020), palaeolakes may be best areas to search for evidence of ancient life on Mars (Fairén, Davila et al. 2010, Summons, Amend et al. 2011). The palaeolakes identified in this thesis represent a range of potentially habitable environments, and sites for the future exploration of Mars with the objective of identifying past signs of life.

Previous works on martian and terrestrial lakes have indicated that shallow lakes tend to have greater biological productivity (Wetzel 2001, Fassett and Head 2008). Therefore the greater number of shallow lakes in the present catalogue, as indicated by mean depth (**Figure 6.13e**), may aid in the identification of past habitable environments. As the climate of Mars changed, habitable conditions may have persisted in local micro-climates within deep closed-basin crater hosted palaeolakes which make up a significant portion of features identified in this thesis, the floors of which are often kilometres lower than surrounding terrains. Atmospheric pressure would have remained marginally

higher in these settings, and geothermal heating could have maintained relatively higher temperatures (Abramov and Kring 2005, Osinski, Tornabene et al. 2013).

The extensive coverage, density, and connectivity exhibited by palaeolakes identified in this thesis, indicates a past environment where life could have spread from one habitable environment to another. This is in stark contrast to the previously mapped palaeolakes in the region (Fassett and Head 2008, Goudge, Aureli et al. 2015), representing deep, isolated environments with great distances in between. Open-basin and closed-basin lakes on Earth exhibit vastly different habitable environments. Open-basin lakes are typically freshwater, and offer greater oxygenation and nutrient recycling. Whilst closed-basin lakes are often saline and acidic, and offering a different suit of nutrients for some specialised extremophile organisms. Again, the combination of these two broad classes of habitable aqueous environments in close proximity, into fluvial and lacustrine chains, provides an even greater variety of possible habitable conditions and environments.

7.4 APPRAISAL OF METHODS

7.4.1 PALAEOLAKE IDENTIFICATION CRITERIA

The methods for identifying palaeolakes utilised in this thesis were based on previous palaeolake studies on Mars (Mangold and Ansan 2006, Fassett and Head 2008, Goudge, Aureli et al. 2015), with the development of some key additions and refinements. Although multiple palaeolake fill levels have been identified in detailed studies of individual open-basin palaeolakes (Goudge and Fassett 2018), the majority of studies only consider a single level approximately equivalent to the valley overflow level described in this thesis (**Section 4.2.1**). The standard identification of all three possible palaeolake fill levels applied in this thesis is new to the field of study, and it is hoped that future research will make use of similar principals. As described above (**Section 7.3.1**), the identification of basin overflow and valley overflow levels records a change in palaeolake levels over time, rather than a static and unchanging single palaeolake level, and although the meaning of the valley extremity level has defied a conclusive interpretation (**Section**

4.4.1.3), the consistent appearance of this feature across so many palaeolakes suggests that it represents some process as yet unidentified, and continuing to record the valley extremity level in future studies will hopefully lead to a better understanding.

Another key feature differentiating the methods used in this thesis from past palaeolake studies, is the identification of open-basin palaeolakes not only where valleys begin within topographic basins, but also where valleys transect through topographic basins. The clearest example of this are the two final palaeolakes in the chain described in Chapter 4 (**Section 4.4.1.1**), but many (20%; n=127) of the palaeolakes identified in Chapter 6 fit this same sub-set. Identifying these palaeolakes is another important aspect in understanding how fluvial and lacustrine systems on Mars have changed over time, and as described in Chapter 5, they provide an opportunity to identify areas where possible palaeolake deposits have been incised and eroded.

The identification of closed-basin palaeolakes on Mars is generally handled conservatively, in order to minimise misidentification of closed-palaeolakes within basins which were drainage sinks, but never hosted standing bodies of water. Within this thesis, this general caution was applied, but with the addition of palaeolakes identified within a wider range of basins besides only impact craters. An additional set of criteria to be examined in future palaeolake studies may be the wider identification of closed-basin palaeolakes where numerous inlet valleys are concentrated at a narrowly constrained elevation, as demonstrated in Chapter 5 (**Section 5.3.5**). There are many deep craters in the highlands which do not meet the established criteria of inlet valleys breaching the crater rim, but do exhibit tens or hundreds of short channels incised into the crater edges. A systematic process to assess these features could involve calculating the vertical elevation difference, and horizontal distance from the palaeolake boundary, for all fluvial terminations within 10 km of the palaeolake boundary.

Although efforts were made in the course of this research to verify the identified palaeolakes, future studies making use of high-resolution topography, and studies characterising additional features such palaeolake deposits and shorelines, will be

required to build more confidence in the methods applied in other palaeolake studies and within this thesis.

7.4.2 Drainage Catchment Delineation

The delineation of ancient drainage catchments on Mars is complicated by the substantial topographic changes that have shaped the landscape subsequent to fluvial and lacustrine processes. On Mars, idealised drainage catchments are generally calculated on a topography with all sinks filled (Goudge, Aureli et al. 2015, Fawdon 2018, Goudge and Fassett 2018), with other various methods including, manual estimations of drainage catchments based on observations of topography and morphology (Fassett and Head III 2005, Fassett and Head 2008), and iterative approaches using a variety of fill depths to find one that produces drainage catchments that best represent observed fluvial landforms (Mest, Crown et al. 2010). In both cases, a consideration of morphological evidence of drainage in addition to topography is essential, and it was on this basis that the method utilised in Chapter 6 (**Section 6.4.3**) was developed.

Due to the significant differences exhibited across Mars regions, in topography, slope, fluvial feature expression, and hydrological histories, drainage catchment delineation methods will likely require adjustment to match the particularities of new study areas. However, digitally filling topographic data will remain a step in the process, and as demonstrated within this thesis, identifying palaeolake fill levels is an effective and efficient way to identify which basins actually filled with water in the past. Therefore palaeolake identification should be an important part of any future studies delineating drainage catchments on Mars.

7.4.3 Data Resolution in Palaeolake Identification

Global topographic data coverage on Mars is limited to relatively low-resolution ~463 m/pixel MOLA DEMs, with 50-250 m/pixel HRSC DEMs produced from stereo imagery representing the next most extensive coverage (~44%). Obtaining topography data at higher resolutions generally requires the bespoke production of DEMs from stereo imagery, such as ~20 m/pixel CTX DEMs and ~1 m/pixel HiRISE DEMs (**Section**

3.2.2.1). The benefits of full coverage of a study area with high-resolution (~20 m/pixel) CTX DEMs were demonstrated in Chapter 4, including the detection and measurement of relatively subtle topographic features, and most importantly, the ability to resolve and measure the depth of narrow valleys (**Section 4.3.1**). Accurately measuring valley depth allowed the most accurate possible level for valley overflow and basin overflow level at palaeolake outlets, as well as the production of longitudinal valley profiles with elevations of both the valley floor and valley bank. As demonstrated in Chapter 5, the use of lower resolution MOLA DEMs precluded the precise measurement of valley depth for the majority of valleys, with the elevations of ~463 m MOLA DEM pixels representing average elevations of valley floor and bank, and resulting in valley overflow levels which are likely higher elevation than would be measured on high-resolution topography.

To demonstrate differences in palaeolake identification resulting from topographic data resolution, palaeolakes in the study area of Chapter 4 are compared here as identified at three different DEM resolutions: (1) ~20 m/pixel CTX DEM mosaic, as originally identified in Chapter 4; (2) ~150 m/pixel HRSC DEM, mapped for this comparison; and (3) ~463 m/pixel MOLA DEM, as identified in the catalogue in Chapter 6. In all three mapping iterations, the same set of mapped fluvial features were used, contours were spaced at 10 m vertical intervals, and palaeolake levels (valley overflow, basin overflow, valley extremity) were identified with the same criteria.

The results in all three instances are broadly similar, with the exception of palaeolake L-A4, which describes a far greater palaeolake area on MOLA topography. This major discrepancy is due to a narrow (~4 km) barrier between two anomalously large and deep basins, which on MOLA topography become one basin at the elevation of the palaeolake. This circumstance, of a very shallow and narrow strait, is not replicated for any other palaeolakes in the catalogue, and does not appear significant to the study as a whole. The other variations in observed palaeolake areas and boundaries due to topographic resolution are minor, and the outlet elevations defining these palaeolakes are generally consistent regardless of resolution. Finally, valley overflow levels are higher on lower resolution topography, whereas basin overflow levels in the same palaeolakes are

consistent between resolutions. As described above, this is most likely due the failure to resolve narrow valley depths on low resolution topography, with the end result of only a slight difference between the elevation of valley overflow and basin overflow levels.

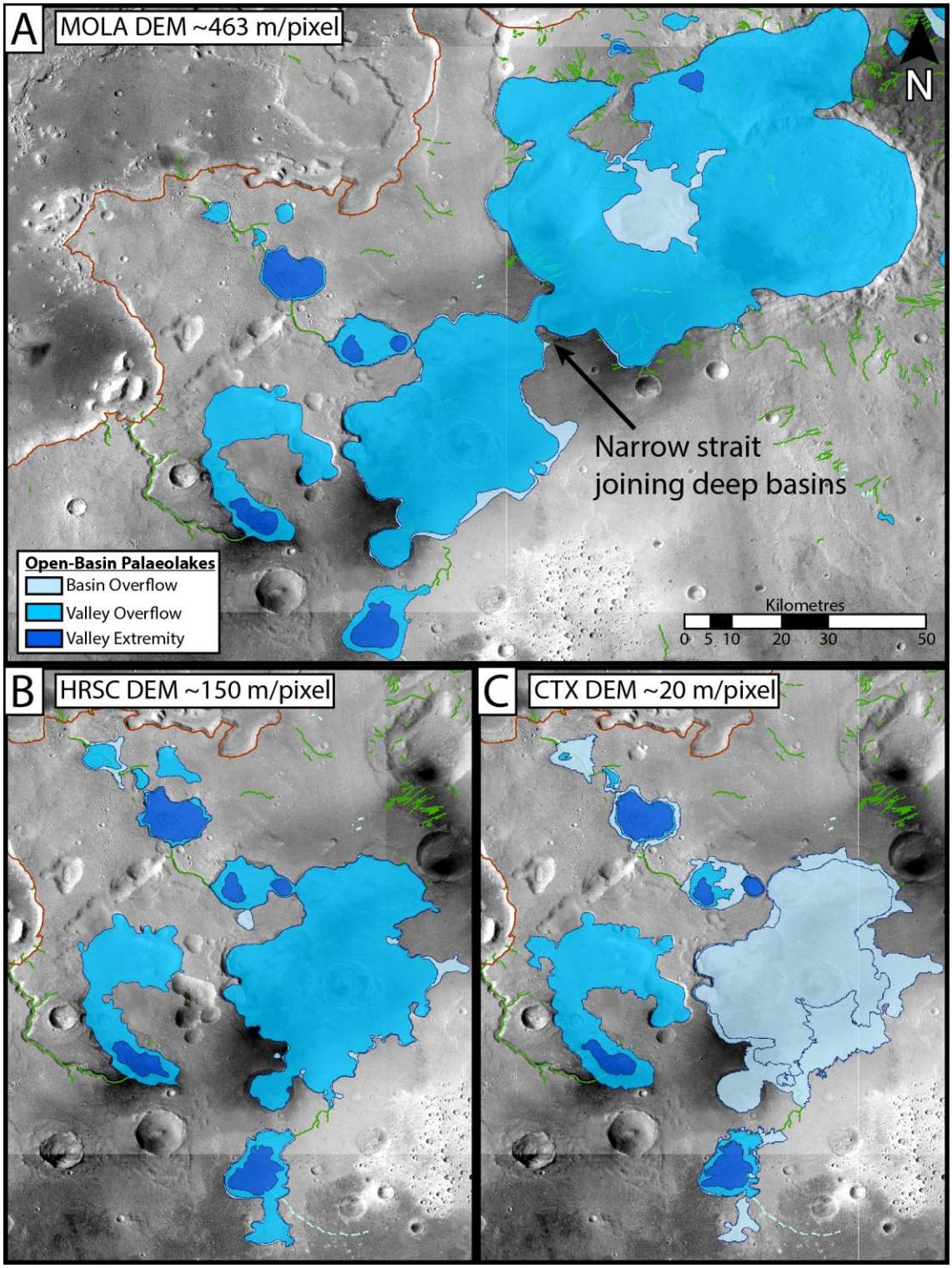

Figure 7.4 *– Demonstration in palaeolakes identified with the use of topography data at different resolutions: (A) 463 m/pixel MOLA DEM, as identified in Chapter 6; (B) 150 m/pixel HRSC DEM; and (C) 20 m/pixel, as identified in Chapter 4. (CTX image mosaic)*

Based on this analysis it can be concluded that lower resolution MOLA and HRSC DEMs produce broadly consistent results to high-resolution DEMs, but do a poorer job of differentiating multiple palaeolake levels in palaeolakes with narrow outlet valleys. In spite of relatively minor differences in palaeolake dimensions, the most important observation here, is that the same major palaeolakes were identified at all resolutions. The use of MOLA topography is the best option for surveys of large areas such as presented in Chapter 6, due to global coverage of the dataset, but with considerations made to identify possible overestimated basins such as in palaeolake L-A4. However, the ability to better define changes in palaeolake levels makes the use of higher resolution topography ideal for the investigation of individual palaeolakes and palaeolake systems, wherever possible.

7.5 FUTURE WORK

7.5.1 PALAEOLAKE DATASETS

The regional catalogue of palaeolakes identified in Chapter 6 presents opportunities for a variety of future research projects, further analysing the data already collected, and as a coverage map, identifying the probable locations and extents of ancient lacustrine environments. Further morphological investigation of the palaeolakes identified in this thesis would help to constrain the nature of palaeolake environments (Kite 2019), and the identification of landforms typical of terrestrial palaeolakes would further test of the veracity of palaeolake identification methods. The identification of lacustrine landforms in the form of palaeoshorelines and palaeolakes deposits represent the greatest potential for future study.

Guiding the identification of palaeoshorelines should be a study of similar palaeolake shorelines on Earth, including: deltas, particularly examples recording changes in base level (Fawdon, Gupta et al. 2018); strandlines (Di Achille, Hynek et al. 2009); wave-cut platforms and terraces (Kraal, Asphaug et al. 2006, Irwin and Zimbelman 2012); and concentric evaporitic mineral deposits (Fernandez-Remolar, Sanchez-Roman et al. 2011). Many sediment fans and deltas were correlated with palaeolake levels in this thesis, and although some candidate strandlines or wave-cut platforms have also been identified

(**Figure 7.5**), a detailed study of high-resolution imagery and topography would be required to test the veracity of these preliminary observations. A regional study focusing on mapped palaeolake boundaries may reveal more such features, but a possible issue in identifying palaeolake shorelines on Mars is the age of these features compared to those on Earth. Well studied examples on Earth are often in the range of hundreds or thousands of years, such as high-stands within Lake Bonneville (13-30 Ka) and Mega-Chad (11 Ka), with reduction in the size of the Aral Sea occurring over the course of decades. Even older examples such as the Paratethys Sea (5-34 Ma) are far younger than the estimated ~3.5-4.0 Ga age of palaeolakes on Mars (Cabrol and Grin 1999, Fassett and Head 2008, Goudge, Fassett et al. 2016, Wilson, Howard et al. 2016). This difficulty has been noted in past studies of possible ocean shorelines on Mars (Malin and Edgett 1999), and a future investigation of martian palaeolake shorelines would benefit from a full review of terrestrial palaeoshoreline evidence as preserved in bedrock.

Palaeolake deposits were considered in the detailed studies of Chapter 4 and 5, and a broader survey across the entire population of palaeolakes presented in Chapter 6 is likely to reveal additional localities (**Figure 7.6**). Deposits have been identified within many open-basin and closed-basin palaeolakes on Mars (Andrews-Hanna, Zuber et al. 2010, Goudge, Head et al. 2012, Grotzinger, Gupta et al. 2015, Fawdon 2018), and the sedimentary structure and mineralogy of palaeolake deposits can reveal the history of lacustrine processes within palaeolake basins, and the climate in general (Grotzinger, Gupta et al. 2015, Goudge, Fassett et al. 2016). Where orbital spectral observations from the CRISM instrument overlap with catalogued palaeolakes, and possible palaeolake deposits in particular, there exists the further opportunity to investigate the mineralogy within ancient palaeolakes on Mars (Goudge, Head et al. 2012, Goudge, Mustard et al. 2015, Tarnas, Mustard et al. 2019). The footprints of 520 CRISM observations overlap the areas of 77 different open-basin palaeolakes identified in this thesis, with an additional coverage of 305 observations overlapping 34 different closed-basin palaeolakes (**Figure 7.7**). This indicates the potential for a new detailed mineralogical investigation of palaeolakes within Arabia Terra, aimed at defining mineralisation and diagenetic

histories within palaeolake basins across the region, and a recent global study has already detected aqueous minerals within some palaeolake deposits in the region (Alemanno, Orofino et al. 2021).

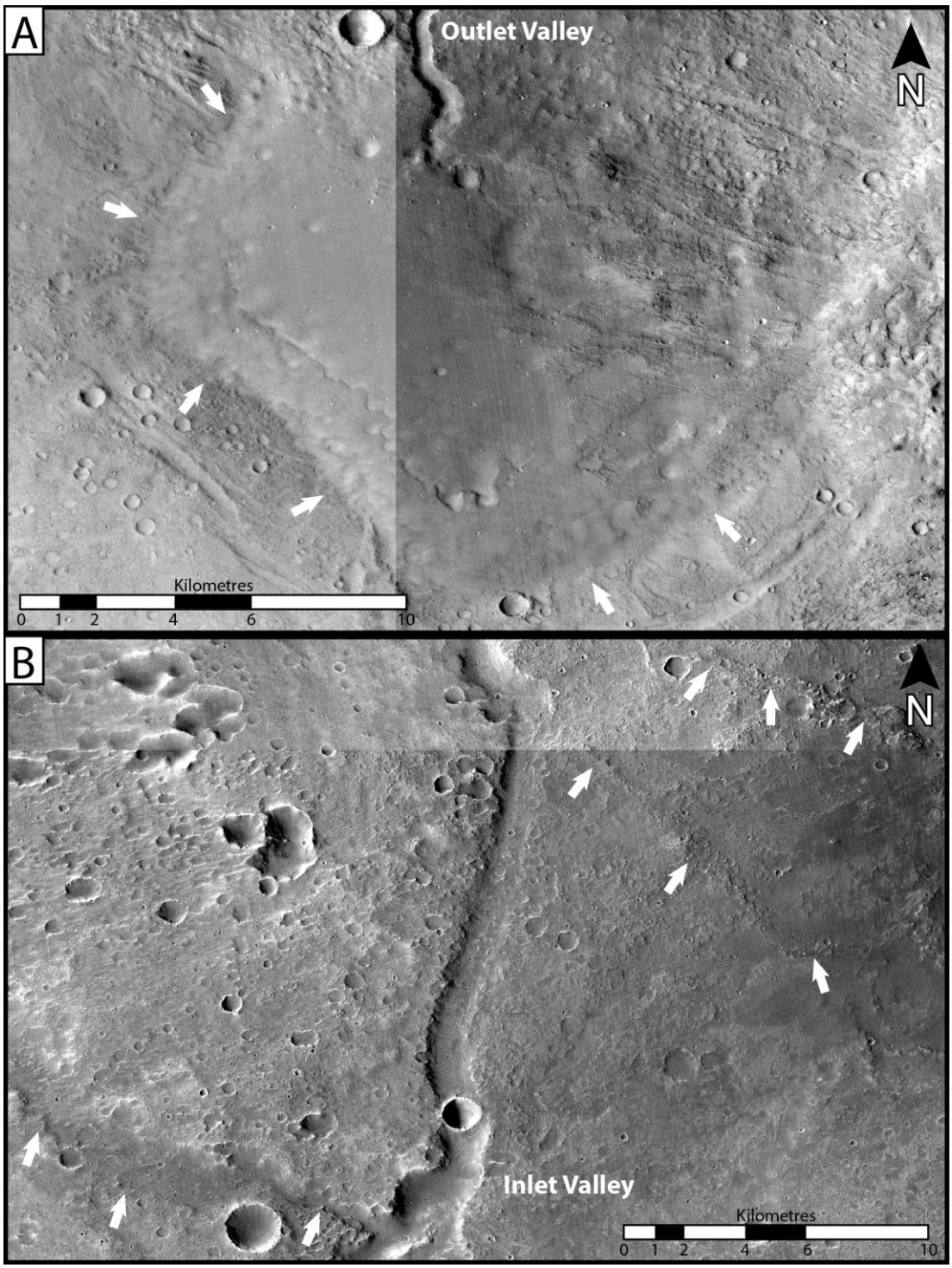

Figure 7.5 *– Examples of possible palaeolake shorelines (white arrows) identified at the margins of palaeolakes identified in Chapter 6. (A) A break in slope apparent near the mapped palaeolake boundary, marks a transition from rugged terrains to the flat floor of the basin. (B) Three possible shorelines at the edge of a palaeolake, roughly parallel to elevation contours, taking the form of linear raised deposits potentially representing strandlines. (CTX image mosaic)*

However, the quality of CRISM observations is patchy (**Section 3.2**), particularly within deep basins which act as sinks for windblown dust and sand, and therefore many spectral observations may not be useful within palaeolake basins (Johnson, Christensen et al. 2002), and the processing and extraction of useful spectra is likely to require a specialist approach. Further study of these deposits could also help determine if they formed contemporaneously with palaeolakes, or if they are the result of later aeolian fill.

Past studies of palaeolakes on Mars have employed numerical models to determine characterised the inundation of past terrains, and constrain values for precipitation, evaporation and infiltration (Andrews-Hanna, Zuber et al. 2010, Wilson, Howard et al. 2016). Given that the majority of the palaeolake chains identified in this thesis terminate within closed-basin palaeolakes, of particular interest is a recent study of the equilibrium reached by coupled open-basin and closed-basin palaeolake systems on Mars, including a comparison to climate models to determine the duration of runoff into these systems (Stucky de Quay, Goudge et al. 2020). The data already collected in this thesis on the volumes, areas, coverage, and connectivity of open-basin and closed-basin palaeolakes is sufficient to begin such analysis for the region of Arabia Terra, and will likely help to place further constraints on the ancient climate.

Due to the uncertainties inherent in delineating the drainage catchments of individual palaeolakes, the relationship between catchment area and palaeolake volume was only quantified for selected large palaeolakes (**Section 6.4.5**). Selection of only the largest palaeolakes naturally excluded many lakes significantly fed by other palaeolakes, and to include smaller palaeolakes in future analysis will require a narrower set of inclusion criteria. A consideration of terrestrial palaeolake studies relating to groundwater influx and surface accumulation will be important to defining the inclusion criteria for palaeolakes within chains (Fassett and Head 2008). Delineating drainage catchments for individual palaeolakes will likely require a combined approach of topographic calculation and assessment of morphological features. Producing catchments on a topography with <100 m sinks filled, such as in Chapter 6, may not be suitable for at this scale, and some development and testing of workable method will likely

be required. Although potentially difficult, defining the relative significance of groundwater or surface accumulation in palaeolake filling would be a great benefit to the further characterisation of ancient hydrology in Arabia Terra.

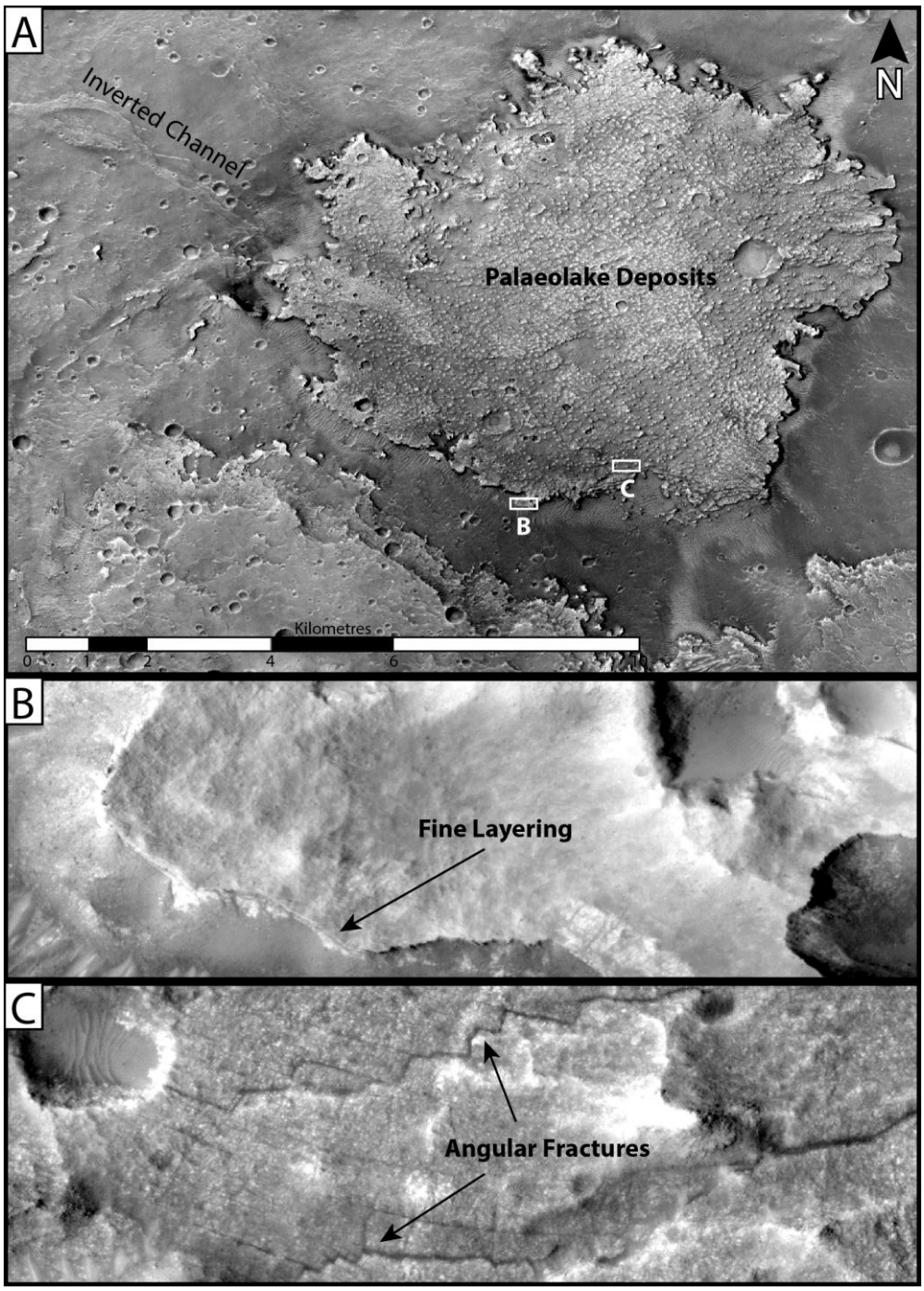

Figure 7.6 *– Example of possible palaeolake deposits within a palaeolake identified in Chapter 6. (A) The deposits are composed of light-toned materials, raised above the surrounding terrains, and apparently the remnants of a wider unit, with a nearby inverted channel which also appears to be preserved in the raised deposits. (B) A high-resolution view of possible fine layering at the edge of the deposits. (C) A high-resolution view of angular fractures in the deposits, similar in morphology to the palaeolake basin deposits identified in Chapter 4. (Top: CTX image mosaic; Bottom: HiRISE images)*

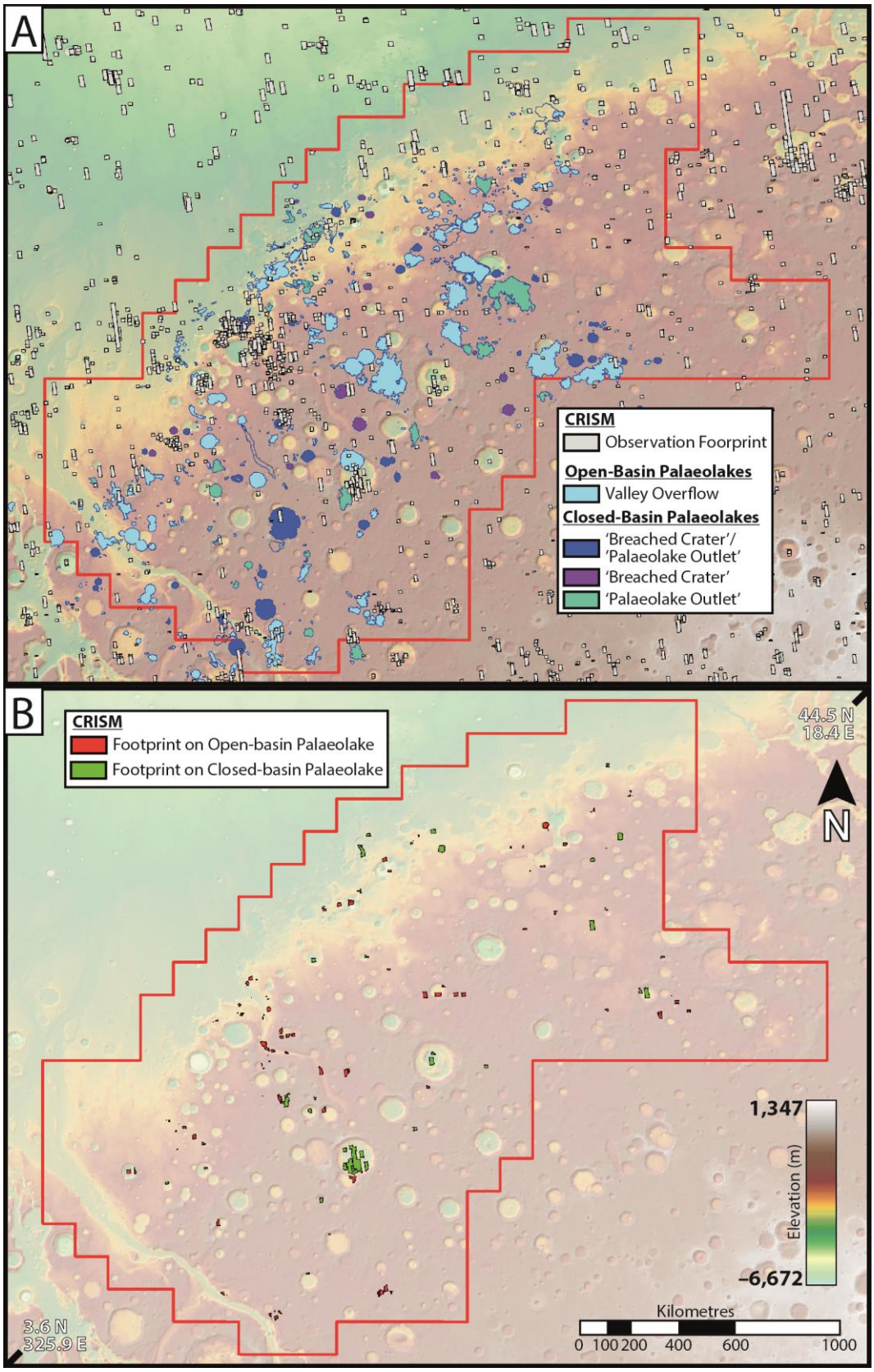

Figure 7.7 – Map of CRISM observations relative to mapped palaeolake boundaries, showing: (A) Complete population of CRISM observations, and open-basin and closed-basin palaeolakes; and (B) Specific localities for future compositional and mineralogical palaeolake studies where CRISM observations overlap open-basin palaeolakes (red areas) and closed-basin palaeolakes (green areas).

7.5.2 FLUVIAL DATASETS

The focus of this thesis was to investigate palaeolakes in Arabia Terra, with the mapping of fluvial features only a preliminary step in the process of identifying palaeolake inlets and outlets. As a result, the >20,000 mapped fluvial features represent an underutilised dataset, and a relatively minor effort to further characterise and attribute additional descriptive data to these features could render the dataset even more useful, and tailor it to a particular set of research aims.

The addition of width and depth values to fluvial features would be useful in further characterising the relative significance of different features in terms of drainage output. More importantly, martian valley depths and volumes have been used to compare the volume of sediment delivered to sediment fans and sinks , and to estimate the longevity of fluvial activity, volume of flow, recycling of water (Luo, Cang et al. 2017). Measurement of valley width is relatively straightforward, but depth is only resolvable for valleys which are ~2 km wide with the use of ~463 m/pixel MOLA DEMs, and similarly, 50-250 m/pixel HRSC DEMs is limited to valleys with widths approximately four times the topographic resolution. Attribution of valley depth and volume will therefore be limited to either: relatively wide valleys across the entire study area; or valleys near to the dichotomy, where HRSC DEM coverage is concentrated. As the coverage of HRSC topography increases, measurement of these attributes may be possible across the entire study region. Additionally, valleys with resolvable depths could be subject to analysis of valley longitudinal profiles, as produced for the study area in Chapter 4 (**Section 4.3.1**), to identify the degree of fluvial maturity, as well as to identify knick points and base level changes.

Investigation of fluvial morphology and distribution also warrants further analysis, such as: the transition to depositional landforms towards the southeast of the study area (Davis, Gupta et al. 2019); and the relatively shallow and braided character of fluvial features in the north east (Wilson, Howard et al. 2016). The fluvial features catalogued in this thesis represent a far more detailed set of data than the study by Wilson et al. (2016), and the area covered between these existing studies presents the opportunity

to better characterise the extents and transitions between these morphologically distinct areas.

7.5.3 EXPANDING REGIONAL PALAEOLAKE CATALOGUES

Central to the research undertaken in this thesis was to not only identify and investigate palaeolakes, but to develop a robust method of palaeolake identification applicable to future research across other Mars regions. Identification and mapping of possible palaeolake basins in future cataloguing efforts could benefit from a degree of automation and standardisation, achieved by developing a GIS toolbox workflow to automatically select only the highest closed contours within each topographic basin across the study area. Displaying only these selected contours would improve the process of identifying valley overflow palaeolake level by showing only those contours relevant to the identification criteria. This processes could be further automated by using an additional GIS toolset to select only the closed basin contours which overlap, or begin within a set distance of a fluvial feature. A manual assessment of identified palaeolakes would still be recommended, but the process described here could significantly reduce the time necessary to identify palaeolakes. Furthermore, this process could even be applied to existing global topography data and valley catalogues, with no additional feature mapping required.

The first choice for a future palaeolake catalogue is an extension to the south-east of the area presented in Chapter 6. The study area would extend south to fully capture the south-eastward transition from depositional landforms at the edge of Arabia Terra, across the valley network terminations concentrated at the steep rise marking the edges of Terra Sabaea and Noachis Terra, and including the full extent of the valley networks and drainage catchments within these regions (**Figure 7.8b**). To the east, the study would be bounded by Ares Vallis and the associated source regions of Iani Chaos and Margaritifer Chaos, and to the west by the edge of the Okavango Valles drainage catchment. However, since the idealised drainage catchments presented in this thesis were revealed to be overestimated, it is likely that the same is true of the Okavango catchment (Mangold and

Howard 2013), and an attempt should be made to extend the palaeolake catalogue across this area.

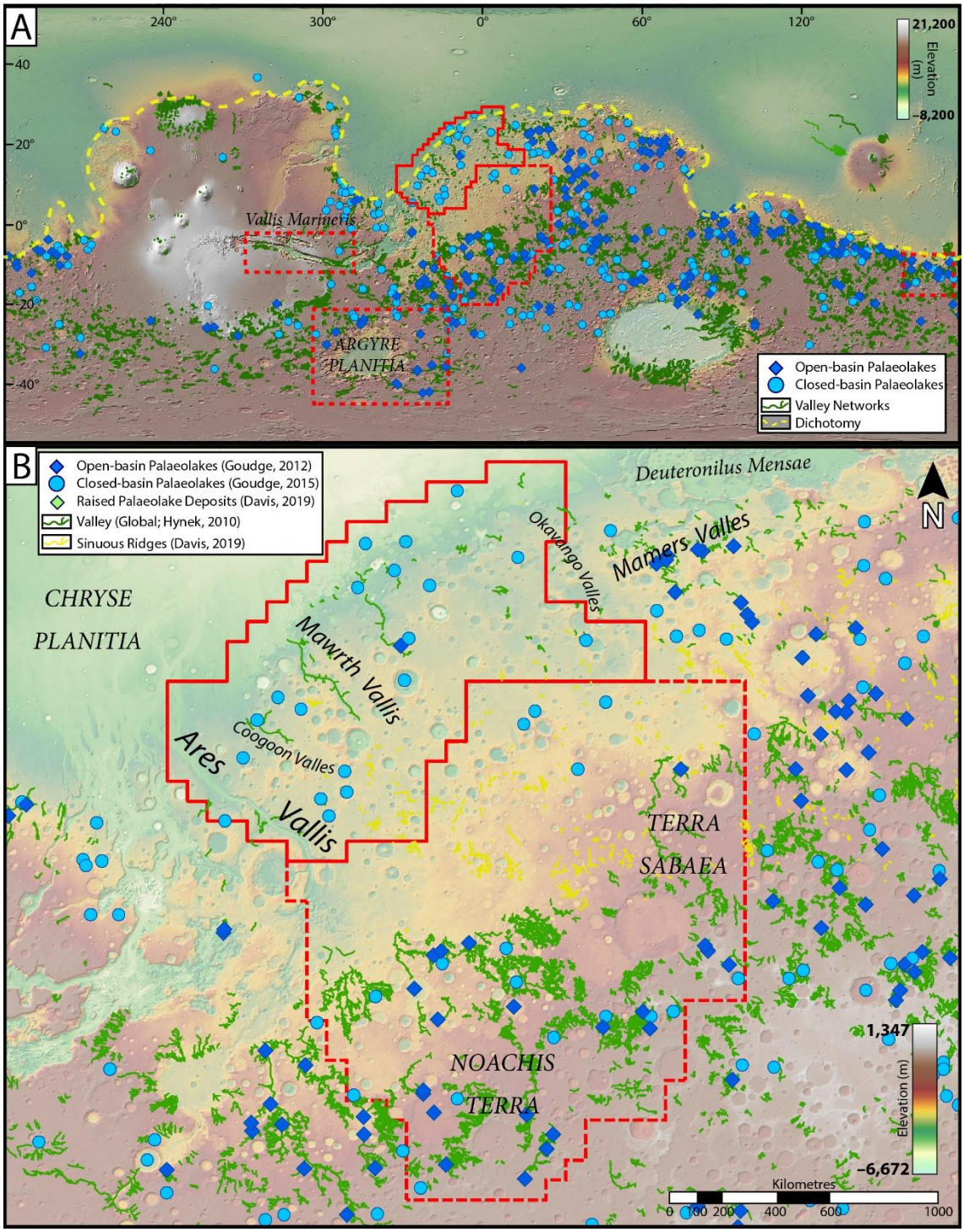

Figure 7.8 – Areas considered for future regional palaeolake catalogues. (A) Global map showing the locations for possible palaeolake catalogues: for the drainage catchment of Argyre Planitia; within Vallis Marineris; and at the dichotomy in Terra Cimmeria. (B) Regional map showing the favoured area for a future palaeolake catalogue, extending southeast from the study area presented in Chapter 6, with the goal of identifying palaeolakes to characterise the transition in hydrological features apparent at the edge of Noachis Terra and Terra Sabaea.

The study area thus defined covers an area of ~6,000,000 km^2, nearly twice as large as the catalogue area of Chapter 6 (3,541,649 km^2). However, with the methods and work flow already well established in this thesis, and with the possible advent of some automation in the palaeolake identification processes, the project scope of the project is manageable. The terminations of valley networks at the south-east edge of Arabia Terra mirrors that observed at the dichotomy, and identifying the fate of water reaching the end of these vast fluvial systems could reveal more about how and why hydrology and fluvial processes appear to change so drastically along this boundary (Davis, Gupta et al. 2019).

The possibilities for additional future palaeolake catalogues are numerous, and other promising areas include (**Figure 7.8a**): (1) the drainage catchment surrounding the basin of Argyre Planitia, which itself shows evidence of being an open-basin palaeolake (Dohm, Ferris et al. 2011), with the aim of defining how one of the largest closed basins on Mars filled to the point of overflow; (2) the floor of Vallis Marineris, in which palaeolakes have been indicated (Lucchitta 2010), and a full catalogue could aid in constraining the timing of tectonic processes in the region; or (3) another study adjacent to the dichotomy in a different region, such as Terra Cimmeria, where numerous palaeolakes have been identified in previous global catalogues, allowing the opportunity to fully contrast the results of a high-resolution regional study. All of these scenarios provide the opportunity to better define regional hydrology, as well as constrain the past climate and availability of water on Mars. Finally, it is hoped that the eventual linking of regional catalogues undertaken with standardised methods will lead to a complete, high-resolution palaeolake catalogue for the whole of Mars.

7.5.4 PROPOSED LANDING SITES IN ARABIA TERRA

The palaeolakes identified in this work also represent areas which may be suitable for future surface exploration on the surface of Mars, based on typical science objectives to explore the sites of ancient aqueous processes and possible habitable environments (Fairén, Davila et al. 2010, Vago, Westall et al. 2017). Landing site selection requires consideration of the relative merits and detractors of candidate sites in relation to the

science objectives and engineering constraints particular to the mission. Science objectives cover a range of mission specific goals, with typical landing site constraints including: (1) morphological and/or mineralogical evidence of past aqueous processes; (2) exposed bedrock surfaces, indicated by thermal inertia units (TIU); (3) ancient aged terrains, typically restricted to Noachian or Hesperian age in the search for life and aqueous environments; and (4) evidence of the exhumation of ancient deposits, important for the potential preservation of biosignatures. Engineering constraints vary significantly for different missions, and are primarily a function of temperature and power considerations, as well as entry, decent, and landing (EDL) technology, often including: (1) latitude, with solar powered missions restricted to equatorial regions; (2) elevation, with low elevation areas favoured to allow aero-braking through a greater depth of atmosphere; and (3) landing ellipse, the size of which varies with the accuracy of EDL technology, and must generally be clear of obstacles, obstructions, and areas of high slope which might endanger landing or rover movement.

The solar-powered ExoMars 'Rosalind Franklin' rover will use a parachute and retrorocket EDL system, with engineering constraints including (Vago, Lorenzoni et al. 2015): (1) latitudes between 5°S and 25°N; (2) elevations <-2000 m; and (3) a landing ellipse with dimensions of ~19 x 120 km, subject to safety constraints such as avoiding slopes >8°. The primary science objective for ExoMars, is to search for preserved biosignatures by drilling into the subsurface, with constraints including (Vago, Westall et al. 2017): (1) morphological and mineralogical evidence of past aqueous processes; (2) terrains of Noachian or Hesperian age; (3) exposed bedrock, identified as <150 TIU; and (3) exhumed ancient deposits, evinced by substantial erosion.

The Mars 2020 'Perseverance' rover, and similarly designed MSL 'Curiosity' rover (Grant, Golombek et al. 2018), are powered by radioisotope thermoelectric generators (RTG), and made use of automated obstacle avoidance software and a 'sky-crane' EDL system, resulting in a less restrictive set of engineering constraints than ExoMars, and including: (1) latitudes between 30°S and 30°N; (2) elevations <0 m; and (3) a landing ellipse with dimensions of 14 x 16 km, subject to fewer safety constraints, but avoiding

slopes >30°. The primary science objective for Mars2020, is to investigate the habitability of an ancient aqueous environment on Mars and collect varied samples for eventual return to Earth, with science constraints similar to ExoMars, excluding those related to drilling for preserved biosignatures.

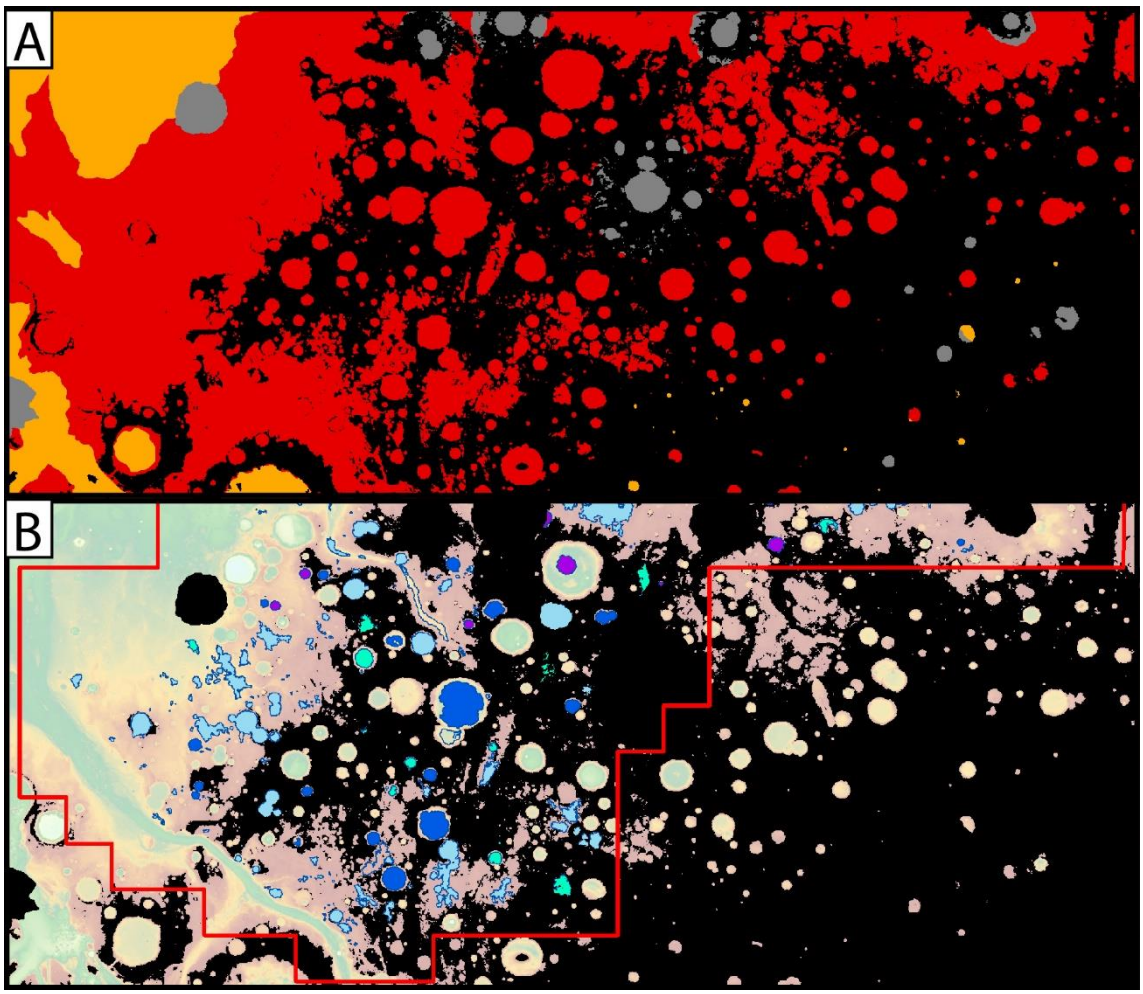

Figure 7.9 *– Illustration of landing site selection using ExoMars type mission criteria, view limited to east, west and south by thesis study area, and to the north at 25°N mission latitude. (A) Blacked out elevations above -2000 m, and greyed out Amazonian aged units, with suitable Noachian (red area) and Hesperian (orange area) terrains distinguished. (B) Unsuitable areas combined and blacked out, showing the locations of possible landing sites within palaeolakes.*

The engineering and science constraints outlined above are not exhaustive, and many of the particular details of site suitability are beyond the scope of this thesis. Identified here are the open-basin and closed-basin palaeolakes which fall within the basic mission criteria, based on: (1) engineering constraints for each mission type individually, only including latitude, and elevation; and (2) the age of terrains as Hesperian or Noachian. The identification of palaeolakes in this thesis constitutes morphological

evidence for aqueous processes, pertinent to the geological and astrobiological investigation of an ancient palaeolake environment. However, a further investigation of these candidate areas will be required to identify suitable landing sites which the full range of engineering constraints, as well as further supporting evidence of lacustrine processes such as observations of palaeolake deposits or mineralogy.

7.6 CONCLUSIONS

The palaeolakes and fluvial features identified and characterised in this thesis represent a significant addition to the understanding of hydrological systems and processes in Arabia Terra, and the ancient climate of Mars. Overall, these results indicate a semi-arid setting, dominated by endorheic drainage systems, and significant coverage and volume of water at the surface of the planet, with lake filling driven by both surface accumulation and groundwater influx.

A key to the approach of this thesis was the use of high-resolution topography to identify detailed attributes within fluvio-lacustrine systems, and build upon those methods and results to develop robust and scalable methods for palaeolake identification and drainage catchment delineation which will be of use to future research in the field.

The low slope of Arabia Terra is broadly southeast to northwest, with the large valleys and drainage catchments indicating a matching trend in flow direction from the highlands, to the dichotomy at the boundary of the lowlands. However, this thesis reveals a far more complex setting, with the local effect of deep local basins, particularly impact craters, having a significant effect on drainage across the region. Through the analysis of these results, a number of possible terrestrial analogue lake regions are identified, which warrant future investigation. By comparison with these analogues, it is hoped that the linking of morphological observations to numerical modelling can be further constrained.

That Arabia Terra was once covered by such extensive areas of water has significant implications for the ancient habitability of the region, with palaeolakes within different settings offering a range of interconnected and varied environments. As

conditions favourable to life gradually declined along with the supply of water, deep crater lakes could have acted as the last refuge for life within the slowly desiccating region. With the exploration of Mars still largely driven by astrobiological objectives, the palaeolakes identified here offer a selection of possible sites which may be suitable for future missions. Not least, the soon to launch, ExoMars 'Rosalind Franklin' rover, which will likely be able to ground truth some of the interpretations made in this thesis.

References

Abe, Y., A. Numaguti, G. Komatsu and Y. Kobayashi (2005). "Four climate regimes on a land planet with wet surface: Effects of obliquity change and implications for ancient Mars." Icarus **178**(1): 27-39.

Abramov, O. and D. A. Kring (2005). "Impact-induced hydrothermal activity on early Mars." Journal of Geophysical Research: Planets **110**(E12).

Acuna, M., J. Connerney, P. a. Wasilewski, R. Lin, K. Anderson, C. Carlson, J. McFadden, D. Curtis, D. Mitchell and H. Reme (1998). "Magnetic field and plasma observations at Mars: Initial results of the Mars Global Surveyor mission." Science **279**(5357): 1676-1680.

Alemanno, G., V. Orofino and F. Mancarella (2018). "Global map of Martian fluvial systems: Age and total eroded volume estimations." Earth and Space Science **5**(10): 560-577.

Alemanno, G., V. Orofino, A. Maturilli, J. Helbert and F. Mancarella (2021). "Detection of aqueous alteration minerals in Martian open and closed paleolake basins." Planetary and Space Science: 105342.

Amante, C. and B. W. Eakins (2009). "ETOPO1 arc-minute global relief model: procedures, data sources and analysis."

Andrews-Hanna, J. C., M. T. Zuber, R. E. Arvidson and S. M. Wiseman (2010). "Early Mars hydrology: Meridiani playa deposits and the sedimentary record of Arabia Terra." Journal of Geophysical Research-Planets **115**.

Andrews-Hanna, J. C., M. T. Zuber and W. B. Banerdt (2008). "The Borealis basin and the origin of the martian crustal dichotomy." Nature **453**(7199): 1212.

Baker, V. (1999). The MEGAOUTFLO hypothesis for long-term environmental change on Mars. Bulletin of the American Astronomical Society.

Baker, V. R. and D. J. Milton (1974). "Erosion by catastrophic floods on Mars and Earth." Icarus **23**(1): 27-41.

Baker, V. R., R. G. Strom, V. C. Gulick, J. S. Kargel, G. Komatsu and V. S. Kale (1991). "ANCIENT OCEANS, ICE SHEETS AND THE HYDROLOGICAL CYCLE ON MARS." Nature **352**(6336): 589-594.

Barabashov, N. P. (1963). Physical conditions on Mars, National Aeronautics and Space Administration.

Barker, D. C. and J. P. Bhattacharya (2018). "Sequence stratigraphy on an early wet Mars." Planetary and Space Science **151**: 97-108.

Barnhart, C., S. Tulaczyk, E. Asphaug, E. Kraal and J. Moore (2005). Ice-Ridge Pile Up and the Genesis of Martian" Shorelines". 36th Annual Lunar and Planetary Science Conference.

Bibring, J.-P., A. Soufflot, M. Berthé, Y. Langevin, B. Gondet, P. Drossart, M. Bouyé, M. Combes, P. Puget and A. Semery (2004). OMEGA: Observatoire pour la Minéralogie, l'Eau, les Glaces et l'Activité. Mars Express: the scientific payload.

Bouley, S., D. Baratoux, I. Matsuyama, F. Forget, A. Séjourné, M. Turbet and F. Costard (2016). "Late Tharsis formation and implications for early Mars." Nature **531**(7594): 344-347.

Bowie, D. (1971). Hunky dory. New York, N.Y., RCA,.

Braun, R. D. and R. M. Manning (2006). Mars exploration entry, descent and landing challenges. 2006 IEEE Aerospace Conference, IEEE.

Brink, U. S. and M. H. Taylor (2002). "Crustal structure of central Lake Baikal: Insights into intracontinental rifting." Journal of Geophysical Research: Solid Earth **107**(B7): ETG 2-1-ETG 2-15.

Cabrol, N. A. and E. A. Grin (1999). "Distribution, classification, and ages of Martian impact crater lakes." Icarus **142**(1): 160-172.

Carr, M. H. (1995). "The Martian drainage system and the origin of valley networks and fretted channels." Journal of Geophysical Research: Planets **100**(E4): 7479-7507.

Carr, M. H. (2000). "Martian oceans, valleys and climate." Astronomy & Geophysics **41**(3): 20-26.

Carr, M. H. (2007). The surface of Mars, Cambridge University Press.

Carr, M. H., W. Baum, G. Briggs, H. Masursky, D. Wise and D. Montgomery (1972). "Imaging experiment: the viking Mars orbiter." Icarus **16**(1): 17-33.

Carr, M. H. and J. W. Head (2003). "Oceans on Mars: An assessment of the observational evidence and possible fate." Journal of Geophysical Research-Planets **108**(E5).

Carr, M. H. and J. W. Head (2010). "Geologic history of Mars." Earth and Planetary Science Letters **294**(3-4): 185-203.

Carr, M. H. and J. W. Head (2015). "Martian surface/near-surface water inventory: Sources, sinks, and changes with time." Geophysical Research Letters **42**(3): 726-732.

Carroll, A. R. and K. M. Bohacs (1999). "Stratigraphic classification of ancient lakes: Balancing tectonic and climatic controls." Geology **27**(2): 99-102.

Carter, J., F. Poulet, J. P. Bibring and S. Murchie (2010). "Detection of Hydrated Silicates in Crustal Outcrops in the Northern Plains of Mars." Science **328**(5986): 1682-1686.

Chamberlain, T., H. Cole, R. Dutton, G. Greene and J. Tillman (1976). "Atmospheric measurements on Mars: The Viking meteorology experiment." Bulletin of the American Meteorological Society **57**(9): 1094-1105.

Chang, C. and L. Liu (2021). "Investigating the formation of the Cretaceous Western Interior Seaway using landscape evolution simulations." Bulletin **133**(1-2): 347-361.

Christensen, P. R., B. Jakosky, H. H. Kieffer, M. C. Malin, H. Y. McSween, K. Nealson, G. L. Mehall, S. H. Silverman, S. Ferry, M. Caplinger and M. Ravine (2004). "The Thermal Emission Imaging System (THEMIS) for the Mars 2001 Odyssey Mission." Space Science Reviews **110**(1-2): 85-130.

Citron, R., M. Manga and D. Hemingway (2018). Evidence of Early Martian Oceans from Shoreline Deformation Due to Tharsis. Lunar and Planetary Science Conference.

Citron, R. I., M. Manga and D. J. Hemingway (2018). "Timing of oceans on Mars from shoreline deformation." Nature **555**(7698): 643-+.

Clifford, S. M. and T. J. Parker (2001). "The evolution of the Martian hydrosphere: Implications for the fate of a primordial ocean and the current state of the northern plains." Icarus **154**(1): 40-79.

Cockell, C. S., T. Bush, C. Bryce, S. Direito, M. Fox-Powell, J. Harrison, H. Lammer, H. Landenmark, J. Martin-Torres and N. Nicholson (2016). "Habitability: a review." Astrobiology **16**(1): 89-117.

Cohen, A. S., M. J. Soreghan and C. A. Scholz (1993). "Estimating the age of formation of lakes: an example from Lake Tanganyika, East African Rift system." Geology **21**(6): 511-514.

Cook, S. J. and D. A. Swift (2012). "Subglacial basins: Their origin and importance in glacial systems and landscapes." Earth-Science Reviews **115**(4): 332-372.

Costard, F., A. Sejourne, K. Kelfoun, S. Clifford, F. Lavigne, I. Di Pietro and S. Bouley (2017). "Modeling tsunami propagation and the emplacement of thumbprint terrain in an early Mars ocean." Journal of Geophysical Research-Planets **122**(3): 633-649.

Davis, J., M. Balme, P. Grindrod, R. Williams and S. Gupta (2016). "Extensive Noachian fluvial systems in Arabia Terra: Implications for early Martian climate." Geology **44**(10): 847-850.

Davis, J. M., S. Gupta, M. Balme, P. M. Grindrod, P. Fawdon, Z. I. Dickeson and R. M. Williams (2019). "A diverse array of fluvial depositional systems in Arabia Terra: Evidence for mid-Noachian to early Hesperian rivers on Mars." Journal of Geophysical Research: Planets **124**(7): 1913-1934.

Di Achille, G. and B. M. Hynek (2010). "Ancient ocean on Mars supported by global distribution of deltas and valleys." Nature Geoscience **3**(7): 459-463.

Di Achille, G., B. M. Hynek and M. L. Searls (2009). "Positive identification of lake strandlines in Shalbatana Vallis, Mars." Geophysical Research Letters **36**(14).

DiBiase, R. A., A. B. Limaye, J. S. Scheingross, W. W. Fischer and M. P. Lamb (2013). "Deltaic deposits at Aeolis Dorsa: Sedimentary evidence for a standing body of water on the northern plains of Mars." Journal of Geophysical Research-Planets **118**(6): 1285-1302.

Dickeson, Z., P. Grindrod, I. Crawford, M. Balme, S. Gupta and J. Davis (2018). Hydrological History of a Complex Lake and Valley System in Western Arabia Terra, Mars. European Planetary Science Congress.

Dickeson, Z. I. and J. M. Davis (2020). "Martian oceans." Astronomy & Geophysics **61**(3): 3.11-13.17.

Dickson, J., L. Kerber, C. Fassett and B. Ehlmann (2018). A Global, Blended CTX Mosaic of Mars with Vectorized Seam Mapping: A New Mosaicking Pipeline Using Principles of Non-Destructive Image Editing. Lunar and Planetary Science Conference.

Dickson, J., M. Lamb, R. Williams, A. Hayden and W. Fischer (2020). "The global distribution of depositional rivers on early Mars." Geology.

Dohm, J., J. Ferris, V. Baker, G. Komatsu, D. Buczkowski, M. El Maarry, T. Hare, W. Mahaney, K. Kim and A. Davila (2011). Did a large Argyre lake source the Uzboi Vallis drainage system?: Post-Viking-era geologic mapping investigation. Lunar and Planetary Science Conference.

Dohm, J. M., J. C. Ferris, V. R. Baker, R. C. Anderson, T. M. Hare, R. G. Strom, N. G. Barlow, K. L. Tanaka, J. E. Klemaszewski and D. H. Scott (2001). "Ancient drainage basin of the Tharsis region, Mars: Potential source for outflow channel systems and putative oceans or paleolakes." Journal of Geophysical Research-Planets **106**(E12): 32943-32958.

Douglas, D. (1964). "Space flight operations plan-Mariner Mars' 64."

Drake, N. and C. Bristow (2006). "Shorelines in the Sahara: geomorphological evidence for an enhanced monsoon from palaeolake Megachad." The Holocene **16**(6): 901-911.

Duran, S., T. J. Coulthard and E. R. Baynes (2019). "Knickpoints in Martian channels indicate past ocean levels." Scientific reports **9**(1): 1-6.

Edgett, K. S. and T. J. Parker (1997). "Water on early Mars: Possible subaqueous sedimentary deposits covering ancient cratered terrain in western Arabia and Sinus Meridiani." Geophysical Research Letters **24**(22): 2897-2900.

Erkaev, N. V., H. Lammer, L. T. Elkins-Tanton, A. Stokl, P. Odert, E. Marcq, E. A. Dorfi, K. G. Kislyakova, Y. N. Kulikov, M. Leitzinger and M. Gudel (2014). "Escape of the martian protoatmosphere and initial water inventory." Planetary and Space Science **98**: 106-119.

Erkeling, G., D. Reiss, H. Hiesinger, F. Poulet, J. Carter, M. A. Ivanov, E. Hauber and R. Jaumann (2012). "Valleys, paleolakes and possible shorelines at the Libya Montes/Isidis boundary: Implications for the hydrologic evolution of Mars." Icarus **219**(1): 393-413.

Fairen, A. G. (2010). "A cold and wet Mars." Icarus **208**(1): 165-175.

Fairen, A. G., A. F. Davila, L. Gago-Duport, J. D. Haqq-Misra, C. Gil, C. P. McKay and J. F. Kasting (2011). "Cold glacial oceans would have inhibited phyllosilicate sedimentation on early Mars." Nature Geoscience **4**(10): 667-670.

Fairen, A. G., J. M. Dohm, V. R. Baker, M. A. de Pablo, J. Ruiz, J. C. Ferris and R. C. Anderson (2003). "Episodic flood inundations of the northern plains of Mars." Icarus **165**(1): 53-67.

Fairén, A., A. Davila, D. Lim and C. McKay (2010). Icebergs on early Mars. Lunar and Planetary Science Conference.

Fairén, A. G., A. F. Davila, D. Lim, N. Bramall, R. Bonaccorsi, J. Zavaleta, E. R. Uceda, C. Stoker, J. Wierzchos and J. M. Dohm (2010). "Astrobiology through the ages of Mars: the study of terrestrial analogues to understand the habitability of Mars." Astrobiology **10**(8): 821-843.

Fassett, C. I. and J. W. Head III (2005). "Fluvial sedimentary deposits on Mars: Ancient deltas in a crater lake in the Nili Fossae region." Geophysical Research Letters **32**(14).

Fassett, C. I. and J. W. Head III (2008). "The timing of Martian valley network activity: Constraints from buffered crater counting." Icarus **195**(1): 61-89.

Fassett, C. I. and J. W. Head (2008). "Valley network-fed, open-basin lakes on Mars: Distribution and implications for Noachian surface and subsurface hydrology." Icarus **198**(1): 37-56.

Fawdon, P. (2018). The Ancient Fluvial Catchment of the Candidate ExoMars 2020 Rover Landing Site in the Oxia Planum Basin. European Planetary Science Congress.

Fawdon, P., M. R. Balme, J. M. Davis, J. C. Bridges, S. Gupta and C. Quantin-Nataf (2021). "Rivers and lakes in Western Arabia Terra: The fluvial catchment of the ExoMars 2022 rover landing site." Journal of Geophysical Research: Planets: e2021JE007045.

Fawdon, P., S. Gupta, J. M. Davis, N. H. Warner, J. B. Adler, M. R. Balme, J. F. Bell III, P. M. Grindrod and E. Sefton-Nash (2018). "The Hypanis Valles delta: The last highstand of a sea on early Mars?" Earth and Planetary Science Letters **500**: 225-241.

Fegley Jr, B. (2003). "Venus." Treatise on geochemistry **1**: 711.

Fernandez-Remolar, D. C., M. Sanchez-Roman, A. C. Hill, D. Gomez-Ortiz, O. Prieto Ballesteros, C. S. Romanek and R. Amils (2011). "The environment of early Mars and the missing carbonates." Meteoritics & Planetary Science **46**(10): 1447-1469.

Forget, F., R. Wordsworth, E. Millour, J.-B. Madeleine, L. Kerber, J. Leconte, E. Marcq and R. M. Haberle (2013). "3D modelling of the early martian climate under a denser CO2 atmosphere: Temperatures and CO2 ice clouds." Icarus **222**(1): 81-99.

Frey, H. (2008). "Ages of very large impact basins on Mars: Implications for the late heavy bombardment in the inner solar system." Geophysical Research Letters **35**(13).

Frey, H. V., J. H. Roark, K. M. Shockey, E. L. Frey and S. E. Sakimoto (2002). "Ancient lowlands on Mars." Geophysical Research Letters **29**(10): 22-21-22-24.

Galofre, A. G., R. S. Bahia, A. M. Jellinek, K. X. Whipple and R. Gallo (2020). "Did Martian valley networks substantially modify the landscape?" Earth and Planetary Science Letters **547**: 116482.

García-Arnay, Á. and F. Gutiérrez (2020). "Reconstructing paleolakes in Nepenthes Mensae, Mars, using the distribution of putative deltas, coastal-like features, and terrestrial analogs." Geomorphology: 107129.

García-Arnay, Á., O. Prieto-Ballesteros, F. Gutiérrez, A. Molina and I. López (2019). "Characterizing the landscape of west Coogoon Valles and southeast Oxia Planum, Mars." Ciencias Planetarias y Exploración del Sistema Solar: 26.

Gautier, F., G. Clauzon, J. Suc, J. Cravatte and D. Violanti (1994). "Age and duration of the Messinian salinity crisis." Comptes Rendus De L Academie Des Sciences Serie Ii **318**(8): 1103-1109.

Ghatan, G. J. and J. R. Zimbelman (2006). "Paucity of candidate coastal constructional landforms along proposed shorelines on Mars: Implications for a northern lowlands-filling ocean." Icarus **185**(1): 171-196.

Golombek, M., F. Anderson and M. Zuber (2001). "Martian wrinkle ridge topography: Evidence for subsurface faults from MOLA." Journal of Geophysical Research: Planets **106**(E10): 23811-23821.

Goudge, T. A., K. L. Aureli, J. W. Head, C. I. Fassett and J. F. Mustard (2015). "Classification and analysis of candidate impact crater-hosted closed-basin lakes on Mars." Icarus **260**: 346-367.

Goudge, T. A. and C. I. Fassett (2018). "Incision of Licus Vallis, Mars, From Multiple Lake Overflow Floods." Journal of Geophysical Research-Planets **123**(2): 405-420.

Goudge, T. A., C. I. Fassett, J. W. Head, J. F. Mustard and K. L. Aureli (2016). "Insights into surface runoff on early Mars from paleolake basin morphology and stratigraphy." Geology **44**(6): 419-422.

Goudge, T. A., J. W. Head, J. F. Mustard and C. I. Fassett (2012). "An analysis of open-basin lake deposits on Mars: Evidence for the nature of associated lacustrine deposits and post-lacustrine modification processes." Icarus **219**(1): 211-229.

Goudge, T. A., A. M. Morgan, G. Stucky de Quay and C. I. Fassett (2021). "The importance of lake breach floods for valley incision on early Mars." Nature **597**(7878): 645-649.

Goudge, T. A., J. F. Mustard, J. W. Head, C. I. Fassett and S. M. Wiseman (2015). "Assessing the mineralogy of the watershed and fan deposits of the Jezero crater paleolake system, Mars." Journal of Geophysical Research: Planets **120**(4): 775-808.

Grant, J. A., M. P. Golombek, S. A. Wilson, K. A. Farley, K. H. Williford and A. Chen (2018). "The science process for selecting the landing site for the 2020 Mars rover." Planetary and Space Science **164**: 106-126.

Grotzinger, J. P., S. Gupta, M. C. Malin, D. M. Rubin, J. Schieber, K. Siebach, D. Y. Sumner, K. M. Stack, A. R. Vasavada and R. E. Arvidson (2015). "Deposition, exhumation, and paleoclimate of an ancient lake deposit, Gale crater, Mars." Science **350**(6257).

Halevy, I. and J. W. Head III (2014). "Episodic warming of early Mars by punctuated volcanism." Nature Geoscience **7**(12): 865.

Hassler, D. M., C. Zeitlin, R. F. Wimmer-Schweingruber, B. Ehresmann, S. Rafkin, J. L. Eigenbrode, D. E. Brinza, G. Weigle, S. Böttcher and E. Böhm (2014). "Mars' surface radiation environment measured with the Mars Science Laboratory's Curiosity rover." science **343**(6169): 1244797.

Hauber, E., S. Acktories, S. Steffens, A. Naß, D. Tirsch, S. Adeli, N. Schmitz, F. Trauthan, K. Stephan and R. Jaumann (2020). "Regional Geologic Mapping of the Oxia Planum Landing Site for ExoMars." Copernicus (GmbH): Göttingen, Germany.

Hauck, S. A. and R. J. Phillips (2002). "Thermal and crustal evolution of Mars." Journal of Geophysical Research: Planets **107**(E7): 6-1-6-19.

Head, J. W., H. Hiesinger, M. A. Ivanov, M. A. Kreslavsky, S. Pratt and B. J. Thomson (1999). "Possible ancient oceans on Mars: Evidence from Mars Orbiter Laser Altimeter data." Science **286**(5447): 2134-2137.

Head, J. W., M. Kreslavsky, H. Hiesinger, M. Ivanov, S. Pratt, N. Seibert, D. E. Smith and M. T. Zuber (1998). "Oceans in the past history of Mars: Tests for their presence using Mars Orbiter Laser Altimeter (MOLA) data." Geophysical Research Letters **25**(24): 4401-4404.

Head, J. W. and D. R. Marchant (2014). "The climate history of early Mars: insights from the Antarctic McMurdo Dry Valleys hydrologic system." Antarctic Science **26**(6): 774-800.

Head, J. W., A. L. Nahm, D. R. Marchant and G. Neukum (2006). "Modification of the dichotomy boundary on Mars by Amazonian mid-latitude regional glaciation." Geophysical Research Letters **33**(8).

Herschel, W. (1784). "XIX. On the remarkable appearances at the polar regions of the planet Mars, and its spheroidical figure; with a few hints relating to its real diameter and atmosphere." Philosophical Transactions of the Royal Society of London **74**: 233-273.

Hess, S. L. (1950). "Some aspects of the meteorology of Mars." Journal of Meteorology **7**(1): 1-13.

Hiesinger, H., J. Head III and S. Pratt (2000). "Deuteronilus Mensae: Testing for a possible shoreline with new MOLA and MOC data." Lunar Planet. Sci.[CD-ROM], XXXI, abstract **1646**.

Hoke, M. R., B. M. Hynek and G. E. Tucker (2011). "Formation timescales of large Martian valley networks." Earth and Planetary Science Letters **312**(1-2): 1-12.

Horton, R. E. (1945). "Erosional development of streams and their drainage basins; hydrophysical approach to quantitative morphology." Geological society of America bulletin **56**(3): 275-370.

Horvath, D. G. and J. C. Andrews-Hanna (2017). "Reconstructing the past climate at Gale crater, Mars, from hydrological modeling of late-stage lakes." Geophysical Research Letters **44**(16): 8196-8204.

Humayun, M., A. Nemchin, B. Zanda, R. Hewins, M. Grange, A. Kennedy, J.-P. Lorand, C. Göpel, C. Fieni and S. Pont (2013). "Origin and age of the earliest Martian crust from meteorite NWA 7533." Nature **503**(7477): 513.

Hutchinson, G. E. (1957). "A Treatise on." limnology **1**: 243.

Hynek, B. M., M. Beach and M. R. T. Hoke (2010). "Updated global map of Martian valley networks and implications for climate and hydrologic processes." Journal of Geophysical Research-Planets **115**.

Iijima, Y., K. Goto, K. Minoura, G. Komatsu and F. Imamura (2014). "Hydrodynamics of impact-induced tsunami over the Martian ocean." Planetary and Space Science **95**: 33-44.

Ireland, R. L., J. F. Poland and F. S. Riley (1984). Land subsidence in the San Joaquin Valley, California, as of 1980, US Government Printing Office.

Irwin, R. P. and J. R. Zimbelman (2012). "Morphometry of Great Basin pluvial shore landforms: Implications for paleolake basins on Mars." Journal of Geophysical Research-Planets **117**.

Ivanov, M., E. Slyuta, E. Grishakina and A. Dmitrovskii (2020). "Geomorphological analysis of ExoMars candidate landing site Oxia Planum." Solar System Research **54**(1): 1-14.

Ivanov, M. A., G. Erkeling, H. Hiesinger, H. Bernhardt and D. Reiss (2017). "Topography of the Deuteronilus contact on Mars: Evidence for an ancient water/mud ocean and long-wavelength topographic readjustments." Planetary and Space Science **144**: 49-70.

Ivanov, M. A. and J. W. Head (2001). "Chryse Planitia, Mars: Topographic configuration, outflow channel continuity and sequence, and tests for hypothesized ancient bodies of water using Mars Orbiter Laser Altimeter (MOLA) data." Journal of Geophysical Research-Planets **106**(E2): 3275-3295.

Ivanov, M. A., H. Hiesinger, G. Erkeling and D. Reiss (2014). "Mud volcanism and morphology of impact craters in Utopia Planitia on Mars: Evidence for the ancient ocean." Icarus **228**: 121-140.

Jakosky, B. M., M. Slipski, M. Benna, P. Mahaffy, M. Elrod, R. Yelle, S. Stone and N. Alsaeed (2017). "Mars' atmospheric history derived from upper-atmosphere measurements of 38Ar/36Ar." Science **355**(6332): 1408-1410.

Janhunen, P. (2002). "Are the northern plains of Mars a frozen ocean?" Journal of Geophysical Research-Planets **107**(E11).

Jaumann, R., G. Neukum, T. Behnke, T. C. Duxbury, K. Eichentopf, J. Flohrer, S. Gasselt, B. Giese, K. Gwinner and E. Hauber (2007). "The high-resolution stereo camera (HRSC) experiment on Mars Express: Instrument aspects and experiment conduct from interplanetary cruise through the nominal mission." Planetary and Space Science **55**(7-8): 928-952.

Johnson, J. R., P. R. Christensen and P. G. J. J. o. G. R. P. Lucey (2002). "Dust coatings on basaltic rocks and implications for thermal infrared spectroscopy of Mars." **107**(E6).

Jones, K. L., R. E. Arvidson, E. A. Guinness, S. L. Bragg, S. D. Wall, C. E. Carlston and D. G. Pidek (1979). "One Mars year: Viking lander imaging observations." Science **204**(4395): 799-806.

Kauffman, E. G. (1985). "Cretaceous evolution of the Western Interior basin of the United States."

Kereszturi, A. (2012). "Review of Wet Environment Types on Mars with Focus on Duration and Volumetric Issues." Astrobiology **12**(6): 586-600.

Kirk, R. L., R. L. Fergason, B. Redding, D. Galuszka, E. Smith, D. Mayer, T. M. Hare and K. Gwinner (2020). "Evaluating stereo DTM quality at Jezero Crater, Mars with HRSC, CTX, and HiRISE images." The International Archives of Photogrammetry, Remote Sensing and Spatial Information Sciences **43**: 1129-1136.

Kirk, R. L., E. Howington-Kraus, M. R. Rosiek, J. A. Anderson, B. A. Archinal, K. J. Becker, D. Cook, D. M. Galuszka, P. E. Geissler and T. M. Hare (2008). "Ultrahigh resolution topographic mapping of Mars with MRO HiRISE stereo images: Meter-scale slopes of candidate Phoenix landing sites." Journal of Geophysical Research: Planets **113**(E3).

Kite, E. S. (2019). "Geologic Constraints on Early Mars Climate." Space Science Reviews **215**(1): 10.

Klein, H. P. (1979). "The Viking mission and the search for life on Mars." Reviews of Geophysics **17**(7): 1655-1662.

Kraal, E. R., E. Asphaug, J. M. Moore and R. D. Lorenz (2006). "Quantitative geomorphic modeling of Martian bedrock shorelines." Journal of Geophysical Research-Planets **111**(E3).

Kreslavsky, M. A. and J. W. Head (2002). "Fate of outflow channel effluents in the northern lowlands of Mars: The Vastitas Borealis Formation as a sublimation residue from frozen ponded bodies of water." Journal of Geophysical Research-Planets **107**(E12).

Kreslavsky, M. A. and J. W. Head (2002). "Mars: Nature and evolution of young latitude-dependent water-ice-rich mantle." Geophysical Research Letters **29**(15).

Kreslavsky, M. A., J. W. Head and D. R. Marchant (2008). "Periods of active permafrost layer formation during the geological history of Mars: Implications for circum-polar and mid-latitude surface processes." Planetary and Space Science **56**(2): 289-302.

Krijgsman, W., M. Garcés, C. Langereis, R. Daams, J. Van Dam, A. Van der Meulen, J. Agustí and L. Cabrera (1996). "A new chronology for the middle to late Miocene continental record in Spain." Earth and Planetary Science Letters **142**(3-4): 367-380.

Kummu, M., S. Tes, S. Yin, P. Adamson, J. Józsa, J. Koponen, J. Richey and J. Sarkkula (2014). "Water balance analysis for the Tonle Sap Lake–floodplain system." Hydrological Processes **28**(4): 1722-1733.

Lamb, M. P., W. E. Dietrich, S. M. Aciego, D. J. DePaolo and M. Manga (2008). "Formation of Box Canyon, Idaho, by megaflood: Implications for seepage erosion on Earth and Mars." science **320**(5879): 1067-1070.

Lammer, H., H. I. M. Lichtenegger, C. Kolb, I. Ribas, E. F. Guinan, R. Abart and S. J. Bauer (2003). "Loss of water from Mars: Implications for the oxidation of the soil." Icarus **165**(1): 9-25.

Lederberg, J. and C. Sagan (1962). "Microenvironments for life on Mars." Proceedings of the National Academy of Sciences of the United States of America **48**(9): 1473.

Lehner, B. and P. Döll (2004). "Development and validation of a global database of lakes, reservoirs and wetlands." Journal of hydrology **296**(1-4): 1-22.

Leighton, R. B., B. C. Murray, R. P. Sharp, J. D. Allen and R. K. Sloan (1965). "Mariner IV photography of Mars: Initial results." Science **149**(3684): 627-630.

Lenardic, A., F. Nimmo and L. Moresi (2004). "Growth of the hemispheric dichotomy and the cessation of plate tectonics on Mars." Journal of Geophysical Research: Planets **109**(E2).

Leverington, D. W. (2004). "Volcanic rilles, streamlined islands, and the origin of outflow channels on Mars." Journal of Geophysical Research: Planets **109**(E10).

Lowell, P. (1895). Mars. Boston and New York, Houghton, Mifflin and Company.

Lowell, P. (1908). Mars as the Abode of Life, The Macmillan Company.

Lucchitta, B. K. (2010). "Lakes in Valles Marineris." Lakes on Mars: 111-161.

Luo, W., X. Z. Cang and A. D. Howard (2017). "New Martian valley network volume estimate consistent with ancient ocean and warm and wet climate." Nature Communications **8**.

Mahaney, W. C., J. M. Dohm, P. Costa and D. H. Krinsley (2010). "Tsunamis on Mars: Earth analogues of projected Martian sediment." Planetary and Space Science **58**(14-15): 1823-1831.

Malin, M. C., J. F. Bell, B. A. Cantor, M. A. Caplinger, W. M. Calvin, R. T. Clancy, K. S. Edgett, L. Edwards, R. M. Haberle, P. B. James, S. W. Lee, M. A. Ravine, P. C. Thomas and M. J. Wolff (2007). "Context Camera Investigation on board the Mars Reconnaissance Orbiter." Journal of Geophysical Research-Planets **112**(E5).

Malin, M. C. and K. S. Edgett (1999). "Oceans or seas in the Martian northern lowlands: High resolution imaging tests of proposed coastlines." Geophysical Research Letters **26**(19): 3049-3052.

Mangold, N. and V. Ansan (2006). "Detailed study of an hydrological system of valleys, a delta and lakes in the Southwest Thaumasia region, Mars." Icarus **180**(1): 75-87.

Mangold, N. and A. D. Howard (2013). "Outflow channels with deltaic deposits in Ismenius Lacus, Mars." Icarus **226**(1): 385-401.

Marinova, M. M., O. Aharonson and E. Asphaug (2008). "Mega-impact formation of the Mars hemispheric dichotomy." Nature **453**(7199): 1216.

Mark, D. M. (1988). "Network models in geomorphology." Modelling Geomorphological Systems. John Wiley and Sons New York. 1988. p 73-97, 11 fig, 3 tab, 60 ref. NSF Grant SES-8420789.

Masursky, H. (1973). "An overview of geological results from Mariner 9." Journal of Geophysical Research **78**(20): 4009-4030.

Matsui, T., I. Takamiya, F. Imamura and E. Tajika (2001). Tsunami generation and propagation in possible ancient ocean on Mars. Lunar and Planetary Science Conference.

McEwen, A. S., E. M. Eliason, J. W. Bergstrom, N. T. Bridges, C. J. Hansen, W. A. Delamere, J. A. Grant, V. C. Gulick, K. E. Herkenhoff, L. Keszthelyi, R. L. Kirk, M. T. Mellon, S. W. Squyres, N. Thomas and C. M. Weitz (2007). "Mars Reconnaissance Orbiter's High Resolution Imaging Science Experiment (HiRISE)." Journal of Geophysical Research-Planets **112**(E5).

McNeil, J. D., P. Fawdon, M. R. Balme and A. L. Coe (2021). "Morphology, Morphometry and Distribution of Isolated Landforms in Southern Chryse Planitia, Mars." Journal of Geophysical Research: Planets **126**(5): e2020JE006775.

Menzel, D. H. (1926). "The atmosphere of Mars." The Astrophysical Journal **63**: 48.

Mest, S. C., D. A. Crown and W. Harbert (2010). "Watershed modeling in the Tyrrhena Terra region of Mars." Journal of Geophysical Research: Planets **115**(E9).

Michalski, J. R., J. Cuadros, P. B. Niles, J. Parnell, A. D. Rogers and S. P. Wright (2013). "Groundwater activity on Mars and implications for a deep biosphere." Nature Geoscience **6**(2): 133.

Milliken, R., R. C. Ewing, W. Fischer and J. Hurowitz (2014). "Wind-blown sandstones cemented by sulfate and clay minerals in Gale Crater, Mars." Geophysical Research Letters **41**(4): 1149-1154.

Milliken, R., J. Grotzinger and B. Thomson (2010). "Paleoclimate of Mars as captured by the stratigraphic record in Gale Crater." Geophysical Research Letters **37**(4).

Molina, A., I. Lopez, O. Prieto-Ballesteros, D. Fernandez-Remolar, M. A. de Pablo and F. Gomez (2017). "Coogoon Valles, western Arabia Terra: Hydrological evolution of a complex Martian channel system." Icarus **293**: 27-44.

Mouginot, J., A. Pommerol, P. Beck, W. Kofman and S. M. Clifford (2012). "Dielectric map of the Martian northern hemisphere and the nature of plain filling materials." Geophysical Research Letters **39**.

Murchie, S., R. Arvidson, P. Bedini, K. Beisser, J. P. Bibring, J. Bishop, J. Boldt, P. Cavender, T. Choo, R. T. Clancy, E. H. Darlington, D. D. Marais, R. Espiritu, D. Fort, R. Green, E. Guinness, J. Hayes, C. Hash, K. Heffernan, J. Hemmler, G. Heyler, D. Humm, J. Hutcheson, N. Izenberg, R. Lee, J. Lees, D. Lohr, E. Malaret, T. Martin, J. A. McGovern, P. McGuire, R. Morris, J. Mustard, S. Pelkey, E. Rhodes, M. Robinson, T. Roush, E. Schaefer, G. Seagrave, F. Seelos, P. Silverglate, S. Slavney, M. Smith, W. J. Shyong, K. Strohbehn, H. Taylor, P. Thompson, B. Tossman, M. Wirzburger and M. Wolff (2007). "Compact reconnaissance Imaging Spectrometer for Mars (CRISM) on Mars Reconnaissance Orbiter (MRO)." Journal of Geophysical Research-Planets **112**(E5).

Neukum, G. and R. Jaumann (2004). HRSC: The high resolution stereo camera of Mars Express. Mars Express: The Scientific Payload.

Oberbeck, V. R. (2009). "Layered ejecta craters and the early water/ice aquifer on Mars." Meteoritics & Planetary Science **44**(1): 43-54.

Ormo, J., J. M. Dohm, J. C. Ferris, A. Lepinette and A. G. Fairen (2004). "Marine-target craters on Mars? An assessment study." Meteoritics & Planetary Science **39**(2): 333-346.

Orosei, R., S. E. Lauro, E. Pettinelli, A. Cicchetti, M. Coradini, B. Cosciotti, F. Di Paolo, E. Flamini, E. Mattei and M. Pajola (2018). "Radar evidence of subglacial liquid water on Mars." Science **361**(6401): 490-493.

Osinski, G. R., L. L. Tornabene, N. R. Banerjee, C. S. Cockell, R. Flemming, M. R. Izawa, J. McCutcheon, J. Parnell, L. J. Preston and A. E. Pickersgill (2013). "Impact-generated hydrothermal systems on Earth and Mars." Icarus **224**(2): 347-363.

Oviatt, C. G. (1997). "Lake Bonneville fluctuations and global climate change." Geology **25**(2): 155-158.

Pacifici, A., G. Komatsu and M. Pondrelli (2009). "Geological evolution of Ares Vallis on Mars: Formation by multiple events of catastrophic flooding, glacial and periglacial processes." Icarus **202**(1): 60-77.

Palucis, M. C., W. E. Dietrich, R. M. Williams, A. G. Hayes, T. Parker, D. Y. Sumner, N. Mangold, K. Lewis and H. Newsom (2016). "Sequence and relative timing of large lakes in Gale crater (Mars) after the formation of Mount Sharp." Journal of Geophysical Research: Planets **121**(3): 472-496.

Palumbo, A. M., J. W. Head and R. D. Wordsworth (2018). "Late Noachian Icy Highlands climate model: Exploring the possibility of transient melting and fluvial/lacustrine activity through peak annual and seasonal temperatures." Icarus **300**: 261-286.

Parker, T. (1998). Mapping of Possible" Oceanus Borealis" Shorelines on Mars: A Status Report. Lunar and Planetary Science Conference.

Parker, T., S. Clifford and W. Banerdt (2000). "Argyre Planitia and the Mars global hydrologic cycle."

Parker, T. J., D. S. Gorsline, R. S. Saunders, D. C. Pieri and D. M. Schneeberger (1993). "Coastal geomorphology of the Martian northern plains." Journal of Geophysical Research: Planets **98**(E6): 11061-11078.

Parker, T. J., R. S. Saunders and D. M. Schneeberger (1989). "TRANSITIONAL MORPHOLOGY IN WEST DEUTERONILUS MENSAE, MARS - IMPLICATIONS FOR MODIFICATION OF THE LOWLAND UPLAND BOUNDARY." Icarus **82**(1): 111-145.

Parker, T. J., D. M. Schneeberger, D. C. Pieri and R. S. Saunders (1986). Geomorphic evidence for ancient seas on Mars. Mars: Evolution of its Climate and Atmosphere.

Pearce, J. (1924). "Oppositions of the Planet Mars." Publications of the Astronomical Society of the Pacific **36**: 276-281.

Perron, J. T., J. X. Mitrovica, M. Manga, I. Matsuyama and M. A. Richards (2007). "Evidence for an ancient martian ocean in the topography of deformed shorelines." Nature **447**(7146): 840-843.

Pieri, D. C. (1980). "Martian valleys: Morphology, distribution, age, and origin." Science **210**(4472): 895-897.

Pollack, J. B. (1991). "Kuiper Prize Lecture: Present and past climates of the terrestrial planets." Icarus **91**(2): 173-198.

Pondrelli, M., A. P. Rossi, L. Marinangeli, E. Hauber, K. Gwinner, A. Baliva and S. Di Lorenzo (2008). "Evolution and depositional environments of the Eberswalde fan delta, Mars." Icarus **197**(2): 429-451.

Popov, S. V., I. G. Shcherba, L. B. Ilyina, L. A. Nevesskaya, N. P. Paramonova, S. O. Khondkarian and I. Magyar (2006). "Late Miocene to Pliocene palaeogeography of the Paratethys and its relation to the Mediterranean." Palaeogeography, Palaeoclimatology, Palaeoecology **238**(1-4): 91-106.

Poulet, F., C. Gross, B. Horgan, D. Loizeau, J. L. Bishop, J. Carter and C. Orgel (2020). "Mawrth Vallis, Mars: a fascinating place for future in situ exploration." Astrobiology **20**(2): 199-234.

Quantin, C., J. Carter, P. Thollot, J. Broyer, L. Lozach, J. Davis, P. Grindrod, M. Pajola, E. Baratti and S. Rossato (2016). Oxia Planum, the landing site for ExoMars 2018. 47th Lunar and Planetary Science Conference Abstracts, Abstract.

Quantin-Nataf, C., J. Carter, L. Mandon, P. Thollot, M. Balme, M. Volat, L. Pan, D. Loizeau, C. Millot and S. Breton (2021). "Oxia Planum: The Landing Site for the ExoMars "Rosalind Franklin" Rover Mission: Geological Context and Prelanding Interpretation." Astrobiology **21**(3): 345-366.

Ramirez, R. M. and R. A. Craddock (2018). "The geological and climatological case for a warmer and wetter early Mars." Nature Geoscience **11**(4): 230.

Ramsdale, J. (2017). Studies of Glacial and Periglacial Environments on Mars, The Open University.

Rapin, W., B. Chauviré, T. Gabriel, A. McAdam, B. L. Ehlmann, C. Hardgrove, P. Y. Meslin, B. Rondeau, E. Dehouck and H. Franz (2018). "In situ analysis of opal in Gale Crater, Mars." Journal of Geophysical Research: Planets **123**(8): 1955-1972.

Rivera-Hernández, F. and M. C. Palucis (2019). "Do deltas along the crustal dichotomy boundary of Mars in the Gale crater region record a northern ocean?" Geophysical Research Letters **46**(15): 8689-8699.

Robbins, S. J., B. M. Hynek, R. J. Lillis and W. F. Bottke (2013). "Large impact crater histories of Mars: The effect of different model crater age techniques." Icarus **225**(1): 173-184.

Rodriguez, J. A. P., A. G. Fairen, K. L. Tanaka, M. Zarroca, R. Linares, T. Platz, G. Komatsu, H. Miyamoto, J. S. Kargel, J. G. Yan, V. Gulick, K. Higuchi, V. R. Baker and N. Glines (2016). "Tsunami waves extensively resurfaced the shorelines of an early Martian ocean." Scientific Reports **6**.

Rosenberg, E. N. and J. W. Head III (2015). "Late Noachian fluvial erosion on Mars: cumulative water volumes required to carve the valley networks and grain size of bed-sediment." Planetary and Space Science **117**: 429-435.

Rosenberg, E. N. and J. W. Head (2015). "Late Noachian fluvial erosion on Mars: cumulative water volumes required to carve the valley networks and grain size of bed-sediment." Planetary and Space Science **117**: 429-435.

Ruiz, J., R. Tejero, D. Gomez-Ortiz and V. López (2006). Paleoshorelines and the evolution of the lithosphere of Mars. Space Science: New Research, Nova Science Publishers Hauppauge, New York**:** 71-96.

Rögl, F. (1999). "Mediterranean and Paratethys. Facts and hypotheses of an Oligocene to Miocene paleogeography (short overview)." Geologica carpathica **50**(4): 339-349.

Salese, F., G. Di Achille, A. Neesemann, G. G. Ori and E. Hauber (2016). "Hydrological and sedimentary analyses of well-preserved paleofluvial-paleolacustrine systems at Moa Valles, Mars." Journal of Geophysical Research: Planets **121**(2): 194-232.

Salese, F., M. G. Kleinhans, N. Mangold, V. Ansan, W. McMahon, T. de Haas and G. Dromart (2020). "Estimated Minimum Life Span of the Jezero Fluvial Delta (Mars)." Astrobiology **20**(8): 977-993.

Salese, F., M. Pondrelli, A. Neeseman, G. Schmidt and G. G. Ori (2019). "Geological Evidence of Planet-Wide Groundwater System on Mars." Journal of Geophysical Research: Planets **124**(2): 374-395.

Sato, H., K. Kurita and D. Baratoux (2010). "The formation of floor-fractured craters in Xanthe Terra." Icarus **207**(1): 248-264.

Schiaparelli, G. V. (1882). "On some observations of Saturn and Mars." The Observatory **5**: 221-224.

Sholes, S., D. Catling and D. Montgomery (2017). Quantified Identification of Paleo-Terraces Along a Proposed Martian Ocean Contact. Lunar and Planetary Science Conference.

Sholes, S. F., Z. I. Dickeson, D. R. Montgomery and D. C. Catling (2021). "Where are Mars' Hypothesized Ocean Shorelines? Large Lateral and Topographic Offsets Between Different Versions of Paleoshoreline Maps." Journal of Geophysical Research: Planets **126**(5): e2020JE006486.

Shreve, R. L. (1966). "Statistical law of stream numbers." The Journal of Geology **74**(1): 17-37.

Smith, D. E., M. T. Zuber, H. V. Frey, J. B. Garvin, J. W. Head, D. O. Muhleman, G. H. Pettengill, R. J. Phillips, S. C. Solomon, H. J. Zwally, W. B. Banerdt, T. C. Duxbury, M. P. Golombek, F. G. Lemoine, G. A. Neumann, D. D. Rowlands, O. Aharonson, P. G. Ford, A. B. Ivanov, C. L. Johnson, P. J. McGovern, J. B. Abshire, R. S. Afzal and X. L. Sun (2001). "Mars Orbiter Laser Altimeter: Experiment summary after the first year of global mapping of Mars." Journal of Geophysical Research-Planets **106**(E10): 23689-23722.

Smith, D. E., M. T. Zuber, S. C. Solomon, R. J. Phillips, J. W. Head, J. B. Garvin, W. B. Banerdt, D. O. Muhleman, G. H. Pettengill and G. A. Neumann (1999). "The global topography of Mars and implications for surface evolution." Science **284**(5419): 1495-1503.

Stepinski, T. and A. Stepinski (2005). "Morphology of drainage basins as an indicator of climate on early Mars." Journal of Geophysical Research: Planets **110**(E12).

Strahler, A. N. (1957). "Quantitative analysis of watershed geomorphology." Eos, Transactions American Geophysical Union **38**(6): 913-920.

Strahler, A. N. (1964). "Part II. Quantitative geomorphology of drainage basins and channel networks." Handbook of Applied Hydrology: McGraw-Hill, New York: 4-39.

Stucky de Quay, G., T. A. Goudge and C. I. Fassett (2020). "Precipitation and aridity constraints from paleolakes on early Mars." Geology **48**(12): 1189-1193.

Summons, R. E., J. P. Amend, D. Bish, R. Buick, G. D. Cody, D. J. Des Marais, G. Dromart, J. L. Eigenbrode, A. H. Knoll and D. Y. Sumner (2011). "Preservation of martian organic and environmental records: final report of the Mars Biosignature Working Group." Astrobiology **11**(2): 157-181.

Tanaka, K., J. Skinner, J. Dohm, R. Irwin, E. Kolb, C. Fortezzo, T. Platz, G. Michael and T. Hare (2014). "Geologic map of Mars, Scientific Investigations Map 3292." US Geol. Sur., do i **10**.

Tanaka, K. L., J. A. Skinner, T. M. Hare, T. Joyal and A. Wenker (2003). "Resurfacing history of the northern plains of Mars based on geologic mapping of Mars Global Surveyor data." Journal of Geophysical Research-Planets **108**(E4).

Tarboton, D., R. Bras and I. Rodriguez-Iturbe (1991). "On the extraction of channel networks from digital elevation data." Hydrological Processes **5**: 81-100.

Tarnas, J., J. Mustard, H. Lin, T. Goudge, E. Amador, M. Bramble, C. Kremer, X. Zhang, Y. Itoh and M. Parente (2019). "Orbital identification of hydrated silica in Jezero crater, Mars." Geophysical Research Letters **46**(22): 12771-12782.

Thomas, N., G. Cremonese, R. Ziethe, M. Gerber, M. Brändli, G. Bruno, M. Erismann, L. Gambicorti, T. Gerber and K. Ghose (2017). "The colour and stereo surface imaging system (CaSSIS) for the ExoMars trace gas orbiter." Space science reviews **212**(3-4): 1897-1944.

Turner, S., P. Fawdon and J. Davis (2021). Mineralogy of the Oxia Planum Catchment Area on Mars and Its Relevance to the ExoMars Rosalind Franklin Rover Mission. Lunar and Planetary Science Conference.

Vago, J., L. Lorenzoni, F. Calantropio and A. Zashchirinskiy (2015). "Selecting a landing site for the ExoMars 2018 mission." Solar System Research **49**(7): 538-542.

Vago, J. L., F. Westall, A. J. Coates, R. Jaumann, O. Korablev, V. Ciarletti, I. Mitrofanov, J. L. Josset, M. C. De Sanctis, J. P. Bibring, F. Rull, F. Goesmann, H. Steininger, W. Goetz, W. Brinckerhoff, C. Szopa, F. Raulin, H. G. M. Edwards, L. G. Whyte, A. G. Fairen, J. Bridges, E. Hauber, G. G. Ori, S. Werner, D. Loizeau, R. O. Kuzmin, R. M. E. Williams, J. Flahaut, F. O. Forget, D. Rodionov, H. Svedhem, E. Sefton-Nash, G. Kminek, L. Lorenzoni, L. Joudrier, V. Mikhailov, A. Zashchirinskiy, S. Alexashkin, F. Calantropio, A. Merlo, P. Poulakis, O. Witasse, O. Bayle, S. Bayon, U. Meierhenrich, J. Carter, J. M. Garcia-Ruiz, P. Baglioni, A. Haldemann, A. J. Ball, A. Debus, R. Lindner, F. Haessig, D. Monteiro, R. Trautner, C. Voland, P. Rebeyre, D. Goulty, F. Didot, S. Durrant, E. Zekri, D. Koschny, A. Toni, G. Visentin, M. Zwick, M. van Winnendael, M. Azkarate, C. Carreau, T. Pasteur Instrument, W. Landing Site Selection and T. ExoMars Project (2017). "Habitability on Early Mars and the Search for Biosignatures with the ExoMars Rover." Astrobiology **17**(6-7): 471-510.

Verdin, K. L. and J. P. Verdin (1999). "A topological system for delineation and codification of the Earth's river basins." Journal of Hydrology **218**(1-2): 1-12.

Villanueva, G. L., M. J. Mumma, R. E. Novak, H. U. Kaufl, P. Hartogh, T. Encrenaz, A. Tokunaga, A. Khayat and M. D. Smith (2015). "Strong water isotopic anomalies in the martian atmosphere: Probing current and ancient reservoirs." Science **348**(6231): 218-221.

Von Paris, P., A. Petau, J. Grenfell, E. Hauber, D. Breuer, R. Jaumann, H. Rauer and D. Tirsch (2015). "Estimating precipitation on early Mars using a radiative-convective model of the atmosphere and comparison with inferred runoff from geomorphology." Planetary and Space Science **105**: 133-147.

Warner, N., S. Gupta, J.-P. Muller, J.-R. Kim and S.-Y. Lin (2009). "A refined chronology of catastrophic outflow events in Ares Vallis, Mars." Earth and Planetary Science Letters **288**(1-2): 58-69.

Watters, T. R., P. J. McGovern and R. P. Irwin Iii (2007). "Hemispheres apart: The crustal dichotomy on Mars." Annu. Rev. Earth Planet. Sci. **35**: 621-652.

Webb, V. E. (2004). "Putative shorelines in northern Arabia Terra, Mars." Journal of Geophysical Research-Planets **109**(E9).

Werner, S. C., K. L. Tanaka and J. A. Skinner (2011). "Mars: The evolutionary history of the northern lowlands based on crater counting and geologic mapping." Planetary and Space Science **59**(11-12): 1143-1165.

Wetzel, R. G. (2001). Limnology: lake and river ecosystems, gulf professional publishing.

White, K., S. McLaren, S. Black and A. Parker (2000). Evaporite minerals and organic horizons in sedimentary sequences in the Libyan Fezzan: implications for palaeoenvironmental reconstruction. Linking Climate Change to Land Surface Change, Springer**:** 193-208.

Wilde, S. A., J. W. Valley, W. H. Peck and C. M. Graham (2001). "Evidence from detrital zircons for the existence of continental crust and oceans on the Earth 4.4 Gyr ago." Nature **409**(6817): 175.

Williams, R. M., J. E. Moersch and R. L. Fergason (2018). "Thermophysical properties of Martian fluvial sinuous ridges: Inferences on "inverted channel" induration agent." Earth and Space Science **5**(9): 516-528.

Wilson, S. A., A. D. Howard, J. M. Moore and J. A. Grant (2016). "A cold-wet middle-latitude environment on Mars during the Hesperian-Amazonian transition: Evidence from northern Arabia valleys and paleolakes." Journal of Geophysical Research-Planets **121**(9): 1667-1694.

Wolfe, S. A., P. D. Morse, S. V. Kokelj and A. J. Gaanderse (2017). Great Slave lowland: the legacy of glacial lake McConnell. Landscapes and Landforms of Western Canada, Springer**:** 87-96.

Woodley, S., P. Fawdon, M. Balme, D. Rothery and E. Favaro (2021). Tectonic Features in Western Arabia Terra and Their Implications for the ExoMars 2022 Rover Landing Site. Lunar and Planetary Science Conference.

Woodworth-Lynas, C. and J. Y. Guigné (2003). "Ice keel scour marks on Mars: evidence for floating and grounding ice floes in Kasei Valles." Oceanography **16**(4): 90-97.

Wordsworth, R., F. Forget, E. Millour, J. Head, J.-B. Madeleine and B. Charnay (2013). "Global modelling of the early martian climate under a denser CO2 atmosphere: Water cycle and ice evolution." Icarus **222**(1): 1-19.

Wordsworth, R., Y. Kalugina, S. Lokshtanov, A. Vigasin, B. Ehlmann, J. Head, C. Sanders and H. Wang (2017). "Transient reducing greenhouse warming on early Mars." Geophysical Research Letters **44**(2): 665-671.

Wordsworth, R. D. (2016). "The Climate of Early Mars." Annual Review of Earth and Planetary Sciences, Vol 44 **44**: 381-408.

Wright, W. H. (1925). "Photographs of Mars made with light of different colors." Lick Observatory Bulletin **12**: 48-61.

Zuber, M. T. (2001). "The crust and mantle of Mars." Nature **412**(6843): 220.

Zuber, M. T., S. C. Solomon, R. J. Phillips, D. E. Smith, G. L. Tyler, O. Aharonson, G. Balmino, W. B. Banerdt, J. W. Head, C. L. Johnson, F. G. Lemoine, P. J. McGovern, G. A. Neumann, D. D. Rowlands and S. J. Zhong (2000). "Internal structure and early thermal evolution of Mars from Mars Global Surveyor topography and gravity." Science **287**(5459): 1788-1793.

Świąder, A. (2014). "Identification and visualisation of possible ancient ocean shoreline on Mars using submeter-resolution Digital Terrain Models." Geologos **20**(4): 289-301.

Appendices

Appendix I – Photogrammetric Processing with SOCET SET

(1) Selection of two suitable images meeting the following criteria: (1) good quality data, with no major artefacts and of similar contrast; (2) difference in incident angles >15° between images; (3) overlap area >50% of the image footprint between images.

(2) Pre-processing with ISIS to generate files for SOCET SET workflow. Data input includes: (1) 'PDS Source EDR' image data linked to from 'Mars Image Explorer'; (2) MOLA DTM; and (3) MOLA shot tracks.

(3) Transfer pre-processed image and MOLA data from the ISIS machine to a dedicated SOCET SET machine, and verify data.

(4) Control the relative orientation, image alignment and absolute orientation of the images to the MOLA shot track data.

(5) Automatically generate tie-points to be compared between the two images. Outlier tie-points with low confidence, and those near the edge of the DEM may require manual removal and re-measurement.

(6) Using 'USGS Tool' add-on to perform vertical adjustment, which adds MOLA elevation data to tie-points. Re-measure tie points, and again remove outliers. Repeat if necessary.

(7) Define DEM resolution to be generated and begin SOCET SET processing, typically taking a few hours.

(8) Export DEMs and orthoimages, and transfer files back to the ISIS machine to generate DEMs and images compatible with 'ArcMap'. Compete export to 'ArcMap' for analysis.

APPENDIX II – GIS DATA FORMATS

The investigation and analysis of orbital data for this thesis was primarily handled using GIS software and environments, and specifically the use of ESRI ArcMap. Four principal GIS data formats were used to store and organise data: (1) rasters; (2) polygons; (3) lines, or polylines; and (4) points. There are a range of methods to combine, contrast, and convert data between these formats, as well as methods for different formats to be used in conjunction.

Rasters are arrays of spatial data in which each pixel is assigned a discrete numerical value, commonly visualised with colours or greyscale stretched across the range of values, with resolution communicated as the dimension of a single pixel, typically as metres per pixel (m/px). Primary imagery and topography data obtained from instrument and space agency sources often comes in this format, as do DEMs produced from stereo imagery. Rasters may constitute secondary products, or intermediary steps produced as part of a workflow in the analysis and interpretation of primary data, with many raster outputs of the hydrological toolbox serving as inputs later in the workflow. Rasters can be converted into other formats, using tools which interpolate and simplify the data contained across multiple pixels based on a desired criteria, such as the production of elevation contours (polyline format) from topography data (raster format).

Polygons are closed, two-dimensional shapes of any geometry, delineated by straight edges linking vertex points attributed with exact coordinates. The space between vertices may be regular or variable, but complex shapes with many vertices often utilising a set distance between vertices to maintain a constant resolution. Interpreted data products in the form of geological units, mineralogy maps, and morphological features are often provided in the form of polygons, and in this thesis polygons are commonly used to define watersheds and study boundaries. Spatial information such as area and perimeter can be extracted from polygons, as well as selecting or generating statistics based on other features or rasters which fall within the boundary of a polygon. Methods commonly used in this thesis include the calculation of minimum, maximum, and mean

elevation, or summarising fluvial feature (line format) attributes within a given polygon area.

Lines are two-dimensional linear features, defined by connected vertex points, with polylines representing a number of disconnected linear segments as a single feature. As with polygons, the distance between vertices set may be set to maintain a constant resolution. Line features are used to represent a wide range of linear features, including: geologic contacts, valleys, and ridges. Line features can also hold directional data, with the terminal vertices of a line defined as start and end points.

Point features are the most basic data format, attributed with a precise set of spatial coordinates. Points are ideal for simplifying more complex shapes, and can significantly reduce the processing time to run some tools. Points are commonly used in this thesis for extracting start and end points from fluvial valleys (line features), or representing the centre point of a mapped palaeolake (polygon feature).

APPENDIX III – QUANTIFICATION OF MORPHOLOGY AND TOPOGRAPHY

Manipulation and analysis of data was achieved with toolboxes included in ArcMap, including the use of established workflows, as well as adaptations of existing tools to meet the research aims of this thesis. The requirement being to extract quantitative data from observed hydrological features, and the three processes most central to the research of this thesis are described here in greater detail: (1) topographic profile production, for fluvial features, palaeolake chains, and other morphological features; (2) delineation of equipotential surfaces, for palaeolakes and possible ocean shorelines; and (3) extracting dimensions for identified palaeolakes, including area, perimeter, depth, and volume.

Two dimensional topographic cross-sectional or longitudinal profiles are useful in characterising and visualising fluvial and lacustrine systems, as well as characterising morphology across local and regional terrains. Profiles have proved useful in Mars research to identify knick-points (Duran, Coulthard et al. 2019), interior fluvial channels (Goudge and Fassett 2018), and sedimentation within basins (Fawdon 2018). The method used to produce profiles in this thesis was to: (1) create a line feature, with a defined direction; (2) automatically generate points along the line at a given spacing, usually 1 km; (3) attributing elevation 'z' values to each point from an input topographic surface raster; and (4) exporting the resulting table to graphing and plotting software. A variation of this method was used to produce approximations of valley bank elevation to accompany longitudinal profiles along valley floors, by: (1) automatically producing parallel line features to either side of a valley centre profile, at a distance representing the half of the maximum valley width, (2) producing elevation attributed points in the same manner described above; (3) and then averaging the elevation of corresponding points from the two parallel lines.

Calculating the approximate boundaries, surface area, and volume of palaeolake basins can be used to model where and how water may have pooled on a surface, and to characterise hydrological processes. Water filling a basin will pool to form an

equipotential surface at a single elevation, with the edge of the water body represented by a single contour line at the equipotential surface elevation. In this work, the areal extents of possible palaeolakes were delineated by producing contour lines from a topographic surface, and converting these closed lines to polygons, with palaeolake perimeter distances and palaeolake areas extracted from the polygons.

Two dimensional palaeolake dimensions, such as area and perimeter were automatically generated for the palaeolake polygons described above. Palaeolake volumes were derived by: (1) using 'Clip' tool, to clip a topography raster to the extent of a palaeolake polygon,, and then using the 'Surface Volume' tool to calculate the volume between a user defined plane (entered as the elevation of the equipotential surface) and the clipped topography raster.

Appendix IV – Catalogue of Palaeolakes in Arabia Terra

Full catalogue of palaeolakes identified in this thesis, based on the catalogue presented in Chapter 6. Dimensions and attributes of palaeolakes which are additionally included in the detailed studies of Chapter 4 and 5 can be found in tables within those respective chapters. Palaeolake attributes presented in this table include:

1. Palaeolake Number – This number represents a palaeolake basin defined by either a single outlet valley, in the case of open-basin palaeolakes, or an inlet valley or valleys, in the case of closed-basin palaeolakes. As three possible fill levels were considered for open-basin palaeolakes, there may be up to three sets of palaeolake attributes associated with a single palaeolake number, with each instance differentiated by the Identification Type.
2. Coordinates – Defined as a point at the geometric centre of the palaeolake, within the mapped palaeolake boundary, and presented as decimal degrees Latitude (N) and Longitude (E). The coordinates of open-basin palaeolakes with different levels all make use of the same centre point.
3. Palaeolake Type – Hydrological classification of the palaeolake defined as either: open-basin, and displaying an outlet; or closed-basin and displaying inlets only.
4. Identification Type – The criteria used to identify the palaeolake, and define its surface elevation and boundary. With a different set of criteria for open-basin and closed-basin types.
    a. VO – Valley Overflow, at the highest elevation on an outlet valley floor
    b. VE – Valley Extremity, at the lowest elevation of an outlet valley head
    c. BO – Basin Overflow, at the highest elevation at an outlet valley bank

d. Term – Termination of a valley issuing from an open-basin palaeolake

e. Crat – Termination of a valley which breaches the raised rim of an impact crater

f. Crat/Term – Termination of a valley issuing from and open-basin palaeolake, which also breaches the raised rim of an impact crater

5. Basin Type – An interpretation of the morphological origin of the basin which hosts the palaeolake.

   a. SC – Basin contained in a single impact crater

   b. MC – Basin defined by multiple impact craters

   c. IC – Basin within the inter-crater plains

   d. UN – Basin of an undetermined origin

6. Submersion – Overlapping relationship of one palaeolake to another in the catalogue. As one lake cannot be submerged under another, this provides an indication of which palaeolakes could not have existed contemporaneously.

   a. O – Palaeolake which overlies another in the catalogue

   b. U – Palaeolake which underlies another in the catalogue

   c. N – Palaeolake which is neither over or under another in the catalogue

7. Chain Order – Value defining the relative position of a palaeolake within a palaeolake chain, and only defined for open-basin palaeolakes. A value of '0' indicates a palaeolake not integrated into a chain, with '1' indicating the first and highest palaeolake in a chain, and higher numbers indicating the number of lake along a chain (eg. A value of '5' indicates the fifth lake in a chain, fed by a chain of four higher lakes.

8. Chain Number – This number indicates the specific palaeolake chain of which a palaeolake is a part. So that all palaeolakes with the same 'Chain Number' are integrated into the same continuous chain.

9. Sediment Fans – A count of the number of sediment fans identified within a palaeolake, and the confidence associated with the identification each fan.

    a. Hx – The number of fans within a palaeolake, identified with high confidence

    b. Lx – The number of fans within a palaeolake, identified with low confidence

    c. NA – No fans identified within a palaeolake

10. Surface Elevation – Elevation of the palaeolake surface, determined by a palaeolake outlet or inlet, and selected from contours spaced at 10 m intervals.

11. Perimeter – Length of palaeolake perimeter defined by a contour at the palaeolake inlet or outlet elevation.

12. Area – Two-dimensional area of the palaeolake surface.

13. Volume – Volume of the palaeolake basin, calculated as the space between the elevation of the palaeolake surface and the present topography of the basin floor.

14. Mean Depth – Palaeolake depth, calculated as palaeolake volume/area.

15. SDI – Shoreline Development Index, used as an indication of palaeolake circularity caused by shoreline processes. Discussed in detail in Section 6.4.2.1 of this thesis.

16. Notes – Other relevant information, including: reference to original palaeolake identification in other catalogues and publications, page and figure reference to detailed palaeolake information elsewhere in this thesis.

Palaeolake Number	Lat (°N)	Lat (°E)	Type	Identification	Basin Type	Submerged	Chain Order	Chain Number	Fan	Surface Elevation (m)	Perimeter (km)	Area (km^2)	Volume (km^3)	Mean Depth (m)	SDI	Notes
1	7.93	348.92	Open	VO	IC	O	2	32	NA	-2100	333	1265	45	36	2.64	
2	7.50	348.6	Open	VO	IC	U	0	32	NA	-2130	26.3	28.4	0.34	12	1.39	
2	7.50	348.6	Open	VE	-	-				-2150	11.3	6.80	0.02	3	1.23	
3	7.82	349.33	Open	VO	IC	N	1	32	NA	-2100	47.3	70.1	0.75	11	1.59	
4	7.59	351.35	Open	VO	CS	N	2	31	NA	-1650	36.2	90.4	8.24	91	1.08	
5	10.13	353.03	Open	VO	IC	N	1	29	NA	-1990	162	1092	84	77	1.38	
5	10.13	353.03	Open	VE	-	-				-2170	5.97	2.32	0.01	3	1.11	
6	9.97	352.64	Open	VO	IC	U	2	29	NA	-2050	26.5	34.6	0.72	21	1.27	
7	-10.03	352.48	Open	VO	IC	U	3	29	NA	-2050	46.9	85.7	1.69	20	1.43	
8	10.01	352.47	Open	VO	IC	O	2	29	NA	-1980	168	609	60	98	1.92	
9	10.48	352.23	Open	VO	IC	N	3(4)	29	NA	-1960	147	512	29	57	1.83	
10	11.34	351.98	Open	VO	IC	N	4(5)	29	NA	-2080	376	1463	87	60	2.77	
11	10.72	351.49	Open	VO	IC	N	5(6)	29	NA	-2080	159	751	31	41	1.64	
12	9.73	351.11	Open	VO	IC	N	0	0	NA	-1720	21.6	24.2	0.51	21	1.24	
13	9.35	347.55	Open	VO	IC	N	1	33	NA	-1970	27.0	31.5	0.65	21	1.36	
14	8.81	346.56	Open	VO	IC	N	3	33	L2	-2100	1017	6053	351	58	3.69	
14	8.81	346.56	Open	VE	-	-				-2120	223	2045	212	104	1.39	
15	12.49	348.422	Open	VO	IC	N	1	28	NA	-1990	26.0	40.6	1.02	25	1.15	

15	12.49	348.422	Open	VE	-	-				-2030	5.58	1.99	0.01	4	1.12
16	14.78	347	Open	VO	UN	N	2	25	NA	-3130	67.4	146	2.17	15	1.57
16	14.78	347	Open	BO	-	-				-3040	175	1456	130	89	1.29
17	15.39	351.8	Open	VO	IC	N	0	0	NA	-1880	105	363	12	32	1.55
18	16.65	352.68	Open	VO	IC	N	0	0	NA	-1980	165	639	17	26	1.84
19	17.50	347.98	Open	VO	IC	N	0	0	NA	-1940	13.0	5.33	0.01	2	1.58
20	16.41	348.33	Open	VO	CS	N	0	0	NA	-2570	27.9	49.4	0.70	14	1.12
20	16.41	348.33	Open	BO	-	-				-2560	36.6	80.3	1.38	17	1.15
21	18.69	345.53	Open	VO	CS	N	2	24	NA	-2320	209	2769	1855	670	1.12
22	18.38	347.16	Open	VO	IC	N	0	0	NA	-2210	82.9	117	3.32	28	2.16
22	18.38	347.16	Open	BO	-	-				-2200	91.9	153	4.62	30	2.10
23	21.20	346.51	Open	VO	IC	N	2	23	NA	-2170	146	617	12	19	1.66
24	19.54	348.43	Open	VO	IC	N	0	0	NA	-1680	4.68	1.46	0.001	1	1.09
25	21.23	355.58	Open	VO	IC	N	0	0	NA	-1920	63.8	108	0.61	6	1.73
26	21.85	354.46	Open	VO	IC	N	0	0	NA	-1850	47.6	89.7	1.99	22	1.42
27	20.85	350.28	Open	VO	IC	N	0	0	NA	-1640	19.0	20.9	0.11	5	1.17
28	21.60	347.03	Open	VO	IC	N	0	22	NA	-2230	30.2	51.1	1.17	23	1.19
28	21.60	347.03	Open	VE	-	-				-2240	28.9	40.7	0.70	17	1.28
29	21.73	347.36	Open	VO	IC	N	0	22	NA	-2150	16.0	11.0	0.04	4	1.36
30	21.96	347.66	Open	VO	IC	N	0	22	NA	-2140	67.3	144	1.93	13	1.58
30	21.96	347.66	Open	BO	-	-				-2130	66.2	191	3.58	19	1.35
31	22.89	354.57	Open	VO	IC	N	1	77	NA	-2090	17.4	21.6	0.19	9	1.05
31	22.89	354.57	Open	VE	-	-				-2110	5.37	1.93	0.003	2	1.09
32	25.17	353.53	Open	VO	IC	N	1	1	NA	-2150	1540	15208	1435	94	3.52
33	25.61	351.36	Open	VO	CM	N	2	1	NA	-2270	828	7219	2283	316	2.75
33	25.61	351.36	Open	BO	-	-				-2260	793	7493	2357	315	2.59
34	25.09	349.088	Open	VO	IC	N	0	0	NA	-2930	14.3	13.6	0.40	30	1.09
34	25.09	349.088	Open	BO	-	-				-2910	16.6	18.1	0.71	39	1.10

35	25.89	349.01	Open	VO	IC	N	0	0	NA	-2370	29.3	34.3	0.39	11	1.41
36	5.66	342.6	Open	VO	UN	N	1	5	NA	-2230	27.9	27.3	0.84	31	1.51
37	6.88	344.06	Open	VO	IC	N	1	6	NA	-2010	196	740	23	31	2.03
38	6.35	342.14	Open	VO	IC	N	4	5	NA	-2260	124	492	18	37	1.58
38	6.35	342.14	Open	VE	-	-				-2290	103	332	5.63	17	1.59
38	6.35	342.14	Open	BO	-	-				-2250	119	536	23	43	1.45
39	6.83	341.76	Open	VO	CS	N	1	4	NA	-2310	112	871	331	380	1.08
39	6.83	341.76	Open	VE	-	-				-2570	106	748	121	161	1.09
39	6.83	341.76	Open	BO	-	-				-2270	114	887	366	413	1.08
40	7.85	339.13	Open	VO	CS	N	0	0	NA	-2920	106	588	59	101	1.23
41	8.46	340.39	Open	VO	IC	N	5	3	NA	-2290	47.4	86.9	0.89	10	1.44
41	8.46	340.39	Open	BO	-	-				-2280	82.8	171	3.83	22	1.78
42	8.68	338.15	Open	VO	UN	N	2	80	NA	-2760	13.3	11.5	0.32	28	1.11
42	8.68	338.15	Open	BO	-	-				-2750	14.3	13.0	0.46	35	1.12
43	8.87	338.27	Open	VO	CS	N	1	80	NA	-2720	61.2	266	21	80	1.06
44	9.26	340.81	Open	VO	IC	N	0	0	NA	-2120	81.2	236	4.64	20	1.49
45	8.55	341.06	Open	VO	IC	N	2	3	NA	-2190	41.9	82.7	0.43	5	1.30
46	8.69	341.47	Open	VO	IC	N	1	3	NA	-2130	24.1	26.8	0.20	7	1.31
47	8.37	341.62	Open	VO	IC	N	1	3	NA	-2090	21.0	26.6	0.33	12	1.15
48	8.10	344.95	Open	VO	IC	N	0	0	NA	-2020	39.3	82.4	2.48	30	1.22
49	9.26	344.05	Open	VO	IC	N	0	34	NA	-2110	77.5	262	5.41	21	1.35
50	9.62	343.64	Open	VO	CS	N	0	34	NA	-2100	14.6	15.1	0.13	8	1.06
50	9.62	343.64	Open	BO	-	-				-2060	449	2677	112	42	2.45
51	11.29	338.29	Open	VO	CS	N	1	79	NA	-1940	35.6	68.2	1.49	22	1.22
51	11.29	338.29	Open	BO	-	-				-1930	39.1	80.8	2.22	27	1.23
52	13.64	338.54	Open	VO	IC	N	2	78	NA	-2050	56.6	101	3.27	32	1.59
53	13.62	338.84	Open	VO	IC	N	1	78	NA	-2050	18.4	16.7	0.08	5	1.27
54	15.32	344.16	Open	VO	IC	N	0	0	NA	-1390	33.8	62.2	1.44	23	1.21

54	15.32	344.16	Open	VE	-	-				-1450	6.42	2.97	0.02	6	1.05
54	15.32	344.16	Open	BO	-	-				-1380	37.9	76.2	2.11	28	1.23
55	15.26	343.18	Open	VO	IC	N	0	0	NA	-1980	45.3	102	1.71	17	1.26
56	14.62	339.09	Open	VO	CS	N	1	12	NA	-2490	87.3	441	109	246	1.17
56	14.62	339.09	Open	VE	-	-				-2560	80.2	394	79	202	1.14
56	14.62	339.09	Open	BO	-	-				-2310	91.4	596	201	337	1.06
57	27.24	349.14	Open	VO	IC	N	4	1	NA	-2700	193	965	40	41	1.75
57	27.24	349.14	Open	VE	-	-				-2730	218	575	16	28	2.56
58	28.09	348.5	Open	VO	IC	N	2	1	L1	-2720	68.6	139	3.77	27	1.64
58	28.09	348.5	Open	BO	-	-				-2700	76.8	206	7.24	35	1.51
59	28.88	346.1	Open	VO	IC	N	0	0	L1	-3030	23.5	26.1	0.20	8	1.30
60	28.44	348.16	Open	VO	IC	N	1	42	NA	-2840	7.73	4.52	0.03	6	1.03
61	28.33	347.97	Open	VO	IC	N	2	42	NA	-2910	44.9	67.3	1.61	24	1.54
61	28.33	347.97	Open	VE	-	-				-2930	35.8	40.5	0.57	14	1.59
61	28.33	347.97	Open	BO	-	-				-2890	52.0	101	3.26	32	1.46
62	28.70	348.216	Open	VO	CS	N	0	0	NA	-2600	27.5	51.4	4.20	82	1.08
62	28.70	348.216	Open	BO	-	-				-2590	28.4	53.9	4.72	88	1.09
63	28.65	348.31	Open	VO	CS	N	0	0	NA	-2590	12.4	10.7	1.33	125	1.07
63	28.65	348.31	Open	VE	-	-				-2680	9.33	6.61	0.58	87	1.02
64	28.67	347.31	Open	VO	IC	N	3	41	NA	-3060	32.3	30.3	0.87	29	1.65
65	28.76	350.07	Open	VO	IC	U	1	74	NA	-3000	16.3	17.6	0.11	6	1.10
66	29.40	349.12	Open	VO	IC	N	6	1	NA	-3320	32.9	43.3	0.58	13	1.41
67	29.66	348.71	Open	VO	IC	N	7	1	L1	-3320	194	901	40	44	1.82
68	28.61	351.08	Open	VO	CS	N	0	0	NA	-2700	28.6	54.8	1.60	29	1.09
68	28.61	351.08	Open	BO	-	-				-2690	31.4	63.3	2.19	35	1.11
69	26.88	355.9	Open	VO	IC	N	1	75	NA	-1940	37.7	29.7	0.55	18	1.95
70	30.65	351.39	Open	VO	IC	N	2	46	NA	-2620	147	516	8.03	16	1.82
71	31.38	351.38	Open	VO	IC	N	3	46	NA	-2720	51.3	84.6	0.58	7	1.57

72	31.53	351.1	Open	VO	IC	N	4	46	NA	-2750	35.8	32.1	0.27	8	1.78
72	31.53	351.1	Open	BO	-	-				-2740	72.5	83.7	0.81	10	2.24
73	30.68	349.72	Open	VO	IC	N	0	45	NA	-3100	20.0	15.6	0.06	4	1.43
74	30.82	349.98	Open	VO	IC	N	0	45	NA	-3100	95.4	158	2.50	16	2.14
75	30.67	348.66	Open	VO	UN	N	11	1	NA	-3760	36.1	70.7	1.39	20	1.21
75	30.67	348.66	Open	VE	-	-				-3780	25.0	32.7	0.38	12	1.24
76	30.23	348.07	Open	VO	CS	N	1	1	NA	-3310	29.6	61.3	4.00	65	1.07
77	31.18	346.37	Open	VO	IC	U	0	0	NA	-4010	47.7	109	6.89	63	1.29
77	31.18	346.37	Open	BO	-	-				-3990	64.2	140	9.39	67	1.53
78	31.89	348.18	Open	VO	IC	N	2	43	NA	-3440	24.1	31.2	0.24	8	1.22
78	31.89	348.18	Open	BO	-	-				-3430	29.0	50.4	0.64	13	1.15
79	32.41	347.81	Open	VO	IC	N	3	43	NA	-3600	186	1049	115	110	1.62
79	32.41	347.81	Open	BO	-	-				-3500	916	9070	4890	539	2.71
80	32.97	346.59	Open	VO	UN	N	6	43	NA	-3870	73.8	207	4.88	24	1.45
80	32.97	346.59	Open	BO	-	-				-3820	229	748	31	42	2.36
81	33.40	347.82	Open	VO	CS	N	1	43	NA	-3460	49.7	126	6.30	50	1.25
82	33.41	347.61	Open	VO	IC	N	2	43	NA	-3510	5.60	1.62	0.003	2	1.24
83	32.91	347.69	Open	VO	UN	N	1	43	NA	-3300	15.1	13.6	0.20	15	1.16
84	33.95	348.268	Open	VO	CS	N	0	0	NA	-3270	12.3	11.3	0.73	65	1.03
85	32.93	348.47	Open	VO	IC	N	1	71	NA	-3620	60.9	165	10	64	1.34
85	32.93	348.47	Open	VE	-	-				-3680	39.3	80.7	3.65	45	1.23
86	33.11	348.9	Open	VO	CS	N	2	71	NA	-4070	19.4	23.4	0.25	11	1.13
87	33.90	349.97	Open	VO	UN	N	4	47	NA	-4050	41.4	98.0	2.28	23	1.18
88	33.42	350.04	Open	VO	CS	N	3	47	NA	-3580	20.1	24.4	0.31	13	1.15
88	33.42	350.04	Open	BO	-	-				-3550	27.3	50.0	1.42	28	1.09
89	32.80	350.05	Open	VO	UN	N	1	47	NA	-3250	61.8	222	11	51	1.17
89	32.80	350.05	Open	VE	-	-				-3340	4.37	1.26	0.002	1	1.10
90	33.51	350.64	Open	VO	CS	N	0	0	NA	-2990	15.2	15.2	1.48	97	1.10

91	32.17	355.02	Open	VO	UN	N	4	65	NA	-2570	295	2191	193	88	1.78
92	32.75	354.94	Open	VO	CS	N	2	64	NA	-2480	33.6	75.2	1.70	23	1.09
93	33.80	355.82	Open	VO	IC	N	1	51	NA	-2310	58.8	67.6	0.65	10	2.02
94	35.73	355.35	Open	VO	CS	N	5	61	L1	-3350	70.9	155	5.35	34	1.60
95	35.24	355.72	Open	VO	IC	N	4	61	NA	-3220	120	425	10	23	1.65
96	35.73	352.82	Open	VO	CS	N	0	0	NA	-3330	12.4	11.5	1.31	114	1.03
97	35.92	352.4	Open	VO	CS	N	0	0	NA	-3610	38.4	84.9	2.66	31	1.17
98	35.51	351.01	Open	VO	IC	N	0	50	NA	-3220	140	428	12	28	1.91
99	34.51	350.01	Open	VO	CS	N	0	0	NA	-3340	29.7	59.2	2.19	37	1.09
100	34.72	349.57	Open	VO	CS	N	0	0	NA	-3250	19.5	28.2	4.67	165	1.04
101	35.45	349.77	Open	VO	IC	N	0	0	L1	-3710	130	623	63	101	1.47
101	35.45	349.77	Open	VE	-	-				-3730	127	542	51	94	1.54
102	34.92	348.41	Open	VO	CS	N	2	48	NA	-3590	36.2	80.0	3.14	39	1.14
103	35.11	348.08	Open	VO	IC	N	3	48	NA	-3730	66.0	138	3.68	27	1.59
104	34.11	348.11	Open	VO	IC	N	0	0	NA	-3280	13.1	10.3	0.10	10	1.15
105	17.22	343.1	Open	VO	IC	N	1	18	NA	-1670	32.1	33.5	0.31	9	1.56
106	17.48	342.87	Open	VO	CS	N	2	18	NA	-2410	17.6	17.4	0.13	7	1.19
107	16.18	342.9	Open	VO	CS	N	0	0	NA	-1670	22.8	31.2	0.26	8	1.15
108	16.22	340.92	Open	VO	IC	N	1	17	NA	-2120	71.9	143	2.42	17	1.70
109	16.15	340.69	Open	VO	IC	N	2	17	NA	-2210	15.8	11.4	0.07	6	1.32
110	15.98	340.72	Open	VO	IC	N	1	17	NA	-2210	13.2	10.4	0.13	12	1.16
110	15.98	340.72	Open	VE	-	-				-2220	10.9	6.42	0.05	8	1.21
111	16.04	340.33	Open	VO	IC	N	3	17	NA	-2230	130	308	5.78	19	2.09
112	16.62	340.05	Open	VO	IC	N	1	17	NA	-2290	7.61	3.87	0.01	2	1.09
113	16.07	339.09	Open	VO	CM	N	1	17	NA	-2300	194	1467	218	148	1.43
114	16.04	337.97	Open	VO	CS	N	2	17	NA	-2450	61.0	189	62	329	1.25
115	16.97	337.45	Open	VO	IC	U	5	17	L1	-2790	301	1388	54	39	2.28
115	16.97	337.45	Open	VE	-	-				-2860	4.01	1.15	0.002	2	1.06

115	16.97	337.45	Open	BO	-	-				-2780	267	1570	68	44	1.90
116	16.37	338.1	Open	VO	IC	N	4	17	NA	-2560	11.2	7.82	0.05	6	1.13
116	16.37	338.1	Open	BO	-	-				-2550	24.0	25.5	0.25	10	1.34
117	16.40	338.36	Open	VO	IC	N	3	17	NA	-2450	7.13	3.38	0.01	4	1.09
118	17.30	339.7	Open	VO	IC	N	1	17	NA	-2340	10.9	5.89	0.02	4	1.27
118	17.30	339.7	Open	BO	-	-				-2330	25.2	28.6	0.20	7	1.33
119	17.07	336.56	Open	VO	UN	N	1	15	NA	-2730	45.2	111	16	149	1.21
120	17.74	336.96	Open	VO	IC	U	6	17	NA	-2820	108	187	4.71	25	2.22
121	17.21	337.28	Open	VO	IC	O	5(6)	17	L1	-2770	604	3501	357	102	2.88
121	17.21	337.28	Open	BO	-	-				-2760	583	3818	393	103	2.66
122	18.06	334.42	Open	VO	IC	N	0	17	NA	-2790	37.0	59.8	1.32	22	1.35
123	18.05	337.77	Open	VO	IC	N	5	17	NA	-2660	104	525	17	33	1.28
123	18.05	337.77	Open	BO	-	-				-2650	141	637	23	36	1.57
124	18.65	337.88	Open	VO	IC	N	4	17	NA	-2500	19.1	15.4	0.13	9	1.38
125	18.77	338.17	Open	VO	IC	N	3	17	NA	-2420	77.8	125	1.55	12	1.96
126	18.97	338.93	Open	VO	IC	N	2	17	NA	-2430	400	2201	93	42	2.40
126	18.97	338.93	Open	VE	-	-				-2470	13.5	10.0	0.02	2	1.20
127	18.70	340.52	Open	VO	IC	N	1	17	NA	-2190	101	259	2.92	11	1.77
128	19.85	341.29	Open	VO	IC	N	0	0	NA	-2180	59.1	225	13	56	1.11
128	19.85	341.29	Open	VE	-	-				-2230	44.3	116	4.17	36	1.16
129	19.39	341.02	Open	VO	IC	N	4	19	NA	-2200	51.3	73.8	0.78	11	1.69
130	19.13	341.2	Open	VO	IC	N	3	19	NA	-2200	42.7	52.1	0.51	10	1.67
131	18.97	341.54	Open	VO	IC	N	1	19	NA	-2140	29.1	40.1	0.52	13	1.30
131	18.97	341.54	Open	VE	-	-				-2160	12.4	8.05	0.04	5	1.23
132	18.63	342.11	Open	VO	IC	N	0	0	NA	-2070	11.3	8.45	0.06	7	1.09
133	19.64	342.52	Open	VO	IC	O	0	0	NA	-1950	116	255	6.34	25	2.05
133	19.64	342.52	Open	VE	-	-				-2000	12.7	10.3	0.05	5	1.12
134	19.50	342.6	Open	VO	IC	U	0	0	NA	-1970	11.5	8.76	0.13	15	1.10

135			Open	VE	-	-				-2000	8.27	3.00	0.004	1	1.35
136	21.91	340.25	Open	VO	IC	N	0	0	NA	-2040	10.1	5.80	0.03	5	1.19
137	21.87	343.6	Open	VO	IC	N	0	0	NA	-1900	3.69	0.95	-	-	1.07
138	21.04	342.58	Open	VO	CM	N	1	20	NA	-1950	217	2665	2865	1075	1.18
138	21.04	342.58	Open	BO	-	-				-1930	219	2689	2918	1085	1.19
139	21.83	342.62	Open	VO	IC	N	2	20	NA	-2070	59.8	141	4.04	29	1.42
139	21.83	342.62	Open	VE	-	-				-2110	29.5	46.6	0.48	10	1.22
140	20.73	338.67	Open	VO	CS	N	0	0	NA	-2550	3.88	1.05	0.001	1	1.07
141	22.93	341.6	Open	VO	UN	O	4	20	H1	-3100	196	806	74	92	1.95
141	22.93	341.6	Open	BO	-	-				-3090	206	847	82	97	2.00
142	23.69	343.01	Open	VO	CM	O	1	35	NA	-2260	206	2133	846	397	1.26
143	23.63	343.27	Open	VO	UN	U	0	0	NA	-2630	24.8	25.3	0.39	15	1.39
143	23.63	343.27	Open	BO	-	-				-2570	65.7	100	4.32	43	1.85
144	21.88	344.71	Open	VO	UN	N	2	21	NA	-2690	68.4	118	7.93	67	1.77
144	21.88	344.71	Open	VE	-	-				-2730	44.8	52.7	1.04	20	1.74
144	21.88	344.71	Open	BO	-	-				-2560	566	2881	302	105	2.97
145	21.92	345.13	Open	VO	IC	N	1	21	NA	-2290	3.33	0.67	0.001	1	1.14
146	25.86	342.22	Open	VO	IC	N	1	37	NA	-2810	12.0	10.7	0.14	13	1.04
147	25.91	341.7	Open	VO	IC	N	2	37	NA	-3360	12.6	7.77	0.05	6	1.27
148	24.87	340	Open	VO	IC	N	0	0	NA	-3150	17.8	10.2	0.06	6	1.57
148	24.87	340	Open	VE	-	-				-3160	7.32	2.96	0.01	3	1.20
148	24.87	340	Open	BO	-	-				-3140	77.0	121	1.63	13	1.98
149	27.01	340.72	Open	VO	CS	N	3	38	NA	-3400	62.1	179	39	216	1.31
149	27.01	340.72	Open	BO	-	-				-3390	169	460	54	118	2.22
150	26.99	341.08	Open	VO	IC	O	1	38	NA	-3230	36.1	98.0	5.42	55	1.03
150	26.99	341.08	Open	VE	-	-				-3360	6.75	3.50	0.06	18	1.02
151	28.18	343.39	Open	VO	IC	N	1	40	NA	-3110	44.8	50.5	0.44	9	1.78
151	28.18	343.39	Open	VE	-	-				-3120	36.0	25.8	0.09	3	2.00

152	28.54	341.9	Open	VO	IC	N	0	0	NA	-3550	27.1	33.6	0.31	9	1.32
152	28.54	341.9	Open	VE	-	-				-3580	3.88	1.07	0.000	0	1.06
153	29.03	342.16	Open	VO	IC	N	2	39	NA	-3600	110	378	21	55	1.60
153	29.03	342.16	Open	VE	-	-				-3630	90.9	242	12	48	1.65
154	29.53	342.84	Open	VO	IC	N	0	0	NA	-3500	49.0	56.9	0.42	7	1.83
155	29.96	345.56	Open	VO	IC	N	1	2	NA	-3290	61.6	159	7.18	45	1.38
155	29.96	345.56	Open	VE	-	-				-3340	33.5	65.5	1.86	28	1.17
156	30.38	345.05	Open	VO	IC	N	0	0	NA	-3510	156	416	70	169	2.16
156	30.38	345.05	Open	VE	-	-				-3640	28.4	40.7	3.08	76	1.26
157	31.09	346.42	Open	VO	CM	O	2	2	H1	-3420	753	5396	2717	504	2.89
157	31.09	346.42	Open	VE	-	-				-3570	16.2	16.9	0.69	41	1.11
157	31.09	346.42	Open	BO	-	-				-3400	635	5858	2842	485	2.34
158	30.94	345.62	Open	VO	CS	U	2	72	NA	-3500	15.3	17.0	1.77	104	1.05
158	30.94	345.62	Open	VE	-	-				-3580	10.7	8.99	0.79	88	1.01
159	31.19	345.24	Open	VO	UN	N	3	2	H2	-3620	42.2	113	14	120	1.12
159	31.19	345.24	Open	VE	-	-				-3650	38.1	94.7	10	110	1.10
160	31.32	345.14	Open	VO	UN	N	4	2	NA	-3660	11.3	6.01	0.06	10	1.30
161	31.41	344.99	Open	VO	UN	N	5	2	NA	-3700	15.7	15.9	0.48	30	1.11
161	31.41	344.99	Open	BO	-	-				-3680	18.2	21.7	0.84	39	1.10
162	31.87	346.67	Open	VO	IC	U	3	67	NA	-3600	18.6	21.0	0.91	43	1.15
162	31.87	346.67	Open	VE	-	-				-3620	15.4	15.6	0.57	36	1.11
162	31.87	346.67	Open	BO	-	-				-3540	170	635	116	182	1.90
163	31.78	346.13	Open	VO	UN	U	0	0	NA	-3550	54.6	165	19	113	1.20
164	32.24	346.73	Open	VO	IC	N	0	44	NA	-3350	4.75	1.72	0.01	6	1.02
165	32.29	346.64	Open	VO	IC	N	2	44	NA	-3350	13.3	5.30	0.01	2	1.62
166	32.55	347.08	Open	VO	IC	N	0	0	NA	-3470	10.7	8.17	0.08	10	1.05
167	32.53	347.27	Open	VO	IC	N	1	43	NA	-3450	21.1	23.2	0.38	17	1.24
168	32.74	346.12	Open	VO	CS	N	0	0	NA	-3550	9.30	6.27	0.27	44	1.05

169	31.99	346.41	Open	VO	IC	N	2	67	NA	-3150	12.6	8.38	0.09	11	1.23
169	31.99	346.41	Open	VE	-	-				-3170	6.62	2.36	0.005	2	1.21
169	31.99	346.41	Open	BO	-	-				-3140	15.5	12.6	0.19	15	1.23
170	31.49	346.45	Open	VO	IC	U	0	0	NA	-3450	6.02	2.46	0.02	9	1.08
171	30.07	348	Open	VO	IC	N	8	1	NA	-3220	24.1	23.2	0.61	26	1.41
172	31.95	351.29	Open	VO	IC	N	5	46	NA	-2810	14.8	11.9	0.24	20	1.21
174	26.40	340.53	Open	VO	CS	N	5	38	NA	-3710	58.3	134	3.27	24	1.42
175	26.70	340.61	Open	VO	CS	N	4	38	NA	-3660	69.5	238	53	221	1.27
176	28.86	342.62	Open	VO	IC	O	1	39	H1	-3520	119	281	4.96	18	2.00
176	28.86	342.62	Open	VE	-	-				-3540	24.8	21.6	0.13	6	1.50
176	28.86	342.62	Open	BO	-	-				-3510	143	400	9.34	23	2.02
177	28.49	343.22	Open	VO	IC	N	2	40	NA	-3240	6.23	2.89	0.01	2	1.03
177	28.49	343.22	Open	BO	-	-				-3230	16.2	12.4	0.07	6	1.29
178	28.83	345.65	Open	VO	IC	N	0	0	NA	-2960	21.8	17.3	0.07	4	1.48
179	31.41	345.23	Open	VO	CS	N	1	2	NA	-3540	12.6	11.8	0.81	69	1.03
180	20.39	350.31	Open	VO	IC	N	0	0	NA	-1500	47.1	132	4.83	37	1.16
181	19.82	344.77	Open	VO	IC	N	0	0	NA	-1610	11.8	9.28	0.11	12	1.09
181	19.82	344.77	Open	BO	-	-				-1600	85.2	140	3.63	26	2.03
182	21.21	344.32	Open	VO	IC	N	0	0	NA	-2050	21.2	19.8	1.16	58	1.34
183	17.13	339.454	Open	VO	IC	N	2	17	NA	-2400	17.4	12.3	0.07	6	1.40
183	17.13	339.454	Open	BO	-	-				-2390	21.0	23.1	0.24	11	1.23
184	12.92	343.67	Open	VO	IC	N	1	26	NA	-1880	6.87	3.18	0.004	1	1.09
185	7.20	341.26	Open	VO	IC	N	3	4	NA	-2330	10.3	8.22	0.12	15	1.02
186	7.32	341.42	Open	VO	IC	N	2	4	NA	-2210	15.2	8.32	0.07	8	1.49
187	7.38	341.64	Open	VO	IC	N	1	4	NA	-2140	5.34	2.05	0.002	1	1.05
188	8.10	338.8	Open	VO	UN	N	0	3	NA	-2600	30.9	25.5	0.27	11	1.72
189	10.84	339.05	Open	VO	IC	N	0	0	NA	-1930	54.0	99.0	1.40	14	1.53
190	9.35	337.51	Open	VO	CS	N	0	0	NA	-2990	60.2	208	12	58	1.18

191	9.31	337.76	Open	VO	UN	N	0	0	NA	-2560	4.21	1.31	0.001	1	1.04
192	9.12	337.74	Open	VO	UN	N	0	0	NA	-2950	6.83	3.50	0.07	21	1.03
192	9.12	337.74	Open	BO	-	-				-2930	9.09	5.61	0.15	26	1.08
193	9.90	337.65	Open	VO	CS	N	0	0	NA	-1920	24.2	40.7	2.36	58	1.07
194	10.26	336.17	Open	VO	IC	N	0	0	NA	-2490	4.19	1.11	0.01	6	1.12
195	11.17	333.89	Open	VO	UN	N	0	0	NA	-3030	53.1	89.4	8.91	100	1.58
195	11.17	333.89	Open	VE	-	-				-3110	49.5	58.2	3.10	53	1.83
195	11.17	333.89	Open	BO	-	-				-2990	52.4	104	13	122	1.45
196	11.42	334.55	Open	VO	IC	N	1	7	NA	-2550	58.2	94.3	1.22	13	1.69
197	11.07	334.08	Open	VO	IC	N	2	7	NA	-2930	78.5	107	1.75	16	2.14
198	13.25	333.25	Open	VO	IC	N	3	8	NA	-2540	19.2	20.1	0.25	13	1.21
199	13.37	333.28	Open	VO	IC	N	2	8	NA	-2520	4.35	1.44	0.002	2	1.02
200	13.38	333.42	Open	VO	IC	N	1	8	NA	-2510	27.6	40.1	0.33	8	1.23
201	13.53	332.59	Open	VO	IC	N	0	0	NA	-2750	6.87	2.31	0.01	2	1.28
201	13.53	332.59	Open	BO	-	-				-2740	8.98	4.55	0.03	7	1.19
203	14.93	335.47	Open	VO	IC	N	0	0	NA	-2520	30.8	47.0	0.78	17	1.27
203	14.93	335.47	Open	VE	-	-				-2540	20.2	18.8	0.17	9	1.32
204	14.99	336.19	Open	VO	IC	O	4	11	NA	-2540	379	2470	150	61	2.15
205	14.54	337.12	Open	VO	IC	N	2	11	NA	-2430	9.34	5.22	0.02	4	1.15
206	14.46	337.04	Open	VO	IC	N	1	11	NA	-2370	9.13	6.15	0.02	3	1.04
207	15.25	337.95	Open	VO	CM	N	2	12	UN	-2410	346	4267	3666	859	1.50
207	15.25	337.95	Open	BO	-	-				-2380	403	4546	3802	836	1.69
208	14.00	335.9	Open	VO	IC	N	0	0	NA	-2560	19.8	15.5	0.06	4	1.42
209	12.06	335.99	Open	VO	IC	N	2	10	NA	-2120	13.1	6.95	0.03	5	1.40
209	12.06	335.99	Open	BO	-	-				-2110	20.9	17.2	0.13	8	1.42
210	17.03	335.73	Open	VO	CM	N	0	0	NA	-2760	93.8	379	46	123	1.36
210	17.03	335.73	Open	BO	-	-				-2740	95.5	395	53	135	1.36
211	17.03	334.71	Open	VO	IC	N	1	14	NA	-2980	62.2	176	2.42	14	1.32

212	17.31	334.3	Open	VO	IC	N	2	14	NA	-2970	47.6	66.8	0.66	10	1.64
213	17.28	334.12	Open	VO	IC	N	0	14	NA	-2960	13.2	10.4	0.03	3	1.15
214	17.11	330.47	Open	VO	UN	N	0	0	NA	-3070	120	550	7.00	13	1.45
215	15.77	334.5	Open	VO	IC	N	1	13	NA	-2670	7.38	3.93	0.01	2	1.05
216	17.19	336.32	Open	VO	IC	N	2	15	NA	-2800	104	235	5.69	24	1.92
217	17.65	336.16	Open	VO	UN	N	2	16	NA	-2950	17.0	16.9	0.42	25	1.16
218	17.37	336.49	Open	VO	UN	N	1	16	NA	-2760	64.8	121	4.99	41	1.66
219	16.53	336.25	Open	VO	UN	N	1	15	NA	-2680	8.41	4.24	0.08	19	1.15
220	35.14	347.53	Open	VO	IC	N	3	49	UN	-3820	14.2	14.7	0.22	15	1.04
221	35.30	347.72	Open	VO	IC	N	2	49	NA	-3750	6.67	3.05	0.01	3	1.08
222	35.38	347.68	Open	VO	IC	N	1	49	NA	-3750	5.22	2.02	0.003	2	1.04
223	32.09	346.6	Open	VO	IC	N	1	44	NA	-3280	18.7	15.9	0.34	21	1.32
224	32.00	347.38	Open	VO	IC	N	1	43	NA	-3280	15.3	14.9	0.81	54	1.12
224	32.00	347.38	Open	BO	-	-				-3270	16.3	17.1	0.95	56	1.11
225	28.41	347.24	Open	VO	IC	N	2	41	NA	-3000	24.2	17.3	0.07	4	1.64
226	28.28	347.26	Open	VO	IC	N	1	41	NA	-2920	6.58	2.71	0.01	6	1.13
227	21.60	346.2	Open	VO	IC	N	1	23	NA	-2040	30.7	32.3	0.35	11	1.52
228	21.69	345.67	Open	VO	IC	N	0	0	NA	-2080	17.1	14.5	0.14	9	1.27
229	19.89	343.5	Open	VO	IC	N	0	0	NA	-1930	21.2	24.4	0.27	11	1.21
230	19.64	340.93	Open	VO	IC	N	6	19	NA	-2230	9.30	5.79	0.05	8	1.09
231	19.55	340.94	Open	VO	IC	N	5	19	NA	-2210	8.43	3.27	0.01	3	1.32
232	18.94	341.32	Open	VO	IC	N	2	19	NA	-2170	10.6	6.03	0.03	5	1.22
233	18.00	342.32	Open	VO	IC	N	0	0	NA	-1900	5.71	2.24	0.01	3	1.08
234	18.82	343.65	Open	VO	IC	N	0	0	NA	-1820	41.1	65.1	1.31	20	1.44
234	18.82	343.65	Open	BO	-	-				-1810	45.0	81.0	2.02	25	1.41
235	18.54	344.87	Open	VO	IC	N	1	24	NA	-1530	6.76	3.07	0.02	6	1.09
236	22.28	341.82	Open	VO	IC	N	2	20	NA	-2430	12.9	10.0	0.30	30	1.15
236	22.28	341.82	Open	BO	-	-				-2390	25.0	23.0	0.87	38	1.47

237	21.93	341.89	Open	VO	IC	N	1	20	NA	-2340	15.7	14.0	0.14	10	1.18
238	15.18	345.91	Open	VO	IC	N	1	25	NA	-1410	7.43	3.86	0.03	8	1.07
238	15.18	345.91	Open	BO	-	-				-1400	9.86	6.64	0.08	13	1.08
239	25.45	340.09	Open	VO	UN	N	0	0	NA	-3470	57.8	148	9.36	63	1.34
240	10.34	340.15	Open	VO	IC	N	0	0	NA	-2120	4.43	1.35	0.002	1	1.08
241	20.14	338.02	Open	VO	UN	N	0	0	L1	-2750	1.48	0.08	-	-	1.43
242	12.25	334.74	Open	VO	IC	N	0	0	NA	-2480	47.2	112	2.63	23	1.26
243	12.30	335.05	Open	VO	IC	N	1	9	NA	-2470	12.5	6.15	0.01	1	1.42
244	10.54	336.12	Open	VO	IC	N	0	0	NA	-2140	43.8	67.0	0.96	14	1.51
245	20.03	352.79	Open	VO	IC	N	0	0	NA	-1560	12.8	9.6	0.02	2	1.16
246	19.25	354.05	Open	VO	UN	N	0	0	NA	-1900	4.59	1.31	0.001	1	1.13
247	36.69	347.85	Open	VO	CS	N	0	0	NA	-3910	58.7	205	13	61	1.16
247	36.69	347.85	Open	VE	-	-				-3920	56.8	192	11	55	1.16
248	36.80	348.01	Open	VO	CS	N	0	0	NA	-3890	8.95	5.81	0.25	44	1.05
249	36.12	352.49	Open	VO	IC	N	0	0	NA	-3550	3.49	0.88	0.000	0	1.05
250	37.47	355.74	Open	VO	IC	N	1	68	NA	-3550	32.6	35.3	0.46	13	1.55
251	37.70	355.39	Open	VO	CS	N	0	0	NA	-3610	4.29	1.33	0.01	8	1.05
252	36.18	359.92	Open	VO	IC	N	3	52	NA	-2970	25.3	18.0	0.26	14	1.68
252	36.18	359.92	Open	BO	-	-				-2960	27.8	25.7	0.48	19	1.55
253	36.16	0.02	Open	VO	IC	N	2	52	NA	-2930	6.22	2.80	0.04	13	1.05
254	36.02	359.69	Open	VO	IC	N	0	0	NA	-2790	7.45	3.41	0.07	20	1.14
254	36.02	359.69	Open	VE	-	-				-2850	2.15	0.18	-	-	1.44
255	36.08	358.92	Open	VO	CM	N	1	53	NA	-2740	8.61	4.30	0.03	7	1.17
256	36.38	358.78	Open	VO	CS	N	2	53	NA	-3610	97.9	502	54	108	1.23
256	36.38	358.78	Open	VE	-	-				-3620	97.9	488	49	101	1.25
257	36.86	357.89	Open	VO	IC	N	0	0	NA	-3090	16.7	16.0	0.09	6	1.18
258	36.39	359.94	Open	VO	IC	N	0	0	NA	-2980	4.86	1.46	0.01	7	1.14
259	37.28	359.49	Open	VO	UN	N	0	0	NA	-3720	47.5	89.3	5.59	63	1.42

259	37.28	359.49	Open	VE	-	-				-3740	46.7	77.8	3.87	50	1.50
260	37.78	358.49	Open	VO	IC	N	1	58	NA	-3370	12.2	7.05	0.02	2	1.30
261	37.57	358.638	Open	VO	CS	N	2	58	NA	-3450	9.12	3.23	0.03	10	1.43
262	37.58	358.51	Open	VO	CS	N	0	0	NA	-3330	4.35	1.26	0.003	2	1.09
262	37.58	358.51	Open	BO	-	-				-3320	6.94	3.19	0.02	6	1.10
263	37.57	358.27	Open	VO	IC	N	0	0	NA	-3280	8.79	5.33	0.01	3	1.07
264	37.39	358.52	Open	VO	CS	N	0	0	NA	-3330	6.17	2.54	0.03	11	1.09
265	37.31	358.46	Open	VO	IC	N	0	0	NA	-3340	5.07	1.62	0.003	2	1.12
266	37.24	358.7	Open	VO	IC	N	3	57	NA	-3550	4.32	1.36	0.01	7	1.05
267	37.21	358.45	Open	VO	IC	N	1	57	NA	-3270	5.74	2.00	0.01	3	1.14
268	36.98	358.54	Open	VO	IC	N	4	54	NA	-3300	14.5	10.7	0.18	17	1.25
269	36.87	358.5	Open	VO	IC	N	3	54	NA	-3260	8.13	3.17	0.01	3	1.29
270	36.93	358.44	Open	VO	IC	N	2	54	NA	-3240	5.03	1.38	0.003	3	1.21
271	36.95	358.37	Open	VO	IC	N	1	54	NA	-3190	6.55	2.32	0.003	1	1.21
272	37.37	357.54	Open	VO	CS	N	0	0	NA	-3100	22.1	35.0	4.46	128	1.05
273	37.11	357.65	Open	VO	IC	N	2	60	NA	-3110	38.4	60.6	1.34	22	1.39
274	37.28	357.29	Open	VO	CS	N	0	0	NA	-3100	5.52	2.21	0.02	10	1.05
275	37.01	357.49	Open	VO	IC	N	1	60	NA	-3020	8.96	5.41	0.06	10	1.09
276	37.13	357.17	Open	VO	IC	N	0	0	NA	-3390	1.89	0.22	-	-	1.14
277	37.70	357.69	Open	VO	IC	N	1	59	NA	-3330	50.5	90.1	1.44	16	1.50
278	37.72	357.89	Open	VO	IC	N	2	59	NA	-3340	5.36	1.71	0.004	2	1.16
279	38.10	356.99	Open	VO	CS	N	0	0	NA	-3400	34.6	58.0	0.39	7	1.28
279	38.10	356.99	Open	VE	-	-				-3410	5.37	1.65	0.003	2	1.18
280	37.58	356.72	Open	VO	CS	N	0	0	NA	-3390	32.6	66.5	9.08	136	1.13
281	37.86	356.37	Open	VO	CS	N	0	0	NA	-3460	16.6	17.2	1.49	87	1.13
282	35.42	359.01	Open	VO	IC	N	1	51	NA	-2660	6.55	2.74	0.004	1	1.12
283	35.77	358.39	Open	VO	IC	N	1	69	NA	-2880	3.56	0.80	-	-	1.12
284	35.87	358.19	Open	VO	IC	N	2	69	NA	-2980	5.59	2.33	0.01	3	1.03

285	35.47	357.93	Open	VO	IC	N	2	62	NA	-2960	23.0	26.2	0.33	13	1.27
286	35.27	357.99	Open	VO	CS	N	1	62	NA	-2840	4.80	1.65	0.02	10	1.06
287	34.83	357.73	Open	VO	IC	N	3	51	NA	-2760	29.3	31.7	0.37	12	1.46
288	34.86	357.52	Open	VO	UN	N	1	51	NA	-2670	5.79	2.41	0.02	7	1.05
288	34.86	357.52	Open	BO	-	-				-2660	7.77	4.03	0.05	12	1.09
289	35.09	357.33	Open	VO	CS	N	1	70	NA	-2840	49.7	164	12	72	1.09
290	35.46	357.207	Open	VO	UN	N	2	70	NA	-3050	8.15	2.36	0.002	1	1.50
290	35.46	357.207	Open	BO	-	-				-3040	14.6	11.1	0.05	5	1.23
291	34.58	357.05	Open	VO	CS	N	2	51	NA	-2630	48.7	147	18	124	1.13
292	35.17	356.19	Open	VO	IC	N	3	61	NA	-3170	10.4	6.28	0.03	4	1.17
293	34.98	356.52	Open	VO	CM	O	2	61	NA	-3140	131	707	137	194	1.39
294	34.81	356.13	Open	VO	CS	U	0	0	NA	-3160	62.5	219	11	49	1.19
294	34.81	356.13	Open	BO	-	-				-3150	61.6	232	13	56	1.14
295	34.74	356.6	Open	VO	IC	N	1	61	NA	-2640	3.54	0.87	0.001	1	1.07
296	34.08	355.97	Open	VO	CS	N	2	51	NA	-2530	36.1	67.3	2.36	35	1.24
296	34.08	355.97	Open	VE	-	-				-2540	34.4	53.6	1.77	33	1.32
296	34.08	355.97	Open	BO	-	-				-2510	39.5	92.9	3.98	43	1.15
297	32.87	356.49	Open	VO	CS	N	1	51		-2730	90.4	306	13	43	1.46
298	34.21	358.4	Open	VO	CM	N	4	51	NA	-2980	765	5303	674	127	2.96
298	34.21	358.4	Open	VE	-	-				-3110	5.38	1.87	0.005	3	1.11
298	34.21	358.4	Open	BO	-	-				-2880	728	9828	1499	153	2.07
299	34.97	359.76	Open	VO	IC	N	1	51	NA	-3200	5.97	2.04	0.01	4	1.18
300	34.91	359.93	Open	VO	IC	N	1	51	NA	-2810	3.39	0.81	0.002	3	1.06
301	33.90	359.87	Open	VO	CS	N	0	0	NA	-2340	25.1	44.9	6.65	148	1.06
302	32.46	358.12	Open	VO	CS	U	0	0	NA	-2590	31.9	44.0	0.18	4	1.36
302	32.46	358.12	Open	VE	-	-				-2600	8.12	2.79	0.005	2	1.37
302	32.46	358.12	Open	BO	-	-				-2580	45.4	91.1	0.87	10	1.34
303	31.71	358.59	Open	VO	CM	O	4	63	NA	-2530	502	6935	961	139	1.70

303	31.71	358.59	Open	BO	-	-				-2470	636	8954	1448	162	1.90
304	31.04	358.45	Open	VO	CS	N	3	63	NA	-2500	146	646	16	25	1.63
304	31.04	358.45	Open	BO	-	-				-2490	147	839	23	28	1.43
305	30.02	357.62	Open	VO	IC	N	2	63	NA	-2360	637	5602	330	59	2.40
306	31.69	357.35	Open	VO	IC	N	1	63	NA	-2260	18.0	15.3	0.10	6	1.29
306	31.69	357.35	Open	BO	-	-				-2250	35.0	40.3	0.38	10	1.56
307	31.59	357.41	Open	VO	IC	N	2	63	NA	-2290	5.32	1.44	0.01	4	1.25
307	31.59	357.41	Open	BO	-	-				-2260	9.88	5.24	0.09	17	1.22
308	32.00	357.13	Open	VO	IC	N	1	63	NA	-2240	71.7	138	1.96	14	1.72
308	32.00	357.13	Open	VE	-	-				-2250	48.2	80.6	0.82	10	1.52
309	32.36	357.44	Open	VO	CS	N	1	63	NA	-2230	31.3	71.2	13	187	1.05
309	32.36	357.44	Open	BO	-	-				-2220	32.0	73.1	14	191	1.05
310	29.48	359.33	Open	VO	IC	N	1	73	NA	-2480	15.8	10.9	0.04	4	1.35
311	29.85	359.45	Open	VO	IC	N	2	73	NA	-2530	47.8	74.3	3.08	41	1.56
311	29.85	359.45	Open	BO	-	-				-2520	72.8	192	4.83	25	1.48
312	29.10	359.53	Open	VO	IC	N	0	0	NA	-2400	79.6	176	4.97	28	1.69
313	28.91	359.72	Open	VO	IC	N	0	0	NA	-2360	14.2	10.3	0.06	6	1.25
314	27.75	357.48	Open	VO	IC	N	1	63	L1	-2270	493	4996	366	73	1.97
315	26.86	356.77	Open	VO	IC	N	0	0	NA	-2120	13.2	7.27	0.02	3	1.38
315	26.86	356.77	Open	VE	-	-				-2130	3.63	0.85	0.000	1	1.11
316	36.12	356.23	Open	VO	CM	N	0	0	NA	-3180	66.9	267	23	86	1.15
317	35.81	354.65	Open	VO	UN	N	6	61	NA	-3610	78.7	121	1.60	13	2.02
318	34.73	357.15	Open	VO	CS	N	1	51	NA	-2570	4.51	1.18	0.004	4	1.17
319	34.68	356.88	Open	VO	IC	N	1	51	NA	-2510	9.80	6.01	0.02	3	1.13
320	34.90	357.59	Open	VO	UN	N	2	51	NA	-2730	8.60	3.38	0.02	6	1.32
320	34.90	357.59	Open	BO	-	-				-2720	13.6	6.06	0.05	9	1.56
321	31.53	357.29	Open	VO	IC	N	1	63	NA	-2150	11.9	6.58	0.10	15	1.31
322	31.89	353.86	Open	VO	CS	N	0	0	NA	-2300	25.7	28.9	0.54	19	1.35

323	31.92	353.54	Open	VO	IC	N	0	0	NA	-2310	7.37	2.73	0.01	2	1.26
324	32.87	354.93	Open	VO	UN	N	1	64	NA	-2410	3.71	0.93	0.002	2	1.08
325	35.85	352.69	Open	VO	CS	N	0	0	NA	-3450	14.7	14.1	1.21	86	1.11
326	37.59	355.58	Open	VO	IC	N	2	68	NA	-3660	17.9	14.7	0.11	8	1.32
327	30.35	351	Open	VO	IC	N	1	46	NA	-2530	50.0	77.1	0.68	9	1.61
328	33.24	350.06	Open	VO	IC	N	2	47	NA	-3530	15.3	13.4	0.25	18	1.18
329	33.15	347.19	Open	VO	UN	N	4	43	NA	-3840	27.8	35.3	0.88	25	1.32
330	33.00	347.16	Open	VO	UN	N	5	43	NA	-3840	14.8	14.4	0.29	20	1.10
331	33.21	347.45	Open	VO	UN	N	3	43	NA	-3690	42.7	98.2	4.90	50	1.22
332	32.04	346.34	Open	VO	IC	N	1	67	NA	-3140	4.61	1.32	0.003	3	1.13
333	32.70	346.32	Open	VO	CS	N	0	0	NA	-3750	18.0	22.6	2.53	112	1.07
334	30.83	348.08	Open	VO	IC	N	10	1	NA	-3580	78.1	220	6.07	28	1.48
335	26.68	341.33	Open	VO	CS	N	1	76	NA	-2980	10.0	7.35	0.14	19	1.04
336	26.60	340.98	Open	VO	IC	N	2	76	NA	-3220	29.3	41.9	0.42	10	1.28
337	27.20	343.04	Open	VO	IC	N	0	0	NA	-2950	21.7	19.0	0.17	9	1.40
338	28.85	342.59	Open	VO	IC	U	0	0	NA	-3530	81.8	147	2.11	14	1.90
339	30.55	347.96	Open	VO	IC	N	9	1	NA	-3570	11.5	7.92	0.06	7	1.15
340	31.66	348.29	Open	VO	IC	N	1	43	NA	-3340	16.4	15.0	0.15	10	1.20
340	31.66	348.29	Open	VE	-	-				-3350	12.1	7.81	0.04	5	1.23
340	31.66	348.29	Open	BO	-	-				-3330	28.0	27.6	0.34	12	1.50
341	31.20	348.95	Open	VO	IC	N	0	0	NA	-3050	18.0	17.8	0.13	7	1.20
342	31.23	347.9	Open	VO	IC	N	1	72	NA	-3330	19.7	20.5	0.31	15	1.23
343	31.35	347.74	Open	VO	IC	N	2	72	NA	-3380	66.9	76.7	2.05	27	2.15
344	31.96	348.46	Open	VO	IC	N	1	43	NA	-3360	15.3	12.1	0.07	6	1.24
345	31.54	347.92	Open	VO	IC	N	1	43	NA	-3330	22.6	30.3	0.29	9	1.16
346	31.69	347.73	Open	VO	IC	N	2	43	NA	-3370	52.8	117	3.78	32	1.38
347	31.49	347.56	Open	VO	IC	N	1	72	NA	-3280	7.93	4.44	0.13	30	1.06
348	30.50	348.63	Open	VO	IC	N	12	1	NA	-3800	9.49	5.30	0.07	13	1.16

349	28.33	349.92	Open	VO	IC	U	2	74	NA	-3140	173	802	125	156	1.72
349	28.35	350.01	Open	VO	IC	O	5	1	NA	-2960	333	2292	407	178	1.96
350	27.69	348.87	Open	VO	IC	N	3	1	NA	-2710	202	844	71	84	1.97
350	27.69	348.87	Open	VE	-	-				-2780	132	389	27	69	1.88
350	27.69	348.87	Open	BO	-	-				-2700	195	908	80	88	1.82
351	28.19	348.68	Open	VO	IC	N	1	1	NA	-2710	13.2	7.00	0.05	7	1.40
351	28.19	348.68	Open	BO	-	-				-2700	16.9	12.2	0.13	11	1.37
352	26.23	349.55	Open	VO	IC	N	3	1	NA	-2540	19.0	12.6	0.20	16	1.51
352	26.23	349.55	Open	BO	-	-				-2490	63.8	108	2.16	20	1.73
353	31.37	349.29	Open	VO	IC	N	0	0	NA	-3070	12.0	8.19	0.04	5	1.19
354	25.85	341.79	Open	VO	CS	N	0	37	NA	-3320	14.4	11.5	0.76	65	1.19
354	25.85	341.79	Open	VE	-	-				-3350	12.1	7.39	0.47	64	1.26
355	25.77	341.75	Open	VO	IC	N	0	0	NA	-3300	24.6	23.2	0.61	27	1.44
355	25.77	341.75	Open	BO	-	-				-3290	27.4	29.6	0.86	29	1.42
356	24.39	342.42	Open	VO	IC	N	2	35	NA	-2480	18.2	18.3	0.18	10	1.20
357	23.39	342.11	Open	VO	IC	N	0	0	NA	-2420	13.9	9.31	0.03	3	1.28
358	25.14	341.83	Open	VO	UN	N	0	0	NA	-3450	148	447	61	136	1.97
358	25.14	341.83	Open	VE	-	-				-3570	11.7	4.44	0.02	5	1.56
359	22.60	342.02	Open	VO	UN	U	4	20	NA	-3110	88.1	228	8.26	36	1.65
360	22.48	342.87	Open	VO	UN	N	3	20	NA	-2990	52.5	80.5	2.26	28	1.65
361	22.37	344.58	Open	VO	CS	N	3	21	L2	-2660	106	720	116	162	1.11
361	22.37	344.58	Open	VE	-	-				-2710	97.9	655	82	125	1.08
362	22.35	346.47	Open	VO	IC	N	0	0	NA	-2060	7.66	2.80	0.004	2	1.29
362	22.35	346.47	Open	BO	-	-				-2040	19.5	18.5	0.20	11	1.28
363	20.84	346.26	Open	VO	IC	N	0	23	NA	-2160	10.5	7.00	0.08	11	1.12
364	16.05	338.63	Open	VO	IC	N	2	17	NA	-2210	2.92	0.56	-	-	1.10
365	15.82	337.95	Open	VO	IC	N	1	17	NA	-2070	7.06	3.69	0.02	7	1.04
366	16.52	339.82	Open	VO	IC	N	2	17	NA	-2390	11.6	7.56	0.03	4	1.19

366	16.52	339.82	Open	BO	-	-				-2380	20.0	19.0	0.15	8	1.29
367	12.41	343.98	Open	VO	IC	N	2	26	NA	-2060	24.0	30.6	0.45	15	1.22
368	12.59	345.45	Open	VO	IC	N	0	27	NA	-2050	65.8	78.6	1.97	25	2.09
369	12.27	345.48	Open	VO	IC	N	2	27	NA	-2060	8.96	5.39	0.02	4	1.09
370	12.27	345.7	Open	VO	IC	N	1	27	NA	-2060	97.6	326	11	35	1.52
371	5.78	342.33	Open	VO	UN	N	2	5	NA	-2460	20.0	23.9	1.42	59	1.15
372	6.68	341.24	Open	VO	IC	N	5	4	NA	-2650	27.8	22.8	0.92	40	1.64
373	7.44	342.91	Open	VO	IC	N	1	6	NA	-2070	106	251	2.72	11	1.89
373	7.44	342.91	Open	BO	-	-				-2060	109	348	5.73	16	1.65
374	7.87	342.8	Open	VO	IC	N	3	6	NA	-2060	219	807	18	23	2.17
375	8.48	340.89	Open	VO	IC	N	3	3	NA	-2190	14.7	8.83	0.02	2	1.39
376	8.54	340.65	Open	VO	IC	N	4	3	NA	-2230	6.33	2.08	0.001	0	1.24
377	11.48	338.61	Open	VO	CM	O	1(3)	79	NA	-1940	276	2639	2325	881	1.52
377	11.48	338.61	Open	BO	-	-				-1910	315	2774	2409	868	1.69
378	12.61	340.5	Open	VO	IC	N	0	0	NA	-1510	5.40	2.08	0.01	4	1.05
379	8.07	338.67	Open	VO	UN	N	0	0	NA	-2610	12.3	9.7	0.25	25	1.12
379	8.07	338.67	Open	BO	-	-				-2600	13.9	11.4	0.35	30	1.16
380	9.31	347.46	Open	VO	IC	N	2	33	NA	-1980	6.47	3.15	0.02	7	1.03
380	9.31	347.46	Open	VE	-	-				-1990	4.23	1.33	0.002	1	1.03
381	10.11	348.13	Open	VO	IC	N	0	0	NA	-1680	22.9	25.6	0.39	15	1.28
382	9.91	348.91	Open	VO	IC	N	0	0	NA	-1940	1.99	0.26	-	-	1.11
382	9.91	348.91	Open	BO	-	-				-1930	6.17	2.58	0.01	3	1.08
383	11.70	351.131	Open	VO	IC	N	0	0	NA	-2060	95.0	162	4.15	26	2.11
384	8.68	351.55	Open	VO	IC	N	0	0	NA	-2000	7.40	3.86	0.01	2	1.06
385	8.57	351.21	Open	VO	IC	N	2	30	NA	-1950	11.2	4.71	0.01	2	1.46
386	8.81	351.2	Open	VO	IC	N	1	30	NA	-1910	43.6	69.9	0.94	13	1.47
387	7.67	352.07	Open	VO	IC	N	0	0	NA	-1850	9.07	4.54	0.03	6	1.20
388	6.19	351.32	Open	VO	IC	N	0	0	NA	-1980	21.5	25.8	0.25	10	1.19

389	7.67	351.23	Open	VO	UN	N	1	31	NA	-1590	10.3	6.54	0.11	16	1.14
390	14.53	332	Open	VO	IC	N	0	0	NA	-2580	55.0	94.8	6.06	64	1.59
391	14.62	333.35	Open	VO	IC	N	1	81	NA	-2120	13.8	11.0	0.05	5	1.17
392	14.14	336.13	Open	VO	IC	N	0	0	NA	-2430	30.7	29.1	0.34	12	1.61
393	12.01	336.19	Open	VO	IC	N	1	10	NA	-2050	6.70	2.56	0.002	1	1.18
394	11.90	335.8	Open	VO	IC	N	3	10	NA	-2280	3.94	1.02	0.002	2	1.10
394	11.90	335.8	Open	BO	-	-				-2270	8.33	4.15	0.02	5	1.15
395	12.77	335.82	Open	VO	IC	N	0	0	NA	-1720	7.06	2.89	0.01	2	1.17
396	12.84	337.92	Open	VO	IC	N	0	0	NA	-1730	9.19	5.78	0.05	8	1.08
397	14.83	337.06	Open	VO	IC	N	3	11	NA	-2540	22.7	19.2	0.10	5	1.46
398	15.02	337.21	Open	VO	CS	N	1	11	NA	-2460	27.8	54.1	3.39	63	1.07
399	14.92	336.86	Open	VO	IC	U	4	11	NA	-2560	45.7	62.5	0.99	16	1.63
400	16.10	334.6	Open	VO	IC	N	2	13	NA	-2760	28.0	39.6	0.37	9	1.26
401	16.06	334.76	Open	VO	IC	N	1	13	NA	-2730	4.94	1.56	0.003	2	1.12
402	16.38	335.42	Open	VO	IC	N	0	0	NA	-2730	52.3	87.3	1.18	14	1.58
403	15.81	333.67	Open	VO	CS	N	0	0	NA	-2620	13.4	10.8	0.11	10	1.15
404	12.47	335.07	Open	VO	IC	N	2	9	NA	-2560	9.79	6.86	0.04	6	1.05
405	12.01	339.05	Open	VO	CM	U	2	79	NA	-2120	207	2129	1705	801	1.27
406	7.20	343.48	Open	VO	IC	N	2	6	NA	-2040	16.6	10.9	0.07	6	1.42
407	6.56	342.52	Open	VO	IC	N	1	5	NA	-2190	51.3	64.4	0.31	5	1.80
408	6.69	342.31	Open	VO	IC	N	2	5	NA	-2200	12.0	9.35	0.04	4	1.10
409	6.76	342.34	Open	VO	IC	N	1	5	NA	-2180	4.74	1.35	0.001	1	1.15
410	6.68	342.21	Open	VO	IC	N	3	5	NA	-2200	18.9	9.9	0.03	3	1.69
411	8.81	345.26	Open	VO	IC	N	0	0	NA	-1820	9.84	6.47	0.04	6	1.09
412	13.19	345.5	Open	VO	IC	N	0	0	NA	-1850	4.93	1.51	0.001	1	1.13
412	13.19	345.5	Open	BO	-	-				-1840	9.16	5.97	0.03	5	1.06
413	13.42	345.73	Open	VO	IC	N	0	0	NA	-1920	20.9	23.5	0.34	14	1.22
413	13.42	345.73	Open	BO	-	-				-1870	54.2	109	5.46	50	1.46

414	13.21	344.97	Open	VO	CS	N	0	0	NA	-2200	12.4	8.85	0.12	13	1.17
415	11.08	347.2	Open	VO	IC	N	0	0	NA	-1640	3.01	0.61	0.001	1	1.09
416	11.14	347.15	Open	VO	IC	N	0	0	NA	-1680	7.86	3.11	0.01	4	1.26
417	9.62	348.43	Open	VO	CS	N	0	0	NA	-1850	5.94	2.69	0.03	13	1.02
418	13.07	348.39	Open	VO	IC	N	2	28	NA	-2070	284	1320	38	29	2.20
419	13.81	348.56	Open	VO	IC	N	3	28	UN	-2090	60.8	97.3	1.14	12	1.74
420	14.72	348.44	Open	VO	IC	N	0	0	NA	-1980	44.1	41.6	0.58	14	1.93
421	15.51	348.89	Open	VO	IC	N	0	0	NA	-2030	6.15	2.80	0.02	6	1.04
422	22.22	354.15	Open	VO	IC	N	0	0	NA	-1950	7.33	3.07	0.01	2	1.18
423	23.03	354.75	Open	VO	IC	N	2	77	NA	-2110	10.8	8.59	0.08	10	1.04
424	24.95	352.19	Open	VO	IC	N	1	1	NA	-2180	10.3	7.66	0.06	8	1.05
425	18.58	350.88	Open	VO	IC	N	0	0	NA	-1910	37.1	40.5	0.20	5	1.64
426	19.89	351.28	Open	VO	CS	N	0	0	NA	-1750	305	5172	3498	676	1.20
426	19.89	351.28	Open	BO	-	-				-1740	308	5209	3550	681	1.20
427	21.04	349.02	Open	VO	IC	N	0	0	NA	-1660	112	218	8.20	38	2.15
428	20.22	347.97	Open	VO	IC	N	0	0	NA	-2030	7.53	3.04	0.004	1	1.22
428	20.22	347.97	Open	BO	-	-				-2020	18.8	16.2	0.09	5	1.32
429	19.98	347.84	Open	VO	IC	N	0	0	NA	-2060	53.3	74.3	0.94	13	1.75
429	19.98	347.84	Open	VE	-	-				-2080	11.3	7.20	0.04	5	1.19
429	19.98	347.84	Open	BO	-	-				-2050	54.0	101	1.80	18	1.52
430	19.94	347.32	Open	VO	IC	N	0	0	NA	-2040	6.67	3.26	0.01	2	1.04
431	21.50	341.51	Open	VO	IC	N	0	0	NA	-2060	15.0	12.6	0.18	14	1.19
432	24.43	338.7	Open	VO	IC	N	1	36	NA	-3070	17.3	16.9	0.25	15	1.18
433	24.52	338.28	Open	VO	IC	N	0	0	NA	-3010	8.93	5.83	0.05	9	1.04
434	24.42	338.58	Open	VO	IC	N	2	36	NA	-3080	7.94	4.31	0.03	6	1.08
435	26.71	355.98	Open	VO	IC	N	2	75	NA	-2040	9.42	5.44	0.06	11	1.14
436	33.85	353.16	Open	VO	CS	N	0	0	NA	-2920	19.2	25.6	2.93	114	1.07
437	34.54	351.7	Open	VO	CS	N	0	0	NA	-2980	15.0	15.6	1.41	91	1.08

438	35.41	350.69	Open	VO	CS	N	0	50	NA	-3240	9.24	5.97	0.32	54	1.07
438	35.41	350.69	Open	VE	-	-				-3280	6.78	3.47	0.16	47	1.03
439	34.81	348.31	Open	VO	UN	N	1	48	NA	-3550	3.05	0.62	-	-	1.10
440	27.83	347.52	Open	VO	IC	N	0	0	NA	-2500	17.9	13.9	0.12	9	1.35
441	35.79	347.38	Open	VO	IC	N	0	0	NA	-3850	5.19	1.84	0.02	10	1.08
441	35.79	347.38	Open	BO	-	-				-3840	7.12	2.89	0.03	11	1.18
442	32.47	345.52	Open	VO	IC	N	0	0	NA	-3580	2.60	0.45	0.000	1	1.09
443	28.97	344.94	Open	VO	IC	N	0	0	NA	-3190	75.5	166	7.19	43	1.65
444	30.25	343.38	Open	VO	IC	N	0	0	NA	-3470	9.60	3.94	0.01	2	1.36
445	27.24	340.91	Open	VO	IC	N	2	38	NA	-3380	15.9	15.6	0.29	18	1.13
445	27.24	340.91	Open	VE	-	-				-3390	13.8	11.2	0.15	13	1.16
445	27.24	340.91	Open	BO	-	-				-3370	17.8	20.0	0.45	23	1.12
446	23.61	357.26	Open	VO	CS	U	0	0	NA	-3310	14.2	14.8	0.60	41	1.05
446	26.97	341.09	Open	VO	IC	N	0	0	NA	-2020	31.8	44.9	16	358	1.34
446	26.97	341.09	Open	VE	-	-				-3340	10.3	8.20	0.27	33	1.02
447	23.16	357.71	Open	VO	IC	N	0	0	NA	-2000	18.5	16.3	0.14	9	1.29
448	27.02	358.5	Open	VO	IC	N	0	0	NA	-2210	16.6	17.0	0.15	9	1.13
448	27.02	358.5	Open	VE	-	-				-2220	13.5	7.78	0.03	3	1.37
449	27.15	0	Open	VO	IC	N	2	97	NA	-2100	75.2	124	1.41	11	1.91
450	27.37	359.23	Open	VO	IC	N	0	0	NA	-2040	76.9	145	4.08	28	1.80
451	27.42	359.54	Open	VO	IC	N	0	0	NA	-2030	21.2	26.1	0.56	21	1.17
452	30.48	359.11	Open	VO	IC	N	0	0	NA	-2460	82.1	228	3.56	16	1.53
453	32.28	356.75	Open	VO	IC	N	1	66	NA	-2070	19.7	15.0	0.18	12	1.44
454	32.05	356.55	Open	VO	IC	N	1	65	NA	-2100	29.1	24.8	0.21	8	1.65
454	32.05	356.55	Open	VE	-	-				-2110	8.71	3.79	0.02	6	1.26
454	32.05	356.55	Open	BO	-	-				-2090	52.8	74.1	0.85	11	1.73
455	31.95	356.22	Open	VO	IC	N	3	65	NA	-2240	38.2	45.5	1.24	27	1.60
455	31.95	356.22	Open	BO	-	-				-2230	41.5	53.2	1.73	33	1.61

456	32.10	356.4	Open	VO	IC	N	2	65	NA	-2090	22.6	24.5	0.68	28	1.29
456	32.10	356.4	Open	VE	-	-				-2130	9.23	4.88	0.04	8	1.18
456	32.10	356.4	Open	BO	-	-				-2080	24.4	28.4	0.94	33	1.29
457	32.13	356.22	Open	VO	IC	N	1	65	NA	-2180	4.46	1.13	0.003	3	1.18
458	32.26	356.41	Open	VO	IC	N	2	65	NA	-2040	14.4	14.1	0.37	26	1.08
459	32.20	356.18	Open	VO	IC	N	3	65	NA	-2280	8.12	4.78	0.08	17	1.05
459	32.20	356.18	Open	VE	-	-				-2320	3.26	0.67	0.001	1	1.12
460	32.24	356.53	Open	VO	IC	N	1	65	NA	-2040	6.42	1.83	0.002	1	1.34
461	32.31	356.96	Open	VO	IC	N	3	66	NA	-2100	5.81	2.09	0.01	3	1.13
462	32.31	356.9	Open	VO	IC	N	2	66	NA	-2100	4.98	0.84	0.002	2	1.53
463	34.84	359.7	Open	VO	CS	N	0	0	NA	-2740	6.73	3.35	0.05	16	1.04
463	34.84	359.7	Open	BO	-	-				-2730	7.75	4.23	0.09	22	1.06
464	35.49	356.63	Open	VO	IC	N	1	61	NA	-3130	35.4	40.6	0.26	6	1.57
465	36.01	356.6	Open	VO	CS	N	0	0	NA	-3040	10.9	8.55	0.60	71	1.06
466	36.99	356.2	Open	VO	CS	N	0	0	NA	-3340	7.23	3.88	0.14	36	1.03
467	39.34	359.53	Open	VO	CS	N	0	0	NA	-3330	12.4	8.76	0.12	13	1.18
468	37.61	358.8	Open	VO	CS	N	0	0	NA	-3570	20.5	28.2	0.57	20	1.09
469	37.04	358.54	Open	VO	IC	N	1	56	NA	-3320	5.48	1.72	0.004	2	1.18
470	37.13	358.58	Open	VO	IC	N	2	56	NA	-3360	3.92	1.13	0.001	1	1.04
471	37.21	358.58	Open	VO	CS	N	2	57	NA	-3380	2.47	0.44	-	-	1.05
472	36.84	358.56	Open	VO	IC	N	1	54	NA	-3220	5.58	2.16	0.01	3	1.07
473	36.78	358.54	Open	VO	IC	N	2	55	NA	-3250	2.22	0.25	-	-	1.25
474	36.79	358.52	Open	VO	IC	N	1	55	NA	-3220	1.79	0.21	-	-	1.11
475	37.18	358.53	Open	VO	IC	N	1	57	NA	-3330	4.54	1.41	0.002	2	1.08
476	35.36	359.67	Open	VO	CS	N	5	51	NA	-3520	155	1125	168	149	1.30
476	35.36	359.67	Open	BO	-	-				-3510	164	1159	179	155	1.36
477	35.36	348.57	Open	VO	CS	N	0	0	NA	-3750	3.41	0.66	-	-	1.19
478	30.32	347.36	Open	VO	IC	N	0	0	NA	-3180	10.1	4.18	0.01	2	1.39

479	36.16	359.4	Open	VO	IC	N	0	0	NA	-3880	5.26	2.01	0.002	1	1.05
479	36.16	359.4	Open	BO	-	-				-3870	29.0	27.3	0.43	16	1.56
480	35.28	356.12	Open	VO	IC	N	2	61	NA	-3170	7.09	3.45	0.01	3	1.08
481	38.02	359.52	Open	VO	CS	N	0	0	NA	-3360	4.00	0.75	-	-	1.30
482	6.91	341.22	Open	VO	IC	N	4	4	NA	-2510	28.1	30.2	2.30	76	1.44
483	15.17	333.26	Open	VO	CS	N	2	81	NA	-2320	196	2415	2986	1237	1.12
483	15.17	333.26	Open	VE	-	-				-2380	187	2347	2843	1211	1.09
484	18.06	336.98	Closed	Crat	CS	-			L1	-3080	66.5	320	41	129	1.05
485	18.99	356.38	Closed	Crat	CS	-			NA	-2510	106	664	228	344	1.16
486	19.53	347.53	Closed	Crat	CS	-			NA	-2580	86.5	442	101	229	1.16
487	20.34	339.11	Closed	Crat	CS	-			NA	-2970	83.3	485	145	299	1.07
488	21.28	355.89	Closed	Crat	CS	-			NA	-2120	36.4	96.8	11	112	1.04
489	21.72	340.4	Closed	Crat	CS	-			L1	-2710	91.8	566	140	247	1.09
490	22.11	351.77	Closed	Crat	CS	-			H2	-3960	169	1782	587	330	1.13
491	24.13	350.69	Closed	Crat	CS	-			NA	-2290	218	1864	400	215	1.42
492	25.96	352.95	Closed	Crat	CS	-			NA	-2440	48.2	173	17	97	1.03
493	26.49	358.84	Closed	Crat	CS	-			H1	-2310	50.4	184	45	248	1.05
494	30.52	352.27	Closed	Crat	CS	-			NA	-2580	92.8	577	102	177	1.09
495	30.68	345.17	Closed	Crat	CS	-			NA	-3680	34.2	78.3	21	269	1.09
496	34.94	352.4	Closed	Crat	CS	-			H2	-3300	92.6	586	193	330	1.08
497	35.76	347.95	Closed	Crat	CS	-			NA	-3780	48.6	173	22	125	1.04
498	35.99	351.91	Closed	Crat	CS	-			H1	-4010	77.4	410	46	112	1.08
499	8.47	344.27	Closed	Crat/Term	CS	-			H1	-2640	205	2831	1740	615	1.08
500	10.05	340.1	Closed	Crat/Term	CS	-			NA	-2480	68.8	203	15	73	1.36
501	10.21	343.38	Closed	Crat/Term	CS	-			NA	-2460	119	867	108	125	1.14
502	10.81	346.01	Closed	Crat/Term	CS	-			L2	-2880	271	4340	851	196	1.16
503	12.10	335.63	Closed	Crat/Term	CS	-			NA	-2620	69.3	322	39	122	1.09
504	12.26	340.49	Closed	Crat/Term	CS	-			NA	-2360	84.2	509	70	137	1.05

505	12.49	335.79	Closed	Crat/Term	CS	-	NA	-2310	80.3	470	227	483	1.05
506	12.98	345.85	Closed	Crat/Term	CS	-	NA	-2430	109	804	228	283	1.09
507	14.27	335.63	Closed	Crat/Term	CS	-	NA	-2860	107	805	273	339	1.06
508	15.97	352.03	Closed	Crat/Term	CS	-	NA	-2480	124	1038	237	228	1.09
509	16.05	347.17	Closed	Crat/Term	CS	-	NA	-3410	466	10136	2446	241	1.31
510	18.79	344.1	Closed	Crat/Term	CS	-	H1	-3310	167	776	127	163	1.69
511	18.87	354.09	Closed	Crat/Term	CS	-	NA	-2350	95.5	564	133	236	1.13
512	19.84	353.27	Closed	Crat/Term	CS	-	NA	-2310	169	1296	281	217	1.32
513	20.18	348.63	Closed	Crat/Term	CS	-	L1	-2370	154	1504	194	129	1.12
514	20.43	338.65	Closed	Crat/Term	CS	-	NA	-2940	67.1	316	51	161	1.07
515	21.66	341.21	Closed	Crat/Term	CS	-	NA	-2330	79.6	466	122	262	1.04
516	22.13	346.85	Closed	Crat/Term	CS	-	NA	-2350	126	929	236	254	1.17
517	26.24	352.132	Closed	Crat/Term	CS	-	L1	-2900	166	1790	383	214	1.11
518	28.13	350.3	Closed	Crat/Term	CS	-	NA	-3480	37.8	105	16	156	1.04
519	28.30	347.65	Closed	Crat/Term	CS	-	H1	-3510	73.0	361	74	205	1.08
520	28.31	344.54	Closed	Crat/Term	CS	-	NA	-3320	276	2443	656	269	1.57
521	30.30	348.54	Closed	Crat/Term	CS	-	NA	-3930	70.7	354	110	311	1.06
522	31.32	0.17	Closed	Crat/Term	CS	-	H1	-2700	123	784	230	293	1.24
523	31.44	347	Closed	Crat/Term	CS	-	H2	-4550	117	716	207	289	1.23
524	31.60	354.29	Closed	Crat/Term	CS	-	H1	-3410	109	772	171	221	1.11
525	32.91	355.3	Closed	Crat/Term	CS	-	NA	-2550	110	679	34	51	1.19
526	33.74	350.67	Closed	Crat/Term	CS	-	NA	-3240	50.7	183	31	169	1.06
527	35.11	350.35	Closed	Crat/Term	CS	-	H1	-3630	138	930	151	163	1.28
528	8.13	351.61	Closed	Term	IC	-	H1L2	-2000	243	1821	70	38	1.60
529	9.34	348.7	Closed	Term	IC	-	NA	-2610	113	808	202	251	1.12
530	10.02	348.86	Closed	Term	IC	-	NA	-1960	27.7	53.2	2.08	39	1.07
531	11.46	338.71	Closed	Term	IC	-	NA	-2580	106	731	293	400	1.10
532	12.28	344.23	Closed	Term	IC	-	NA	-2080	89.5	369	4.90	13	1.31

533	13.51	345.02	Closed	Term	IC	-	L1	-2310	95.0	614	179	291	1.08
534	14.83	342.96	Closed	Term	IC	-	NA	-2000	78.1	150	2.26	15	1.80
535	15.74	342.62	Closed	Term	IC	-	NA	-1850	87.2	167	3.00	18	1.91
536	17.59	350.91	Closed	Term	IC	-	NA	-1940	350	2593	105	40	1.94
537	18.03	342.97	Closed	Term	IC	-	NA	-2950	161	1751	350	200	1.09
538	18.59	335.56	Closed	Term	IC	-	NA	-3120	158	565	11	19	1.88
539	19.55	343.1	Closed	Term	IC	-	NA	-1990	227	1358	46	34	1.74
540	20.25	347.8	Closed	Term	IC	-	NA	-2090	18.5	21.7	0.39	18	1.12
541	21.24	349.12	Closed	Term	IC	-	NA	-1660	13.2	10.9	0.12	11	1.12
542	21.52	355.13	Closed	Term	IC	-	NA	-1980	268	1652	86	52	1.86
543	23.66	342.86	Closed	Term	IC	-	L1	-2730	121	907	165	182	1.13
544	24.40	338.45	Closed	Term	IC	-	NA	-3170	24.0	36.6	1.42	39	1.12
545	25.06	340.03	Closed	Term	IC	-	NA	-3340	19.9	29.3	0.97	33	1.04
546	25.19	349.07	Closed	Term	IC	-	NA	-3050	17.4	21.0	2.65	126	1.07
547	25.98	340.81	Closed	Term	IC	-	NA	-3710	278	687	21	31	3.00
548	26.52	356.13	Closed	Term	IC	-	NA	-2120	55.1	123	3.02	24	1.40
549	26.72	358.39	Closed	Term	IC	-	NA	-2270	128	862	34	39	1.23
550	26.99	356.89	Closed	Term	IC	-	NA	-2230	15.2	6.15	0.01	2	1.73
551	26.69	359.43	Closed	Term	IC	-	NA	-2160	302	2427	119	49	1.73
552	28.46	341.61	Closed	Term	IC	-	H1	-3630	36.0	39.8	0.25	6	1.61
553	28.81	347.28	Closed	Term	IC	-	NA	-3130	44.8	37.9	0.66	17	2.05
554	29.15	346.2	Closed	Term	IC	-	NA	-3110	98.2	434	32	73	1.33
555	29.41	342.02	Closed	Term	IC	-	NA	-3770	35.0	51.8	0.56	11	1.37
556	29.98	359.09	Closed	Term	IC	-	NA	-2480	30.8	37.4	0.19	5	1.42
557	30.74	348.071	Closed	Term	IC	-	NA	-3490	417	2435	470	193	2.39
558	31.43	346.19	Closed	Term	IC	-	NA	-4320	48.7	165	72	433	1.07
559	32.51	350.93	Closed	Term	IC	-	NA	-3170	117	361	7.82	22	1.74
560	33.43	348.67	Closed	Term	IC	-	L3	-4430	329	2415	865	358	1.89

561	34.66	347.66	Closed	Term	IC	-			L1	-3820	197	741	54	73	2.04
562	35.95	357.09	Closed	Term	IC	-			NA	-3110	205	1533	93	61	1.48
563	36.78	359.41	Closed	Term	IC	-			L1	-3830	262	2612	702	269	1.45
564	14.18	348.6	Closed	Term	IC	-			NA	-2080	96.4	370	28	76	1.41
565	41.13	1.18	Open	VO	IC	N	2	82	NA	-3540	56.7	112	2.44	22	1.51
566	41.47	1.75	Open	VO	IC	N	0	0	NA	-3510	10.7	4.32	0.01	2	1.46
567	41.30	1.7	Open	VO	IC	N	0	0	NA	-3600	9.13	5.18	0.03	6	1.13
568	41.07	1.67	Open	VO	IC	N	5	82	NA	-3550	6.41	2.81	0.01	5	1.08
569	41.15	1.6	Open	VO	IC	N	3	82	NA	-3540	7.06	2.67	0.004	2	1.22
570	41.11	1.64	Open	VO	IC	N	4	82	NA	-3540	6.16	2.16	0.001	0	1.18
571	39.42	1.61	Open	VO	CS	N	0	0	NA	-3410	15.9	13.4	0.55	41	1.23
571	39.42	1.61	Open	VE	-	-				-3420	14.5	11.7	0.44	38	1.20
572	39.14	1.88	Open	VO	UN	N	0	0	NA	-3320	6.68	3.11	0.005	1	1.07
573	38.21	0.88	Open	VO	CS	N	0	0	NA	-2760	26.9	52.2	4.72	90	1.05
574	37.87	0.73	Open	VO	UN	N	2	83	NA	-2920	8.79	3.25	0.01	2	1.38
575	37.83	0.51	Open	VO	CS	N	3	83	NA	-3000	15.8	12.1	0.07	6	1.28
575	37.83	0.51	Open	VE	-	-				-3010	6.83	3.15	0.01	2	1.08
576	37.72	0.3	Open	VO	UN	N	4	83	NA	-3050	38.8	83.1	0.85	10	1.20
576	37.72	0.3	Open	VE	-	-				-3070	7.37	3.38	0.005	1	1.13
577	37.73	1.86	Open	VO	CS	N	1	84	NA	-2380	12.2	10.9	0.94	86	1.04
578	37.66	1.11	Open	VO	IC	C	1	83	NA	-2740	43.8	77.4	3.78	49	1.41
578	37.66	1.11	Open	VE	-	-				-2790	35.3	41.5	0.88	21	1.55
579	37.40	0.54	Open	VO	IC	N	0	0	NA	-3010	9.09	5.74	0.03	6	1.07
580	37.47	0.37	Open	VO	CS	N	0	0	NA	-3010	18.9	21.8	1.59	73	1.14
581	36.16	0.13	Open	VO	IC	N	1	52	NA	-2820	4.11	1.19	0.004	4	1.06
582	36.08	0.14	Open	VO	IC	N	1	52	NA	-2730	3.99	1.11	0.003	2	1.07
583	36.73	0.2	Open	VO	UN	N	0	0	NA	-3180	25.1	22.7	0.24	10	1.49
584	36.48	0.35	Open	VO	UN	N	8	85	NA	-3000	15.1	10.1	0.12	11	1.34

585	36.53	0.67	Open	VO	UN	N	7	85	NA	-2810	8.24	2.64	0.005	2	1.43
586	36.25	1.25	Open	VO	UN	N	5	85	NA	-2630	31.4	26.2	0.22	8	1.73
586	36.25	1.25	Open	VE	-	-				-2640	15.6	7.22	0.02	3	1.64
587	36.36	1.29	Open	VO	IC	N	1	85	NA	-2570	4.22	1.32	0.005	4	1.04
588	36.08	1.44	Open	VO	IC	N	4	85	NA	-2620	28.8	21.4	0.24	11	1.76
588	36.08	1.44	Open	VE	-	-				-2630	8.90	5.88	0.09	15	1.04
589	36.35	0.26	Open	VO	IC	N	1	85	NA	-2930	3.08	0.67	0.000	1	1.06
590	36.43	0.27	Open	VO	IC	N	2	85	NA	-2960	4.38	1.30	0.003	3	1.08
591	36.33	0.57	Open	VO	IC	N	2	85	NA	-2830	12.8	6.42	0.03	4	1.42
592	36.28	0.59	Open	VO	IC	N	1	85	NA	-2810	4.09	1.20	0.003	2	1.05
593	36.44	0.1	Open	VO	IC	N	2	87	NA	-2930	10.1	6.80	0.11	16	1.10
593	36.44	0.1	Open	VE	-	-				-2960	5.91	1.81	0.003	2	1.24
594	36.37	0.08	Open	VO	IC	N	1	87	NA	-2910	12.1	8.72	0.17	20	1.16
595	40.76	5.75	Open	VO	IC	N	2	88	NA	-3490	5.14	1.36	-	-	1.24
596	40.79	5.83	Open	VO	IC	N	1	88	NA	-3460	7.31	3.44	0.01	4	1.11
597	40.50	5.57	Open	VO	IC	N	2	88	NA	-3450	13.0	6.19	0.02	3	1.47
598	40.49	5.68	Open	VO	IC	N	1	88	NA	-3420	26.1	32.5	0.34	10	1.29
599	37.39	5.8	Open	VO	IC	N	2	89	NA	-2250	16.1	11.3	0.10	9	1.35
600	37.27	5.76	Open	VO	IC	N	1	89	NA	-2150	4.81	1.64	0.01	5	1.06
601	36.73	5.86	Open	VO	IC	N	0	0	NA	-2130	10.3	5.36	0.01	3	1.26
602	36.84	5.65	Open	VO	IC	N	0	0	NA	-2150	4.29	1.15	0.001	1	1.13
603	36.22	3.57	Open	VO	IC	N	1	90	NA	-2370	8.15	5.00	0.04	8	1.03
604	36.22	3.09	Open	VO	IC	N	0	0	NA	-2410	5.01	1.24	-	-	1.27
605	36.23	3.07	Open	VO	IC	N	0	0	NA	-2410	1.96	0.25	-	-	1.10
606	36.37	2.97	Open	VO	IC	N	0	0	NA	-2450	4.22	1.33	0.004	3	1.03
607	36.70	3	Open	VO	IC	N	2	90	NA	-2530	223	1032	20	19	1.96
608	36.55	0.57	Open	VO	IC	N	1	85	NA	-2820	5.22	1.95	0.01	5	1.05
609	36.57	0.94	Open	VO	IC	N	1	85	NA	-2760	7.41	2.45	0.005	2	1.34

610	36.52	0.86	Open	VO	UN	N	6	85	NA	-2760	9.91	4.89	0.02	5	1.26
611	36.66	0.86	Open	VO	IC	N	1	85	NA	-2770	26.1	24.1	0.19	8	1.50
612	36.41	1.18	Open	VO	IC	N	1	85	NA	-2620	8.86	4.45	0.04	9	1.18
613	37.02	1.05	Open	VO	IC	N	0	0	NA	-2710	8.65	4.27	0.01	3	1.18
614	37.34	1.83	Open	VO	IC	N	2	84	NA	-2630	61.7	166	4.55	27	1.35
614	37.34	1.83	Open	VE	-	-				-2640	48.5	126	3.11	25	1.22
615	37.05	1.52	Closed	Crat/Term	CS	-			L1	-2900	102	628	102	162	1.15
616	38.37	2.46	Open	VO	IC	N	0	0	NA	-2900	8.23	4.52	0.03	7	1.09
617	38.12	0.63	Closed	Crat/Term	CS	-			NA	-3020	35.0	83.7	6.80	81	1.08
618	39.33	3.52	Open	VO	IC	N	5	92	NA	-3150	24.3	21.9	0.24	11	1.46
618	39.33	3.52	Open	VE	-	-				-3160	8.13	3.56	0.01	4	1.22
619	39.71	3.73	Open	VO	IC	N	6	92	NA	-3540	5.10	1.84	0.01	3	1.06
620	38.34	3.5	Open	VO	IC	N	0	0	NA	-2740	8.84	5.75	0.03	5	1.04
621	38.50	3.86	Open	VO	IC	N	2	92	NA	-2760	10.6	6.50	0.11	17	1.17
622	38.46	3.98	Open	VO	IC	N	1	92	NA	-2750	19.1	22.7	0.36	16	1.13
622	38.46	3.98	Open	VE	-	-				-2790	3.02	0.67	0.002	2	1.04
623	38.07	3.93	Open	VO	IC	N	4	92	NA	-2740	95.6	368	15	42	1.41
624	37.72	4.37	Open	VO	IC	N	3	92	NA	-2620	106	691	293	423	1.14
624	37.72	4.37	Open	BO	-	-				-2600	108	703	306	436	1.15
625	37.70	3.85	Open	VO	UN	N	2	92	NA	-2620	9.79	5.66	0.06	11	1.16
626	37.50	3.88	Open	VO	UN	N	1	92	NA	-2590	13.4	6.12	0.03	5	1.53
627	37.29	4.67	Open	VO	IC	N	0	0	NA	-2310	14.5	8.46	0.07	8	1.41
628	37.40	4.7	Open	VO	IC	N	1	92	NA	-2310	13.9	12.1	0.21	17	1.12
629	37.56	4.96	Open	VO	IC	N	2	92	NA	-2410	81.2	326	34	103	1.27
629	37.56	4.96	Open	BO	-	-				-2400	84.8	353	37	105	1.27
630	37.81	5.5	Open	VO	IC	N	0	0	NA	-2270	3.35	0.74	0.001	2	1.10
631	38.28	4.74	Open	VO	UN	N	1	91	NA	-2570	11.1	6.17	0.02	3	1.27
632	38.39	4.75	Open	VO	IC	N	2	91	NA	-2610	3.77	1.07	0.002	2	1.03

633	38.37	4.92	Open	VO	IC	N	3	91	NA	-2850	13.5	10.3	0.22	21	1.18
634	38.67	4.474	Open	VO	IC	N	0	0	NA	-2740	14.8	16.9	0.40	24	1.02
635	40.21	5.45	Open	VO	IC	N	0	0	NA	-3190	7.69	4.24	0.05	12	1.05
636	35.58	1.66	Open	VO	IC	N	3	85	NA	-2510	251	1791	230	129	1.67
636	35.58	1.66	Open	VE	-	-				-2530	200	1506	192	127	1.46
637	34.97	1.81	Open	VO	UN	N	1	85	NA	-2430	5.89	2.55	0.01	5	1.04
638	34.63	2.1	Open	VO	IC	N	1	85	NA	-2370	111	437	13	30	1.50
639	35.73	359.83	Open	VO	IC	N	0	0	NA	-2680	5.06	1.72	0.01	5	1.09
640	35.02	0.46	Open	VO	IC	N	1	51	NA	-2730	26.9	45.5	1.00	22	1.12
641	35.13	0.38	Open	VO	IC	N	1	51	NA	-2650	32.4	31.8	1.05	33	1.62
642	34.70	0.37	Open	VO	CS	N	0	0	NA	-2160	3.09	0.68	-	-	1.05
643	34.91	0.85	Open	VO	IC	N	0	0	NA	-2280	6.31	2.65	0.01	5	1.09
644	35.09	0.95	Open	VO	IC	N	1	86	NA	-2280	26.3	35.8	0.36	10	1.24
645	35.78	0.02	Open	VO	IC	N	1	51	NA	-2530	11.0	6.13	0.08	13	1.26
646	35.07	1.44	Open	VO	UN	N	1	85	NA	-2430	7.34	4.08	0.07	17	1.03
646	35.07	1.44	Open	VE	-	-	1	85		-2440	5.95	2.73	0.04	13	1.01
647	35.12	1.16	Open	VO	IC	N	2	86	NA	-2350	17.2	11.8	0.10	8	1.41
648	34.95	2.48	Open	VO	IC	N	0	0	NA	-2340	4.83	1.72	0.01	5	1.04
649	34.85	2.62	Open	VO	IC	N	0	0	NA	-2290	12.7	10.2	0.14	14	1.12
650	35.28	2.92	Open	VO	IC	N	3	93	NA	-2440	24.7	21.9	0.33	15	1.49
650	35.28	2.92	Open	VE	-	-				-2460	11.7	6.06	0.06	9	1.34
651	35.24	3.24	Open	VO	IC	N	2	93	NA	-2230	18.4	13.4	0.20	15	1.42
651	35.24	3.24	Open	VE	-	-				-2240	17.5	9.47	0.10	10	1.60
651	35.24	3.24	Open	BO	-	-				-2210	23.7	20.6	0.51	25	1.47
652	35.14	3.32	Open	VO	IC	N	1	93	NA	-2160	21.4	22.7	0.53	24	1.27
652	35.14	3.32	Open	VE	-	-				-2180	18.7	13.7	0.18	13	1.43
653	35.33	3.16	Open	VO	IC	N	1	93	NA	-2160	3.49	0.72	-	-	1.16
654	35.40	3.15	Open	VO	UN	N	2	94	NA	-2150	6.19	2.20	0.02	10	1.18

655	35.41	3.22	Open	VO	IC	N	1	94	NA	-2050	1.67	0.10	-	-	1.52
656	34.44	0.9	Open	VO	IC	N	1	85	NA	-2200	41.5	50.8	0.22	4	1.64
657	34.74	1.1	Open	VO	IC	N	2	85	NA	-2280	16.7	16.0	0.16	10	1.18
658	34.05	1.25	Open	VO	CS	N	2	95	NA	-2510	142	1021	77	75	1.26
659			Open	VE	-	-				-2560	29.5	34.8	0.57	16	1.41
660	34.25	1.66	Closed	Crat/Term	CS	-			NA	-2560	52.6	197	33	170	1.06
661	33.97	1.9	Open	VO	IC	N	1	95	NA	-2360	44.5	63.9	0.38	6	1.57
662	35.70	3.3	Closed	Crat	CS	-			NA	-2740	94.9	633	196	310	1.06
663	33.56	2.36	Open	VO	IC	N	0	0	NA	-2240	11.6	4.97	0.04	8	1.47
664	32.78	1.99	Open	VO	IC	N	0	0	NA	-2120	7.36	3.39	0.01	2	1.13
665	31.31	2.43	Open	VO	IC	N	0	0	NA	-2470	5.81	2.60	0.02	9	1.02
665	31.31	2.43	Open	BO	-	-				-2460	8.10	4.87	0.06	12	1.04
666	30.95	2.53	Closed	Crat/Term	CS	-			NA	-2660	97.7	425	115	271	1.34
667	31.09	3.23	Open	VO	IC	N	0	0	NA	-2420	4.95	1.37	0.000	0	1.19
668	28.63	0.34	Open	VO	CS	N	1	96	NA	-2440	29.1	59.9	1.75	29	1.06
669	28.91	0.18	Open	VO	IC	N	2	96	NA	-2510	13.9	9.20	0.04	5	1.29
670	27.31	0.35	Open	VO	IC	N	1	97	NA	-1990	19.2	17.3	0.24	14	1.30
671	26.56	1.06	Open	VO	IC	N	0	0	NA	-2090	4.47	1.36	0.000	0	1.08
672	26.48	1.55	Closed	Crat/Term	CS	-			NA	-2370	57.5	209	2.46	12	1.12
673	26.70	2.54	Open	VO	IC	N	1	98	NA	-2330	16.1	12.9	0.07	6	1.26
674	26.23	2.58	Open	VO	IC	U	0	0	NA	-2490	50.3	89.3	0.57	6	1.50
675	26.65	3.75	Open	VO	IC	U	1	99	NA	-2550	94.1	148	1.75	12	2.18
675	26.65	3.75	Open	VE	-	-				-2560	23.5	19.5	0.09	5	1.50
676	26.27	3.32	Open	VO	IC	U	0	0	NA	-2580	188	1115	37	33	1.59
677	25.89	3.42	Closed	Term	IC	-			NA	-2710	14.0	13.0	0.31	24	1.10
678	26.27	3.48	Open	VO	IC	U	2	99	NA	-2610	133	426	10	23	1.81
679	26.70	3.09	Closed	Crat/Term	CS	-			NA	-2890	27.9	30.6	2.14	70	1.42
680	25.96	3.1	Open	VO	IC	O	3	98	NA	-2420	653	9345	776	83	1.91

681	27.10	4.33	Open	VO	IC	N	2	98	NA	-2390	56.7	85.9	1.18	14	1.73
681	27.10	4.33	Open	VE	-	-				-2420	13.7	7.90	0.03	3	1.37
682	27.40	6.06	Closed	Crat/Term	CS	-			H1	-2750	133	1011	182	180	1.18
683	27.26	5.33	Open	VO	IC	N	1	98	NA	-2070	26.8	38.7	0.47	12	1.22
684	28.34	5.29	Open	VO	UN	N	0	0	NA	-2280	28.5	42.6	1.10	26	1.23
685	29.02	5.17	Open	VO	IC	N	0	0	NA	-2320	12.5	9.9	0.07	7	1.12
686	26.40	4.53	Open	VO	UN	N	4	98	NA	-2570	18.7	19.8	1.09	55	1.18
687	26.04	5.01	Closed	Crat/Term	CS	-			H1	-2770	194	1973	466	236	1.23
688	26.23	359.78	Open	VO	UN	N	0	0	NA	-2130	13.8	5.85	0.02	4	1.61
689	28.83	2.07	Open	VO	IC	N	0	0	NA	-2510	17.6	14.7	0.10	7	1.30
689	28.83	2.07	Open	VE	-	-				-2520	9.70	5.20	0.02	3	1.20
690	28.47	1.2	Open	VO	IC	N	0	0	NA	-2210	72.1	137	2.02	15	1.74
690	28.47	1.2	Open	BO	-	-				-2200	75.1	167	3.51	21	1.64
691	28.23	0.38	Open	VO	IC	N	0	0	NA	-2130	10.9	5.18	0.04	8	1.35
692	27.94	0.35	Open	VO	IC	N	0	0	NA	-2140	2.86	0.43	-	-	1.23
693	25.94	2.8	Closed	Term	IC	-			NA	-2520	70.5	319	6.97	22	1.11
694	25.30	4.98	Open	VO	IC	N	1	100	NA	-2070	9.27	5.93	0.06	9	1.07
694	25.30	4.98	Open	VE	-	-				-2080	6.91	3.17	0.02	5	1.09
695	25.33	5.73	Open	VO	IC	U	0	0	NA	-2360	7.85	2.00	0.002	1	1.57
696	23.60	3.79	Open	VO	IC	N	0	0	NA	-2010	8.40	4.67	0.03	7	1.10
697	23.48	3.66	Open	VO	IC	N	0	0	NA	-2040	4.32	1.37	0.001	1	1.04
698	23.82	2.61	Open	VO	IC	N	0	0	NA	-2030	28.4	54.1	1.10	20	1.09
699	23.81	2.96	Closed	Term	IC	-			NA	-2110	201	874	41	47	1.92
700	23.93	2.35	Open	VO	IC	N	0	0	NA	-1970	4.41	1.27	0.001	1	1.11
701	22.98	0.89	Closed	Crat	CS	-			NA	-2090	153	1284	220	171	1.20
702	24.97	0.59	Closed	Crat	CS	-			NA	-2310	121	641	87	135	1.35
703	22.05	1.52	Open	VO	CS	N	0	0	NA	-2000	49.3	142	15	103	1.17
703	22.05	1.52	Open	VE	-	-				-2020	41.1	120	12	101	1.06

704	24.61	4.43	Open	VO	IC	N	1	98	NA	-2120	197	1143	53	47	1.64
705	25.31	6.36	Open	VO	IC	O	2	100	NA	-2210	971	9701	863	89	2.78
706	25.81	7.65	Open	VO	CS	U	3	101	NA	-2370	46.5	153	20	130	1.06
707	25.62	7.52	Open	VO	CS	U	2	101	NA	-2330	23.1	39.3	2.96	75	1.04
708	25.46	7.69	Open	VO	IC	U	1	101	NA	-2280	60.4	184	3.04	16	1.26
709	25.95	7.97	Closed	Crat/Term	CS	-			NA	-2470	76.6	323	33	104	1.20
710	26.81	8.35	Open	VO	IC	N	0	0	NA	-2180	45.3	92.5	1.04	11	1.33
711	27.83	6.07	Open	VO	IC	N	0	0	NA	-2280	21.5	21.6	0.19	9	1.31
711	27.83	6.07	Open	VE	-	-				-2290	13.9	10.4	0.05	5	1.21
712	28.31	6.77	Open	VO	IC	N	0	0	NA	-2260	77.6	155	5.00	32	1.76
712	28.31	6.77	Open	BO	-	-				-2230	92.9	238	11	45	1.70
713	28.27	5.97	Closed	Crat/Term	CS	-			H1	-2380	102	475	118	247	1.32
714	28.48	7.8	Open	VO	IC	N	2	102	NA	-2040	4.47	1.14	0.003	3	1.18
715	28.53	7.85	Open	VO	IC	N	1	102	NA	-2020	3.95	0.78	-	-	1.26
716	27.83	7.5	Open	VO	IC	N	0	0	NA	-2130	43.6	65.2	0.59	9	1.52
716	27.83	7.5	Open	VE	-	-				-2140	26.8	27.3	0.14	5	1.45
717	27.95	6.8	Closed	Crat	CS	-			NA	-2530	37.0	104	15	148	1.02
718	26.01	10	Closed	Crat/Term	CS	-			L1	-2540	85.1	508	115	227	1.07
719	25.92	9.46	Open	VO	IC	N	1	103	NA	-2220	95.4	247	2.86	12	1.71
720	25.94	9.7	Open	VO	IC	N	2	103	NA	-2260	3.40	0.77	0.001	1	1.09
721	26.38	10.38	Open	VO	IC	N	0	0	NA	-1730	5.65	2.30	0.01	3	1.05
722	26.47	11.27	Open	VO	IC	N	0	0	NA	-2180	20.6	17.4	0.08	4	1.39
723	23.09	8.92	Closed	Crat/Term	CS	-			L1	-2560	58.1	245	37	152	1.05
724	22.78	9.07	Open	VO	IC	N	0	0	NA	-2230	115	170	2.24	13	2.48
725	22.72	8.62	Open	VO	UN	N	0	0	NA	-2160	19.2	14.8	0.11	7	1.41
726	26.10	6.01	Closed	Crat/Term	CS	-			H1	-2650	92.1	587	139	237	1.07
727	29.91	1.82	Closed	Term	IC	-			NA	-2590	1144	11694	783	67	2.98
728	31.70	0.9	Closed	Crat	CS	-			NA	-2570	30.4	50.4	3.35	67	1.21

729	37.33	6.31	Open	VO	IC	N	0	0	NA	-2210	8.39	3.67	0.01	3	1.24
730	37.37	6.24	Open	VO	UN	N	0	0	NA	-2210	5.19	1.88	0.01	4	1.07
731	37.39	6.09	Open	VO	IC	N	0	0	NA	-2180	7.17	3.81	0.05	12	1.04
732	41.12	7.85	Open	VO	IC	N	2	104	NA	-3390	8.19	4.27	0.04	8	1.12
733	41.02	7.67	Open	VO	IC	N	1	104	NA	-3280	3.52	0.87	0.001	1	1.06
734	40.17	1.14	Open	VO	IC	N	0	0	NA	-3440	4.51	1.54	0.001	1	1.03
735	41.06	3.76	Open	VO	IC	N	0	0	NA	-3830	149	580	4.05	7	1.75
735	41.06	3.76	Open	BO	-	-				-3810	673	5822	126	22	2.49
736	40.93	0.93	Open	VO	IC	N	1	82	NA	-3420	13.2	12.9	0.14	11	1.04
737	40.70	5.58	Open	VO	UN	N	3	88	NA	-3500	45.8	100	5.18	52	1.29
737	40.70	5.58	Open	BO	-	-				-3490	48.3	110	6.21	56	1.30